

EXPERIMENTAL AND MODELLING INVESTIGATION OF A NOVEL
TETRAFUNCTIONAL INITIATOR IN FREE RADICAL
POLYMERIZATION

by
Matthew Justin Scorah

A thesis
presented to the University of Waterloo
in fulfillment of the
thesis requirement for the degree of

Doctor of Philosophy
in
Chemical Engineering

Waterloo, Ontario, Canada 2005

© Matthew Justin Scorah 2005

I hereby declare that I am the sole author of this thesis. This is a true copy of the thesis, including any required final revisions, as accepted by my examiners.

I understand that my thesis may be made electronically available to the public.

Abstract

An experimental and modelling investigation of a tetrafunctional initiator designed for free radical polymerizations is presented. Multifunctional initiators are believed to provide two advantages over traditional monofunctional initiators. With a higher number of functional sites per molecule, they are able to increase polymer production while simultaneously maintaining or increasing polymer molecular weight. Examination of the literature indicates the majority of academic and industrial published studies have investigated difunctional initiators with most focusing on styrene. In this thesis, a tetrafunctional initiator, JWEB50, was systematically investigated for a variety of monomer systems in order to develop a better understanding of the behaviour of multifunctional initiators in free radical polymerizations.

A kinetic study comparing the tetrafunctional initiator to a monofunctional counterpart, TBEC, demonstrated that the impact of a multifunctional initiator is dependent upon monomer type. Regardless of the homo- or copolymer system examined, it was observed that the tetrafunctional initiator could produce higher rates of polymerization due to the greater number of labile groups per initiator molecule. However, the influence of the tetrafunctional initiator on the polymer molecular weight was dictated by the polymerization characteristics of the system in question. In the case of styrene, the tetrafunctional initiator maintained similar molecular weights compared to the monofunctional initiator while for methyl methacrylate (MMA), switching from a mono- to a tetrafunctional initiator actually decreased the polymer molecular weight. Other monomers such as butyl acrylate and vinyl acetate and copolymers of MMA and styrene or α -methyl styrene were examined to study the effect of initiator functionality in free radical polymerizations.

Subsequent to the kinetic investigation, polystyrene and poly(methyl methacrylate) samples produced with the tetrafunctional initiator were characterized in detail in order to examine the effects of initiator functionality on polymer properties. Samples generated with the monofunctional initiator were used for comparison purposes. Chromatographic

and dilute solution methods were able to detect significant levels of branching in the polystyrene sample produced with JWEB50, while poly(methyl methacrylate) samples showed no evidence of branching. Rheological tests involving a combination of oscillatory and creep shear measurements were completed in order to detect differences between samples. The presence of branching using rheological techniques was clearly observed for both polystyrene and poly(methyl methacrylate) samples produced with the tetrafunctional initiator.

In order to explain the experimental results observed in the kinetic and polymer properties studies, a reaction mechanism for polymerizations initiated with a tetrafunctional initiator was proposed and used in the development of a mathematical model. Reactions involving the fate/efficiency of functional groups are properly accounted for, while in the past this had been ignored by modelling work in the literature. Based on model predictions, di-radical concentrations were estimated to be several orders of magnitude smaller than mono-radical concentrations and their contribution in the reaction mechanism was found to be negligible. Modelling results also demonstrated that the concentration and chain length of various polymer structures (i.e., linear, star or coupled stars) depend upon monomer type and reaction conditions.

Acknowledgments

I am indebted to my supervisor, Professor Alexander Penlidis, for his invaluable guidance, support and insight in both my academic work and life in general. I consider myself fortunate to have had the chance to learn from such an excellent mentor. I would also like to express my gratitude to my co-supervisor, Professor Ramdhane Dhib, for his support and encouragement during the course of my research.

Many thanks are extended to Professor Neil McManus, for sharing his seemingly unending wealth of laboratory and chemistry knowledge and Professor Costas Tzoganakis, for his helpful discussions on polymer rheology. I would like to acknowledge the assistance of ATOFINA Chemicals, specifically Dr. Jerry Wicher and Dr. Leo Kasehagen, for supplying samples of the initiators used in this study and their patience in answering my questions. My thanks go out to Renato Cosentino, for his help running the experiments with butyl acrylate.

My sincere gratitude goes out to those friends I have made during the course of my studies in Waterloo, many thanks to Brian Barclay, Jennifer Chen, Luke Coleman, Luigi D'Agnillo, Deborah Sarzotti and William Ripmeester, for making life in graduate school much more enjoyable.

I am extremely grateful for the support of my family, particularly my brother, Ed, for his generosity, support and friendship. I would never have finished grad school without his help. Lastly, I would like to thank my fiancée, Dr. Julie Smith, for her patience, love and friendship. I still have no clue how you manage to put up with me.

TABLE OF CONTENTS

Abstract.....	iii
Acknowledgments.....	v
List of Figures.....	ix
List of Tables.....	xv
Abbreviations.....	xvi
Symbols.....	xvii
CHAPTER 1 - INTRODUCTION.....	1
CHAPTER 2 - BACKGROUND AND LITERATURE REVIEW.....	4
2.1 Free Radical Polymerization.....	4
2.2 Multifunctional Initiators.....	5
2.3 Branching in Polymers.....	8
2.3.1 Branched Polymer Properties.....	10
2.3.2 Detection of Long-Chain Branching.....	36
2.4 References.....	53
CHAPTER 3 - EXPERIMENTAL METHODS.....	70
3.1 Initiator Selection.....	70
3.2 Reagent Purification.....	71
3.3 Polymer Synthesis.....	71
3.4 Polymer Characterization.....	72
3.4.1 Size Exclusion Chromatography.....	72
3.4.2 ¹ H-Nuclear Magnetic Resonance.....	75
3.4.3 Differential Scanning Calorimetry (DSC).....	75
3.4.4 Soxhlet Extraction.....	75
3.4.5 Rheological characterization.....	77
3.5 References.....	81
CHAPTER 4 - POLYMERIZATION OF METHYL METHACRYLATE.....	82
4.1 Introduction.....	82
4.2 Experimental.....	83
4.2.1 Reagents Purification.....	83
4.2.2 Polymer Synthesis.....	83
4.2.3 Characterization.....	84
4.2.4 Experimental Design.....	85
4.3 Results and Discussion.....	85
4.3.1 Temperature.....	85
4.3.2 Initiator Concentration.....	89
4.3.3 Initiator Functionality.....	92
4.3.4 Detection of Branching.....	96

4.4 Conclusions	103
4.5 References	103
CHAPTER 5 - COPOLYMERIZATION OF METHYL METHACRYLATE/ STYRENE AND METHYL METHACRYLATE/ α -METHYL STYRENE	106
5.1 Introduction	106
5.2 Experimental	106
5.2.1 Reagent Purification	106
5.2.2 Polymer Synthesis.....	106
5.2.3 Polymer Characterization	107
5.2.4 Experimental Design.....	108
5.3 Results and Discussion.....	109
5.3.1 Styrene-Methyl Methacrylate Copolymer	109
5.3.2 Methyl Methacrylate and α -Methyl Styrene Copolymer.....	129
5.4 Conclusions	132
5.5 References	133
CHAPTER 6 - POLYMERIZATION OF BUTYL ACRYLATE AND VINYL ACETATE	135
6.1 Introduction	135
6.2 Experimental	136
6.2.1 Reagent Purification	136
6.2.2 Polymer Synthesis.....	136
6.2.3 Polymer Characterization	137
6.2.4 Experimental Design.....	138
6.3 Results and Discussion.....	139
6.3.1 Butyl Acrylate.....	139
6.3.2 Vinyl Acetate	145
6.4 Conclusions	148
6.5 References	149
CHAPTER 7 - DETECTION OF BRANCHING IN POLYSTYRENE AND POLY(METHYL METHACRYLATE)	151
7.1 Introduction	151
7.2 Experimental Methods	153
7.2.1 Materials	153
7.2.2 Characterization	153
7.3 Results and Discussion.....	157
7.3.1 SEC	157
7.3.2 ThFFF	161
7.3.3 DSC.....	162
7.3.4 Rheology.....	163
7.4 Conclusions	195

7.5 References	197
CHAPTER 8 - MATHEMATICAL MODELLING OF TETRAFUNCTIONAL	
INITIATORS.....	201
8.1 Introduction	201
8.2 Model Development.....	201
8.2.1 Polymerization Mechanism	202
8.2.2 Mathematical Modelling.....	210
8.3 Modelling Results.....	213
8.3.1 Determination of Model Parameters.....	213
8.3.2 Validation of Model.....	217
8.3.3 Validation of Model Assumptions	229
8.3.4 Case Studies.....	235
8.4 Conclusions	240
8.5 References	242
CHAPTER 9 - CONTRIBUTIONS TO RESEARCH AND RECOMMENDATIONS	245
APPENDIX A – BENCH-MARKING OF DIFUNCTIONAL INITIATORS.....	248
APPENDIX B – TEMPERATURE PROGRAMMING WITH DIFUNCTIONAL	
INITIATORS.....	267
APPENDIX C – TETRAFUNCTIONAL MODEL DEVELOPMENT.....	270

LIST OF FIGURES

Figure 2.1. Various polymer molecular architectures: (a) star; (b) comb; (c) H-shaped; (d) pom-pom; (e) dendrimer; (f) randomly branched (contains tri- and tetrafunctional branch points with branches on branches).....	10
Figure 2.2. Theoretical and experimental g values as a function of star functionality. Data points are taken from Table 2.2.	17
Figure 2.3. Radius of gyration as a function of molecular weight for monodisperse polystyrene stars. Data from ref. (63, 67). Parameters for linear polystyrene from ref. (60).....	17
Figure 2.4. Intrinsic viscosity as a function of weight-average molecular weight for branched polystyrenes. Data taken from refs. (93, 94).	21
Figure 2.5. Zero-shear viscosity at 169.5°C as a function of weight-average molecular weight for polystyrene melts: open and closed circles and squares, linear; triangles, H-polymers. Data from ref. (94).	31
Figure 2.6. ^{13}C -NMR spectrum of polyethylene sample measured at 120°C using deuterium <i>o</i> -dichlorobenzene and 1,2,4-trichlorobenzene as solvents. Taken from ref. (204).....	37
Figure 2.7. Intrinsic viscosity, radius of gyration and contraction factors as a function of molecular weight for polystyrene (SEC at 30°C with 1.0 mL/min of tetrahydrofuran). Ref. (257).....	43
Figure 2.8. Zero-shear viscosity as a function of the number of branches per chain for polyethylene of a constant molecular weight, based on the model of Janzen and Colby (261).	45
Figure 2.9. Zero-shear viscosity as a function of weight-average molecular weight for various polyethylene samples at 190°C: circles, fairly narrow MWD ($M_w/M_n \sim 2-6$) linear samples; crosses, broad to very broad MWD ($M_w/M_n \sim 6.6-30$) branched samples but with narrow rheological polydispersity ($E_R \sim 1.7-3.7$); squares, broad MWD ($M_w/M_n \sim 6.0-14$) branched samples with large rheological polydispersity ($E_R \sim 6.0-14$). Data from ref. (175).	48
Figure 2.10. Loss angle as a function of frequency at 150°C obtained for high-density, metallocene catalyzed polyethylene samples of increasing long-chain branching. Taken from ref. (265).	50
Figure 2.11. Loss angle as a function of the reduced modulus (ratio of complex modulus and plateau modulus) for polystyrene samples. Taken from ref. (268).....	50
Figure 3.1. Decomposition of tetrafunctional initiator, JWEB50.....	70
Figure 3.2. Decomposition of monofunctional initiator, TBEC.....	70
Figure 3.3. Diagram representing the separation of low and high molecular weight polymer molecules.	73
Figure 3.4. Soxhlet extraction apparatus.....	76
Figure 3.5. Examples of the storage modulus for three linear polymers. A is monodisperse with a low molecular weight. B is monodisperse with a high molecular weight. C is polydisperse with a high molecular weight. Taken from ref. (5).....	79

Figure 3.6. Typical storage and loss modulus curves for a monodisperse high molecular weight polymer. Taken from ref. (5).....	79
Figure 4.1. Monomer conversion as a function of time for the polymerization of MMA with JWEB50 at T_1 (110°C) and T_2 (100°C).....	86
Figure 4.2. Molecular weight averages as a function of conversion for the polymerization of MMA with JWEB50 at T_1 (110°C) and T_2 (100°C).	88
Figure 4.3. Polydispersity as a function of conversion for the polymerization of MMA with JWEB50 at T_1 (110°C) and T_2 (100°C).....	88
Figure 4.4. Monomer conversion as a function of time for the polymerization of MMA with JWEB50 at C_1 (1×10^{-3} M) and C_2 (5×10^{-4} M).	90
Figure 4.5. Molecular weight averages as a function of conversion for the polymerization of MMA with JWEB50 at C_1 (1×10^{-3} M) and C_2 (5×10^{-4} M).....	91
Figure 4.6. Polydispersity as a function of conversion for the polymerization of MMA with JWEB50 at C_1 (1×10^{-3} M) and C_2 (5×10^{-4} M).	91
Figure 4.7. Monomer conversion as a function of time for the polymerization of MMA: comparing Tetra to Mono at T_2 (100°C) and C_2 (5×10^{-4} M).....	92
Figure 4.8. Monomer conversion as a function of time for the polymerization of MMA at T_1 (110°C): comparing Tetra at C_2 (5×10^{-4} M), Mono at C_2 (5×10^{-4} M) and Mono at $4C_2$ (2×10^{-3} M).....	94
Figure 4.9. Weight-average molecular weights as a function of conversion for the polymerization of MMA at T_1 (110°C): comparing Tetra at C_2 (5×10^{-4} M), Mono at C_2 (5×10^{-4} M) and Mono at $4C_2$ (2×10^{-3} M).....	95
Figure 4.10. SEC chromatograms for polymer produced with Tetra at T_1 (110°C) and C_2 (5×10^{-4} M).	98
Figure 4.11. SEC chromatograms for polymer produced with Mono at T_1 (110°C) and $4C_2$ (2×10^{-3} M).	99
Figure 4.12. Radius of gyration as a function of molecular weight for PMMA samples from runs Tetra, T_1 (110°C), C_2 (5×10^{-4} M) and Mono, T_1 (110°C), $4C_2$ (2×10^{-3} M) with similar weight-average molecular weights.....	101
Figure 4.13. Chromatograms depicting the effect that the linear fraction in a polymer has on the detection of branching by SEC-MALLS.....	102
Figure 5.1. Monomer conversion as a function of time for the bulk polymerization of styrene at 110°C ($C = 0.004$ M, $4C = 0.016$ M).	111
Figure 5.2. Weight-average molecular weight as a function of conversion for the bulk polymerization of styrene at 110°C ($C = 0.004$ M, $4C = 0.016$ M).....	111
Figure 5.3. Polydispersity as a function of conversion for the bulk polymerization of styrene at 110°C ($C = 0.004$ M, $4C = 0.016$ M).	112
Figure 5.4. SEC chromatograms for polymer samples from experiment S-TC (from SEC1).....	113
Figure 5.5. SEC chromatograms for polymer samples from experiment S-MC (from SEC1).....	114
Figure 5.6. Monomer conversion as a function of time for the bulk polymerization of MMA at 110°C ($C = 0.004$ M, $4C = 0.016$ M).....	115
Figure 5.7. Weight-average molecular weight as a function of conversion for the bulk polymerization of MMA at 110°C ($C = 0.004$ M, $4C = 0.016$ M).....	116

Figure 5.8. Effect of mode of termination on degree of polymerization.	117
Figure 5.9. Monomer conversion as a function of time for the bulk copolymerization of styrene and MMA at 110°C (C = 0.004 M, 4C = 0.016 M).....	118
Figure 5.10. Weight-average molecular weight as a function of conversion for the bulk copolymerization of styrene and MMA at 110°C (C = 0.004 M, 4C = 0.016 M).....	119
Figure 5.11. Copolymer composition as a function of conversion for the bulk copolymerization of styrene and MMA at 110°C (C = 0.004 M, 4C = 0.016 M).....	119
Figure 5.12. Radius of gyration and corresponding branching factor as a function of molecular weight: (a) polystyrene; (b) poly(methyl methacrylate); (c) styrene-methyl methacrylate copolymer; (d) g values for PS, PMMA and copolymer samples produced with the tetrafunctional initiator.....	122
Figure 5.13. Intrinsic viscosity and corresponding branching factor as a function of molecular weight: (a) polystyrene; (b) poly(methyl methacrylate); (c) styrene-methyl methacrylate copolymer; (d) g' values for PS, PMMA and copolymer samples produced with the tetrafunctional initiator.....	125
Figure 5.14. Weight-average molecular weight as a function of conversion for the bulk polymerization of styrene at 120°C (all samples are >99% conversion).	127
Figure 5.15. SEC chromatograms for polymer samples from experiment S-TC120 (from SEC2).....	128
Figure 5.16. Weight-average molecular weight as a function of conversion for the bulk polymerization of MMA at 120°C (all samples are >99% conversion).....	129
Figure 5.17. Monomer conversion as a function of time for the bulk copolymerization of α -methyl styrene and MMA at 110°C (C = 0.004 M, 4C = 0.016 M).	130
Figure 5.18. Weight-average molecular weight as a function of conversion for the bulk copolymerization of α -methyl styrene and MMA at 110°C (C = 0.004 M, 4C = 0.016 M).	131
Figure 5.19. Intrinsic viscosity contraction factor as a function of molecular weight for polymer produced with the tetrafunctional initiator.....	132
Figure 6.1. Monomer conversion as a function of time for the bulk polymerization of butyl acrylate at 80°C.....	139
Figure 6.2. Gel fraction as a function of conversion for butyl acrylate experiments with no chain transfer agent.	140
Figure 6.3. Weight average molecular weight of soluble material extracted from poly(butyl acrylate) samples.	141
Figure 6.4. Molecular weight averages as a function of conversion for the bulk polymerization of butyl acrylate with [CTA] = 0.05 wt.%.....	143
Figure 6.5. Molecular weight averages as a function of conversion for the bulk polymerization of butyl acrylate with [CTA] = 0.5 wt.%.....	143
Figure 6.6. Polydispersity index as a function of conversion for the bulk polymerization of butyl acrylate at 80°C (SEC1).	144
Figure 6.7. Conversion as a function of time for the bulk polymerization of vinyl acetate at 100°C.....	146

Figure 6.8. Weight average molecular weight as a function of conversion for the bulk polymerization of vinyl acetate at 100°C. Insert: weight average molecular weight for less than 60% conversion.	146
Figure 7.1. Plots of radius of gyration, intrinsic viscosity and their respective branching factors as a function of molecular weight for polystyrene samples (circles – PS-M; triangles – PS-T).	158
Figure 7.2. Plots of radius of gyration, intrinsic viscosity and their respective branching factors as a function of molecular weight for poly(methyl methacrylate) samples (circles – PMMA-M; triangles – PMMA-T).	159
Figure 7.3. Number of long-chain branches per molecule as a function of molecular weight for PS-T. The subscript number denotes the type of branching (tri- or tetrafunctional) while the subscript w indicates a weight average.	160
Figure 7.4. Number of long-chain branches per molecule as a function of molecular weight for PS-T and PS-M samples. The subscript number denotes the type of branching (tri- or tetrafunctional) while the subscript w indicates a weight average.	161
Figure 7.5. Maxwell element.	164
Figure 7.6. Logarithm of horizontal shift factors as a function of temperature for polystyrene and poly(methyl methacrylate) samples.	169
Figure 7.7. 95% Joint probability contour regions for WLF parameters estimated from polystyrene data.	170
Figure 7.8. 95% Joint probability contour regions for WLF parameters estimated from poly(methyl methacrylate) data.	170
Figure 7.9. Logarithm of horizontal shift factors as a function of inverse temperature for polystyrene and poly(methyl methacrylate) samples.	171
Figure 7.10. Storage and loss moduli master curves at 220°C for polystyrene samples.	175
Figure 7.11. Storage and loss moduli master curves at 250°C for poly(methyl methacrylate) samples.	176
Figure 7.12. Shear compliance as a function of time for sample PS-M at varying shear stress and 220°C.	177
Figure 7.13. Shear creep compliance versus time for polystyrene samples at 220°C and poly(methyl methacrylate) samples at 250°C.	178
Figure 7.14. Complex compliance as a function of frequency for polystyrene samples at 220°C and poly(methyl methacrylate) samples at 250°C. Data points are master curves obtained from dynamic experiments while lines were generated by converted creep data.	183
Figure 7.15. Storage and loss modulus master curves generated by combining dynamic and creep data for polystyrene at 220°C and poly(methyl methacrylate) at 250°C.	184
Figure 7.16. Cole-Cole plot for polystyrene and poly(methyl methacrylate) samples.	185
Figure 7.17. Reduced Van Gorp-Palmen plot for polystyrene and poly(methyl methacrylate) samples.	187

Figure 7.18. Relaxation spectra for polystyrene and poly(methyl methacrylate) samples.....	189
Figure 7.19. Viscosity versus shear rate for polystyrene and poly(methyl methacrylate) samples. Parameters for the Cross-Carreau model are given in Table 7.4 for sample.	194
Figure 7.20. Reduced viscosity as a function of shear rate for polystyrene and poly(methyl methacrylate) samples.	195
Figure 8.1. Molecular structure of tetrafunctional initiator, JWEB50.	203
Figure 8.2. Conversion as a function of time for the bulk polymerization of styrene initiated with TBEC at varying concentrations and reaction temperatures.	219
Figure 8.3. Molecular weight as a function of conversion for the bulk polymerization of styrene initiated with TBEC at varying concentrations and reaction temperatures.	220
Figure 8.4. Molecular weight as a function of conversion for the bulk polymerization of styrene initiated with TBEC at varying concentrations and reaction temperatures (Figure 8.3 continued).	221
Figure 8.5. Conversion as a function of time for the bulk polymerization of styrene initiated with JWEB50 at varying concentrations and reaction temperatures.	222
Figure 8.6. Molecular weight as a function of conversion for the bulk polymerization of styrene initiated with JWEB50 at varying concentrations and reaction temperatures.	223
Figure 8.7. Conversion as a function of time for the bulk polymerization of MMA initiated with TBEC at varying concentrations and reaction temperatures.	224
Figure 8.8. Molecular weight as a function of conversion for the bulk polymerization of MMA initiated with TBEC at varying concentrations and 110°C.....	225
Figure 8.9. Molecular weight as a function of conversion for the bulk polymerization of MMA initiated with TBEC at varying concentrations and 100°C.....	226
Figure 8.10. Conversion as a function of time for the bulk polymerization of MMA initiated with JWEB50 at varying concentrations and reaction temperatures.	227
Figure 8.11. Molecular weight as a function of conversion for the bulk polymerization of MMA initiated with JWEB50 at varying concentrations and reaction temperatures.	228
Figure 8.12. Mono- and di-radical concentrations as a function of conversion for the bulk polymerization of styrene (110°C, 4.0 mmol/L of JWEB50).	230
Figure 8.13. Mono-radical concentrations of linear, star (1 core) and coupled star (2 cores) chains as a function of conversion for the bulk polymerization of styrene (110°C, 4.0 mmol/L of JWEB50).	231
Figure 8.14. Concentration of linear, star (1 core) and coupled (2 cores) star polymer species for the bulk polymerization of styrene (110°C, 4.0 mmol/L of JWEB50).	232

Figure 8.15. Concentration of polymer species with varying number of functional groups as a function of time for the bulk polymerization of styrene (110°C, 4.0 mol/L of JWEB50).....	234
Figure 8.16. Number- and weight-average molecular weight for the bulk polymerization of styrene (110°C, 1 mmol/L of JWEB50).....	236
Figure 8.17. (a) Mole fraction of various polymer species. (b) Weight-average chain length. Identical conditions as reported in Figure 8.15. For combination data: solid line – linear, line and open circles – 1 core, line and grey circles – 2 cores. For disproportionation data: dashed line – linear, line and diamonds – 1 core, linear and grey diamonds – 2 cores.	237
Figure 8.18. Weight-average molecular weight as a function of conversion for increasing transfer to monomer in the bulk polymerization of styrene (110°C, 1 mmol/L of JWEB50).....	239
Figure 8.19. Mole fraction and chain length of star and coupled star polymer chains for increasing transfer to monomer in the bulk polymerization of styrene (110°C, 1 mmol/L of JWEB50). Solid line – 0.1 mol/(L·min), line and circles – 1 mol/(L·min), dashed line – 10 mol/(L·min), line and triangles – 50 mol/(L·min).	239

LIST OF TABLES

Table 2.1. Theoretical equations for mean-square radius contraction factor (g) for several branched structures.	14
Table 2.2. Experimental g values for star polymers in theta and good solvents.....	16
Table 2.3. Values of ε for polyethylene.....	20
Table 4.1. Effect of temperature on the rate of polymerization of MMA with JWEB50.....	87
Table 5.1. Styrene-methyl methacrylate experiment conditions.	109
Table 5.2. α -Methyl styrene-methyl methacrylate experiment conditions.....	109
Table 5.3. Power law coefficients for radius of gyration-molecular weight relationship and Kuhn-Mark-Houwink-Sakurada coefficients.....	123
Table 6.1. Butyl acrylate and vinyl acetate experiment conditions.....	138
Table 7.1. Molecular weight characterization of polystyrene and poly(methyl methacrylate) samples.....	156
Table 7.2. Material properties for polystyrene and poly(methyl methacrylate) samples.....	156
Table 7.3. Model parameters for horizontal shift factors.....	168
Table 7.4. Cross-Carreau model parameters.....	195
Table 8.1. Database entries for styrene, methyl methacrylate and their polymers.....	215
Table 8.2. Database entries for TBEC and JWEB50.....	216
Table 8.3. Estimated parameters for monofunctional and tetrafunctional models.....	217

ABBREVIATIONS

α -MS	α -Methyl styrene
ATRP	Atom transfer radical polymerization
DSC	Differential scanning calorimetry
EPM	Ethylene propylene copolymer
FFF	Field-flow fractionation
GPC	Gel permeation chromatography
IC	Interaction chromatography
JCR	Joint confidence region
KMHS	Kuhn-Mark-Houwink-Sakurada equation
LALLS	Low-angle laser light scattering
LCB	Long-chain branching
LDPE	Low-density polyethylene
LS	Light scattering
MALLS	Multi-angle laser light scattering
MMA	Methyl methacrylate
MW	Molecular weight
MWD	Molecular weight distribution
NMP	Nitroxide-mediated polymerization
NMR	Nuclear magnetic resonance
PDI	Polydispersity index
PS	Polystyrene
PMMA	Poly(methyl methacrylate)
RAFT	Reversible addition-fragmentation chain transfer polymerization
RALLS	Right-angle laser light scattering
RI	Refractive index detector
SANS	Small-angle neutron scattering
SAXS	Small-angle X-ray scattering
SEC	Size exclusion chromatography
TGIC	Temperature-gradient interaction chromatography
TTS	Time-temperature superposition
ThFFF	Thermal field-flow fractionation
Visc	Viscometer
UV	Ultra-violet light detector
WLF	Williams-Landel-Ferry equation

SYMBOLS

α	Kuhn-Mark-Houwink-Sakurada parameter
β	Exponent for A_2 - M power law
γ	Shear rate
δ	Loss angle
ε	Exponent relating g and g'
η_0	Zero-shear viscosity
η^*	Complex viscosity
$[\eta]$	Intrinsic viscosity
θ	Theta condition
ν	Exponent for R_g - M power law
ρ	Density
σ	Shear stress
τ	Relaxation time
τ^*	Characteristic shear stress of Cross-Carreau model
ω	Frequency
A_2	Second virial coefficient
a	Cross-Carreau model parameter
a_T	Frequency shift factors
b_T	Modulus shift factors
dn/dc	Specific refractive index increment
E_a	Activation energy
f	Branch point functionality
f	Initiator efficiency
G_N^o	Plateau modulus
G'	Storage modulus
G''	Loss modulus
G^*	Complex modulus
G_{red}	Reduced modulus
g	Mean-square radius contraction factor
g'	Intrinsic viscosity contraction factor
H	Relaxation modulus
h	Hydrodynamic radius contraction factor
J	Shear compliance
J^*	Complex compliance
J_e^o	Zero-shear or steady-state recovery compliance
K_{A_2}	Pre-exponential constant for A_2 - M power law
K_{R_g}	Pre-exponential constant for R_g - M power law
$K_{[\eta]}$	Kuhn-Mark-Houwink-Sakurada parameter
k_d	Functional group decomposition rate constant
k_p	Propagation rate constant
k_t	Termination rate constant

k_{tc}	Termination by combination rate constant
k_{td}	Termination by disproportionation rate constant
M	Molecular weight
M_a	Arm molecular weight
M_c	Critical molecular weight
M_e	Molecular weight between entanglements
M_n	Number-average molecular weight
M_w	Weight-average molecular weight
M_z	z -average molecular weight
n	Rate index of viscosity power-law model
R	Ideal gas law constant
R_g	Radius of gyration
R_h	Hydrodynamic radius
R_p	Rate of polymerization
T	Temperature
T_g	Glass transition temperature
V	Volume
V_f	Free volume

CHAPTER 1 - INTRODUCTION

The focus of this work has been to explore the use of multifunctional initiators in free radical polymerization. This has been completed through experimental and modelling studies of a novel tetrafunctional peroxide initiator with the following objectives in mind:

1. Study the kinetics of a tetrafunctional initiator and compare to an appropriate monofunctional counterpart.
2. Examine the effects of using a multifunctional initiator on polymer properties.
3. Model the behaviour of tetrafunctional initiators in free radical polymerization.

In Chapter 2, a brief review of the nature of free radical polymerization is given followed by advances in multifunctional initiators and their application. An inherent property of initiators with functionalities greater than two is the ability to introduce branching into the final polymer product. As such, a detailed discussion of branched polymers, their properties and the detection of branching in polymers is presented.

The experimental techniques used to study the polymerization kinetics of the tetrafunctional initiator and its monofunctional counterpart are described in Chapter 3. The methods employed in characterizing the polymer samples are also discussed in detail with relevant background information provided.

The first of several experimental studies is presented in Chapter 4. Previous work found in the literature on the use of multifunctional initiators, the majority of which are difunctional, has centered on the polymerization of styrene. In this chapter, the tetrafunctional initiator is employed in a kinetic study of the bulk polymerization of methyl methacrylate (MMA). The performance of the tetrafunctional initiator is evaluated based on rates of polymerization, molecular weights and evidence of branching for a range of conversions and under different operating conditions. These results are

then compared to experiments where an appropriate monofunctional counterpart is run under identical conditions. The behavior of the tetrafunctional initiator in the polymerization of MMA was observed to be unlike that of styrene.

In Chapter 5, the experimental kinetic study is extended to systems of two monomers. The homopolymerizations of methyl methacrylate and styrene and the copolymerizations of MMA/styrene and MMA/ α -methyl styrene were investigated. A similar procedure for evaluating the tetrafunctional initiator's behaviour was performed where conversion and molecular weight results are compared to identical runs completed with the monofunctional initiator. Dilute solution properties such as the radius of gyration and intrinsic viscosity were utilized in the detection of branching.

Chapter 6 provides the final segment of the kinetic study where the homopolymerizations of butyl acrylate and vinyl acetate initiated with the tetrafunctional initiator were explored. The polymerization of both monomers is characterized by significant transfer reactions. As such, they were chosen in order to examine the behaviour of a multifunctional initiator when transfer reactions to both monomer and polymer dominate. The impact of a chain transfer agent on a multifunctional initiator was also investigated.

In Chapter 7, the characterization of polystyrene and poly(methyl methacrylate) samples produced by both the mono- and tetra-functional initiators is presented. Size exclusion chromatography setups equipped with a light scattering detector and viscometer were used to detect evidence of branching in the polymer samples. Rheological characterization was performed by dynamic and creep tests. As seen with previous studies on polymer branching, rheological methods are far more sensitive to the presence of branched chains, and differences detected in the rheological characterization are not seen by dilute solution methods.

A mathematical model for free radical polymerization initiated with a tetrafunctional initiator is developed and discussed in Chapter 8. The model is able to accurately predict the experimental data collected for the tetrafunctional initiator. The validity of two major

model assumptions is assessed. Case studies are presented investigating the effect of termination and transfer reactions. The model is found to be a useful tool in understanding the behaviour of multifunctional initiators in various monomer systems.

CHAPTER 2 - BACKGROUND AND LITERATURE REVIEW

2.1 Free Radical Polymerization

Free radical polymerizations are characterized by a series of reactions that occur at any time during the reaction. The chemical reactions can be grouped into the following four categories: initiation, propagation, termination, and chain transfer reactions.

Initiation

The polymerization of a monomer begins with the generation of radicals from the decomposition of an initiator molecule. These radicals are then able to add one monomer unit and form primary radicals. Equation 2.1 and 2.2 demonstrate the mechanism for the generation of primary radicals.



In the above equations, I is an initiator molecule, R_{in}^{\bullet} an initiator radical, M a monomer unit and R_1^{\bullet} a primary radical.

Propagation

With the generation of primary radicals, the driving reaction involved in a polymerization may proceed, namely propagation. This step involves the sequential addition of monomer units to a radical chain.



In Equation 2.3, R_n^{\bullet} is a radical chain with n monomers units.

Termination

The termination of radicals can occur by two processes: combination and disproportionation. The former involves two radical chains reacting together to form one dead polymer chain (Equation 2.4), while the latter produces two dead polymer chains (Equation 2.5).



P_n is a dead polymer molecule of chain length n.

Chain Transfer Reactions

Depending on the nature of the reaction mixture, radical chains may react with other molecules and transfer the active radical site. Equation 2.6 provides the general mechanism for transfer reactions where Z can be any species in the reaction mixture such as monomer, solvent, impurities, chain transfer agent or polymer.



2.2 Multifunctional Initiators

Multifunctional initiators are believed to provide two advantages over traditional monofunctional initiators. Firstly, research has shown that they aid in increasing polymer production (1-7). It is known from free radical polymerization theory that the molecular weight is inversely proportional to the rate of polymerization. As such, with the use of a monofunctional initiator it is not possible to simultaneously obtain high rates and high molecular weights for bulk or solution processes. Multifunctional initiators are seen as an alternative to this problem. It has been shown that initiators containing two or more functional groups can generate high rates of polymerization while producing polymer of similar or higher molecular weight when compared to a monofunctional initiator. Such an effect has been attributed to the sequential decomposition of the functional groups, thus allowing repeated initiation, propagation and termination of the same molecule.

The second advantage of multifunctional initiators is their ability to introduce branching into the final polymer product. When three or more labile groups are contained within a single molecule, the resulting polymer chain will have a structure resembling a star. Star polymers are the simplest class of branched structures and as such, they have received a great deal of interest (8, 9). The introduction of branching is seen as advantageous from the polymer processing viewpoint, especially in polymer stretching operations where branching has been found to improve such properties as melt strength (10, 11).

Multifunctional initiators is an area of research that has grown rapidly in the last few decades with the majority of studies dealing with controlled/living polymerizations such as atom transfer radical polymerization (ATRP)(12), reversible addition-fragmentation chain transfer polymerization (RAFT)(13), nitroxide-mediated polymerization (NMP)(14), anionic polymerization (15) and cationic polymerization (16). In comparison, there are relatively few studies that investigated the use of multifunctional initiators in free radical polymerizations. And those that have researched this area typically deal with difunctional initiators for the polymerization of styrene.

Interest in the use of multifunctional initiators for free radical polymerization began over three decades ago. Prisyazhnyuk and Ivanchev produced fundamental work on understanding the mechanism of polymerization with difunctional initiators (1). The authors examined the kinetics of several diperoxides having labile functional groups of differing thermal stability in the polymerization of styrene. Work was also completed on the use of unsymmetrical difunctional initiators to produce block copolymers. Polymerization was first carried out in styrene at a lower temperature to form polystyrene macroinitiators. These macroinitiators were then used in the polymerization of methyl methacrylate (MMA) at a higher temperature to form block copolymers. Nearly a decade later, Ivanchev (1979) reviewed the current state of free radical polymerization initiation, summarizing most of the past work on difunctional initiators (17). Another significant review came from Simionescu et al. (1986) who compiled an extensive list of work involving the synthesis, decomposition and use of difunctional and multifunctional free

radical polymerization initiators (18). Although some of the synthesis and decomposition studies dealt with initiators with a functionality greater than two, very little work was completed on the use of these initiators in actual polymerizations.

Similar to earlier work, recent studies on multifunctional initiators are concerned more with difunctional molecules. The group of Choi and coworkers have written numerous papers starting with the employment of symmetrical difunctional initiators in the polymerization of styrene and developing a kinetic model of this system (3, 19). The group advanced to experimental and modeling work for unsymmetrical difunctional initiators (20, 21), then to combinations of initiators (22) and finally, modified their batch model for a tubular reactor (23). Villalobos et al. (1991) found that previous models using difunctional initiation had serious limitations for the prediction of molecular weights and molecular weight distributions at high conversion. They modified and extended current models in the literature making comparisons to their experimental work (4). Similarly, González et al. (1996) adapted a model to allow for the use of mixtures of mono- and difunctional initiators and compared their results to experimental data (5). Estenoz et al. (1996) evaluated several difunctional initiators for the synthesis of high-impact polystyrene and attempted to predict their experimental behaviour (24). More recently, Cavin et al. (2000) completed a thorough kinetic and modeling investigation of 2,5-dimethyl-2,5-bis(2-ethyl hexanoyl peroxy)hexane in the polymerization of styrene (6). By combining and adapting various models found in the literature, the group was able to accurately predict conversion data but molecular weights up to only 70% conversion. Dhib et al. (2000) compiled an extensive review of the work to date on difunctional initiators and incorporated the results into a computer simulation/database package (25). All of these studies have shown, either through experimental or modeling results, the ability of difunctional initiators over their monofunctional counterparts to reduce batch times while maintaining or increasing the polymer molecular weight.

As for initiators of functionality higher than two, a limited amount of work has been done in free radical polymerization. Menciloglu et al. (1992) reported on the synthesis of three tetrafunctional initiators based on the reaction of tetrakis(dimethylamino)titanium

with either 2,2'-azoisobutyronitrile, tetracyanoethylene or isophorone diisocyanate (26). Very little polymerization information was reported. Cerna et al. (2002) reported a kinetic study showing that the use of difunctional and trifunctional cyclic initiators would allow for high rates of polymerization while producing high molecular weight polymer (7). Holzinger and Kickelbick (2002) are another group that has used multifunctional initiators in free radical polymerization (27). Their work examined the synthesis of various initiators for thermal or photoinduced free radical polymerization from modified cubic spherosilicate cages. The data showed that polymer with a broad polydispersity was being produced which the authors attributed to the formation of various molecular architectures. Kwon et al. (2003) synthesized a novel tetrafunctional photoiniferter for the production of star polystyrene by radical polymerization (28). The resulting polymer was found to have a broad molecular weight distribution (≥ 2.5) with roughly 3 out of the 4 arms retaining their functional groups. As such, this star polystyrene was used as a polymeric photoiniferter for further polymerization of styrene.

2.3 Branching in Polymers

Branched polymers are defined as macromolecules containing points where three or more long chains are attached together. In other words, a branched polymer is characterized by more than two chain ends. These macromolecules lie in between the two extremes of linear polymers and polymer networks; however, they are more related to linear polymers. Branching can be deliberately or inadvertently introduced into a polymer either in the polymerization or extrusion process. During polymerization of many monomers, a variety of side reactions such as transfer to polymer can occur inadvertently leading to branch points. Branching can also be introduced deliberately during polymerization with the choice of the proper initiator or the addition of a polyfunctional monomer or agent. In extrusion, branching may be caused by thermal degradation, radiation or chemical means. The determination of long-chain branching (LCB) both qualitatively and quantitatively has been the focus of polymer researchers for over seventy years. The reason for such an interest can be attributed to the fact that the occurrence of even a small amount of branching can considerably influence the properties of a polymer. LCB is known to influence several solution and melt properties varying

from intrinsic viscosity to swell during blow molding. As many commercially produced polymers contain significant amounts of branched material, the detection of LCB is of tremendous practical importance.

This section deals with the detection of branching in polymers and is divided into two parts. The first segment encompasses the various properties influenced by branching while the second part reviews methods to detect or estimate branching. Short-chain branching (e.g., the result from copolymerization with a monomer containing side groups or from back-biting) is not considered in this chapter. The properties and characterization of macromolecular rings or polymer networks are also not within the scope of this text.

The occurrence of branching was postulated, roughly seventy years ago, by the work of Staudinger and Schulz in order to explain certain unexpected observations with polystyrene (29). Flory later showed that transfer reactions during the free radical polymerization of styrene could produce long-chain branches (30). Already by the early 1950's, a noteworthy amount of work dealt with the mechanism and kinetics of branching reactions, the effect of branching on polymer properties and the possible determination of LCB. In 1953, Stockmayer and Fixman reviewed the state of dilute solution properties of branched polymers (31). A short time later, Melville published an account of linear and branched polymers discussing the implication of branching and its possible detection (32). Since that era, numerous reviews of branching have been compiled. In 1968, Graessley summarized methods for the detection of branching based on dilute solution methods (33). In that same year, Dexheimer and coworkers compiled a list of studies not only including the effects of branching on polymer properties but also the kinetics and mechanism of branching (34). Small wrote a notable review of long-chain branching examining its influence on various polymer properties and the estimation of LCB (35). The work also included a survey of branching in specific polymers such as polyethylene, poly(vinyl acetate), polystyrene, poly(methyl methacrylate) and poly(vinyl chloride). More recent reviews include work by Burchard (36, 37), and Mays and Hadjichristidis (38), who examined the solution properties of branched macromolecules, and Roovers (39) who provided comprehensive surveys of the literature for branched polymers in

general. Reviews on the effect of branching in the melt state include those of Graessley (40) and Vega and coworkers (41).

Branched polymers can have various structures depending upon their synthesis. Figure 2.1 shows the architecture of some typical model branch structures and an example of random branching. A great deal of research has involved the synthesis of model branched polymers (42, 43) with narrow molecular weight distributions (MWD) in order to specifically observe the effect of branching. These results help to construct fundamental theories which can aid in the investigation of randomly branched polymers.

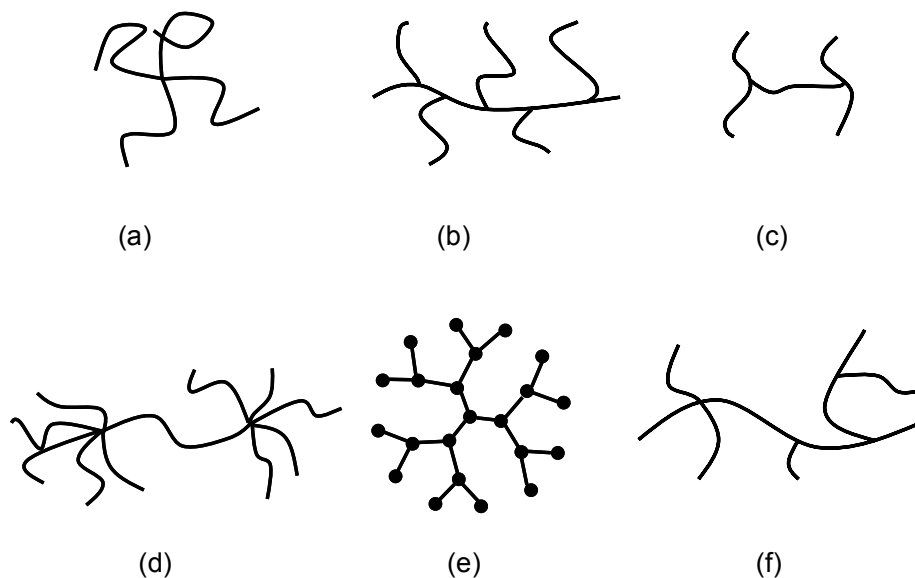


Figure 2.1. Various polymer molecular architectures: (a) star; (b) comb; (c) H-shaped; (d) pom-pom; (e) dendrimer; (f) randomly branched (contains tri- and tetrafunctional branch points with branches on branches).

2.3.1 Branched Polymer Properties

2.3.1.1 Dilute Solution Properties

2.3.1.1.1 Mean-square radius

The size of a macromolecule is one of its most fundamental properties. Although there are several ways to represent the dimensions of a polymer chain, the mean-square radius is a typical measure of size, given by the following:

$$\langle s^2 \rangle = \left\langle \sum_{i=1}^N \frac{r_i^2}{N} \right\rangle \quad (2.7)$$

where the polymer molecule is considered to be comprised of N small elements of identical mass and r_i is the distance of the i^{th} unit from the polymer molecule's centre of gravity. The use of angled brackets denotes that the summation is averaged over all possible conformations that the polymer chain can assume. The term radius of gyration is widely used when referring to a polymer molecule's size and is simply the square root of the mean-square radius:

$$R_g = \langle s^2 \rangle^{1/2} \quad (2.8)$$

Theoretical calculations for the mean-square radius of gyration usually assume that a polymer molecule can be represented by a random flight chain made up of N freely jointed units. Discrepancies between the model and actual chains arise for two reasons, known as short and long range effects. The short range effects are due to units not being completely free to rotate but having bond restrictions, while long range effects occur because intersections of units are impossible. Short range effects are addressed by dividing the polymer chain into longer segments of several bonds so that each unit can be considered to be freely jointed. If long range effects, also known as volume exclusion, are absent, then chains obey the random flight model and take an "unperturbed" state. In this case, the mean-square radius is represented by $\langle s_0^2 \rangle$ (the subscript 0 denotes an unperturbed value). From the work of Flory (44), long range effects are nonexistent at the θ point (particular temperature, T_θ , for a specific solvent) and

$$\langle s_0^2 \rangle = \langle s_\theta^2 \rangle \quad (2.9)$$

Compared to a linear chain of the same number of units, a branched chain is more compact. As a result, the impact of branching on the size of a polymer chain is to

decrease the mean-square radius as branching increases. To assess the decrease in size due to branching, the mean-square radius of a branched polymer is compared to the size of a linear analog of identical molecular weight. Quantitatively, this was defined by Zimm and Stockmayer (45) with the following branching or contraction factor:

$$g = \frac{\langle s^2 \rangle_{br}}{\langle s^2 \rangle_l} \Big|_M = \frac{R_{g\ br}^2}{R_{g\ l}^2} \Big|_M \quad (2.10)$$

The subscript M indicates that both the branched (br) and linear (l) chains have identical molecular weights. Because branched polymers are more compact and have smaller dimensions, g will always be less than unity with smaller values being an indication of a higher amount of branching. Theoretical equations for the calculation of contraction factors for various types of branching have been developed and are given in Table 2.1. Although not a complete list of the results in the literature, Table 2.1 does summarize the earlier work which provided expressions for more common types of branching. Other groups who derived identical equations or equations for other types of branching structures include Orofino (46, 47), Kurata and Fukatsu (48), Forsman (49), Burchard (36), Nakamura and coworkers (50), and Roovers (51). The equations for g given in Table 2.1 are based on the random flight model where chains are assumed to be in an unperturbed state. If Equation 2.9 is assumed to hold, these equations can be compared to experimental values of g_θ , where the mean-square radius for both linear and branched chains is measured at the θ point.

Values of $\langle s^2 \rangle$ can be obtained experimentally from radiation or neutron scattering experiments. By measuring the angular dependence of the intensity of scattered radiation between the particles and the probing radiation, the particle size can be determined. Well developed techniques for determining a particle's size include light scattering (LS), small-angle X-ray scattering (SAXS), and small-angle neutron scattering (SANS) (52). The theory of light scattering from macromolecular solutions is provided in the works of Debye and Zimm (53-55) and is reviewed and applied to branched polymers by Burchard

(36). Light scattering experiments provide a z -average estimate of the radius of gyration ($R_{g(z)}$). For samples with a narrow molecular weight distribution, this does not provide a problem and $R_g = R_{g(z)}$. However, when samples with a broad molecular weight distribution are analyzed, the increase in polydispersity (M_w/M_n) has a substantial effect and $R_{g(z)}$ will increase. This increase in the z -average radius of gyration is significant enough that it will counterbalance the decrease in size due to branching. As a result, the $R_{g(z)}$ for a polydisperse branched polymer may seem identical to that of a polydisperse linear sample. Therefore some fractionation method must be used in order to obtain monodisperse fractions where the contraction factor can be calculated. Further discussion concerning the determination of g for polydisperse samples will be provided in the section for detecting LCB.

Values of experimentally determined contraction factors for stars of varying functionality are provided in Table 2.2 and plotted in Figure 2.2. The theoretical equations for stars with monodisperse and polydisperse arms in an unperturbed state are also shown. The experimental results are for stars with narrow molecular weight distributions. Studies have found that g_0 values for stars with less than roughly 10 arms are predicted quite well by Equation 2.12. However, at higher functionalities, g_0 is observed to be greater than the theoretical values. Deviations between the two values have been attributed to various factors including a greater number of segment-segment interactions (56) and a higher density of segments near the core (57, 58). The discrepancy has also been observed with other types of branching structures such as combs and random branching (59).

The radius of gyration can be related to a molecular weight by an equation of the following form:

$$R_g = K_{R_g} M^v \quad (2.11)$$

where K_{R_g} and v are constants. The exponent can vary between 0.33 for hard spheres to 1 for a rigid rod. In the case of linear chains, an exponent of 0.5 refers to an unperturbed

state while in good solvents, ν is closer to 0.6. An excellent summary of R_g - M data in the literature by Fetters and coworkers provides estimates for these parameters in both θ and good solvents for a number of linear polymers (60). The parameters in Equation 2.11 are not only influenced by the experimental conditions (solvent, temperature) but are also affected by the polymer's structure. For monodisperse stars it has been found that increasing the number of arms decreases K_{R_g} while ν remains identical to that of the linear polymer (see Figure 2.3). However, for randomly branched polymers it has been found that ν is closer to 0.5 and in some cases much lower. Such low values of this exponent might be considered an indication of the branched polymer being in an unperturbed state; however, this is not the case. An explanation as to why ν is so small for randomly branched polymers has been found using fractal behaviour and an overview is given by Burchard (37).

Table 2.1. Theoretical equations for mean-square radius contraction factor (g) for several branched structures.

Branching type	Theoretical branching factor	Ref.
Regular stars		
monodisperse arms	$g = \frac{3f - 2}{f^2}$	(2.12) (45)
polydisperse arms	$g = \frac{6f}{(f + 1)(f + 2)}$	(2.13) (45)
	$\langle g \rangle_z = \frac{3f}{(f + 1)^2}$	(2.14) (37)
Stars with unreacted functional groups		
monodisperse arms	$g = \frac{1 + 3(f - 1)\alpha}{(2 + (f - 1)\alpha)^2}$	(2.15) (61)
polydisperse arms	$g = 4 \frac{1 + (f - 1)\alpha}{(2 + (f - 1)\alpha)^2}$	(2.16) (61)
Symmetrical combs	$g = \lambda - \frac{1}{n+1} \lambda^2 (1 - \lambda) + \frac{2}{n} \lambda (1 - \lambda)^2 + \left(\frac{3n - 2}{n^2} \right) (1 - \lambda)^3$	(2.17) (62)

Table 2.1. Continued

Random combs	
n is constant	$g = \lambda + \frac{2}{n} \lambda (1 - \lambda)^2 + \left(\frac{3n - 2}{n^2} \right) (1 - \lambda)^3 \quad (2.18) \quad (62)$
n varies	$g = \lambda + \frac{3(1 - \lambda)^2}{\bar{n}} + \frac{(1 - \lambda)^3}{\bar{n}^2} \quad (2.19) \quad (62)$
Random branching	
n is constant	$g \doteq 3 \left(\frac{\pi}{2(f-1)(f-2)n} \right)^{1/2} - \frac{2(6-f)}{(f-1)(f-2)n} \quad (2.20) \quad (45)$
n varies	$g_3 = \left[\left(1 + \frac{\bar{n}}{7} \right)^{1/2} + \frac{4\bar{n}}{9\pi} \right]^{-1/2} \quad (2.21)$
	(45)
	$g_4 = \left[\left(1 + \frac{\bar{n}}{6} \right)^{1/2} + \frac{4\bar{n}}{3\pi} \right]^{-1/2} \quad (2.22)$
n varies polydisperse	$\langle g_3 \rangle_w = \frac{6}{n_w} \left[\frac{1}{2} \left(\frac{2 + n_w}{n_w} \right)^{1/2} \ln \left(\frac{(2 + n_w)^{1/2} + n_w^{1/2}}{(2 + n_w)^{1/2} - n_w^{1/2}} \right) - 1 \right] \quad (2.23)$
	$\langle g_4 \rangle_w = \frac{1}{n_w} \ln(1 + n_w) \quad (2.24) \quad (45)$
	$\langle g \rangle_z = \frac{1}{1 + \frac{(f-1)(f-2)n_w}{6}} \quad (2.25)$

Notes:

f is the functionality of the branch point (i.e., number of chains attached to branch point); α is the number of unreacted functional groups; λ is the fraction of polymer in the backbone chain; n is the number of branch points per chain; \bar{n} is the average number of branch points per chain; n_w is the weight-average number of branch points per chain; π is 3.14159...; g_3 and g_4 denote trifunctional and tetrafunctional branch points; subscripts n , w or z represent the number, weight and z -averages.

Table 2.2. Experimental g values for star polymers in theta and good solvents.

f	g		Polymer	Conditions		Ref.
	θ solvent	Good solvent		θ Solvent	Good solvent	
3	0.82	0.79	PS	Cyclohexane (35°C)	Toluene (35°C)	(63)
4	0.63		PS	Cyclohexane (35°C)		(64)
	0.58		PS	Cyclohexane (35°C)		(65)
	0.65		PI	Dioxane (34°C)		(66)
		0.60	PS		Toluene (35°C)	(67)
6	0.46		PS	Cyclohexane (35°C)		(64)
	0.46		PI	Dioxane (34°C)		(66)
		0.47	PS		Toluene (35°C)	(67)
7	0.68	0.51	PS	Cyclohexane (35°C)	Benzene (25°C)	(68)
8	0.42		PI	Dioxane (34°C)		(69)
	0.44	0.34	PI	Dioxane (34°C)	Cyclohexane (25°C)	(70)
8.7	0.31	0.37	PS	Cyclohexane (35°C)	Benzene (25°C)	(68)
10.7	0.28	0.33	PS	Cyclohexane (35°C)	Benzene (25°C)	(68)
12	0.28	0.24	PS	Cyclohexane (35°C)	Toluene (35°C)	(71)
	0.34	0.25	PS	Cyclohexane (35°C)	Toluene (35°C)	(63)
	0.33		PI	Dioxane (34°C)		(69)
	0.37	0.25	PI	Dioxane (34°C)	Cyclohexane (25°C)	(70)
12.3	0.26	0.33	PS	Cyclohexane (35°C)	Benzene (25°C)	(68)
15.5	0.23	0.24	PS	Cyclohexane (35°C)	Benzene (25°C)	(68)
18	0.23	0.20	PS	Cyclohexane (35°C)	Toluene (35°C)	(71)
	0.20	0.19	PB	Dioxane (27°C)	Cyclohexane (25°C)	(72)
	0.29	0.18	PI	Dioxane (34°C)	Cyclohexane (25°C)	(70)
32	0.15	0.12	PB	Dioxane (27°C)	Cyclohexane (25°C)	(73)
64	0.092	0.068	PB	Dioxane (27°C)	Cyclohexane (25°C)	(74)
128	0.060	0.043	PB	Dioxane (27°C)	Cyclohexane (25°C)	(74)
270	0.06	0.03	PB	Dioxane (27°C)	Cyclohexane (25°C)	(75)

Notes:

PI represents polyisoprene; PS represents polystyrene; PB represents polybutadiene.

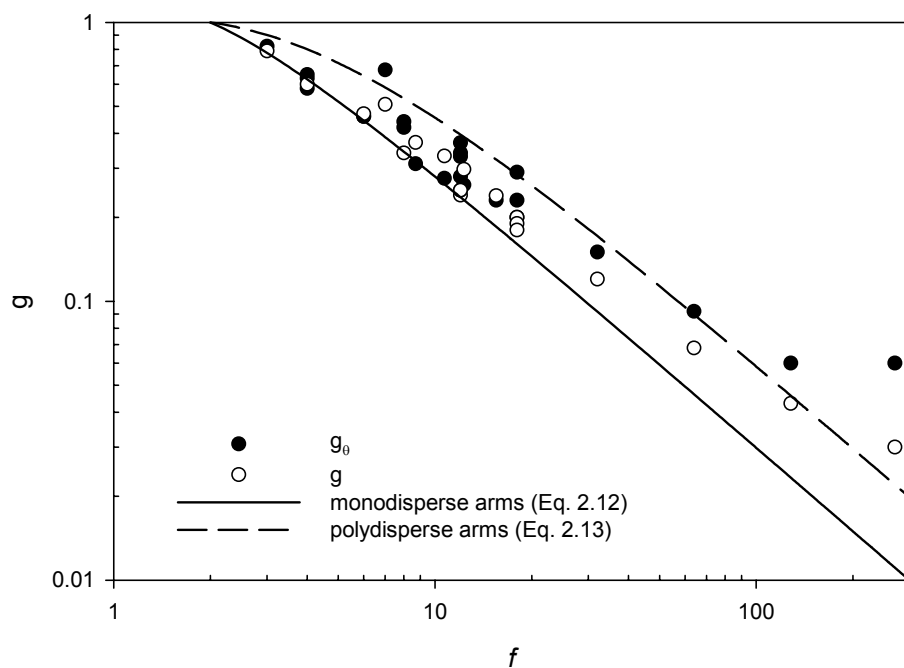


Figure 2.2. Theoretical and experimental g values as a function of star functionality. Data points are taken from Table 2.2.

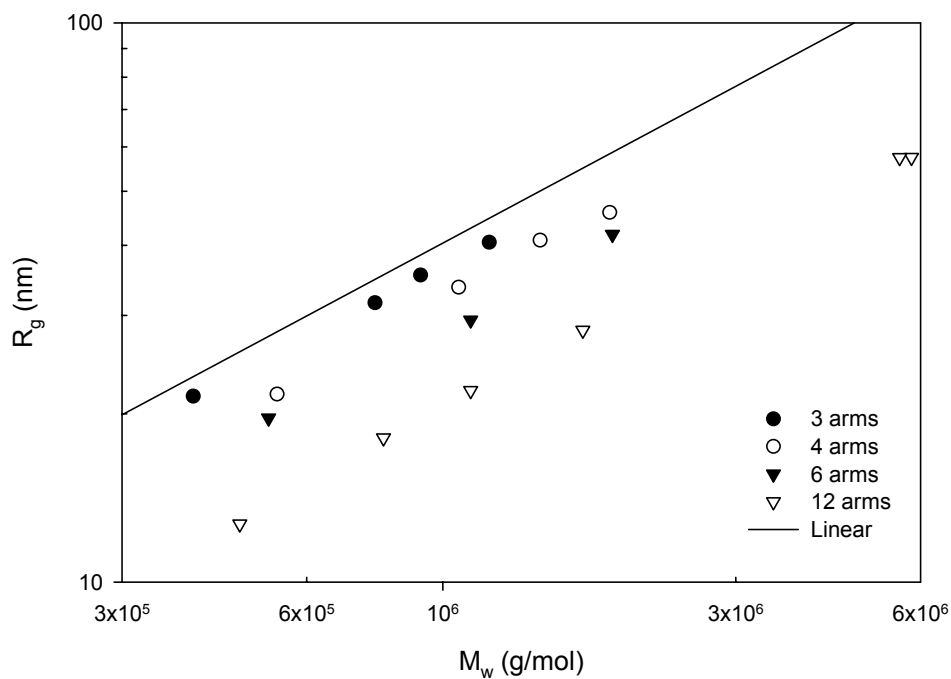


Figure 2.3. Radius of gyration as a function of molecular weight for monodisperse polystyrene stars. Data from ref. (63, 67). Parameters for linear polystyrene from ref. (60).

2.3.1.1.2 Intrinsic viscosity

The increase in viscosity with the addition of a polymer into a solvent is an important property. By measuring the solution viscosity as a function of polymer concentration, useful information about the polymer's molecular properties can be determined. From solution data, the intrinsic viscosity (also known as limiting viscosity number or Staudinger index) can be calculated:

$$[\eta] = \lim_{c \rightarrow 0} \frac{1}{c} \left(\frac{\eta}{\eta_o} - 1 \right) \quad (2.26)$$

where c is the concentration of polymer in solution, η the solution viscosity and η_o the viscosity of the pure solvent. The presence of branching leads to smaller intrinsic viscosity values. Comparable to Equation 2.10, a branching factor can be also defined using the intrinsic viscosity:

$$g' = \frac{[\eta]_{br}}{[\eta]_l} \Big|_M \quad (2.27)$$

Because of the ease in measuring intrinsic viscosity relative to the radius of gyration, considerably more experimental work has reported intrinsic viscosity data for branched molecules. As a result, attempts have been made to relate the two contraction factors. However, the efforts to find an encompassing relationship have not been completely successful. Thurmond and Zimm (76) proposed the following equation:

$$g' = g^\varepsilon \quad (2.28)$$

with a value of 1.5 for ε but found results supporting and opposing the use of such a value for their polystyrene star samples. Zimm and Kilb (77) later came to the numerical conclusion that $\varepsilon = 0.5$ for certain star polymers. For combs, it was found ε varied between the two limits of 1.5 and 0.5 (48, 65). Burchard proposed that the relationship

between the two branching factors could not be adequately described by a simple power law and proposed the following equation for star polymers (37):

$$g' = (a + (1 - a)g^p)g^\varepsilon \quad (2.29)$$

with $a = 1.104$, $p = 7$ and $\varepsilon = 0.906$.

Overall, studies have found that ε varies with experimental conditions and the type of branching. Typically, stars have been found to have the lowest values ($\varepsilon = 0.5$) while combs are the upper limit ($\varepsilon = 1.5$). Results for randomly branched polymers tend to fall somewhere between these limits. However, these are only general trends and upon examination of the results for polyethylene, a variety of values for ε can be shown (see Table 2.3). For randomly branched polystyrene with tetra-branch points, values ranging from 0.5 in cyclohexane to 0.72 in toluene have been found (78). Further work found that styrene copolymerized with divinylbenzene produced polymer with an exponent varying from 0.65 at low conversion to 1.41 at higher conversions (79). Berry and Orofino determined that for their poly(vinyl acetate) combs in benzene, ε varied from 0.5-1.0 while randomly branched poly(vinyl acetate) in benzene exhibited a range of 0.7-0.9 (80). Foster and coworkers also found $\varepsilon = 1$ for randomly branched poly(vinyl acetate) in tetrahydrofuran (81). Values of ε greater than 1.5 have been observed including work with styrene-butadiene graft copolymer where ε was estimated to be 2 (82). An extensive review on the dilute solution properties of star polymers has found that over a large range of functionalities, no constant exponent could be found (83).

Table 2.3. Values of ε for polyethylene.

ε	Conditions	Method	Ref
1.0-1.5	diphenyl at 118°C (theta point)	light scattering and viscosity measurements on fractionated samples to obtain g and g' .	(84)
1.3	decalin at 130°C	light scattering and viscosity measurements on fractionated samples to obtain g and g' .	(85)
1.0±0.3	tetralin at 130°C	light scattering and viscosity measurements	(86)
1.3±0.2	a-chloronaphthalene at 125°C	on fractionated samples to obtain g and g' .	
1.2	autoclave	light scattering and viscosity measurements	(87)
2	tubular reactor tetralin at 120°C	on fractionated samples to obtain g and g' .	
0.8-1	TCB at 135°C	SEC to fractionate sample and then use LS and viscometer to obtain g and g' .	(88)
0.75	TCB at 140°C	SEC with calibration curve and Eqn. 2.22 to calculate average number of branches. This is compared to average number of branches obtained from NMR data and best agreement gives ε .	(81)
0.7-0.9	autoclave	SEC-Visc to determine g' and fractions	(89)
0.9-1	tubular reactor TCB at 135°C	collected from SEC analyzed with MALLS to obtain g .	
0.68- 0.88	TCB at 145°C	SEC-LALLS and NMR data to calculate ε .	(90)
1-1.5	autoclave reactor	SEC-MALLS to calculate g and KMHS	(91)
1.2-1.8	tubular reactor TCB at 140°C	equation with universal calibration to get g' .	
0.2-1.8	TCB at 135°C	SEC-MALLS-Visc to obtain g and g' .	(92)

Notes:

TCB, 1,2,4-trichlorobenzene; SEC, size exclusion chromatography; NMR, nuclear magnetic resonance; LALLS, low-angle laser light scattering; MALLS, multi-angle laser light scattering; Visc, viscometer; KHMS, Kuhn-Mark-Houwink-Sakurada equation.

The intrinsic viscosity in turn can be related to a molecular weight with a power law expression known as the Kuhn-Mark-Houwink-Sakurada (KMHS) equation:

$$[\eta] = K_{[\eta]} M^\alpha \quad (2.30)$$

Similar to the behaviour of R_g - M for stars, the exponent α does not vary with star functionality (see Figure 2.4). However, for randomly branched polymers it is found that α is smaller compared to the exponent for a linear polymer. In fact, α decreases with increasing molecular weight for randomly branched polymers. Due to the nature of branching reactions in randomly branched polymers (e.g., transfer to polymer), the number of branches per macromolecule increases with molecular weight. It is for this reason that α decreases with increasing molecular weight.

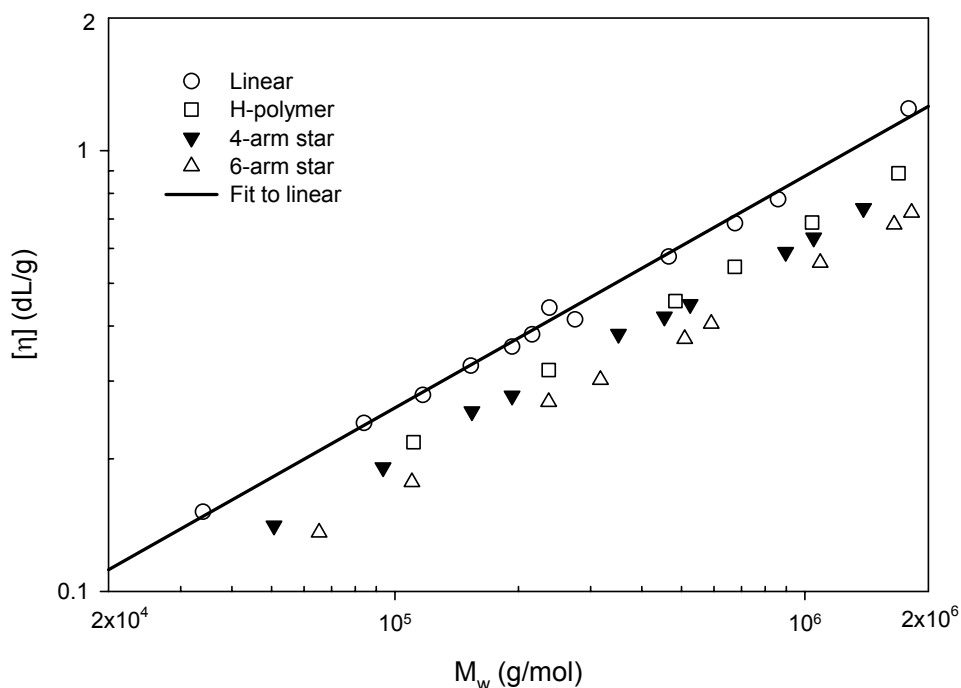


Figure 2.4. Intrinsic viscosity as a function of weight-average molecular weight for branched polystyrenes. Data taken from refs. (93, 94).

2.3.1.1.3 Friction coefficient

The size of a polymer molecule can be represented by other measures aside from the radius of gyration. From sedimentation or diffusion experiments, the translational friction coefficient, F , of a particle can be determined and related to the hydrodynamic radius with the Stokes equation:

$$F = 6\pi\eta_o R_h \quad (2.31)$$

where R_h is a hydrodynamically effective sphere radius. The hydrodynamic radius can also be determined from dynamic light scattering (DLS) experiments where the translational diffusion coefficient is measured and can be related to the friction coefficient of a particle with Einstein's equation:

$$D = \frac{kT}{F} \quad (2.32)$$

where D is the translation diffusion coefficient, T is temperature and k is Boltzmann's constant. Stockmayer and Fixman defined a ratio of hydrodynamic radii of the branched and linear polymers similar to g and g' (31):

$$h = \frac{R_{hbr}}{R_{hl}} \Big|_M \quad (2.33)$$

They found that the segment densities for branched and linear polymers differed even though the two polymers had the same radius of gyration. Therefore, branched and linear polymers with the same radius of gyration will not necessarily have equivalent hydrodynamic properties. Based on their theoretical calculations, Stockmayer and Fixman proposed that for star polymers (31):

$$g' = h^3 \quad (2.34)$$

Calculations for other types of branching structures (uniform and randomly distributed stars, combs and randomly branched structures) led to the following limits for h (48):

$$1 \leq \frac{h}{g^{1/2}} \leq 1.39 \quad (2.35)$$

2.3.1.1.4 Second virial coefficient

Two types of interactions between particles need to be considered in dilute polymer solutions: thermodynamic and hydrodynamic interactions. The first arises from repulsion or attraction of particles while the second is due to the distortion of laminar flow by the particles. Thermodynamic interactions can be measured independently of hydrodynamic interactions by static light scattering or osmotic pressure measurements. For static light scattering:

$$\frac{Kc}{R_0} = \frac{1}{M_w} + 2A_2c \quad (2.36)$$

where K is a constant, R_0 the normalized scattering intensity (Rayleigh ratio) at zero angle, M_w the weight-average molecular weight, and A_2 the second virial coefficient. A_2 can also be obtained from osmometry data from:

$$\frac{\pi}{RTc} = \frac{1}{M_n} + A_2c \quad (2.37)$$

where π is the osmotic pressure, M_n the number-average molecular weight, and R the ideal gas constant. The second virial coefficient is a measure of the thermodynamic quality of the solvent; the higher the A_2 , the better the solvent. According to Flory, the θ point is characterized by a value of $A_2 = 0$ (44). The second virial coefficient has been well studied for linear flexible chains. Qualitatively, the effect of branching produces a decrease in the second virial coefficient.

A_2 can be related to molecular weight according to the following:

$$A_2 = K_{A_2} M^{-\beta} \quad (2.38)$$

where K_{A_2} and β are constants. For linear polymers, β ranges from 0.15 to 0.35 while for randomly branched molecules, the second virial coefficient decreases much more rapidly with molecular weight. Exponents of 0.55 to 0.8 have been found for randomly branched polymers. Similar to the drastic change in v (see Equation 2.11), the significant difference between β values for linear and branched molecules has been explained with fractal behaviour (37). As branching influences the second virial coefficient, it is also found that the temperature at which A_2 is zero (T_θ) is lower for branched polymers (67-70, 95-98).

2.3.1.2 Molecular Weight and Molecular Weight Distribution

The effect of branching on molecular weight and molecular weight distribution (MWD) is found to depend upon the type/nature of the branching reaction. Random branching reactions such as transfer reactions in free radical polymerization lead to increases in molecular weight and a broadening of the MWD. However, the addition of a polyfunctional monomer or initiator to the polymerization may narrow the molecular weight distribution.

Various mathematical modeling methods have been used to derive the molecular weight averages and the molecular weight distribution for randomly branched polymers. Some of the earliest work concerning the influence of branching on MWD was performed with statistical methods. Schulz derived approximate relationships for the MWD in polymers with a fixed number of chains of random length (99). The following expression was obtained for the instantaneous molecular weight distribution:

$$w(x) = \left[\frac{x(x+f-2)!}{(f-1)!(x-1)!} \right] \left[\frac{(1-p)^{f+1}}{fp+1-p} \right] p^{x-1} \quad (2.39)$$

where $w(x)$ is the weight fraction of chains with a degree of polymerization of x and p is the probability that a functional group has reacted ($p \rightarrow 1$ as the coupling tends towards

completion). The original work was intended for polymers produced during free radical polymerization; however, this type of polymerization leads to random branching and the results could not be applied to these particular polymers. Schaeffgen and Flory did realize that the results could be applied to the coupling of f arms having a most probable distribution (100). Both groups found that as the extent of reaction reached completion the polydispersity could be approximated by:

$$PDI = \frac{M_w}{M_n} = 1 + \frac{1}{f} \quad (2.40)$$

Equations 2.39 and 2.40 are valid for f coupled linear chains having a most probable distribution. In the case of randomly branched polymers, Stockmayer (1943) and Flory (1946) developed instantaneous distributions for the post-gelation of polyfunctional condensations (101, 102):

$$w(x) = \frac{(1-\alpha)^2}{\alpha} f \frac{(fx-x)!}{(x-1)!(fx-2x+2)!} \beta^x \quad (2.41)$$

where $\beta = \alpha(1-\alpha)^{f-2}$ and α is the fraction of unreacted functional groups (also can be thought of as the probability of a functional group reacting or the extent of reaction). An important result of their work is that with random branching, the polydispersity increases roughly linearly with the weight-average molecular weight.

Using Flory's idea of an extent of reaction, Gordon (1962) adapted the cascade approach (based on stochastic process theory) to model branched polymers and several studies have thus employed the cascade approach (103-107). However, Tobita and Hatanaka have noted that this method is not applicable to polymers produced by free radical polymerization (108). The Flory-Stockmayer approach assumes that the probability α is independent of chain size and that excluded volume effects could be neglected. In order to avoid such approximations, other statistical techniques have been employed. Simulations of branching processes on a lattice were used with bond percolation to derive

the molecular weight distribution of branched chains. The method involved placing x units on a lattice with N^3 sites where a bond is formed if two units lie on adjacent lattices. Studies have examined the differences between the Flory-Stockmayer, cascade and percolation approaches (37, 109-112).

Recently, Zhu and coworkers have derived analytical expressions for the MWD of star polymers based on the statistical connection of pre-formed chains onto cores. The model was also found to apply for core-first methods for the formation of stars and included the effect of star degradation on average molecular weights (113). In the case of polyolefins, a bivariate distribution for chain length and branching has also been developed for polymers produced with single-site coordination catalysts. The model assumes that long-chain branching is the result of macromonomer insertion where the macromonomer is formed due to β -hydride elimination or transfer to ethylene (114).

The main drawback of the previous statistical approaches is that they are static theories providing instantaneous distributions that do not account for the growth rate of chains. Although instantaneous distributions can be altered to account for non-steady state conditions (115), methods employing population balances are more commonly used for these instances. For this particular technique, a reaction scheme is proposed and population balances for each species in the reaction mixture are developed. Early studies calculating the effects of branching on the molecular weight distribution from kinetic models include those of Beasley (1953), and Bamford and Tompa (1954) (116, 117). They derived branching and molecular weight distribution functions for free radical polymerization when long-chain branching is due to transfer to polymer. The former developed equations for a stirred tank reactor and assumed monomer and polymer concentrations were constant. In the case of the latter, Laplace transforms were employed to solve the kinetic equations of a batch reactor with time dependent concentrations. Based on this early work, groups have expanded the model's complexity to include further reactions in the polymerization mechanism, unsteady-state kinetics and various reactor configurations (118-122).

Through the use of population balances the molecular weight and branching distributions of various branching processes have been derived. Expressions for the MWD of stars formed during the polycondensation of monomers with the addition of a multifunctional compound have been developed (123). Analytical equations have also been derived to predict the branching and molecular weight distributions for comb polymers formed by the copolymerization with a macromonomer (124). Müller and coworkers developed batch and semi-batch models for the molecular weight and branching distribution for hyperbranched polymers produced by self-condensing vinyl polymerization with the addition of a multifunctional molecule (125, 126). Results found that during a batch reaction, the narrowing of the MWD was proportional to $1/f^2$ and that in the case of a semi-batch process, Equation 2.40 was obtained.

Recently, groups have used numerical fractionation techniques to help derive branching and molecular weight distributions. In this approach, a broad and complex distribution is divided into a series of narrow distributions. This allows for a difficult problem to be separated into several smaller problems that are easier to solve. In the case of branched polymers, chains with the same number of branches per molecule are separated into classes (127-129).

Another statistical method for the determination of the full MWD of branched polymers is the Monte Carlo approach. The technique estimates possible outcomes from a set of random variables by simulating the growth of a polymer chain a large number of times. A reaction mechanism is proposed and the probabilities of possible outcomes are related to the rate constants. A considerable amount of information about the polymer molecules can be obtained with this method as the chains are individually built during the simulation. The group of Tobita has used Monte Carlo simulations extensively to model various branching reactions including cross-linking copolymerization (130-133); random cross-linking and degradation (134, 135); free radical polymerization with long-chain branching due to transfer reactions and terminal double bond polymerization (108, 136-140); use of a polyfunctional chain transfer agent in free radical polymerization (141, 142); and copolymerization with a monomer having a high chain transfer constant (143,

144). Beigzadeh and coworkers have also used Monte Carlo simulations for the modeling of branching in polyolefins (145).

2.3.1.3 Rheological Properties

Rheological properties of polymers are highly sensitive to macromolecular structure. In some cases, the incorporation of minute amounts of branching can alter the flow properties of a polymer even though the dilute solution properties are unchanged. The rheological behaviour of branched polymers is influenced by a variety of factors including the number, location, architecture and length of branches (40). Similar to dilute solution properties, the differences between the viscoelastic behaviour of linear and branched polymers can be masked by large polydispersities.

There has been a considerable amount of research on the rheological properties of polymers with uniform model structures such as stars and combs with narrow molecular weight distributions. These studies provide insight into the effects of branching. The presence of branching has two opposing effects. Firstly, branching is known to decrease the size of polymer molecules compared to a linear chain of identical molecular weight. In such a case, a smaller size will result in fewer chain entanglements. Secondly, when the branch lengths reach a critical molecular weight, they become long enough to become entangled and the overall number of entanglements has increased. It is because of these two opposing effects that the impact of branching on rheological properties is highly dependent upon the nature of branching present in the polymer.

2.3.1.3.1 Zero-shear properties

The zero-shear viscoelastic properties of concentrated polymer solutions or polymer melts are typically defined by two parameters: the zero-shear viscosity (η_0) and the zero-shear recovery compliance (J_e^0). The former is a measure of the dissipation of energy while the latter is a measure of energy storage. For model polymers, the influence of branching is best established for the zero-shear viscosity. When the branch length is short or the concentration of polymer is low (i.e., for solution rheology), it is found that

the zero-shear viscosity of the branched polymer is lower than that of the linear. This has been attributed to the smaller mean-square radius of the branched chains and has led to the following relation (146-148):

$$\eta_{0br} = g^a \eta_{0l} \quad \begin{cases} a = 1 & \text{when } M < M_c \\ a = 3.4 & \text{when } M > M_c \end{cases} \quad (2.42)$$

where g is the ratio of mean-square radii of the branched and linear polymers of identical molecular weight in the unperturbed state and M_c is a critical molecular weight where the exponent in Equation 2.42 changes from 1 (unentangled linear polymers) to 3.4 (entangled linear polymers). Experimental evidence of a smaller zero-shear viscosity for branched polymers has been shown for a variety of polymer architectures such as stars (93, 149), combs (150, 151) and randomly branched polymers (152). In some cases, the reduction in zero-shear viscosity has been observed at higher polymer concentrations (149) and even in the melt state (40).

In certain cases the behaviour of branched polymers cannot be described by Equation 2.42. These situations can arise for higher molecular weights, higher polymer concentrations, longer branch lengths or longer spacing between branch points (i.e., situations where branching can increase the number of chain entanglements). For these conditions, it has been found that the zero-shear viscosity of the branched polymer can be considerably higher than that of the linear. This viscosity enhancement has been detected for several polymers of varying branching structure such as randomly branched polybutadiene (153); randomly branched poly(vinyl acetate) (154); star poly(α -methylstyrene) (155); comb polystyrene (155, 156); H-shaped polystyrene (94); star polyethylene (157); comb, regular and irregular stars, H-shaped, and pom-pom polyethylene (158); and star polyisoprene (149, 159). Figure 2.5 shows the behaviour of the zero-shear viscosity versus molecular weight for a series of H-shaped polystyrenes. At low molecular weights and hence smaller branch lengths, there is a viscosity reduction while at higher molecular weights, there is a viscosity enhancement.

In order to understand this viscosity enhancement it is easier to start with the theory for linear polymers. The behaviour of linear polymers can be described by the reptation model introduced by Edwards (160) and extended by de Gennes (161, 162), and Doi and Edwards (163). For a linear polymer of high molecular weight in the melt, chains can be modeled as a confined tube where the diffusion of the chain is restricted along the tube contour. Entanglements form between chains where the reptation of a chain along its contour becomes the dominant mode of movement. The addition of a branch point prevents reptation and other forms of movement must occur in order for the chain to change its configuration. In the case of a star polymer, the arms retract partway down its contour tube and then move outwards along a different trajectory (163). This process is slow relative to that of linear polymers and is influenced by the branching length. For longer branches, there are a higher number of entanglements per branch leading to a higher zero-shear viscosity. In the case of star polymers, it has been found that the viscosity increases exponentially with arm molecular weight (159, 162-164) and that the effect of functionality is no longer significant above $f > 4$ (i.e., total star molecular weight does not influence viscosity, only arm molecular weight) (159). For star polymers the exponential dependence of zero-shear viscosity on the number of entanglements per arm is given by (159, 165):

$$\eta_0 \propto \left(\frac{M_a}{M_e} \right)^{1/2} \exp \left(v' \frac{M_a}{M_e} \right) \quad (2.43)$$

where M_a is the arm molecular weight, M_e is the molecular weight between entanglements and v' is a constant. In order to properly describe the dynamics of branched melts, other effects aside from arm retraction that were not included in the original treatment of linear polymers such as contour length fluctuations and dynamic tube dilation are important (164, 166). In the case of comb and H-shaped polymers, the length of branches is not the only factor as it has been found that the length between branch points is a significant variable (150, 167).

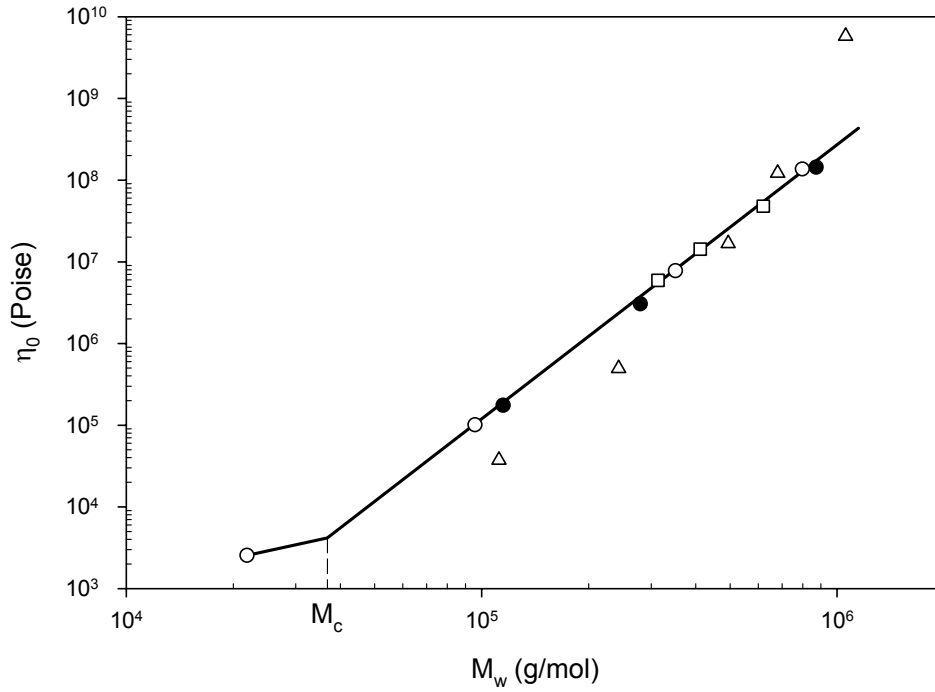


Figure 2.5. Zero-shear viscosity at 169.5°C as a function of weight-average molecular weight for polystyrene melts: open and closed circles and squares, linear; triangles, H-polymers. Data from ref. (94).

The zero-shear recovery compliance is another viscoelastic property of polymers that is noticeably influenced by the presence of branching and similar to viscosity, the effect of branching is dependent upon several factors including polymer concentration and molecular weight. In dilute solutions, J_e^0 is expected to decrease with branching according to (146):

$$J_e^0 = \frac{2g_2M}{5cRT} \quad (2.44)$$

where c is the concentration of polymer and g_2 defined as follows:

$$g_2 = \left[\frac{\langle s^4 \rangle - \langle s^2 \rangle^2}{\langle s^2 \rangle^2} \right]_{br} / \left[\frac{\langle s^4 \rangle - \langle s^2 \rangle^2}{\langle s^2 \rangle^2} \right]_{l,M} \quad (2.45)$$

Similar to other branching factors, g_2 is unity for linear polymers and less than one for branched polymers. Equations for the determination of g_2 for certain branching structures have been determined including those for uniform stars and combs (168). This reduction in J_e^0 has been observed for low molecular weight star polymers at low and high concentrations and with high molecular weight stars at low concentrations (149). However, in most instances, J_e^0 is much larger for branched polymers compared to a linear polymer of similar molecular weight (94, 149, 151-154, 169) and Equation 2.44 does not accurately predict the behaviour of a branched polymer. Based on the theory used to derive Equation 2.43, a similar relationship for the zero-shear compliance and molecular weight of star polymers was expressed as follows:

$$J_e^0 = v' \frac{M_a}{M_e} \frac{1}{G_N^0} \quad (2.46)$$

where G_N^0 is the plateau modulus which has been found to be independent of branching (169). As well, the enhancement of η_0 and J_e^0 does not necessarily coincide at the same polymer concentration and some polymers (e.g., polystyrene) are less prone to enhancement than others (40).

2.3.1.3.2 Shear rate dependency

Knowing that branching influences the zero-shear viscosity, it would be expected to have an impact on the dependency of shear viscosity with shear rate. The characteristic shear rate ($\dot{\gamma}_0$) has been defined as the point at which the viscosity has dropped to 80% of η_0 and provides an indication of the onset of non-Newtonian flow (i.e., shear thinning behaviour). Depending upon a branched polymer's structure, smaller and larger values of the characteristic shear rate have been observed. For linear polymers the following relation was determined (170):

$$\eta_0 J_e^0 \dot{\gamma}_0 = 0.6 \pm 0.2 \quad (2.47)$$

This relationship has also been found to hold for branched polymers (149). The effect of branching can either increase or decrease both η_0 and J_e^0 and the influence on $\dot{\gamma}_0$ can be seen from Equation 2.47. For the cases where branching leads to less entanglements (e.g., higher branching densities, shorter branches), η_0 and J_e^0 can be reduced and higher characteristic shear rates are observed. However, when there is enhancement of the zero-shear viscosity and recovery compliance, the dependency of viscosity on shear rate occurs at much lower values of $\dot{\gamma}_0$ (149). The degree of shear thinning is also influenced by the presence of branching. In general, for those cases where a lower zero-shear viscosity and a higher characteristic shear rate are observed, less shear thinning is observed (41). Higher degrees of shear thinning are found for polymers with viscosity enhancement and lower values of $\dot{\gamma}_0$ (149, 158, 171).

2.3.1.3.3 Thermorheological behaviour

For most polymers, the temperature dependence of viscoelastic properties can be accounted using the principles of Time-Temperature Superposition (TTS), the results of which are that time (a_T) and modulus (b_T) shift factors may be used to superimpose data at various temperatures to generate a single curve:

$$\eta_0(T) = a_T(T) b_T(T) \eta_0(T_0) \quad (2.48)$$

$$G_N^0(T) = b_T(T) G_N^0(T_0) \quad (2.49)$$

where T_0 is a reference temperature. Materials that exhibit this behaviour where curves at multiple temperatures may be superimposed to generate a master curve are said to be thermorheologically simple. In such cases, the activation energy may be determined by an Arrhenius equation:

$$a_T = \exp\left[\frac{E_a}{R}\left(\frac{1}{T} - \frac{1}{T_0}\right)\right] \quad (2.50)$$

The activation energy, E_a , for viscous flow is influenced by several factors including chain flexibility, intermolecular interactions and short-chain branching. Polymer chains that are highly flexible tend to have lower values of the activation energy while the incorporation of short branches increases E_a (172). However, the effect of long-chain branching on the activation energy is not completely understood. Some studies have found that E_a increases with the presence of long-chain branching (173) while others have declared that there is no trend (174, 175).

Another difficulty with the thermorheological behaviour of branched polymers is that in some cases the principles of TTS are no longer valid and curves at varying temperatures cannot be superimposed with only one time shift factor per temperature (174-177). It is still not well understood why some branched polymers are thermorheologically complex while others are not. Polystyrene (169), polybutadiene (178) and polyisoprene (179) stars have been found to be thermorheologically simple while stars of polyethylene have not (157).

2.3.1.3.4 Extensional flow

Although not as well studied as shear flow, branched polymer melts in extensional flow have shown differing behaviour compared to linear polymers. It has been found that the presence of long-chain branching in polymers may lead to strain hardening behaviour in elongational flow (180-185). Strain hardening is found when comparing the stress in start-up flow to the results predicted by the theory of linear viscoelasticity (186). If the stress rises above that predicted by theory, the material is said to be strain hardening. For either very small or slow deformations, the theory of linear viscoelasticity predicts the following:

$$\lim_{\dot{\epsilon} \rightarrow 0} \eta_E^+(t, \dot{\epsilon}) = 3\eta^+(t) \quad (2.51)$$

where $\eta_E^+(t, \dot{\epsilon})$ is the tensile stress growth coefficient that is measured at the start-up of simple extension, $\eta^+(t)$ is the shear growth coefficient and $\dot{\epsilon}$ is the Hencky strain rate. Thus plots of $\eta_E^+(t, \dot{\epsilon})$ divided by $3\eta^+(t)$ as a function of time can provide an indication of strain hardening where values above unity are evidence of such an effect.

2.3.1.3.5 Non-linear viscoelasticity

The non-linear viscoelastic properties of branched polymers are not as well investigated as those of the linear regime. Early studies found that the shear history of branched polymers influences their rheology in a manner different from linear polymers (187-190). After extensive shearing, it was found that branched polymers required much longer relaxation times to recover. A possible reason for this behaviour is that high shear will destroy the entanglements in branched polymers responsible for the enhanced viscosity and elasticity. Because these entanglements are slow to come apart it is reasonable to assume that they would be slow to form (186). Studies have also examined the impact of branching on the strain dependence of rheological functions. A weaker dependency of the damping function on strain has been found for branched polymers, both experimentally (184, 191, 192) and theoretically (193, 194). The application of the Cox-Merz rule for branched polymers has also been investigated. The Cox-Merz rule relates nonlinear and linear viscoelastic data and can be expressed as follows:

$$\eta(\dot{\gamma}) = |\eta^*(\omega)| \quad (2.52)$$

where $\eta(\dot{\gamma})$ is the shear viscosity obtained as a function of shear rate and $|\eta^*(\omega)|$ is the complex viscosity as a function of frequency. Some studies have found that the rule does not apply to branched polymers (182, 195) while others have confirmed its validity for polymers with branching (196).

2.3.2 Detection of Long-Chain Branching

For the most part, detection of long-chain branching relies upon indirect methods that compare the properties of a branched polymer to the corresponding linear polymer. However, spectroscopic or chemical methods can quantitatively determine the number of branches or end groups without needing a linear reference. The results from different techniques typically do not agree as each technique has a different criterion as to how long a branch must be in order to be considered “long”. Long-chain branches are usually defined as being comparable in length to the main chain. Using polyethylene as an example, it has been found that size exclusion chromatography (SEC) can detect a minimum length for a straight chain alkane branch somewhere between six and twelve carbons (90, 197). It is generally accepted that six carbons or longer can be detected by ^{13}C nuclear magnetic resonance (NMR) spectroscopy (198-200). In the case of rheology, a definite length is not completely established. It has been proposed that the length of a LCB corresponds to the critical entanglement molecular weight (200). For polyethylene, this equates to 270 carbon atoms or greater (reported values of M_c vary from 2100 to 5200 (41)). Other sources have found that branches longer than twice the molecular weight between entanglements are considered long in rheological terms (201). In the case of polyethylene, this corresponds to 180 carbon atoms in length. Due to this variability in the methods of detecting LCB, agreement between techniques can be considered fortuitous.

2.3.2.1 Spectroscopic Methods

Spectroscopic methods rely on the chemical difference between end groups or branch points in a polymer. In the case of polyethylene, the most common spectroscopic technique for determining long-chain branching has been nuclear magnetic resonance spectroscopy. Using ^{13}C -NMR, branches of 1 to 5 carbon atoms can be distinguished while a 6 carbon atom branch produces the same spectral pattern as any subsequent branch of greater length (199). Peak assignments for various chemical shifts in polyethylene have been well documented (202, 203). Figure 2.6 is a typical ^{13}C -NMR spectrum of polyethylene showing the various peak assignments (204). Recent studies

employing NMR have reported long-chain branching as low as 0.2 branches per 10 000 carbon atoms in polyethylene (204-206). Although NMR is seen as an absolute technique for determining LCB in polyethylene, studies have found limitations when compared to methods utilizing rheological measurements. A series of commercial high-density polyethylenes (HDPE) with similar molecular weight and molecular weight distributions were found to have large and systematic increases in zero-shear viscosity which were attributed to long-chain branching (200). However, the number of branches determined with NMR showed random scatter. In the same study, it was found that NMR could not detect the presence of long-chain branching in peroxide modified high-density polyethylene nor could it identify LCB in multiple pass extruded HDPE. In both cases, samples showed large changes in their rheological behaviour relative to the unmodified samples.

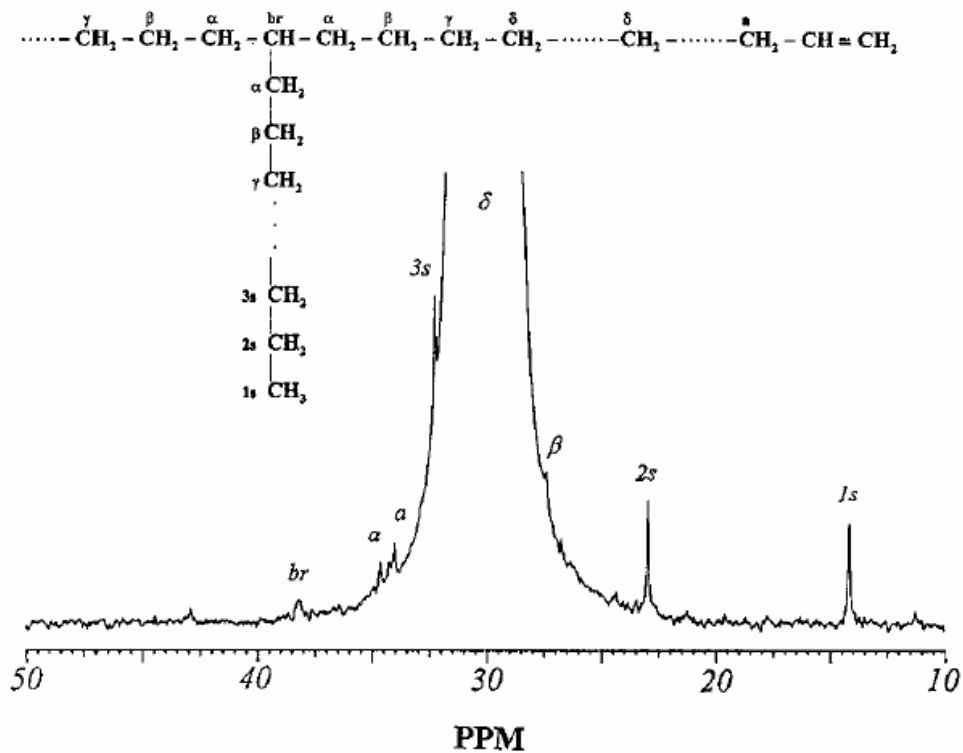


Figure 2.6. ^{13}C -NMR spectrum of polyethylene sample measured at 120°C using deuterium o-dichlorobenzene and 1,2,4-trichlorobenzene as solvents. Taken from ref. (204)

The determination of branching is sometimes possible through the use of mass spectroscopic (MS) techniques. For the case of polydisperse polymers, separation of the polymer into monodisperse fractions must be performed prior to analysis. The fractions are then analyzed by matrix-assisted laser desorption/ionization time of flight mass spectrometry (MALDI-TOF MS) and branching can be determined by analysis of end groups or branch points (207).

2.3.2.2 Chromatographic Methods

Introduced in 1964 (208), size exclusion chromatography (SEC), also known as gel permeation chromatography (GPC), has developed into one of the most popular and convenient methods for polymer characterization (209). Using size exclusion chromatography, a mixture of polymer molecules of varying size passes through a column packed with porous particles, where the molecules that are too large to penetrate the pores elute first. Thus SEC separates polymer molecules based upon their size in dilute solution; however, the choice of an appropriate size has been debated by several workers (210). Grubisic and coworkers proposed that SEC separates polymer molecules, regardless of chemical composition and large-scale structure, according to a hydrodynamic volume, V_H (211). Based on the Flory-Fox equation (212), they found this hydrodynamic volume to be proportional to the product of intrinsic viscosity and molecular weight:

$$V_H \propto [\eta]M \quad (2.53)$$

The excellent correlation between hydrodynamic volume and $([\eta]M)$ has become the basis of the universal calibration curve (UCC) for polymers. Although other size parameters, namely those dependent on R_g , have been suggested, the applicability of UCC has recently been verified for a variety of polymers including those with a high chemical and molecular weight asymmetry (e.g., miktoarm stars where arms are of different composition) (213).

Methods for determining long-chain branching in polymers through the use of SEC depend upon the type of detectors employed and thus, the type of information collected. For conventional SEC equipped with only a concentration detector, a calibration curve is constructed where molecular weight is a function of elution volume. For a linear and branched macromolecule of the same molecular weight, it is known that the branched macromolecule will have a smaller intrinsic viscosity ($[\eta]_{br} < [\eta]_l$) and as a result, it will elute later than the linear macromolecule. Because of this, SEC with only a concentration detector will underpredict the molecular weight of branched polymer. Using the KMHS relation for the linear polymer, two branching ratios can be defined for SEC (88):

$$g'_{[\eta]} = \left(\frac{[\eta]_{br}}{[\eta]^*} \right)^{\alpha+1} \quad (2.54)$$

$$g'_M = \left(\frac{M^*}{M_{br}} \right)^{\alpha+1} \quad (2.55)$$

where $[\eta]^*$ and M^* are the intrinsic viscosities and molecular weight of linear molecules leaving the column at the same elution volume as the branched molecules having intrinsic viscosity and molecular weight of $[\eta]_{br}$ and M_{br} . Several workers have applied an iterative method in order to derive the branching density (λ) based on SEC chromatograms (214-217). Assuming a value of λ , the number of branches are calculated as a function of molecular weight ($n = \lambda M$) and using the appropriate equation, g can be determined for each molecular weight (see Table 2.1). Then assuming a value for ε , g' and then $[\eta]_{br}$ can be calculated for each elution volume. The total intrinsic viscosity can be determined as a weighted sum of the individual elution volumes. This total intrinsic viscosity calculated from SEC data can be compared to the measured value. The process is repeated by changing λ until the two values agree. Problems with this method arise from the various assumptions made including constant values of λ and ε . Several studies have found that the branching density varies with molecular weight for a particular sample and a constant value of ε cannot be assumed (79, 83, 92). Another problem lies in the fact that theoretical equations for g are for chains in an unperturbed state, best

represented by a θ solvent and temperature. SEC measurements are typically made in good solvents. For these reasons, values of the branching density based on this method are only valid for relative comparisons.

Most SEC studies of branching employ at least one other detector aside from a concentration detector. In the past, the most common additional detector for measuring long-chain branching was an online viscometer (218-222). By using UCC and a viscometer, both molecular weight and intrinsic viscosity distributions can be determined for a polymer sample. Low-angle light scattering detectors with UCC have also been employed for the determination of molecular weight and intrinsic viscosity distributions and in turn, the detection of long-chain branching (81, 223-225). However, the use of a viscometer has been found to be more appropriate for studying branched polymers (226, 227). If a branched sample has a distribution in the extent or type of branching, the fractionation with SEC will not be complete. It is possible for two polymer molecules, one more branched than the other, to have the same hydrodynamic volume ($[\eta]M$) and coelute. The more highly branched chain will have a smaller intrinsic viscosity but it may also have a higher molecular weight. In this case, the detector cells do not contain monodisperse fractions and the results from the detectors at each elution volume are average results. Light scattering is known to provide a weight-average molecular weight estimate and from the work of Hamielec and Ouano (228), it was determined that UCC provides the number-average molecular weight for polymer molecules of the same hydrodynamic volume but differing molecular weight.

With the intrinsic viscosity distributions obtained either from a viscometer or light scattering detector, previous studies have attempted to quantitatively determine the amount of long-chain branching. First, g' was related to g using an assumed value of ε and the appropriate equation from Table 2.1 was used to calculate the number of branches per molecule. However, due to the assumptions involved, it is more appropriate to determine the level of branching in a more qualitative manner. From the molecular weight and intrinsic viscosity data collected, a KMHS plot can be constructed for each polymer sample and comparisons can be made to the linear polymer. Figure 2.7 shows

an example of a KMHS plot for branched polystyrene compared to a linear sample obtained using SEC. As the level of branching increases, the $[\eta]$ - M relationship can no longer be expressed as a linear relation in a log-log plot. Therefore, deviations from the KMHS plot for a linear sample are an indication of branching with more curvature being an indication of higher levels of branching.

The introduction of commercial LALLS detectors for SEC in the seventies was followed by multi-angle laser light scattering detectors in the eighties (229). Coupled with SEC, a MALLS detector allows for the determination of the radius of gyration as a function of molecular weight for a polymer sample. In plots of R_g - M , the presence of branching is detected by lower trends for branched polymers compared to a linear sample (see Figure 2.7). The use of MALLS also allows for the determination of g directly and the branching density can be determined from a suitable equation in Table 2.1. Most studies now involve the combination of three detectors in the analysis of branched polymers (92, 230-237). Mourey, Balke and coworkers have reported on a unique method to analyze branched polymers with triple detector SEC (233, 238-241). Because light scattering reports a weight-average molecular weight and viscometry with UCC provides an estimate of the number-average molecular weight, it is possible to determine the local polydispersity for each elution volume. However, significant molecular weight heterogeneity is needed between the types of branched macromolecules in order to detect any local polydispersity (241).

Due to the difficulties of SEC to resolve branched polymers other chromatographic techniques such as field-flow fractionation (FFF) and interaction chromatography (IC) have been employed for the analysis of branching. Originally developed in the late 1960's, field-flow fractionation is seen as a relatively new technique as commercial units were not available until the beginning of the nineties (242, 243). In FFF, the columns are replaced by a channel containing no stationary phase or packing. Retention and separation in the channel is achieved by the action of an externally generated field, applied perpendicularly to flow (243). Although FFF has several advantages including a separation range of 5 nm ($\sim 10^3$ g/mol) to 100 μ m, its use is definitely not as widespread

as SEC (244). This is partially because there is no set method for the analysis of a particular sample. One must choose the appropriate subtechnique (i.e., what type of external field to employ) and the proper experimental variables. Nevertheless, there are studies where FFF has been used in the analysis of branched polymers (245-247). In particular, one study has found that the retardation in the elution of highly branched polymers during SEC could be avoided by using thermal FFF (247).

Temperature-gradient interaction chromatography (TGIC) is another technique used for the characterization of polymers (248-250). Unlike SEC which relies on an entropic separation, TGIC utilizes the enthalpic interaction between polymer segments and the stationary phase to separate polymer molecules. While SEC separates molecules based on hydrodynamic size, retention in TGIC is mainly determined by molecular weight and not as much by chain architecture (250). This technique has been useful in the characterization of model branched systems where a higher number of branches greatly increases the molecular weight but the increase in size is not as large (251-256). This is especially the case for star polymers of uniform arms. As of yet, IC methods have not been used for the characterization of randomly branched polymers.

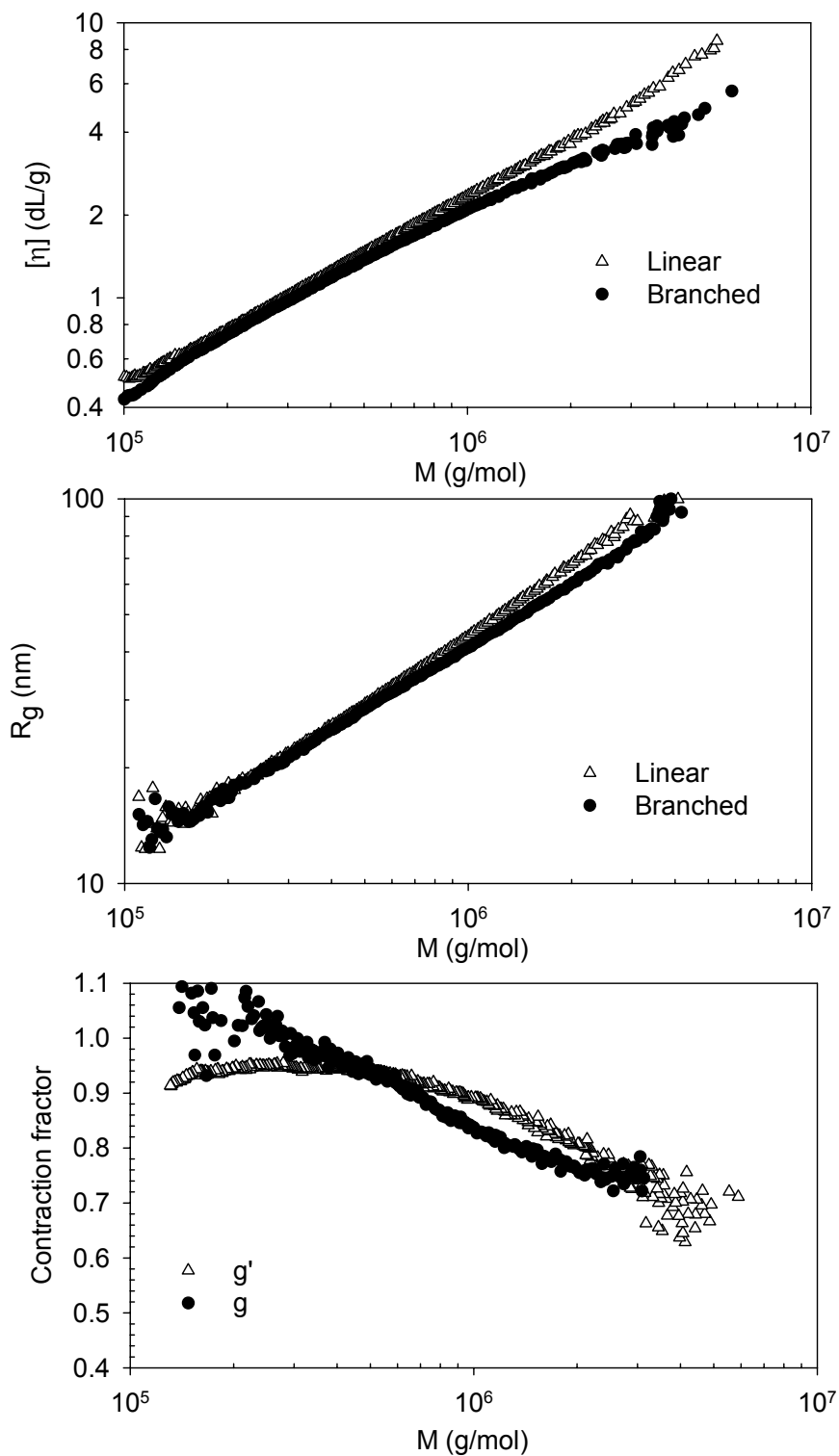


Figure 2.7. Intrinsic viscosity, radius of gyration and contraction factors as a function of molecular weight for polystyrene (SEC at 30°C with 1.0 mL/min of tetrahydrofuran). Ref. (257).

2.3.2.3 Rheological Methods

The flow behaviour of polymers is extremely sensitive to large-scale architecture. As such, techniques that rely on rheology are much more sensitive to the presence of long-chain branching than dilute solution, chromatographic and spectroscopic methods (40, 200). However, the theoretical understanding of the rheology of branched polymers is not fully developed and in most cases, a quantitative analysis of branching is not possible. The other issue with rheological methods is that polydispersity affects rheological properties in the same manner as branching and hence, discrimination of the two effects can be difficult.

The most common rheological method is to compare the zero-shear viscosity of the branched polymer to that of the linear. It is well established that for linear polymers above the critical molecular weight for entanglement, zero-shear viscosity scales with a molecular weight to a power of 3.4. For the most part, η_0 is independent of the molecular weight distribution (186, 258) as long as there is no significant fraction of low molecular weight material below the entanglement threshold (258). Thus deviation from the power law for linear samples implies the presence of branching. Whether there is a reduction or enhancement of zero-shear viscosity depends upon polymer molecular weight and branching characteristics (number, length, and architecture). Gabriel and Münstedt (2002) completed a study on the long-chain branching in polyethylene where reduction and enhancement was observed in various samples (258). For highly branched low-density polyethylene (LDPE), a reduction in zero-shear viscosity was observed as high branching densities (i.e., a high number of branches of relatively short length) led to a lower radius of gyration and less entanglements. However, for metallocene-catalyzed polyethylenes with very low levels of long-chain branching, a significant increase in η_0 was observed and attributed to a higher number of entanglements from longer branches.

Recently, a model has been proposed for the relationship between zero-shear viscosity and weight-average molecular weight to also account for the effect of branching (259-261). Although the model has limitations and uncertainties in some parameters, it was found to predict the reduction and enhancement in the η_0 - M behaviour of branched

polyesters and branched polyethylenes. Colby and coworkers attribute an increase in η_0 to cases where the molecular weight between branch points is much larger than the entanglement molecular weight, while decreases in η_0 are found in polymers with high branching densities where the molecular weight between branch points is small (261). The main limitation of the model is to account for varying types of branching within a polymer sample. Figure 2.8 illustrates how the number of branches per chain can influence the zero-shear viscosity based upon this model.

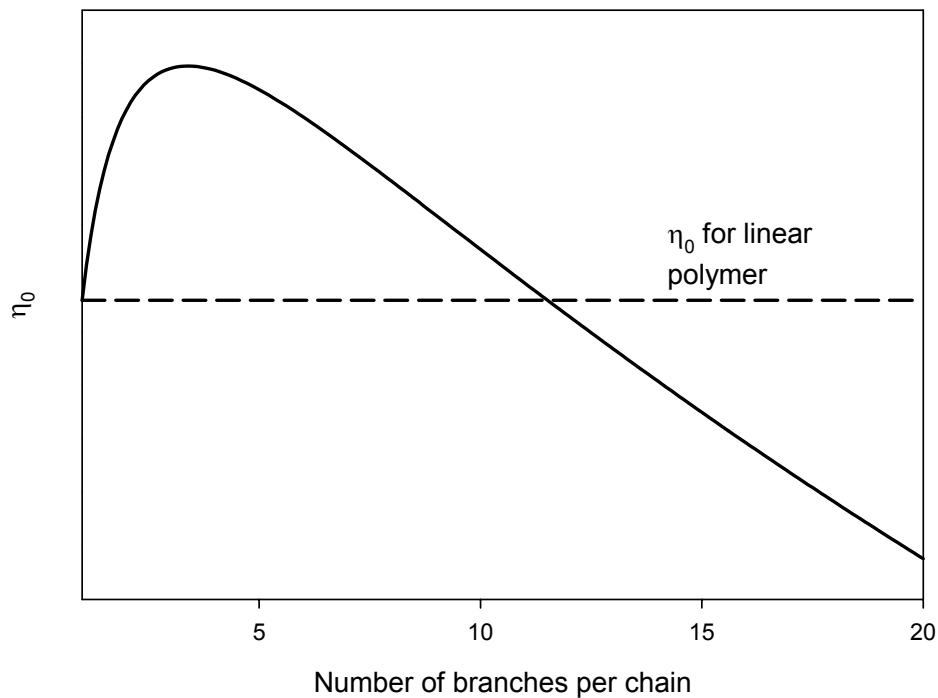


Figure 2.8. Zero-shear viscosity as a function of the number of branches per chain for polyethylene of a constant molecular weight, based on the model of Janzen and Colby (261).

Unlike the zero-shear viscosity, the zero-shear compliance is significantly influenced by the molecular weight distribution, particularly the high molecular weight fractions. For linear polymers, increases in polydispersity correspond to an increase in elasticity (increase in J_e^0). In the case of branched polymers, the zero-shear compliance can experience a reduction or enhancement depending on a number of factors including molecular weight; number, length and type of branching; and molecular weight between

branch points. Fewer studies rely on the detection of long-chain branching from zero-shear compliance estimates (258). This is most likely due to the difficulties in separating the effects of polydispersity and LCB.

Shroff and Mavridis have completed a number of studies on the determination of branching in polyethylene (174, 175, 200, 262). The authors have reviewed and proposed several indices relying on rheological data to quantify the amount of long-chain branching including what they have termed as the long-chain branching index (LCBI) (175):

$$\text{LCBI} = \frac{\eta_0^{1/a_3}}{[\eta]_{br}} \frac{1}{k_3^{1/a_3}} - 1 \quad (2.56)$$

where k_3 and a_3 are the constants for a linear polymer in a η_0 - $[\eta]$ power law equation as follows:

$$\eta_0 = k_3 [\eta]^{a_3} \quad (2.57)$$

The LCBI is zero for linear polymers with larger numbers denoting higher levels of long-chain branching. A significant advantage of this index is that it is independent of molecular weight and molecular weight distribution. The LCBI has been developed for essentially linear polymers and its derivation relies upon the assumption that $g \approx g' \approx 1$. In other words, the LCBI is only valid for low levels of long-chain branching not detected by solution methods. A modification of Equation 2.56 has been proposed to accommodate those polymers where $g' < 1$. However, this method relies on assuming a value for ε and as previously noted, this parameter is found to vary with long-chain branching and molecular weight. As Shroff and Mavridis show with a series of low-density polyethylenes where branching was detected with solution methods, the expected trend of samples with increasing LCB is only found at $\varepsilon = 0.5$ and not for other values of ε reported for polyethylene in the literature (175). Shroff and Mavridis have also

reviewed and extended a list of rheological polydispersity indices (262). It was found that the presence of even small amounts of long-chain branching significantly alters most of the measures of rheological polydispersity while no changes were observed in the MWD obtained from SEC. One such measure proposed by the authors is the E_R , which is independent of molecular weight but influenced by molecular weight distribution and long-chain branching (262):

$$E_R = C_1 G'' \Big|_{\text{at } G''_{ref}} \quad (2.58)$$

where G''_{ref} is a reference low modulus value corresponding to low frequencies and C_1 is a constant. For polyolefin melts, the authors have suggested $G''_{ref} = 5000 \text{ dyn/cm}^2$ and $C_1 = 1.781 \times 10^{-3} \text{ cm}^2/\text{dyn}$. Figure 2.9 provides an example of a η_0 - M_w plot for various polyethylene samples where very small amounts of LCB produced an increase in the zero-shear viscosity but were not detected with SEC. The samples categorized as having lower E_R values do not display as much viscosity enhancement as the samples with much higher values of E_R .

Another index developed to detect long-chain branching is the Dow rheology index (DRI) (263). It was specifically derived for polyethylenes with similar, narrow molecular weight distributions ($M_w/M_n \sim 2$) and is not able to distinguish between the effects of polydispersity and branching.

$$\text{DRI} = 3.65 \times 10^5 \frac{\tau_0}{\eta_0} - 0.1 \quad (2.59)$$

where τ_0 is a characteristic time determined from the Cross equation.

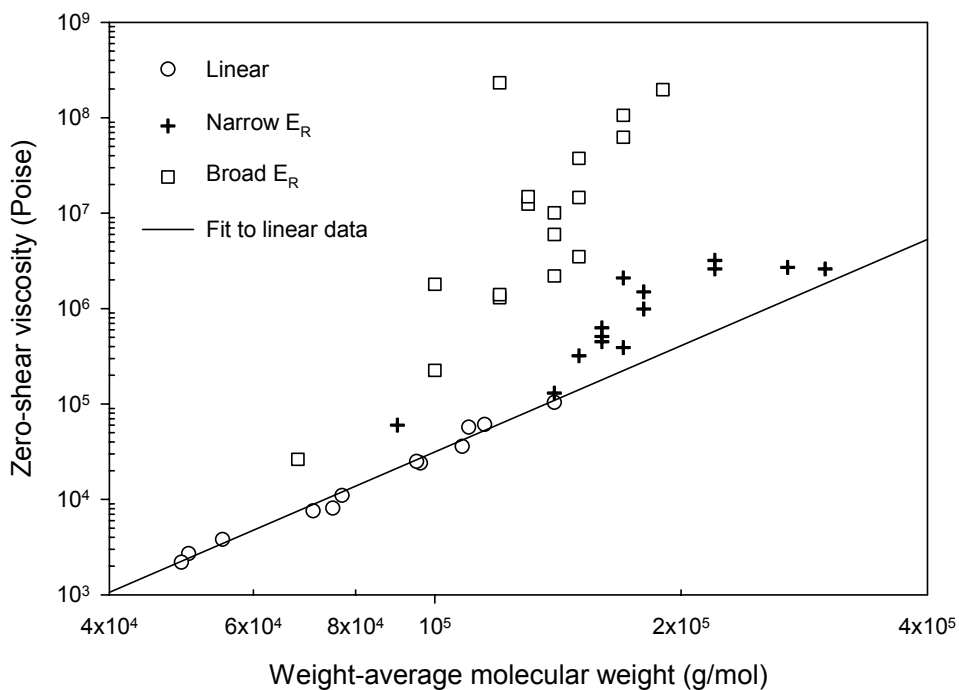


Figure 2.9. Zero-shear viscosity as a function of weight-average molecular weight for various polyethylene samples at 190°C: circles, fairly narrow MWD ($M_w/M_n \sim 2-6$) linear samples; crosses, broad to very broad MWD ($M_w/M_n \sim 6.6-30$) branched samples but with narrow rheological polydispersity ($E_R \sim 1.7-3.7$); squares, broad MWD ($M_w/M_n \sim 6.0-14$) branched samples with large rheological polydispersity ($E_R \sim 6.0-14$). Data from ref. (175).

Another technique to calculate the amount of LCB in polymers was developed by Wood-Adams and Dealy (183). Based upon the work of Shaw and Tuminello (264), the procedure involves transforming the complex viscosity data as a function of frequency into a molecular weight distribution. This distribution is then compared to that obtained from SEC and the difference in the location of peaks is correlated to a level of branching.

Although only providing a qualitative determination of the level of branching, comparing the linear viscoelastic data of samples from dynamic rheology measurements is a common technique. Plots of the loss angle, δ , as a function of frequency are altered due to branching.

$$\delta = \tan^{-1}\left(\frac{G''(\omega)}{G'(\omega)}\right) \quad (2.60)$$

where $G''(\omega)$ and $G'(\omega)$ are the loss and storage modulus and ω is the angular frequency. For a perfectly elastic solid, the loss modulus is zero and thus, so is the loss angle. For a perfectly viscous fluid, the storage modulus is zero and the loss angle is 90° . Figure 2.10 provides a plot of the loss angle as a function of frequency for high-density polyethylenes from metallocene catalysts. In general, the presence of branching causes a plateau in the loss angle with the magnitude and breadth of the plateau depending on the degree of LCB (265, 266). A variation of this technique is known as the reduced van Gorp-Palmen plot where the loss angle is plotted as function of the ratio of the complex modulus and plateau modulus ($G_{red} = |G^*|/G_N^0$) (267, 268). The plot is found to be temperature invariant and because a reduced modulus is used, the curves are not influenced by polymer composition. Figure 2.11 provides an example of a reduced van Gorp-Palmen plot. For a linear polymer, the loss angle starts as a plateau at 90° for low G_{red} . As the reduced modulus increases, the loss angle decreases past an inflection point towards a minimum at $G_{red} = 1$ and then increases again. The effect of molecular weight is to lower the value of the loss angle at the minimum while a broader molecular weight distribution tends to cause a less steep drop in δ towards the minimum (i.e., δ begins to decrease from 90° at much lower values of G_{red}). The impact of branching is to produce a plateau or even a second minimum at the inflection point of $G_{red} < 1$. This presence of a second minimum has also been found for blends of linear high and low molecular weight materials (267).

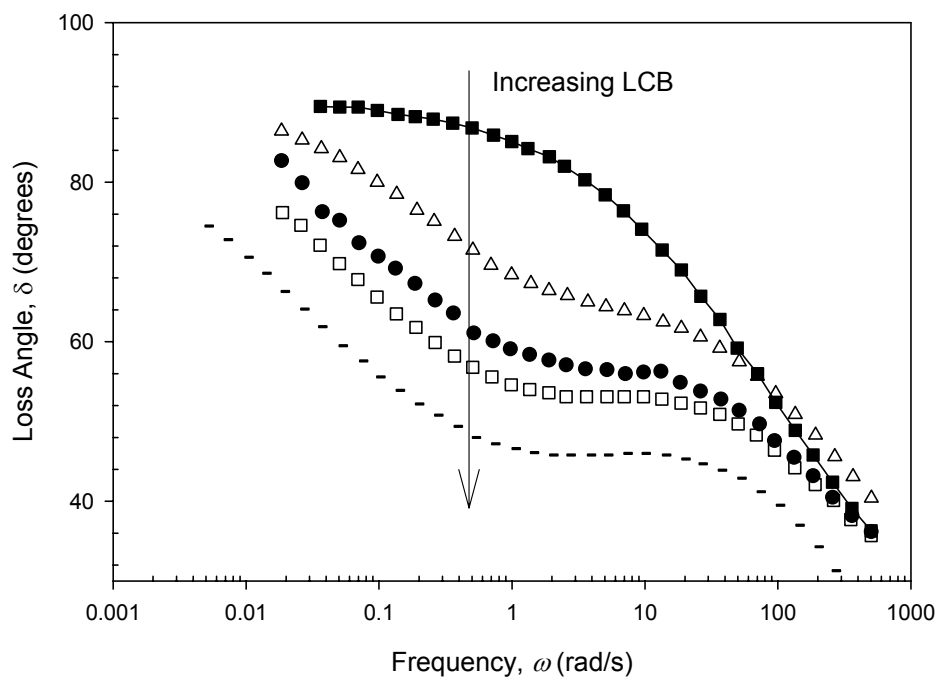


Figure 2.10. Loss angle as a function of frequency at 150°C obtained for high-density, metallocene catalyzed polyethylene samples of increasing long-chain branching. Taken from ref. (265).

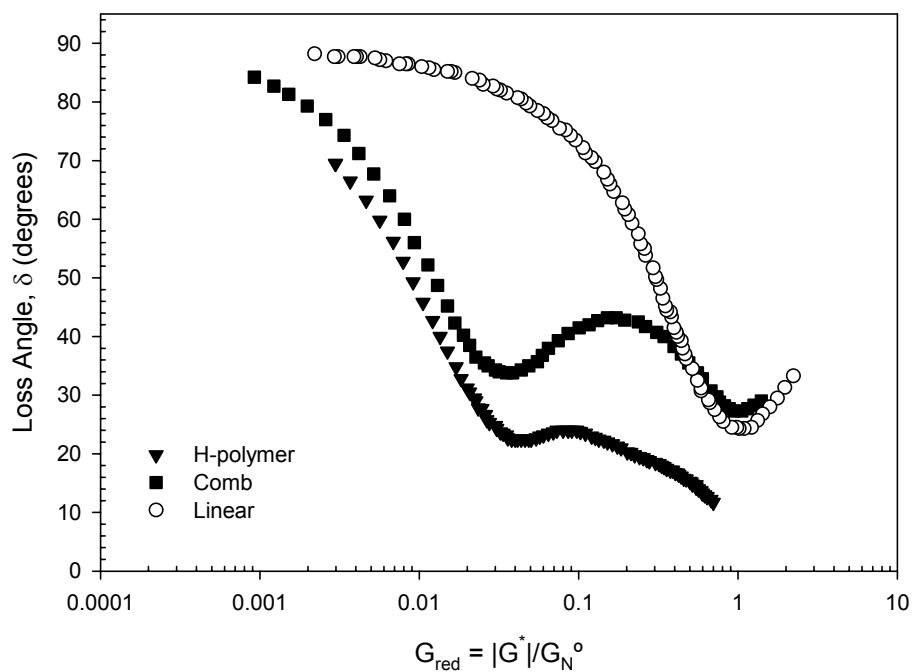


Figure 2.11. Loss angle as a function of the reduced modulus (ratio of complex modulus and plateau modulus) for polystyrene samples. Taken from ref. (268).

Other techniques employed in the detection of branching from rheological data include:

- Viscosity dependence on frequency (or shear rate): The effect of branching produces either a reduction (e.g., LDPE) or enhancement (e.g., metallocene PE) of η_0 . In a similar manner, branching can also increase (e.g. LDPE) or decrease (e.g. metallocene PE) the critical shear rate for the onset of shear thinning.
- Modified Cole-Cole plot (G' vs. G''): The plot is invariant of molecular weight and thus, useful for comparing various samples. Differences between samples of similar polydispersity may be assigned to LCB.
- Activation energy for flow: The enhancement of E_a can be attributed to the presence of LCB; however, the reverse is not always true as LCB does not always increase the value of E_a . A general rule is that the absence of an enhanced E_a does not necessarily rule out the presence of long-chain branching (175, 269).
- Thermorheological complexity: Failure of the TTS implies that a polymer is thermorheologically complex. This can be seen from plots of $\tan \delta$ as a function of G^* where curves for various temperatures should superimpose in order for TTS to be valid. As other factors may cause a polymer to be thermorheologically complex, this method cannot conclusively determine LCB (270).
- Extensional rheology: Branching may be detected from strain hardening behaviour where the tensile stress growth coefficient increases above the linear viscoelastic response (183-185, 271). However, strain hardening has been observed for a number of linear polymers (180, 184, 272-274) and thus, it alone cannot be used for detecting branching. In general, the presence of LCB provides much greater strain hardening relative to linear polymers (185).

2.3.2.4 Summary

LCB affects a variety of polymer properties from the dilute to melt state. Because many commercial polymers contain a fraction of branched material, understanding the relationship between polymer properties and molecular architecture is of tremendous importance. Branched polymers are denser than linear polymers and hence have a smaller size. Various contraction factors can be used to quantify this reduction. In the case of polydisperse polymers, a broad molecular weight distribution can mask the effects of branching and as such, these samples must be fractionated in order to detect any evidence of LCB. The effect of branching on rheological properties is somewhat more complex as there are two opposing effects. The first effect is due to the fact that branching reduces a polymer molecule's size and leads to less entanglements. Secondly, when the branch is sufficiently long to become entangled, the overall number of entanglements is increased. Because of these effects, reduction or enhancement of various rheological properties is observed.

The task of quantifying branching in polymers is complicated by their very nature. Typical branched macromolecules are extremely heterogeneous in terms of the number, type, and length of branches, molecular weight variations, and in most instances, the presence of linear or crosslinked fractions. Spectroscopic methods such as NMR are some of the best methods for quantitatively determining the level of branching. Chromatographic techniques can provide more information such as molecular weight and branching distributions depending upon the detectors employed. Yet both spectroscopic and chromatographic methods are not sensitive enough to be able to detect the very low levels of branching that can still significantly alter a polymer's flow behaviour. In such instances, rheological characterization becomes the only solution. However, the rheology of branched polymers is still not fully understood and techniques typically provide a qualitative view on branching.

2.4 References

1. Prisyazhnyuk, A. I., Ivanchev, S. S. Diperoxides with differing thermal stabilities of the peroxide group as initiators of radical polymerization and block copolymerization. *Polymer Science USSR* **1970**, *12* (2), 514-524.
2. Kamath, V. R. New initiators for PS offer big efficiencies. *Modern Plastics* **1981**, *58* (9), 106-110.
3. Choi, K. Y., Lei, G. D. Modeling of free radical polymerization of styrene by bifunctional initiators. *AIChE Journal* **1987**, *33* (12), 2067-2076.
4. Villalobos, M. A., Hamielec, A. E., Wood, P. E. Kinetic model for short-cycle bulk styrene polymerization through bifunctional initiators. *Journal of Applied Polymer Science* **1991**, *42*, 629-641.
5. González, I. M., Meira, G. R., Oliva, H. M. Synthesis of polystyrene with mixtures of mono- and bifunctional initiators. *Journal of Applied Polymer Science* **1996**, *59*, 1015-1026.
6. Cavin, L., Rouge, A., Meyer, T., Renken, A. Kinetic modeling of free radical polymerization of styrene initiated by the bifunctional initiator 2,5-dimethyl-2,5-bis(2-ethyl hexanoyl peroxy)hexane. *Polymer* **2000**, *41*, 3925-3935.
7. Cerna, J. R., Morales, G., Eyler, G. N., Canizo, A. I. Bulk Polymerization of Styrene Catalyzed by Bi- and Trifunctional Cyclic Initiators. *Journal of Applied Polymer Science* **2002**, *83*, 1-11.
8. Bywater, S. Preparation and Properties of Star-branched Polymers. *Advances in Polymer Science* **1979**, *30* (2), 89-116.
9. Roovers, J. Dilute Solution Properties of Regular Star Polymers. *Plastics Engineering* **1999**, *53*, 285-341.
10. Krupiniski, Steven M. (Nova Chemicals Inc.). Tetrafunctional initiator. US Patent 6,166,099, **2000**.
11. Kasehagen, L., Wicher, J., Brennan, J., Debaud, F., Suehisa, T. A New Multifunctional Peroxide Initiator for High Molecular Weight, High Productivity, and Long-Chain Branching. *ANTEC - Soc. Plast. Eng.* **2002**, *60* (2), 1837-1841.
12. Matyjaszewski, K. The Synthesis of Functional Star Copolymers as an Illustration of the Importance of Controlling Polymer Structures in the Design of New Materials. *Polymer Int.* **2003**, *52*, 1559-1565.
13. Barner, L., Barner-Kowollik, C., Davis, T. P., Stenzel, M. H. Complex molecular architecture polymers via RAFT. *Australian Journal of Chemistry* **2004**, *57* (1), 19-24.
14. Hawker, C. J., Bosman, A. W., Harth, E. New Polymer Synthesis by Nitroxide Mediated Living Radical Polymerization. *Australian Journal of Chemistry* **2004**, *57*, 19-24.
15. Charleux, B., Faust, R. Synthesis of Branched polymers by Cationic Polymerization. *Advances in Polymer Science* **1999**, *142*, 1-69.
16. Hadjichristidis, N., Pitsikalis, M., Pispas, S., Iatrou, H. Polymers with Complex Architecture by Living Anionic Polymerization. *Chemical Reviews* **2001**, *101*, 3747-3792.

17. Ivanchev, S. S. New Views on Initiation and Radical Polymerization in Homogeneous and Heterogeneous Systems. *Polymer Science USSR* **1979**, *20* (9), 2157-2181.
18. Simionescu, C. I., Comanita, E., Pastravanu, M., Dumitriu, S. Progress in the field of bi- and poly-functional free-radical polymerization initiator. *Progress in Polymer Science* **1986**, *12*, 1-109.
19. Choi, K. Y., Liang, W. R., Lei, G. D. Kinetic bulk styrene polymerization catalyzed by symmetrical bifunctional initiators. *Journal of Applied Polymer Science* **1988**, *35*, 1547-1562.
20. Kim, K. J., Choi, K. Y. Modeling of free radical polymerization of styrene catalyzed by unsymmetrical bifunctional initiators. *Chemical Engineering Science* **1989**, *44* (2), 297-312.
21. Kim, K. J., Liang, W. R., Choi, K. Y. Bulk free radical polymerization of styrene with unsymmetrical bifunctional initiators. *Industrial and Engineering Chemistry Research* **1989**, *28*, 131-138.
22. Yoon, W. J., Choi, K. Y. Free radical polymerization of styrene with a binary mixture of symmetrical bifunctional initiators. *Journal of Applied Polymer Science* **1992**, *46*, 1353-1367.
23. Yoon, W. J., Choi, K. Y. Polymerization of styrene in a continuous filled tubular reactor. *Polymer Engineering and Science* **1996**, *36* (1), 65-77.
24. Estenoz, D. A., Leal, G. P., Lopez, Y. R., Oliva, H. M., Meira, G. R. Bulk Polymerization of Styrene in the Presence of Polybutadiene. The Use of Bifunctional Initiators. *Journal of Applied Polymer Science* **1996**, *62*, 917-939.
25. Dhib, R., Gao, J., Penlidis, A. Simulation of free radical bulk/solution homopolymerization using mono- and bi-functional initiators. *Polymer Reaction Engineering Journal* **2000**, *8*, 299-464.
26. Menciloglu, Y. Z., Baysal, B. M. Synthesis and characterization of multifunctional initiators for preparation of four-branched polymers. *Die Angewandte Makromolekulare Chemie* **1992**, *200*, 37-47.
27. Holzinger, D., Kickelbick, G. Modified cubic spherosilicates as macroinitiators for the synthesis of inorganic-organic starlike polymers. *Journal of Polymer Science Part A-Polymer Chemistry* **2002**, *40* (21), 3858-3872.
28. Kwon, T. S., Takagi, K., Kunisada, H., Yuki, Y. Synthesis of star polystyrene by radical polymerization with 1,2,4,5-tetrakis(*p-tert*-butylphenylselenomethyl)benzene as a novel photoiniferter. *European Polymer Journal* **2003**, *39*, 1437-1441.
29. Staudinger, H., Schulz, G. V. Highly polymerized compounds. CXXXVI. Comparison of Osmotic and Viscosimetric Molecular-Weight Determinations of Polymer-Homologous Series. *Ber.* **1935**, *68B*, 2320-2335.
30. Flory, P. J. Mechanism of Vinyl Polymerizations. *J. Am. Chem. Soc.* **1937**, *59*, 241-253.
31. Stockmayer, W. H., Fixman, M. Dilute Solutions of Branched Polymers. *Ann. N. Y. Acad. Sci.* **1953**, *57* (4), 334-352.
32. Melville, H. W. New Kinds of Macromolecules. *Trans. Plast. Inst. Lond.* **1955**, *23*, 146-163.

33. Graessley, W. W. Detection and Measurement of Branching in Polymers. In *Characterization of Macromolecular Structure*; National Academy of Sciences: Washington, D.C., 1968; 371-388.
34. Dexheimer, H., Fuchs, O., Suhr, H. Branching of Macromolecules and its Effect on Properties. *Deut. Farben-Z.* **1968**, *22* (11), 481-494.
35. Small, P. A. Long-Chain Branching in Polymers. *Adv. Polym. Sci.* **1975**, *18*, 1-64.
36. Burchard, W. Static and Dynamic Light Scattering From Branched Polymers and Biopolymers. *Adv. Polym. Sci.* **1983**, *48*, 1-124.
37. Burchard, W. Solution Properties of Branched Macromolecules. *Adv. Polym. Sci.* **1999**, *143*, 113-194.
38. Mays, J. W., Hadjichristidis, N. Dilute Solution Properties of Branched Macromolecules. *J. Appl. Polym. Sci. : Appl. Polym. Symp.* **1992**, *51*, 55-72.
39. Roovers, J. Branched Polymers. In *Encyclopedia of Polymer Science and Engineering*; John Wiley: New York, 1983; 478-499.
40. Graessley, W. W. Effect of Long Branches on the Flow Properties of Polymers. *Acc. Chem. Res.* **1977**, *10*, 332-339.
41. Vega, J., Aguilar, M., Peon, J., Pastor, D., Martinez-Salazar, J. Effect of long chain branching on linear-viscoelastic melt properties of polyolefins. *E-Polymers* **2002**,
42. Barner, L., Barner-Kowollik, C., Davis, T. P., Stenzel, M. H. Complex Molecular Architecture Polymers via RAFT. *Aust. J. Chem.* **2004**, *57* (1), 19-24.
43. Hadjichristidis, N., Pitsikalis, M., Pispas, S., Iatrou, H. Polymers with Complex Architecture by Living Anionic Polymerization. *Chem. Revs.* **2001**, *101* (12), 3747-3792.
44. Flory, P. J. *Principles of Polymer Chemistry*; Cornell Univ. Press: Ithaca, New York, 1953.
45. Zimm, B. H., Stockmayer, W. H. The Dimensions of Chain Molecules Containing Branches and Rings. *J. Chem. Phys.* **1949**, *17* (12), 1301-1314.
46. Orofino, T. A. Branched Polymers. II – Dimensions in Non-Interacting Media. *Polymer* **1961**, *2*, 305-314.
47. Berry, G. C., Orofino, T. A. Branched Polymers. III – Dimensions of Chains with Small Excluded Volume. *J. Chem. Phys.* **1964**, *40* (6), 1614-1621.
48. Kurata, M., Fukatsu, M. Unperturbed Dimension and Translational Friction Constant of Branched Polymers. *J. Chem. Phys.* **1964**, *41* (9), 2934-2944.
49. Forsman, W. C. Matrix Method for Determining the Dimensions of Branched Random-Flight Chains. *Macromolecules* **1968**, *1* (4), 343-347.
50. Nakamura, Y., Wan, Y., Mays, J. W., Iatrou, H., Hadjichristidis, N. Radius of Gyration of Polystyrene Combs and Centipedes in Solution. *Macromolecules* **2000**, *33*, 8323-8328.
51. Roovers, J. Conformational Properties of Dendritic Polymers with Variable Branching Functionality in Their Generational Shells. *E-Polymers* **2000**,
52. Chu, B., Lui, T. Characterization of Nanoparticles by Scattering Techniques. *J. Nanopart. Res.* **2000**, *2*, 29-41.
53. Debye, P. Light Scattering in Solutions. *J. Appl. Phys.* **1944**, *15*, 338-342.

54. Zimm, B. H. Molecular Theory of the Scattering of Light in Fluids. *J. Chem. Phys.* **1945**, *13*, 141-145.
55. Zimm, B. H. The Dependence of the Scattering of Light on Angle and Concentration in Linear Polymer Solutions. *J. Chem. Phys.* **1948**, *52*, 260-267.
56. Candau, F., Rempp, P., Benoit, H. A New Theoretical Approach to the Problem of Solution Behavior of Branched Polymers. *Macromolecules* **1972**, *5*, 627-632.
57. Mazur, J., McCrackin, F. L. Configurational Properties of Star-Branched Polymers. *Macromolecules* **1977**, *10*, 326-332.
58. Daoud, M., Cotton, J. P. Star Shaped Polymers - A Model for the Conformation and Its Concentration-Dependence. *J. Phys.* **1982**, *43* (3), 531-538.
59. Roovers, J. Synthesis and dilute solution characterization of comb polystyrenes. *Polymer* **1979**, *20*, 843-849.
60. Fetters, L. J., Hadjichristidis, N., Lindner, J. S., Mays, J. W. Molecular Weight Dependence of Hydrodynamic and Thermodynamic Properties for Well-Defined Linear Polymers in Solution. *J. Phys. Chem. Ref. Data* **1994**, *23* (4), 619-640.
61. Burchard, W. Statistics of Star-Shaped Molecules. II. Stars with Homodisperse Side Chains. *Macromolecules* **1974**, *7* (6), 841-846.
62. Casassa, E. F., Berry, G. C. Angular Distribution of Intensity of Rayleigh Scattering from Comblike Branched Molecules. *J. Polym. Sci. , Part A: Polym. Chem.* **1996**, *4*, 881-897.
63. Khasat, N., Pennisi, R. W., Hadjichristidis, N., Fetters, L. J. Dilute Solution Behavior of Asymmetric Three-Arm and Regular Three- and Twelve-Arm Polystyrene Stars. *Macromolecules* **1988**, *21*, 1100-1106.
64. Roovers, J. E. L., Bywater, S. Preparation of Six-Branched Polystyrene. Thermodynamic and Hydrodynamic Properties of Four- and Six-Branched Star Polystyrenes. *Macromolecules* **1974**, *7*, 443-449.
65. Berry, G. C. Thermodynamic and Conformational Properties of Polystyrene. III. Dilute Solution Studies on Branched Polymers. *J. Polym. Sci. , Part A: Polym. Chem.* **1971**, *9* (4), 687-715.
66. Hadjichristidis, N., Roovers, J. E. L. Synthesis and Solution Properties of Linear, Four-Branched, and Six-Branched Star Polyisoprenes. *J. Polym. Sci. : Polym. Phys. Ed.* **1974**, *12*, 2521-2533.
67. Douglas, J. F., Roovers, J., Freed, K. F. Characterization of Branching Architecture through "Universal" Ratios of Polymer Solution Properties. *Macromolecules* **1990**, *23*, 4168-4180.
68. Zilliox, J.-G. Etude Morphologique en Solution Diluée de Polymères en Étoile. *Makromol. Chemie* **1972**, *156*, 121-141.
69. Bauer, B. J., Hadjichristidis, N., Fetters, L. J., Roovers, J. E. L. Star-Branched Polymers. 5. The θ Temperature Depression for 8- and 12-Arm Polyisoprenes in Dioxane. *J. Am. Chem. Soc.* **1980**, *102* (7), 2410-2413.
70. Bauer, B. J., Fetters, L. J., Graessley, W. W., Hadjichristidis, N., Quack, G. F. Chain Dimensions in Dilute Polymer Solutions: A Light-Scattering and

- Viscometric Study of Multiarmed Polyisoprene Stars in Good and θ Solvents. *Macromolecules* **1989**, *22*, 2337-2347.
71. Roovers, J., Hadjichristidis, N., Fetters, L. J. Analysis and Dilute Solution Properties of 12- and 18-Arm-Star Polystyrenes. *Macromolecules* **1983**, *16*, 214-220.
 72. Toporowski, P. M., Roovers, J. Synthesis and Properties of Eighteen-arm Polybutadienes. *J. Polym. Sci. , Part A: Polym. Chem.* **1986**, *24*, 3009-3019.
 73. Zhou, L.-L., Hadjichristidis, N., Toporowski, P. M., Roovers, J. Synthesis and Properties of Regular Star Polybutadienes With 32 Arms. *Rubber Chem. Technol.* **1992**, *65*, 303-314.
 74. Roovers, J., Zhou, L.-L., Toporowski, P. M., van der Zwan, M., Iatrou, H., Hadjichristidis, N. Regular Star Polymers with 64 and 128 Arms. Models for Polymeric Micelles. *Macromolecules* **1993**, *26*, 4324-4331.
 75. Roovers, J., Toporowski, P. M., Martin, J. Synthesis and Characterization of Multiarm Star Polybutadienes. *Macromolecules* **1989**, *22*, 1897-1903.
 76. Thurmond, C. D., Zimm, B. H. Size and Shape of the Molecules in Artificially Branched Polystyrene. *J. Polym. Sci.* **1952**, *8* (5), 477-494.
 77. Zimm, B. H., Kilb, R. W. Dynamics of Branched Molecules in Dilute Solution. *J. Polym. Sci.* **1959**, *37*, 19-42.
 78. Kurata, M., Abe, M., Masamichi, I., Matsushima, M. Randomly Branched Polymers. I. Hydrodynamic Properties. *Polymer J.* **1972**, *3* (6), 729-738.
 79. Ambler, M. R., McIntyre, D. Randomly Branched Styrene/Divinylbenzene Copolymers. II. Solution Properties and Structure. *J. Appl. Polym. Sci.* **1977**, *21*, 2268-2282.
 80. Berry, G. C., Orofino, T. A. Branched Polymers. III - Dimensions of Chains with Small Excluded Volume. *J. Chem. Phys.* **1964**, *40* (6), 1614-1621.
 81. Foster, G. N., Hamielec, A. E., MacRury, T. B. The Molecular Weight and Branching Distribution Method. *ACS Symposium Series* **1980**, *138*, 131-148.
 82. Vega, J. R., Estenoz, D. A., Oliva, H. M., Meira, G. R. Analysis of a Styrene-Butadiene Graft Copolymer with the Help of a Polymerization Model. *Int. J. Polym. Anal. Charact.* **2001**, *6*, 81-87.
 83. Roovers, J. Dilute Solution Properties of Regular Star Polymers. *Plast. Eng.* **1999**, *53*, 285-341.
 84. Moore, W. R. A. D., Millns, W. Long-Chain Branching in Low-Density Polyethylene. *Brit. Polym. J.* **1969**, *1* (2), 81-87.
 85. Völker, H., Luig, F. J. Long Chain Branching in Polyethylenes. *Angew. Makromol. Chem.* **1970**, *12*, 43-57.
 86. Hama, T., Yamaguchi, K., Suzuki, T. Long-Chain Branching and Solution Properties of Low-Density Polyethylene. *Makromol. Chem.* **1972**, *155* (4), 283-298.
 87. Kuhn, V. R., Krömer, H., Rossmannith, G. Structure and Properties of Differently Prepared High Pressure Polyethylene. *Angew. Makromol. Chem.* **1974**, *40/41*, 361-389.
 88. Scholte, Th. G., Meijerink, N. L. J. Gel Permeation Chromatography on Branched Polymers. *Polymer J.* **1977**, *9* (2), 133-139.

89. Hert, M., Strazielle, C. Study of the Branching Structure of Low-Density Polyethylene by Viscosity and Light Scattering Measurements on fractions from Exclusion GPC. *Makromol. Chem.* **1983**, *184* (1), 135-145.
90. Grinshpun, V., Rudin, A., Russell, K. E., Scammell, M. V. Long-Chain Branching Indexes from Size-Exclusion Chromatography of Polyethylenes. *J. Polym. Sci. , Part B: Polym. Phys.* **1986**, *24* (5), 1171-1176.
91. Tackx, P., Tacx, J. C. J. F. Chain Architecture of LDPE as a Function of Molar Mass Using Size Exclusion Chromatography and Multi-Angle Laser Light Scattering (SEC-MALLS). *Polymer* **1998**, *39* (14), 3109-3113.
92. Wang, W.-J., Kharchenkob, S., Miglerb, K., Zhu, S. Triple-detector GPC Characterization and Processing Behavior of Long-Chain-Branched Polyethylene Prepared by Solution Polymerization with Constrained Geometry Catalyst. *Polymer* **2004**, *45* (19), 6495-6505.
93. Utracki, L. A., Roovers, J. E. L. Viscosity and Normal Stresses of Linear and Star Branched Polystyrene Solution. I. Application of Corresponding States Principle to Zero-Shear Viscosities. *Macromolecules* **1973**, *6* (3), 366-372.
94. Roovers, J. Melt Rheology of H-Shaped Polystyrenes. *Macromolecules* **1984**, *17*, 1196-1200.
95. Noda, I., Horikawa, T., Kato, T., Fujimoto, T., Nagasawa, M. Solution Properties of Comb-Shaped Polystyrenes. *Macromolecules* **1970**, *3* (6), 795-799.
96. Grest, G. S., Fetters, L. J., Huang, J. S., Richter, D. Star Polymers: Experiment, Theory, and Simulation. *Adv. Chem. Phys.* **1996**, *94*, 67-163.
97. Gauthier, M., Chung, J., Choi, L., Nguyen, T. T. Second Virial Coefficient of Arborescent Polystyrenes and Its Temperature Dependence. *J. Phys. Chem. B* **1998**, *102* (17), 3138-3142.
98. Striolo, A., Prausnitz, J. M., Bertucco, A. Osmotic Second Virial Coefficient, Intrinsic Viscosity and Molecular Simulation for Star and Linear Polystyrenes. *Macromolecules* **2000**, *33* (26), 9583-9586.
99. Schulz, G. V. The Kinetics of Chain Polymerization. V. The Effect of Various Reaction Species on the Multimolecularity. *Z. Physik. Chem.* **1939**, *B43*, 25-46.
100. Schaeffgen, J. R., Flory, P. J. Synthesis of Multichain Polymers and Investigation of their Viscosities. *J. Am. Chem. Soc.* **1948**, *70*, 2709-2718.
101. Stockmayer, W. H. Theory of Molecular Size Distribution and Gel Formation in Branched-Chain Polymers. *J. Chem. Phys.* **1943**, *11* (2), 45-55.
102. Flory, P. J. Fundamental Principles of Condensation Polymerization. *Chem. Revs.* **1946**, *39*, 137-197.
103. Gordon, M. Good's theory of cascade processes applied to the statistics of polymer distributions. *Proc. Roy. Soc. Lond. Ser. A* **1962**, *268*, 240-259.
104. Burchard, W. Angular Distribution of Rayleigh Scattering from Branched Polycondensates. Amylopectin and Glycogen Types. *Macromolecules* **1972**, *5* (5), 604-610.
105. Ullisch, B., Burchard, W. Branching in Free Radical Polymerization Due to Chain Transfer, 2) Theory of the Effect of Polyfunctional Transfer Reagents. *Makromol. Chem.* **1977**, *178*, 1403-1426.

106. Ullisch, B., Burchard, W. Branching in Free Radical Polymerization Due to Chain Transfer, 3) Polymerization of Styrene in the Presence of a Tetrafunctional Chain Transfer Agent. *Makromol. Chem.* **1977**, *178*, 1427-1437.
107. Spouge, J. L. Asymmetric Bonding of Identical Units: A General A_gRB_{f-g} Polymer Mode. *Macromolecules* **1983**, *16* (5), 831-835.
108. Tobita, H., Hatanaka, K. Branched Structure Formation in Free Radical Polymerization of Vinyl Acetate. *J. Polym. Sci. , Part B: Polym. Phys.* **1996**, *34* (4), 671-681.
109. Patton, E. V., Wesson, J. A., Rubinstein, M., Wilson, J. C., Oppenheimer, L. E. Scaling Properties of Branched Polyesters. *Macromolecules* **1989**, *22*, 1946-1959.
110. Bauer, J., Lang, P., Burchard, W., Bauer, M. Critical Behavior of a Trifunctional, Randomly Branched Polymer. Percolation versus Cascade Theory. *Macromolecules* **1991**, *24*, 2634-2636.
111. Colby, R. H., Rubinstein, M., Gillmor, J. R., Mourey, T. H. Scaling Properties of Branched Polyesters. 2. Static Scaling above the Gel Point. *Macromolecules* **1992**, *25*, 7180-7187.
112. Weissmüller, M., Burchard, W. Molar Mass Distributions of End-linked Polystyrene Star Macromolecules. *Polymer Int.* **1997**, *44*, 380-390.
113. Zhu, S., Li, D., Yu, Q., Hunkeler, D. Change in Molecular Weight Distribution During Formation and Degradation of Star Polymers. *J. M. S. - Pure Appl. Chem.* **1998**, *A35* (1), 33-56.
114. Soares, J. B. P., Hamielec, A. E. Bivariate Chain Length and Long Chain Branching Distribution for Copolymerization of Olefins and Polyolefin Chains Containing Terminal Double-Bonds. *Macromol. Theory Simul.* **1996**, *5* (3), 547-572.
115. Sachs, W. H. Simulating Cumulative Distributions under Transient Conditions in Well-Mixed, Continuous and Batch Polymerization Reactors. *Macromol. Symp.* **2004**, *206*, 29-42.
116. Beasley, J. K. The Molecular Structure of Polyethylene. IV. Kinetic Calculations of the Effect of Branching on Molecular Weight Distribution. *J. Am. Chem. Soc.* **1953**, *75*, 6123-6127.
117. Bamford, C. H., Tompa, H. Calculation of Molecular-Weight Distributions from Kinetic Schemes. *Trans. Farad. Soc.* **1954**, *50*, 1097-1115.
118. Graessley, W. W., Mittelhauser, H., Maramba, R. Molecular Weight Distribution in Free Radical Polymers. The Effect of Branching on Distribution Breadth, and the Prediction of Gel Points in Diene Polymerization. *Makromol. Chem.* **1965**, *86*, 129-138.
119. Saito, O., Nagasubramanian, K., Graessley, W. W. Molecular Weight Distribution in Branched Polymers. *J. Polym. Sci. : Polym. Phys. Ed.* **1969**, *7* (11), 1937-1954.
120. Jackson, R. A., Small, P. A., Whiteley, K. S. Prediction of Molecular Weight Distributions in Branched Polymers. *J. Polym. Sci. : Polym. Chem. Ed.* **1973**, *11*, 1781-1809.

121. Taylor, T. W., Reichert, K. H. The Influence of Reactor Type and Operating Conditions on the Molecular Weight Distribution in Vinyl Acetate Polymerization. *J. Appl. Polym. Sci.* **1985**, *30*, 227-250.
122. Yoon, W. J., Kim, Y. S., Kim, I. S., Choi, K. Y. Recent Advances in Polymer Reaction Engineering: Modeling and Control of Polymer Properties. *Korean J. Chem. Eng.* **2004**, *21* (1), 147-167.
123. Yan, D., Zhou, Z., Jiang, H., Wang, G. Kinetic Model of Star-Branched Polycondensation. *Macromol. Theory Simul.* **1998**, *7*, 13-18.
124. Zhu, S., Li, D., Zhou, W., Crowe, C. M. Molecular Weight Distribution of Comb Polymers by Chain Polymerization with Macromonomer. *Polymer* **1998**, *39* (21), 5203-5208.
125. Radke, W., Litvinenko, G., Müller, A. H. E. Effect of Core-Forming Molecules on Molecular Weight Distributions and Degree of Branching in the Synthesis of Hyperbranched Polymers. *Macromolecules* **1998**, *31*, 239-248.
126. Yan, D., Zhou, Z., Müller, A. H. E. Molecular Weight Distribution of Hyperbranched Polymers Generated by Self-Condensing Vinyl Polymerization in Presence of a Multifunctional Initiator. *Macromolecules* **1999**, *32*, 245-250.
127. Pladis, P., Kiparissides, C. A. Comprehensive Model for the Calculation of Molecular Weight-Long Chain Branching Distribution in Free-Radical Polymerizations. *Chem. Eng. Sci.* **1998**, *53* (18), 3315-3333.
128. Butté, A., Ghielmi, A., Storti, G., Morbidelli, M. Calculation of Molecular Weight Distributions in Free-Radical Polymerization with Chain Branching. *Macromol. Theory Simul.* **1999**, *8*, 498-512.
129. Yiannoulakis, H., Yiagopoulos, A., Pladis, P., Kiparissides, C. Comprehensive Dynamic Model for the Calculation of the Molecular Weight and Long Chain Branching Distributions in Metallocene-Catalyzed Ethylene Polymerization Reactors. *Macromolecules* **2000**, *33*, 2757-2766.
130. Tobita, H. Molecular Weight Distribution in Free-Radical Crosslinking Copolymerization. *Macromolecules* **1993**, *26* (4), 836-841.
131. Tobita, H. Kinetics of Network Formation in Free-Radical Crosslinking Copolymerization. *Macromolecules* **1993**, *26* (20), 5427-5435.
132. Tobita, H. Simulation Model for Network Formation in Free-Radical Crosslinking Copolymerization: Pregelation Period. *Makromol. Chem. Theory Simul.* **1993**, *2* (5), 761-776.
133. Tobita, H. Dimensions of Cross-Linked Polymers Formed in Living Vinyl/Divinyl Copolymerization. *Macromolecules* **1994**, *27* (19), 5413-5420.
134. Tobita, H. Molecular Weight Distribution in Random Crosslinking of Polymer Chains. *J. Polym. Sci. , Part B: Polym. Phys.* **1995**, *33* (8), 1191-1202.
135. Tobita, H. Simulation Model for the Modification of Polymers via Crosslinking and Degradation. *Polymer* **1995**, *36* (13), 2585-2596.
136. Tobita, H. Molecular Weight Distribution in Free Radical Polymerization with Long-Chain Branching. *J. Polym. Sci. , Part B: Polym. Phys.* **1993**, *31* (10), 1363-1371.

137. Tobita, H. Simulation Model for Long-Chain Branching in Vinyl Acetate Polymerization: 1. Batch Polymerization. *J. Polym. Sci. , Part B: Polym. Phys.* **1994**, *32* (5), 901-910.
138. Tobita, H. A Simulation Model for Long-Chain Branching in Vinyl Acetate Polymerization: 2. Continuous Polymerization in Stirred Tank Reactor. *J. Polym. Sci. , Part B: Polym. Phys.* **1994**, *32* (5), 911-919.
139. Tobita, H., Hatanaka, K. Long-Chain Branching in Free-Radical Polymerization Due to Chain Transfer to Polymer. *J. Polym. Sci. , Part B: Polym. Phys.* **1995**, *33* (5), 841-853.
140. Tobita, H. Bimodal molecular weight distribution formed in emulsion polymerization with long-chain branching. *Polym. React. Eng. J.* **2003**, *11* (4), 855-868.
141. Tobita, H. Random Sampling Technique To Predict the Molecular Weight Distribution in Free-Radical Polymerization That Involves Polyfunctional Chain Transfer Agents. *Macromolecules* **1996**, *29* (2), 693-704.
142. Tobita, H., Mima, T., Okada, A., Mori, J., Tanabe, T. Molecular Weight Distribution Formed During Free-Radical Polymerization in the Presence of Polyfunctional Chain Transfer Agents. *J. Polym. Sci. , Part B: Polym. Phys.* **1999**, *37* (12), 1267-1275.
143. Tobita, H. Copolymerization with Chain Transfer Monomer. 1. Distribution of Branch Points. *Macromolecules* **1997**, *30* (6), 1685-1692.
144. Tobita, H. Copolymerization with Chain Transfer Monomer. 2. Molecular Weight Distribution. *Macromolecules* **1997**, *30* (6), 1693-1700.
145. Beigzadeh, D., Soares, J. B. P., Duever, T. A., Hamielec, A. E. Analysis of Branching Structure in Polyethylene Resins Synthesized with Constrained-Geometry Catalyst Systems Using Monte Carlo Simulation. *Polym. React. Eng. J.* **1999**, *7* (2), 195-205.
146. Ham, J. S. Viscoelastic Theory of Branched and Cross-Linked Polymers. *J. Chem. Phys.* **1957**, *26* (3), 625-633.
147. Bueche, F. Viscosity of Molten Branched Polymers and Their Concentrated Solutions. *J. Chem. Phys.* **1964**, *40* (2), 484-487.
148. Berry, G. C., Fox, T. G. The Viscosity of Polymers and Their Concentrated Solutions. *Adv. Polym. Sci.* **1968**, *5* (3), 262-357.
149. Graessley, W. W., Masuda, T., Roovers, J. E. L., Hadjichristidis, N. Rheological Properties of Linear and Branched Polyisoprene. *Macromolecules* **1976**, *9* (1), 127-141.
150. Roovers, J., Graessley, W. W. Melt Rheology of Some Model Comb Polystyrenes. *Macromolecules* **1981**, *14* (3), 766-773.
151. Nagasawa, M., Fujimoto, T. Preparation, Characterization and Viscoelastic Properties of Branched Polymers. *Prog. Polym. Sci. Japan* **1972**, *3*, 263-314.
152. Masuda, T., Nakagawa, Y., Ohta, Y., Onogi, S. Viscoelastic Properties of Concentrated Solutions of Randomly Branched Polystyrenes. *Polymer J.* **1972**, *3* (1), 92-99.
153. Valentine, R. H., Ferry, J. D., Homma, T., Ninomiya, K. Viscoelastic Properties of Polybutadienes - Linear and Lightly Crosslinked Near the Gel Point. *J. Polym. Sci. , Part A-2* **1968**, *6*, 479-492.

154. Graessley, W. W., Shinbach, E. S. Flow Properties of Branched Polydisperse Polymers. *J. Polym. Sci. : Polym. Phys. Ed.* **1974**, *12* (10), 2047-2063.
155. Takahashi, Y., Suzuki, F., Miyachi, M., Noda, I., Nagasawa, M. Zero-Shear Viscosity of Branched Polymer Solutions. *Polymer J.* **1986**, *1968* (18), 1-89.
156. Isono, Y., Fujimoto, T., Kajiura, H., Nagasawa, M. Viscoelastic Properties of Branched Polymers. II. In Concentrated Solutions. *Polymer J.* **1980**, *12* (6), 369-378.
157. Raju, V. R., Rachapudy, H., Graessley, W. W. Properties of Amorphous and Crystallizable Hydrocarbon Polymers. IV. Melt Rheology of Linear and Star-Branched Hydrogenated Polybutadiene. *J. Polym. Sci. : Polym. Phys. Ed.* **1979**, *17* (7), 1223-1235.
158. Lohse, D. J., Milner, S. T., Fetters, L. J., Xenidou, M., Hadjichristidis, N., Mendelson, R. A., Garcia-Franco, C. A., Lyon, M. K. Well-Defined, Model Long Chain Branched Polyethylene. 2. Melt Rheological Behavior. *Macromolecules* **2002**, *35* (8), 3066-3075.
159. Fetters, L. J., Kiss, A. D., Pearson, D. S., Quack, G. F., Vitus, F. J. Rheological Behavior of Star-Shaped Polymers. *Macromolecules* **1993**, *26* (4), 647-654.
160. Edwards, S. F. Statistical Mechanics of Polymerized Material. *Proc. Phys. Soc.* **1967**, *92* (1), 9-16.
161. de Gennes, P. G. Reptation of a Polymer Chain in the Presence of Fixed Obstacles. *J. Chem. Phys.* **1971**, *55* (2), 572-579.
162. de Gennes, P. G. *Scaling Concepts in Polymer Physics*; Cornell Univ. Press: Ithaca, New York, 1979.
163. Doi, M.; Edwards, S. F. *The Theory of Polymer Dynamics*; Oxford Univ. Press: Oxford, England, 1986.
164. Milner, S. T., McLeish, T. C. B. Parameter-Free Theory for Stress Relaxation in Star Polymer Melts. *Macromolecules* **1997**, *30* (7), 2159-2166.
165. Pearson, D. S., Hefland, E. Viscoelastic Properties of Star-Shaped Polymers. *Macromolecules* **1984**, *17* (4), 888-895.
166. Vega, D. A., Sebastian, J. M., Russel, W. B., Register, R. A. Viscoelastic Properties of Entangled Star Polymer Melts: Comparison of Theory and Experiment. *Macromolecules* **2002**, *35* (1), 169-177.
167. Juliani, Archer, L. A. Relaxation Dynamics of Entangled and Unentangled Multiarm Polymer Solutions: Comparisons with Theory. *Macromolecules* **2002**, *35* (27), 10048-10053.
168. Pearson, D. S., Raju, V. R. Configurational and Viscoelastic Properties of Branched Polymers. *Macromolecules* **1982**, *15* (2), 294-298.
169. Graessley, W. W., Roovers, J. Melt Rheology of Four-Arm and Six-Arm Polystyrenes. *Macromolecules* **1979**, *12* (5), 959-965.
170. Graessley, W. W. The Entanglement Concept in Polymer Rheology. *Adv. Polym. Sci.* **1974**, *16*, 1-179.
171. Mendelson, R. A., Bowles, W. A., Finger, F. L. Effect of Molecular Structure on Polyethylene Melt Rheology. II. Shear-Dependent Viscosity. *J. Polym. Sci. , Part A-2* **1970**, *8*, 127-141.

172. Carella, J. M., Graessley, W. W., Fetters, L. J. Effects of Chain Microstructure on the Viscoelastic Properties of Linear Polymer Melts: Polybutadienes and Hydrogenated Polybutadienes. *Macromolecules* **1984**, *17* (12), 2775-2786.
173. Yan, D., Wang, W.-J., Zhu, S. Effect of Long Chain Branching on Rheological Properties of Metallocene Polyethylene. *Polymer* **1999**, *40*, 1737-1744.
174. Mavridis, H., Shroff, R. N. Temperature Dependence of Polyolefin Melt Rheology. *Polym. Eng. Sci.* **1992**, *32* (23), 1778-1791.
175. Shroff, R. N., Mavridis, H. Long-Chain Branching Index for Essentially Linear Polyethylenes. *Macromolecules* **1999**, *32*, 8454-8464.
176. Graessley, W. W. Effect of Long Branches on the Temperature Dependence of Viscoelastic Properties in Polymer Melts. *Macromolecules* **1982**, *15* (4), 1164-1167.
177. Wood-Adams, P., Costeux, S. Thermorheological Behavior of Polyethylene: Effects of Microstructure and Long Chain Branching. *Macromolecules* **2001**, *34* (18), 6281-6290.
178. Rochefort, W. E., Smith, G. G., Rachapudy, H., Raju, V. R., Graessley, W. W. Properties of Amorphous and Crystallizable Hydrocarbon Polymers. II. Rheology of Linear and Star-Branched Polybutadiene. *J. Polym. Sci. : Polym. Phys. Ed.* **1979**, *17* (12), 2767-2775.
179. Gotro, J. T., Graessley, W. W. Model Hydrocarbon Polymers: Rheological Properties of Linear Polyisoprenes and Hydrogenated Polyisoprenes. *Macromolecules* **1984**, *17* (12), 2767-2775.
180. Münstedt, H., Laun, H. M. Elongational Properties and Molecular Structure of Polyethylene Melts. *Rheol. Acta* **1981**, *20* (3), 211-221.
181. Hingmann, R., Marcinke, B. L. Shear and Elongational Flow Properties of Polypropylene Melts. *J. Rheol.* **1994**, *38* (3), 573-587.
182. Ferri, D., Lomellini, P. Melt Rheology of Randomly Branched Polystyrenes. *J. Rheol.* **1999**, *43* (6), 1355-1372.
183. Wood-Adams, P. M., Dealy, J. M. Using Rheological Data To Determine the Branching Level in Metallocene Polyethylenes. *Macromolecules* **2000**, *33* (20), 7481-7488.
184. Kasehagen, L. J., Macosko, C. W. Nonlinear Shear and Extensional Rheology of Long-Chain Randomly Branched Polybutadiene. *J. Rheol.* **1998**, *42* (6), 1303-1327.
185. Gotsis, A. D., Zeevenhoven, B. L. F., Tsenoglou, C. Effect of Long Branches on the Rheology of Polypropylene. *J. Rheol.* **2004**, *48* (4), 895-914.
186. Dealy, J.; Wissbrun, K. F. *Melt Rheology and its Role in Plastics Processing*; Van Nostrand Reinhold: New York, 1989.
187. Prichard, H., Wissbrun, K. F. Reversible Melt Flow Rate Increase of Branched. *J. Appl. Polym. Sci.* **1969**, *13* (1), 233-239.
188. Howells, E. R., Benbow, J. J. Flow Defects in Polymer Melts. *Trans. J. Plast. Inst.* **2004**, *30* (88), 240-253.
189. Rokudai, M., Fujiki, T. Influence of Shearing History on the Rheological Properties and Processability of Branched Polymers. III. An Amorphous Long-Chain Branched Polymer. *J. Appl. Polym. Sci.* **1979**, *23* (11), 3295-3300.

190. Rokudai, M. Influence of Shearing History on the Rheological Properties and Processability of Branched Polymers. V. Effect of Molecular Structural Parameters on Die Swell of Low-Density Polyethylenes. *J. Appl. Polym. Sci.* **1981**, *26* (4), 1427-1429.
191. Laun, H. M. Description of the Non-Linear Shear Behavior of a Low Density Polyethylene Melt by Means of an Experimentally Determined Strain Dependent Memory Function. *Rheol. Acta* **1978**, *17* (1), 1-15.
192. Osaki, K. On the Damping Function of Shear Relaxation Modulus for Entangled Polymers. *Rheol. Acta* **1993**, *32* (5), 429-437.
193. Larson, R. G. A Constitutive Equation for Polymer Melts Based on Partially Extending Strand Convection. *J. Rheol.* **1984**, *28* (5), 545-571.
194. Bick, D. K., McLeish, T. C. B. Topological Contributions to Nonlinear Elasticity in Branched Polymers. *Phys. Rev. Lett.* **1996**, *76* (14), 2587-2590.
195. Kalika, D. S., Denn, M. M. Wall Slip and Extrudate Distortion in Linear Low-Density Polyethylene. *J. Rheol.* **1987**, *31* (8), 815-834.
196. Wood-Adams, P. The effect of long chain branches on the shear flow behavior of polyethylene. *J. Rheol.* **2001**, *45* (1), 203-210.
197. Rudin, A., Grinshpun, V., O'Driscoll, K. F. Long Chain Branching in Polyethylene. *J. Liq. Chromatogr.* **1984**, *7* (9), 1809-1821.
198. Bovey, F. A., Schilling, F. C., McCrackin, F. L., Wagner, H. L. Short-Chain and Long-Chain Branching in Low-Density Polyethylene. *Macromolecules* **1976**, *9* (1), 76-80.
199. Randall, J. C. Characterization of long-chain branching in polyethylenes using high-field ¹³C-NMR. *ACS Symposium Series* **1980**, *142*, 93-118.
200. Shroff, R. N., Mavridis, H. Assessment of NMR and Rheology for the Characterization of LCB in Essentially Linear Polyethylenes. *Macromolecules* **2001**, *34* (21), 7362-7367.
201. Jordan, E. A., Donald, A. M., Fetters, L. J., Klein, J. Transition from Linear to Star-Branched Diffusion in Entangled Polymer Melts. *Polym. Prepr.* **1989**, *30* (1), 63-64.
202. De Pooter, M., Smith, P. B., Dohrer, K. K., Bennett, K. F., Meadows, M. D., Smith, C. G., Schouwenaars, H. P., Geerards, R. A. Determination of the Composition of Common Linear Low Density Polyethylene Copolymers by ¹³C-NMR Spectroscopy. *J. Appl. Polym. Sci.* **1991**, *42* (2), 399-408.
203. Hansen, E. W., Blom, R., Bade, O. M. NMR Characterization of Polyethylene with Emphasis on Internal Consistency of Peak Intensities and Estimation of Uncertainties in Derived Branch Distribution Numbers. *Polymer* **1997**, *38* (17), 4295-4304.
204. Wang, W.-J., Yan, D., Zhu, S., Hamielec, A. E. Kinetics of Long Chain Branching in Continuous Solution Polymerization of Ethylene Using Constrained Geometry Metallocene. *Macromolecules* **1998**, *31* (25), 8677-8683.
205. Wang, W.-J., Yan, D., Charpentier, P. A., Zhu, S., Hamielec, A. E., Sayer, B. G. Long-Chain Branching in Ethylene Polymerization Using Constrained Geometry Metallocene Catalyst. *Macromol. Chem. Phys.* **1998**, *199* (11), 2409-2416.

206. Malmberg, A., Kokko, E., Lehmus, P., Löfgren, B., Seppälä, J. V. Long-Chain Branched Polyethylene Polymerized by Metallocene Catalysts Et[Ind]2ZrCl2/MAO and Et[IndH4]2ZrCl2/MAO. *Macromolecules* **1998**, *31* (24), 8448-8454.
207. Montaudo, G.; Montaudo, M. S. Polymer characterization methods. In *Mass Spectrometry of Polymers*; CRC Press: New York, 2002; 41-112.
208. Moore, J. C. Gel Permeation Chromatography. I. New Method for Molecular-Weight Distribution of High Polymers. *J. Polym. Sci.* **1964**, *1964* (2), 2-835.
209. Mori, S.; Barth, H. G. *Size Exclusion Chromatography*; Springer: New York, 1999.
210. Sun, T., Chance, R. R., Graessley, W. W., Lohse, D. J. A Study of the Separation Principle in Size Exclusion Chromatography. *Macromolecules* **2004**, *37* (11), 4304-4312.
211. Grubisic, Z., Rempp, P., Benoit, H. Universal Calibration for Gel Permeation Chromatography. *J. Polym. Sci.* **1967**, *5* (9), 753-759.
212. Flory, P. J., Fox, T. G. Treatment of Intrinsic Viscosities. *J. Am. Chem. Soc.* **1951**, *73*, 1904-1908.
213. Stogiou, M., Kapetanaki, C., Iatrou, H. Examination of the Universality of the Calibration Curve of Size Exclusion Chromatography by Using Polymers Having Complex Macromolecular Architectures. *Int. J. Polym. Anal. Charact.* **2002**, *7*, 273-283.
214. Drott, E. E., Mendelson, R. A. Determination of Polymer Branching with Gel-Permeation Chromatography. I. Theory. *J. Polym. Sci. : Polym. Phys. Ed.* **1970**, *8*, 1361-1371.
215. Drott, E. E., Mendelson, R. A. Determination of Polymer Branching with Gel-Permeation Chromatography. II. Experimental Results for Polyethylene. *J. Polym. Sci. : Polym. Phys. Ed.* **1970**, *8*, 1373-1385.
216. Ram, A., Miltz, J. New Method for Molecular Weight Distribution (MWD) Determination in Branched Polymers. *J. Appl. Polym. Sci.* **1971**, *15* (11), 2639-2644.
217. Kurata, M., Okamoto, H., Iwama, M., Abe, M., Homma, T. Randomly Branched Polymers. II. Computer Analysis of the Gel-Permeation Chromatogram. *Polymer J.* **1972**, *3* (6), 739-748.
218. Grubisic-Gallot, Z., Picot, M., Gramain, Ph., Benoit, H. Characterization of Homopolymers and Copolymers by Coupling of Gel Permeation Chromatography and Automatic Viscometry. *J. Appl. Polym. Sci.* **1972**, *16* (11), 2931-2945.
219. Meunier, J. C., Gallot, Z. Study of Starlike Polymers Using a Gel Permeation Chromatography Apparatus with a Viscometric Detector. *Makromol. Chem.* **1972**, *156*, 117-120.
220. Servotte, A., De Bruille, R. Determination of Long-Chain Branching Distribution in Polyethylene by Combination of Gel Permeation Chromatography and Viscometry. *Makromol. Chem.* **1975**, *176*, 203-212.
221. Constantin, D. Coupling of Gel Permeation Chromatography and Automatic Viscometry. Application to the Study of Long Chain Branched Polyethylene. *Eur. Polym. J.* **1977**, *13* (11), 907-913.

222. Mirabella, F. M., Jr., Wild, L. Determination of Long-Chain Branching Distributions of Polyethylenes by Combined Viscometry-Size Exclusion Chromatography Technique. *Polym. Mater. Sci. Eng.* **1988**, *59*, 7-11.
223. Kato, T., Kanda, A., Takahashi, A., Noda, I., Maki, S., Nagasawa, M. Determination of the Degree of Branching of Comb-Shaped Branched Polystyrenes by a GPC/LS Method. *Polymer J.* **1979**, *11* (7), 575-581.
224. Jordan, R. C., McConnell, M. L. Characterization of branched polymers by size exclusion chromatography with light scattering detection. *ACS Symposium Series* **1980**, *138*, 107-129.
225. Hamielec, A. E., Ouano, A. C., Nebenzahl, L. L. Characterization of branched poly(vinyl acetate) by GPC and low angle laser light scattering photometry. *J. Liq. Chromatogr.* **1978**, *1* (4), 527-554.
226. Grinshpun, V., Rudin, A., Potter, D. Comments on the Measurement of Long Chain Branching by Size Exclusion Chromatography. *Polym. Bull.* **1985**, *13* (1), 71-75.
227. Rudin, A. Measurement of long-chain branch frequency in synthetic polymers. *Chemical Analysis* **1991**, *113*, 103-112.
228. Hamielec, A. E., Ouano, A. C. Generalized Universal Molecular Weight Calibration Parameter in GPC. *J. Liq. Chromatogr.* **1978**, *1* (1), 111-120.
229. Podzimek, S. The Use of GPC Coupled with a Multiangle Laser Light Scattering Photometer for the Characterization of Polymers. On the Determination of Molecular Weight, Size, and Branching. *J. Appl. Polym. Sci.* **1994**, *54* (1), 91-103.
230. Vilenchik, L., Ayotte, R. New developments in Liquid-Chromatographic Analysis of Branched Polymers. *J. Appl. Polym. Sci. : Appl. Polym. Symp.* **1992**, *51*, 73-90.
231. Pang, S., Rudin, A. Size-exclusion chromatographic assessment of long-chain branch frequency in polyethylenes. *ACS Symposium Series* **1993**, *521*, 254-269.
232. Wintermantel, M., Antonietti, M., Schmidt, M. Structure Determination of Polymers by Size-Exclusion Chromatography Equipped with Multiangle Light Scattering and Viscosity Detectors. *J. Appl. Polym. Sci. : Appl. Polym. Symp.* **1993**, *52*, 91-103.
233. Mourey, T. H., Vu, K. A., Balke, S. T. Use of multidetector SEC for determining local polydispersity. *ACS Symposium Series* **1999**, *731*, 20-34.
234. Yau, W. W., Gillespie, D. New Approaches Using MW-Sensitive Detectors in GPC-TREF for Polyolefin Characterization. *Polymer* **2001**, *42* (21), 8947-8958.
235. Lu, J., Hammons, K., Sue, H.-J., Yau, W. W. Investigation of Long-Chain Branching in HDPE Using Triple-Detector GPC. *ANTEC - Soc. Plast. Eng.* **2002**, *60* (2), 2051-2055.
236. Lapienis, G., Penczek, S. Multibranching Star-Shaped Polyethers. *Macromol. Symp.* **2003**, *195*, 317-327.
237. Striegel, A. M. Influence of chain Architecture on the Mechanochemical Degradation of Macromolecules. *J. Biochem. Biophys. Methods* **2003**, *56*, 117-139.

238. Mourey, T. H., Balke, S. T. Detecting Local Polydispersity with Multidetector SEC from Reconstructed DRI Chromatograms. *J. Appl. Polym. Sci.* **1998**, *70* (4), 831-835.
239. Thitiratsakul, R., Balke, S. T., Mourey, T. H., Schunk, T. C. Detecting "Perfect Resolution" Local Polydispersity in Size Exclusion Chromatography. *Int. J. Polym. Anal. Charact.* **1998**, *4* (4), 357-377.
240. Balke, S. T., Mourey, T. H., Karami, A. Evaluating Size Exclusion Chromatography Fractionation. *Int. J. Polym. Anal. Charact.* **2000**, *6* (1), 13-33.
241. Balke, S. T., Mourey, T. H. Local Polydispersity Detection in Size Exclusion Chromatography: Method Assessment. *J. Appl. Polym. Sci.* **2001**, *81* (2), 370-383.
242. Giddings, J. C. Field-Flow Fractionation: Analysis of Macromolecular, Colloidal, and Particulate Materials. *Science* **1993**, *260* (5113), 1456-1465.
243. Giddings, J. C. The field-flow fractionation family: underlying principles. In *Field-Flow Fractionation Handbook*; John Wiley: New York, 2000; 3-30.
244. White, R. J. FFF-MALS - A New Tool for the Characterization of Polymers and Particles. *Polymer Int.* **1997**, *43* (4), 373-379.
245. Schimpf, M. E., Giddings, J. C. Measurement of Effects of Polymer Composition and Solvent Parameters on Thermal Field-Flow Fractionation. *Polym. Prepr.* **1986**, *27* (2), 158-160.
246. Schimpf, M. E., Giddings, J. C. Characterization of Thermal Diffusion in Polymer Solutions by Thermal Field-Flow Fractionation: Effects of Molecular Weight and Branching. *Macromolecules* **1987**, *20* (7), 1561-1563.
247. Podzimek, S., Vlcek, T., Johann, C. Characterization of Branched Polymers by Size Exclusion Chromatography Coupled with Multiangle Light Scattering Detector. I. Size Exclusion Chromatography Elution Behavior of Branched Polymers. *J. Appl. Polym. Sci.* **2001**, *81* (7), 1588-1594.
248. Lee, H. C., Chang, T. Polymer Molecular Weight Characterization by Temperature Gradient High Performance Liquid Chromatography. *Polymer* **1996**, *37* (25), 5747-5749.
249. Lee, W., Lee, H. C., Chang, T., Kim, S. B. Characterization of Poly(methyl methacrylate) by Temperature Gradient Interaction Chromatography with On-Line Light Scattering Detection. *Macromolecules* **1998**, *31* (2), 344-348.
250. Chang, T. Recent Advances in Liquid Chromatography Analysis of Synthetic Polymers. *Adv. Polym. Sci.* **2003**, *163*, 1-60.
251. Lee, H. C., Chang, T., Harville, S., Mays, J. W. Characterization of Linear and Star Polystyrene by Temperature-Gradient Interaction Chromatography with a Light-Scattering Detector. *Macromolecules* **1998**, *31* (3), 690-694.
252. Lee, H. C., Lee, W., Chang, T., Yoon, J. S., Frater, D. J., Mays, J. W. Linking Reaction Kinetics of Star Shaped Polystyrene by Temperature Gradient Interaction Chromatography. *Macromolecules* **1998**, *31* (13), 4114-4119.
253. Perny, S., Allgaier, J., Cho, D., Lee, W., Chang, T. Synthesis and Structural Analysis of an H-Shaped Polybutadiene. *Macromolecules* **2001**, *34* (16), 5408-5415.

254. Cho, D., Park, S., Chang, T., Avgeropoulos, A., Hadjichristidis, N. Characterization of a 4-miktoarm Star Copolymer of the (PS-b-PI)₃ PS Type by Temperature Gradient Interaction Chromatography. *Eur. Polym. J.* **2003**, *39* (11), 2155-2160.
255. Park, S., Cho, D., Im, K., Chang, T., Uhrig, D., Mays, J. W. Utility of Interaction Chromatography for Probing Structural Purity of Model Branched Copolymers: 4-Miktoarm Star Copolymer. *Macromolecules* **2003**, *36* (15), 5834-5838.
256. Im, K., Park, S., Cho, D., Chang, T., Lee, K., Choi, N. HPLC and MALDI-TOF MS Analysis of Highly Branched Polystyrene: Resolution Enhancement by Branching. *Anal. Chem.* **2004**, *76* (9), 2638-2642.
257. Scoria, M. J., R. Dhib, and A. Penlidis *Journal of Macromolecular Science Pure and Applied Chemistry* 2005; **A42** (4), 403-426.
258. Gabriel, C., Münstedt, H. Influence of Long-Chain Branches in Polyethylenes on Linear Viscoelastic Flow Properties in Shear. *Rheol. Acta* **2002**, *41* (3), 232-244.
259. Lusignan, C. P., Mourey, T. H., Wilson, J. C., Colby, R. H. Viscoelasticity of Randomly Branched Polymers in the Critical Percolation Class. *Phys. Rev. E* **1995**, *52* (6), 6271-6280.
260. Lusignan, C. P., Mourey, T. H., Wilson, J. C., Colby, R. H. Viscoelasticity of Randomly Branched Polymers in the Vulcanization Class. *Phys. Rev. E* **1999**, *60* (5), 5657-5669.
261. Janzen, J., Colby, R. H. Diagnosing Long-Chain Branching in Polyethylenes. *J. Molecul. Struct.* **1999**, *485-486*, 569-584.
262. Shroff, R., Mavridis, H. New Measures of Polydispersity from Rheological Data on Polymer Melts. *J. Appl. Polym. Sci.* **1995**, *57* (13), 1605-1626.
263. Lai, S., Plumley, T. A., Butler, T. I., Knight, G. W., Kao, C. I. Dow Rheology Index (DRI) for Insite Technology Polyolefins (ITP): Unique Structure-Processing Relationships. *ANTEC - Soc. Plast. Eng.* **1994**, *52* (2), 1814-1815.
264. Shaw, M. T., Tuminello, W. H. A Closer Look at the MWD-Viscosity Transform. *Polym. Eng. Sci.* **1994**, *34* (2), 159-165.
265. Wood-Adams, P., Dealy, J. M., deGroot, A. W., Redwine, O. D. Effect of Molecular Structure on the Linear Viscoelastic Behavior of Polyethylene. *Macromolecules* **2000**, *33* (20), 7489-7499.
266. Karjala, T. P., Sammler, R. L., Huang, W., Mangnus, M. A., Johnson, M. S. Rheological Methods for the Detection of Low Levels of Long-Chain Branching in Polyolefins. *ANTEC - Soc. Plast. Eng.* **2004**, *62* (1), 1018-1022.
267. Trinkle, S., Friedrich, C. Van Gorp-Palmen-Plot: A Way to Characterize Polydispersity of Linear Polymers. *Rheol. Acta* **2001**, *40* (4), 322-328.
268. Trinkle, S., Walter, P., Friedrich, C. Van Gorp-Palmen Plot II - Classification of Long Chain Branched Polymers by their Topology. *Rheol. Acta* **2002**, *41* (1-2), 103-113.
269. Wasserman, S. H., Graessley, W. W. Prediction of Linear Viscoelastic Response for Entangled Polyolefin Melts from Molecular Weight Distribution. *Polym. Eng. Sci.* **1996**, *36* (6), 853-861.

270. van Gorp, M., Palmen, J. Time-Temperature Superposition for Polymeric Blends. *Rheol. Bull.* **1998**, *67*, 5-8.
271. Bin Wadud, S. E., Baird, D. G. Shear and Extensional Rheology of Sparsely Branched Metallocene-Catalyzed Polyethylenes. *J. Rheol.* **2000**, *44* (5), 1151-1167.
272. Berger, L., Meissner, J. Linear Viscoelasticity, Simple and Planar Melt Extension of Linear Polybutadienes with Bimodal Molar Mass Distributions. *Rheol. Acta* **1992**, *31* (1), 63-74.
273. Münstedt, H. Dependence of the Elongational Behavior of Polystyrene Melts on Molecular Weight and Molecular Weight Distribution. *J. Rheol.* **1980**, *24* (6), 847-867.
274. Takahashi, T., Takimoto, J., Koyama, K. Elongational Viscosity for Miscible and Immiscible Polymer Blends. II. Blends with a Small Amount of UHMW Polymer. *J. Appl. Polym. Sci.* **1999**, *72*, 961-969.

CHAPTER 3 - EXPERIMENTAL METHODS

3.1 Initiator Selection

Produced by ATOFINA Chemicals Inc., Luperox JWEB50 is a multifunctional initiator with four monoperoxycarbonate functional groups. Its structure and decomposition are shown in Figure 3.1 with the R group shown in the diagram being a linkage ATOFINA has kept proprietary. JWEB50 is shipped in a 50 wt. % solution of ethyl benzene and has a molecular weight of 965.0 g/mol. With respect to the tetrafunctional initiator's thermal stability, the functional groups are found to have 1-hour and 10-hour half-life temperatures of 119 °C and 100 °C in ethyl benzene and an approximate 1-hour half-life temperature of 121 °C in dodecane.

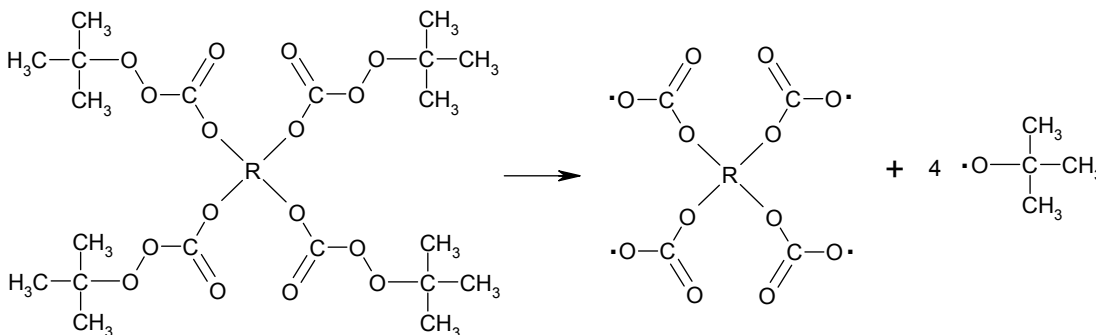


Figure 3.1. Decomposition of tetrafunctional initiator, JWEB50.

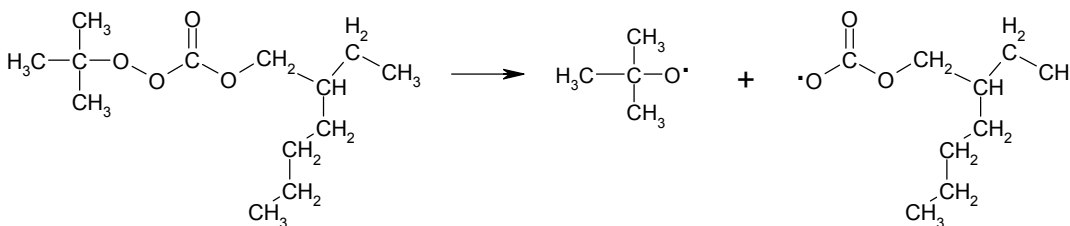


Figure 3.2. Decomposition of monofunctional initiator, TBEC.

In order to examine the effect of initiator functionality, a suitable monofunctional initiator had to be chosen such that when varying initiator type, there would be minimal variation in structure and stability of the labile groups. As such, the monofunctional counterpart used in this study is tert-butylperoxy 2-ethylhexyl carbonate (Luperox TBEC, ATOFINA Chemicals Inc.). Figure 3.2 shows the structure and decomposition of TBEC. This monofunctional initiator has a similar thermal stability to JWEB50 as it has 1-hour and 10-hour half life temperatures of 121 °C and 100 °C in dodecane. Luperox TBEC is diluted with 5 wt. % of 2-ethylhexanol.

The decarboxylation of the alkoxy-carbonyloxy radicals is not shown in Figures 3.1 and 3.2 as past studies have found that the rate of this step is relatively slow and is not competitive with the addition of an alkene (1, 2).

3.2 Reagent Purification

Monomers (styrene, methyl methacrylate, α -methyl styrene and butyl acrylate) (Sigma-Aldrich Canada Ltd.) were washed three times with a 10 w/v % sodium hydroxide solution, washed three times with distilled water, dried over calcium chloride and distilled under vacuum. Purification of vinyl acetate did not involve washing with sodium hydroxide solution or distilled water as it is highly water soluble. Solvents such as ethanol, dichloromethane, and toluene used during the course of the experiment and both initiators (JWEB50 and TBEC) were used as received from suppliers without further purification. Dodecanethiol which was used as a chain transfer agent and hydroquinone as a radical inhibitor were also used in experiments without further purification.

3.3 Polymer Synthesis

Ampoule experiments were completed in borosilicate glass ampoules (capacity ~4 mL). Reagents were weighed, mixed and pipetted into ampoules. Ampoules were then degassed by several vacuum-freeze-thaw cycles, sealed under vacuum with a gas/oxygen torch and then immersed in a silicone oil bath having a temperature control of ± 0.1 °C. Ampoules were removed at selected time intervals to ensure a well-defined conversion

versus time plot. Once removed from the bath, the ampoules were placed in liquid nitrogen to stop the polymerization. Ampoules were then thawed, weighed, opened and the contents poured into a flask containing ethanol to precipitate the polymer and facilitate the removal of residual monomer. A small amount of radical inhibitor (hydroquinone) was added to prevent any radical formation and further reactions. The weights of the empty ampoules were recorded. For the higher conversion levels where it became difficult to remove the reaction mixture, the ampoules were not thawed before being opened. In these cases, a frozen piece of the reaction mixture was removed from the ampoule, weighed, allowed to dissolve in a dichloromethane with hydroquinone and then precipitated with ethanol before being dried in a vacuum oven.

3.4 Polymer Characterization

A general explanation of the various analytical methods used for polymer characterization is given in this section. A more detailed description is given in the chapters dealing with the discussion of experimental results (Chapters 4-7).

3.4.1 Size Exclusion Chromatography

Size exclusion chromatography (SEC), also referred to as gel permeation chromatography (GPC), is the most popular and convenient method for determining the average molecular weight and molecular weight distribution (MWD) of a polymer. As its name implies SEC works on the principle of size exclusion. A very low concentration polymer solution is passed through a column of porous particles. As shown in Figure 3.3, the molecules that are too large cannot enter the pores of the packing and as such, they elute first. Smaller molecules that can penetrate or diffuse into the pores are retained in the column and elute at a later time. Thus a sample is fractionated by molecular hydrodynamic volume and the resulting profile describes the molecular weight distribution. A concentration detector (e.g., differential refractometer (RI) or UV detector) is placed downstream of the columns to measure the concentration of each fraction as a function of time. The actual method for determining the molecular weight averages and the MWD depend upon the presence of any accompanying detectors.

Comprehensive references have been written on the various methods of MWD determination from SEC (3).

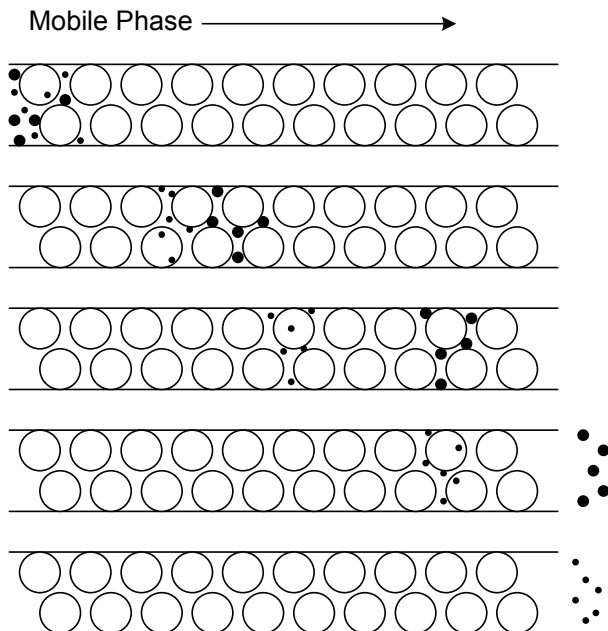


Figure 3.3. Diagram representing the separation of low and high molecular weight polymer molecules.

In this study, two SEC setups were employed in the characterization of polymer samples. Both systems were maintained at 30°C with tetrahydrofuran as the mobile phase flowing at a rate of 1.0 mL/min. The first setup included an RI detector followed by a multi-angle laser light scattering (MALLS) detector while the second system consisted of an RI detector, low-angle (LALS) and right-angle (RALS) laser light scattering detectors, a UV detector and a viscometer. Both the MALLS and LALS provide a “true” estimate of the molecular weight; however, it is only the MALLS that allows for the calculation of the radius of gyration. Light scattered at an angle θ from a volume of very dilute macromolecular solution is governed by the following equation:

$$\frac{Kc}{R_{\theta}} = \frac{1}{MP(\theta)} + 2A_2c + \dots \quad 3.1$$

where c is the concentration of polymer molecules, R_θ is the excess Rayleigh ratio at angle θ , M is the molecular weight, $P(\theta)$ is the particle scattering function and A_2 is the second virial coefficient. K is a constant for vertically polarized incident light,

$$K = \frac{4\pi^2 n_0^2}{\lambda_0^4 N_A} \left(\frac{dn}{dc} \right)^2 \quad 3.2$$

n_0 is the refractive index of the solvent for the given wavelength λ_0 in a vacuum, N_A is Avogadro's number and dn/dc is the specific refractive index increment of the polymer in a given solvent at a specific wavelength. Values of dn/dc are reported in the literature (4). Higher order concentrations terms are typically ignored in equation 3.1 and in the analysis of SEC data, even the $2A_2c$ term is dropped because sufficiently low concentrations are used. The particle scattering function is defined as:

$$P(\theta) = \frac{R_\theta}{R_0} \quad 3.3$$

where R_θ and R_0 are the excess Rayleigh ratios at the angle of observation θ and zero. The particle scattering function accounts for the interference of light scattered from different points on the same molecule and thus can be used to provide information about a molecule's size.

$$P(\theta) \approx 1 + \frac{16\pi^2}{3\lambda^2} \sin^2\left(\frac{\theta}{2}\right) \langle r_g^2 \rangle \quad 3.4$$

λ is the wavelength of incident light in a given solvent ($\lambda = \lambda_0/n_0$) and $\langle r_g^2 \rangle$ is the mean square radius ($\langle r_g^2 \rangle = R_g^2$). In the case of LALS, a very low angle is used such that $P(\theta) \approx 1$ and Equation 3.1 can be used to calculate the molecular weight. With MALLS, however, the excess Rayleigh ratio is measured at various angles and a plot of R_θ/Kc as a

function of $\sin^2(\theta/2)$ allows for the determination of the molecular weight (intercept) and radius of gyration (slope).

3.4.2 ^1H -Nuclear Magnetic Resonance

In the case of comonomer feeds, polymer composition was determined by ^1H -NMR using a Bruker AVANCE 500 NMR spectrometer. Deuterated chloroform was used as the solvent and the measurements were taken at room temperature. The relative amounts of each monomer incorporated in the copolymer were estimated from absorption peaks of the spectra. In the case of methyl methacrylate, the three protons in the $-\text{OCH}_3$ group were found at $\delta = 3.6$ ppm while for α -methyl styrene and styrene the five protons in the $-\text{C}_6\text{H}_5$ group were taken at 6.7-7.3 ppm.

3.4.3 Differential Scanning Calorimetry (DSC)

Differential scanning calorimetry is a technique employed to measure the enthalpic changes in a sample. Thermal transitions such as the melting of a crystalline polymer or the glass transition can be observed by monitoring the energy supplied as a function of temperature. The polymers produced in this study are non-crystalline and therefore, do not exhibit any crystallization or melting transitions. A Q100 DSC (TA Instruments) was used to determine the glass transition temperature, T_g , of the polymer samples. A standard heating rate of $10^\circ\text{C}/\text{min}$ was chosen.

3.4.4 Soxhlet Extraction

In the characterization of poly(butyl acrylate) samples, soxhlet extractions were used to separate the insoluble gel fraction from the uncrosslinked sol fraction. Figure 3.4 provides a diagram of a soxhlet extraction setup. A solvent reservoir is heated such that a suitable amount of vapour can be condensed overhead of the thimble. The warm solvent then flows over the polymer in the paper thimble dissolving and extracting the soluble fraction of the polymer sample. When enough vapour has been condensed, the solvent will drain through the siphon tube into the solvent reservoir.

Due to the fact that such low amounts of polymer were used, losses in the weight of the paper thimble during the procedure hindered the determination of reliable gel contents. For this reason, prior to the extraction process, the paper thimbles were placed inside the apparatus, refluxed with toluene for one hour, dried under vacuum and then weighed. In the extraction procedure, toluene was refluxed over approximately 1 gram of polymer for 8 hours. The thimble and insoluble polymer were removed from the setup, dried under vacuum and then weighed to allow for the calculation of the gel content. The soluble fraction of the polymer was recovered from the solvent reservoir and analyzed with SEC.

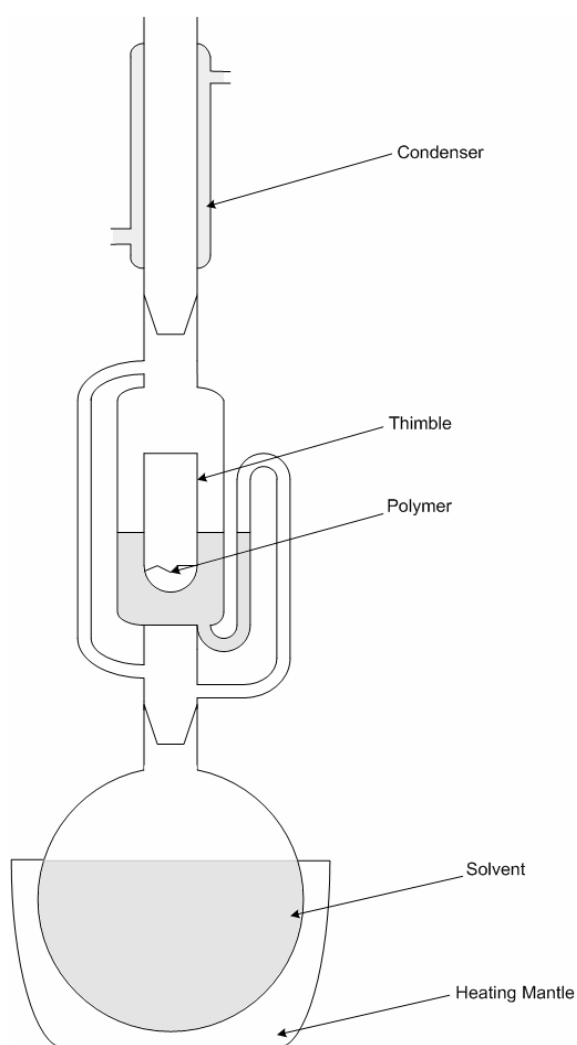


Figure 3.4. Soxhlet extraction apparatus.

3.4.5 Rheological characterization

The rheological properties of a polymer are not only important as they help to decide the type of application a polymer may have but they can also provide insight into a polymer's molecular properties. The manner in which polymers deform when forces are applied depends upon numerous factors including composition, molecular weight, molecular weight distribution and molecular architecture. Although exact relationships between rheological and molecular properties are not always available, comparisons of the behaviour of various polymers are useful in finding differences that other characterization methods may not detect (e.g., branching).

Polymers exhibit a behaviour that is a combination of solid-like and liquid-like characteristics known as viscoelasticity. The simplest and most commonly measured type of this behaviour is linear viscoelasticity. In this situation, the deformation is sufficiently small that the polymer molecules are only negligibly disturbed from their equilibrium configuration and entanglement state. The linear viscoelastic region of a polymer is determined by performing a strain sweep. The limit of the linear region is found when certain viscoelastic properties are no longer constant but vary with strain.

3.4.5.1 Oscillatory Shear Experiments

Oscillatory shear experiments are the most prevalent means for measuring the linear viscoelastic properties of a polymer. In such an experiment, a thin disc is deformed according to oscillatory shear strain and the shear stress is measured.

$$\gamma(t) = \gamma_o \sin(\omega t) \quad 3.5$$

$$\sigma(t) = \sigma_o \sin(\omega t + \delta) \quad 3.6$$

where γ_o is the strain amplitude, σ_o is the stress amplitude, ω is the frequency and δ is the phase shift. The shear stress can also be represented as:

$$\sigma(t) = \gamma_o [G'(\omega) \sin(\omega t) + G''(\omega) \cos(\omega t)] \quad 3.7$$

where $G'(\omega)$ is the storage (elastic) modulus and $G''(\omega)$ is the loss (viscous) modulus. The phase shift or loss angle is simply given by:

$$\tan \delta = \frac{G''}{G'} \quad 3.8$$

For a completely elastic material, $G''=0$ while for a perfectly viscous fluid, $G'=0$. From the storage and loss modulus, other material properties such as the complex modulus (G^*), compliance (J^*) and viscosity (η^*) can be calculated. Using the Cox-Merz rule, the complex viscosity versus frequency plot can be viewed as a viscosity versus shear rate plot.

Figure 3.5 is an illustration of typical curves for $G'(\omega)$ for three different polymers. At high frequencies (equivalent to short time spans), polymer molecules do not have sufficient enough time to accommodate the sudden strain and only very small scale molecular motions occur (i.e., bond distortion). This segment of the curve is called the glassy region and it is not dependent on molecular weight or MWD. As the frequency is lowered, a transition zone is observed and molecular rearrangement becomes possible during a cycle. In the case of material A, the transition zone is followed by a terminal zone where $G'(\omega)$ drops dramatically. For material B which has a much higher molecular weight we find that there is a plateau separating the transition and terminal regions. Material C shows the effect of polydispersity where we do not observe a well-defined plateau nor a clear transition to the terminal region. The appearance of a plateau is found for those polymers with a sufficiently high molecular weight to produce entanglements. These entanglements reproduce the effect produced by cross-linked or rubbery materials. Figure 3.6 is a sketch of the storage and loss modulus for material B. At low frequencies, the viscous response (G'') dominates while at higher frequencies, the elastic response (G') is more important. An important point to note is that G'' passes through a minimum while G' has a plateau indicating that very little dissipation of energy occurs in this region.

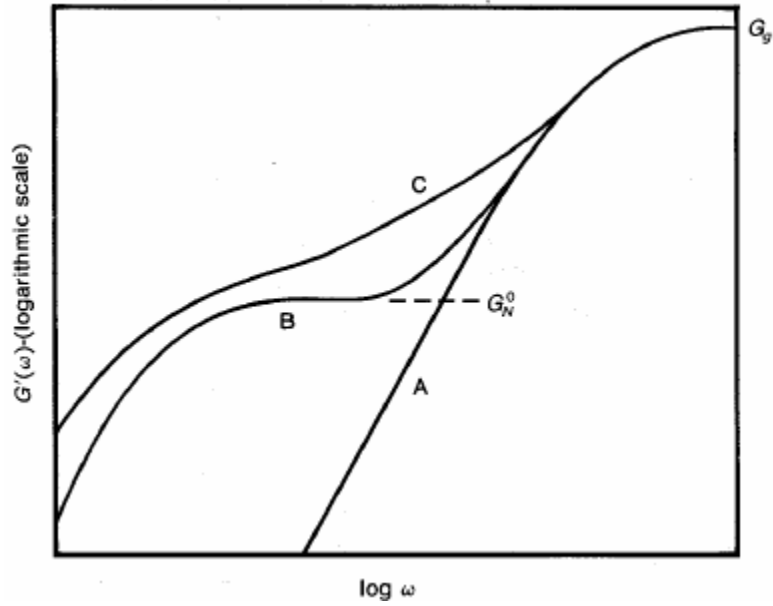


Figure 3.5. Examples of the storage modulus for three linear polymers. A is monodisperse with a low molecular weight. B is monodisperse with a high molecular weight. C is polydisperse with a high molecular weight. Taken from ref. (5).

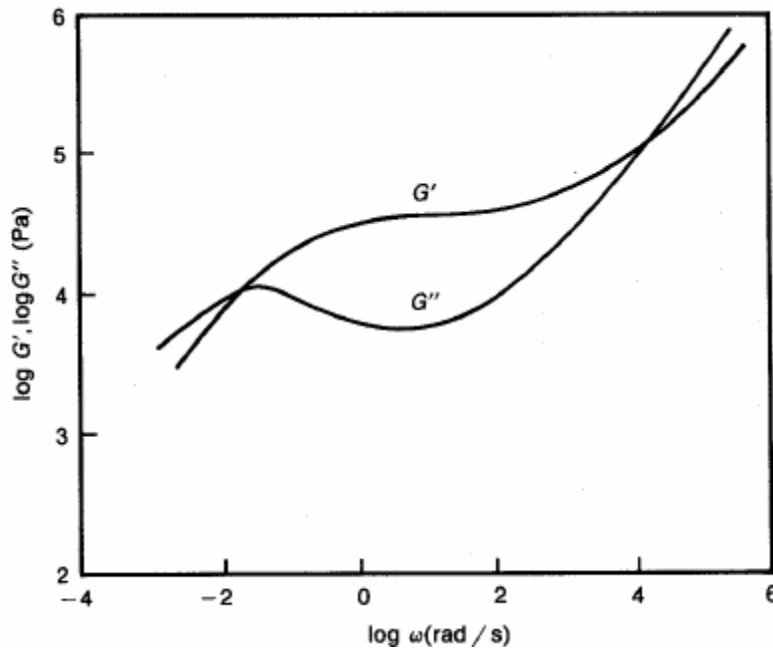


Figure 3.6. Typical storage and loss modulus curves for a monodisperse high molecular weight polymer. Taken from ref. (5).

Aside from frequency, temperature is another important variable that affects rheological properties. It has been found that both frequency and temperature are related. The glassy behaviour observed at high frequencies is similar to the effect produced at low temperatures. As well, at lower frequencies polymer chains have time to relax and a terminal region is achieved that can be reproduced by increasing the temperature. Past studies have found that the rheological data collected at several temperatures could be brought together to form a single “master” curve. The relationship is known as time-temperature superposition (TTS). From a practical viewpoint, this allows for the construction of curves over a wider range of frequencies than is realistically possible when data is collected for a fixed temperature. By raising the temperature, information about the lower frequency regions can be measured without performing extremely long experiments.

Oscillatory shear experiments were performed on a TA Instruments AR2000 rheometer with a parallel-plate geometry (2.5 cm diameter). An environmental test chamber was used to maintain the temperature and allowed an inlet of 10 L/min of N₂ to prevent polymer degradation. The plate gap was set to approximately 2 mm. Strain sweeps were carried out to determine the limit of the linear viscoelastic region before conducting frequency sweeps from 0.01 Hz to 100 Hz for varying temperatures. After completing the frequency sweep at the highest temperature, a frequency sweep was done again at the lowest temperature. Good reproducibility between the two experiments for the lower temperature ensured that no polymer degradation occurred. As well, SEC analysis was performed on the samples after rheological testing to verify that no cross-linking or degradation occurred.

3.4.5.2 Shear Creep Experiments

Another useful rheological test is the creep experiment where a material, initially in its equilibrium state, is subjected to a constant shear stress. The shear strain is then measured as a function of time and the material function, the compliance, may be determined as follows:

$$J(t) = \frac{\gamma(t)}{\sigma} \quad 3.9$$

The creep test is a simple method to study the linear viscoelastic region over a broad time range. As a result, it is useful in providing information about the terminal region (e.g., zero shear viscosity) that may not be easily obtained from oscillatory shear experiments. For a melt, the shear rate will eventually become constant and at long times the compliance is given by

$$J(t) = J_e^0 + \frac{t}{\eta_0} \quad 3.10$$

A TA Instruments AR2000 rheometer with environmental test chamber was used in the creep test of polystyrene and poly(methyl methacrylate) samples. A 2.5 cm parallel-plate geometry was used with a plate gap of approximately 2 mm. Similar precautions and testing of polymer degradation to the oscillatory experiments was performed. The linear viscoelastic region was found by conducting creep experiments with incrementing levels of shear stress. The limit of the linear region was found when the shear stress began to influence the compliance.

3.5 References

1. Watanabe, Y., Ishigaki, H., Okada, H., Suyama, S. Study on radical chemistry of monoperoxycarbonates by alpha-methylstyrene dimer trapping technique. *Polymer Journal* **1998**, *30* (3), 192-196.
2. Mekarbane, P. G., Tabner, B. J. An EPR spin-trap study of the radicals present during the thermolysis of some novel monoperoxycarbonates and peroxydicarbonates. *Journal of the Chemical Society-Perkin Transactions 2* **2000**, (7), 1465-1470.
3. Mori, S.; Barth, H. G. *Size Exclusion Chromatography*; Springer: New York, 1999.
4. Brandrup, J.; Immergut, E. H.; Grulke, E. A. *Polymer Handbook*; Wiley: New York, 1999.
5. Dealy, J.; Wissbrun, K. F. *Melt Rheology and its Role in Plastics Processing*; Van Nostrand Reinhold: New York, 1989.

CHAPTER 4 - POLYMERIZATION OF METHYL METHACRYLATE

4.1 Introduction

Due to the nature of free radical polymerization, high rates of polymer production and high molecular weights cannot always be obtained. From research done on monofunctional initiators, the polymerization mechanism shows that attempts to increase the rate of polymerization will cause a decrease in the molecular weight according to the following equation (1):

$$v = \frac{k_p^2 [M]^2}{k_t R_p} \quad (4.1)$$

where v is the kinetic chain length defined as the average number of monomer molecules consumed by each radical; k_p and k_t are the propagation and termination rate constants, respectively; $[M]$ is the monomer concentration; and R_p is the rate of polymerization. The kinetic chain length is a measure of the polymer molecular weight and as seen by the above equation, it is inversely proportional to the rate of polymerization. Due to this relationship, the possibilities of increasing production rate without affecting the molecular weight are limited. Manufacturers are left with a few possible solutions such as changing the reactor design or employing a finishing catalyst to increase conversion. In the case of the former, the capital costs can be too great with adverse effects on molecular weight and branching, while the latter only produces a marginal increase in production (2).

Multifunctional initiators are another possible solution, as one of their main benefits is that they allow higher rates of polymerization while increasing or maintaining similar molecular weights when compared to a monofunctional counterpart. Their second advantage is that if the initiator has a functionality greater than two, branching such as

star polymers can be introduced into the final product. Star polymers are the most elementary group of branched molecules since there is only one branching point. These polymers have found applications in several areas such as rheological modifiers and pressure sensitive adhesives (3). From the standpoint of polymer-stretching operations, the incorporation of branching in a polymer product is seen as a desirable property as it can improve melt strength (4).

This study examines the effects of employing a novel tetrafunctional peroxide initiator in the free radical polymerization of methyl methacrylate. A study on this tetrafunctional initiator for the polymerization of styrene has been reported (5). The performance of the tetrafunctional initiator is evaluated based on rates of polymerization, molecular weights and evidence of branching for a range of conversions and under different operating conditions. These results are then compared to experiments where a monofunctional counterpart is run under identical conditions.

4.2 Experimental

4.2.1 Reagents Purification

Methyl methacrylate (Sigma-Aldrich Canada Ltd.) was washed 3 times with a 10% sodium hydroxide solution, washed 3 times with distilled water, dried over calcium chloride, and distilled under vacuum at 26°C. All solvents (ethanol, dichloromethane and acetone) used during the course of the experiment and both initiators (JWEB50 and TBEC) were used as obtained from suppliers without further purification.

4.2.2 Polymer Synthesis

The bulk polymerization of MMA was carried out in borosilicate glass ampoules (capacity ~4 mL) for the full range of conversions. The monomer and initiator were weighed and pipetted into ampoules. The ampoules were degassed by 4 vacuum-freeze-thaw cycles, sealed under vacuum and then immersed in a temperature-regulated oil bath. The ampoules were removed from the oil bath after a set time period and placed in liquid nitrogen to quench the reaction. Next, the ampoules were thawed, weighed, opened and

the contents poured into a flask containing ethanol with a radical inhibitor (hydroquinone). The empty ampoules were weighed. The precipitated polymer was dried in a vacuum oven at 60°C until a constant weight was achieved. For samples having a conversion of approximately 50% or greater, it was too difficult to pour the reaction mixture from the ampoule because of the mixture's high viscosity. In these cases, the ampoules were not thawed before being opened. A frozen piece of the reaction mixture was removed from the ampoule, weighed, kept in a solution of dichloromethane and hydroquinone until dissolved, precipitated with ethanol and then allowed to dry in a vacuum oven.

4.2.3 Characterization

A Waters size exclusion chromatograph (SEC) equipped with a multi-angle laser light scattering (MALLS) detector (DAWN DSP, Wyatt Technology Corp.) followed by a refractive index (RI) detector (2410 RI, Waters) in series was maintained at 30°C and used to determine molecular weight and radius of gyration estimates. The SEC was equipped with one PLgel 10 μm guard column (50 x 7.5 mm) and three PLgel 10 μm MIXED-B columns (300 x 7.5 mm) (Polymer Laboratories Inc.). Tetrahydrofuran (THF) (HPLC Grade, Caledon Laboratories Inc.) was filtered and used as the eluent at a flowrate of 1 mL/min. The polymer was dissolved in THF to obtain concentrations of ~0.2 wt. % and the injection volume was 100 μL . Prior to injection, the polymer solution was filtered through a 0.45 μm filter (GHP Acrodisc GF, Waters) to remove any insoluble gels, if present.

The DAWN DSP laser operated at 633 nm and the light-scattering intensity was measured at 18 angles between 14 and 152°. A value of 0.083 mL/g was used in this study as the specific refractive index increment of poly(methyl methacrylate) (PMMA) in THF. Molecular weight and radius of gyration (R_g) estimates were determined using the Astra version 4.7 software (Wyatt Technology Corp.) and by selecting the Zimm method for analysis. Past studies have found that the Zimm method or “Inverse Debye method” (plot of Kc/R_θ vs. $\sin^2(\theta/2)$) is linear over a much broader range of molecular weights

while other methods require increasing the order of the polynomial to better fit the light scattering data as the molecular weight increased throughout a sample (6). The second virial coefficient for the light-scattering equation was assumed to be negligible as very low concentrations of polymer were employed.

4.2.4 Experimental Design

A factorial design was used to investigate the bulk polymerization of MMA with JWEB50 where three factors and two levels were examined: temperature ($T_1 = 110^\circ\text{C}$, $T_2 = 100^\circ\text{C}$), initiator concentration ($C_1 = 1 \times 10^{-3} \text{ M}$, $C_2 = 5 \times 10^{-4} \text{ M}$) and initiator functionality (monofunctional, tetrafunctional). When looking at the full decomposition of the initiators (see Figures 3.1 and 3.2) it can be seen that each molecule of JWEB50 has the potential of producing a total of four times as many radical sites than one molecule of TBEC. To compare the initiators at similar potential radical concentrations (i.e., assuming all functional sites decompose and react to produce growing polymer chains), an additional set of experiments were carried out with the monofunctional initiator at a concentration four times that of the tetrafunctional initiator ($4C_1 = 4 \times 10^{-3} \text{ M}$, $4C_2 = 2 \times 10^{-3} \text{ M}$) at both temperatures. The complete design comprised a total of 12 experiments.

4.3 Results and Discussion

4.3.1 Temperature

The effect of temperature on the polymerization of MMA initiated by JWEB50 was evaluated by determining rates of polymerization from conversion versus time plots. By selecting regions of the curves that were linear, the rate of polymerization was approximated by the slope of a line fit to the data. Figure 4.1 presents the conversion versus time data for the polymerization of MMA with $1 \times 10^{-3} \text{ M}$ (C_1) of JWEB50 at two different temperatures of 110 (T_1) and 100°C (T_2). Linear regression was completed on two segments of the data for each run: low conversion ($X < 0.35$, approximately) and mid to high conversion ($0.40 < X < 0.90$, approximately). From the values of the slopes, it was determined that the rate of polymerization (rate of change of conversion) at T_1 (rate

at low $X = 0.0096 \text{ min}^{-1}$, rate at mid to high $X = 0.062 \text{ min}^{-1}$) is approximately twice as great than the rate observed at T_2 (rate at low $X = 0.0043 \text{ min}^{-1}$, rate at mid to high $X = 0.032 \text{ min}^{-1}$) for both conversion regions (see also Table 4.1). Another point to note from Figure 4.1 is the replicate for the run Tetra, T_2 , C_1 . It can be seen that data from the two experiments agree very well showing good reproducibility.

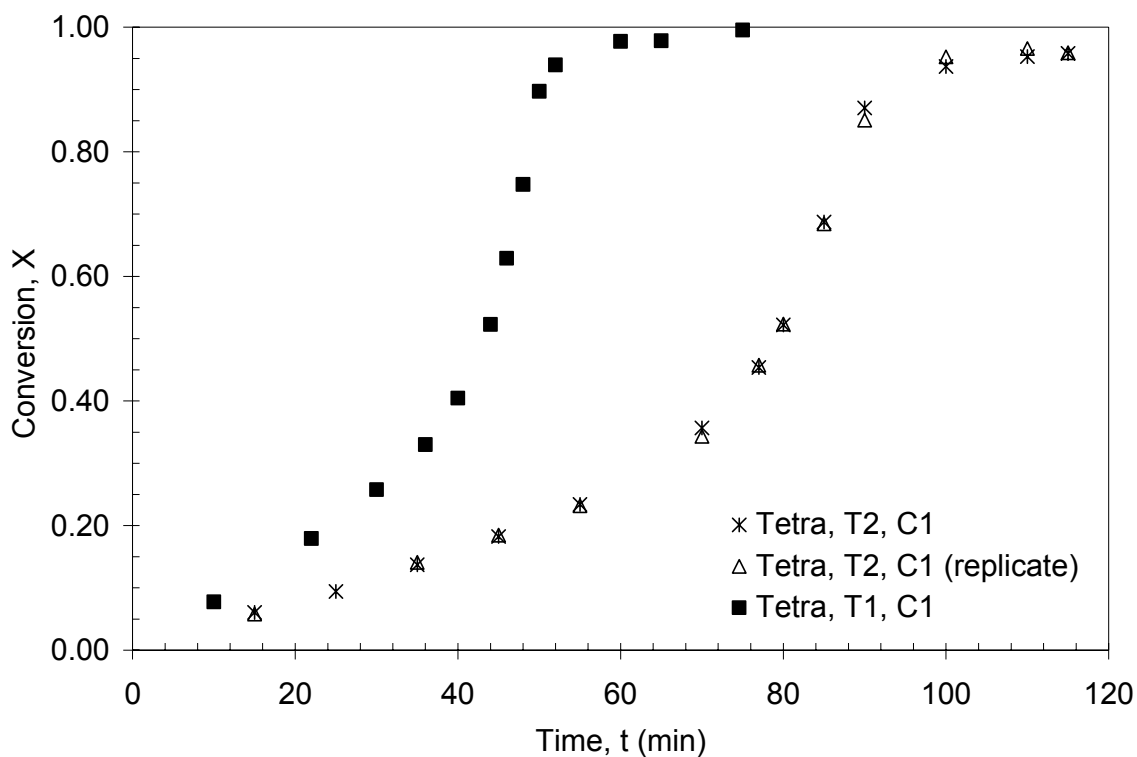


Figure 4.1. Monomer conversion as a function of time for the polymerization of MMA with JWEB50 at T_1 (110°C) and T_2 (100°C).

Table 4.1. Effect of temperature on the rate of polymerization of MMA with JWEB50.

Conversion Range	Run Conditions	Estimate of Rate (min ⁻¹)	Ratio of Rates (T ₁ /T ₂)
Low	Tetra, T ₁ , C ₁	0.0096	2.2
	Tetra, T ₂ , C ₁	0.0043	
	Tetra, T ₁ , C ₂	0.0065	2.0
	Tetra, T ₂ , C ₂	0.0033	
Mid to High	Tetra, T ₁ , C ₁	0.062	1.9
	Tetra, T ₂ , C ₁	0.032	
	Tetra, T ₁ , C ₂	0.043	2.3
	Tetra, T ₂ , C ₂	0.019	

Figure 4.2 shows weight- and number-average molecular weight estimates for the polymerization of MMA initiated with JWEB50 at C₁ for both temperatures T₁ and T₂. As expected, the increase in temperature has produced a decrease in the molecular weight averages. The polydispersity ($PDI = M_w/M_n$) of the polymer was calculated and it was found that there was no discernable difference between the trends produced at both temperatures (see Figure 4.3).

Similar results with respect to the effect of temperature on the rate of polymerization, molecular weight averages and polydispersities were observed for the polymerization of styrene with JWEB50 (5). Altering the reaction temperature had a similar effect on the polymerization of MMA with the monofunctional initiator. With a 10°C increase in the temperature, the rate of polymerization approximately doubled. As well, molecular weight averages were found to decrease as temperature increased as expected and there was no noticeable difference between the PDI at T₁ and T₂.

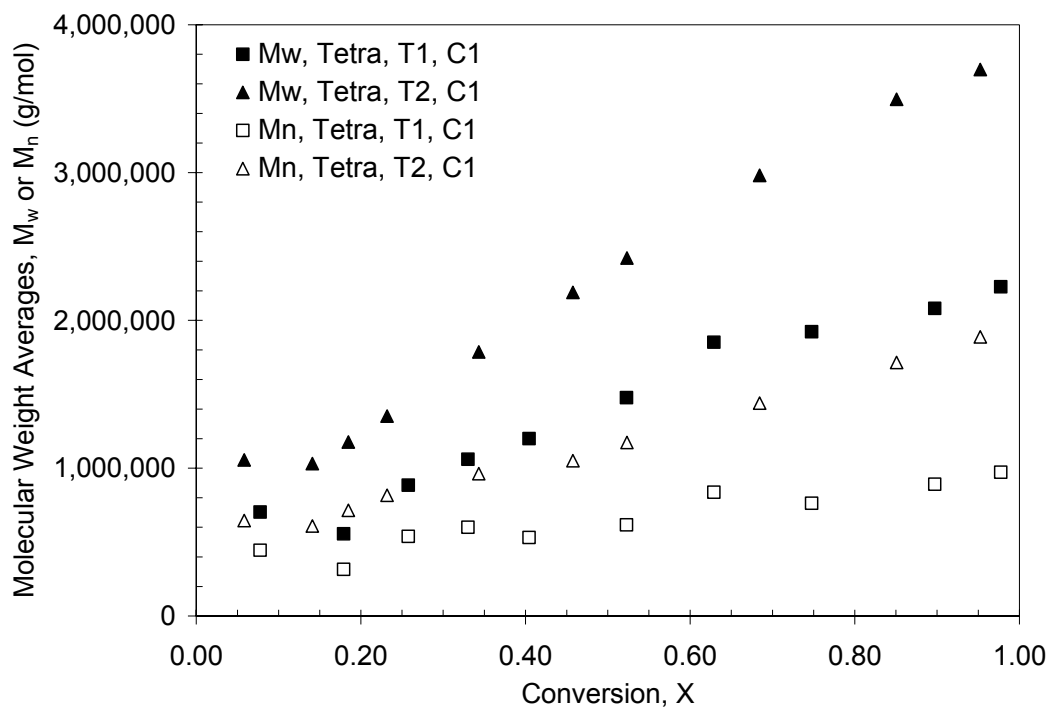


Figure 4.2. Molecular weight averages as a function of conversion for the polymerization of MMA with JWEB50 at T_1 (110°C) and T_2 (100°C).

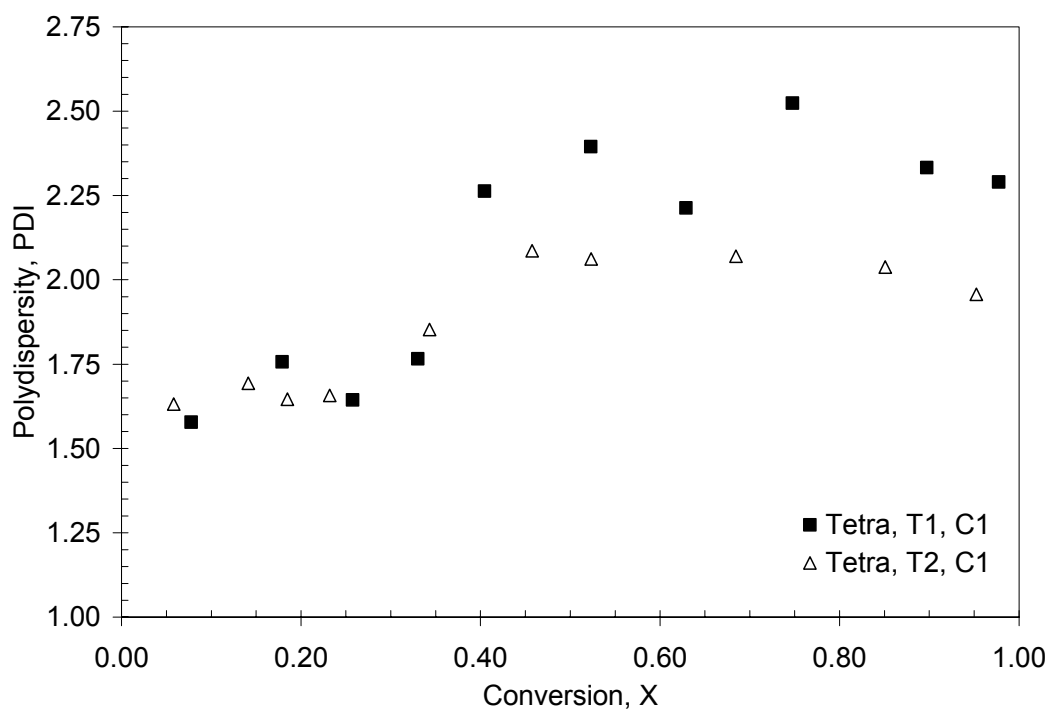


Figure 4.3. Polydispersity as a function of conversion for the polymerization of MMA with JWEB50 at T_1 (110°C) and T_2 (100°C).

4.3.2 Initiator Concentration

Due to the fact that the rate of polymerization is proportional to the square root of the initiator concentration, when the concentration is doubled a factor of $\sqrt{2}$ is expected between rates:

$$R_p = k_p [M] \left(\frac{fk_d [I]}{k_t} \right)^{\frac{1}{2}} \quad (4.2)$$

where f is the initiator efficiency, k_d is the initiator decomposition rate constant and $[I]$ is the initiator concentration. By comparing the rate estimates given in Table 4.1, it was found that the ratio of the polymerization rates ($\text{rate}(C_1)/\text{rate}(C_2)$) was in the range of 1.3 and 1.6, which bounds the expected value of 1.4. Figure 4.4 shows the effect of initiator concentration by presenting monomer conversion for the polymerization of MMA with JWEB50 at the two concentrations. Note that the second experiment (Tetra, T₁, C₂) has been replicated and there is good agreement between the two sets of data. For molecular weight averages, initiator concentration had a similar effect as temperature in that an increase in concentration caused the molecular weights to decrease (see Figure 4.5). The molecular weight averages of the replicate run have also been plotted and coincide well with the original run. Figure 4.6, showing polydispersity data, indicates that initiator concentration had no noticeable effect on the PDI.

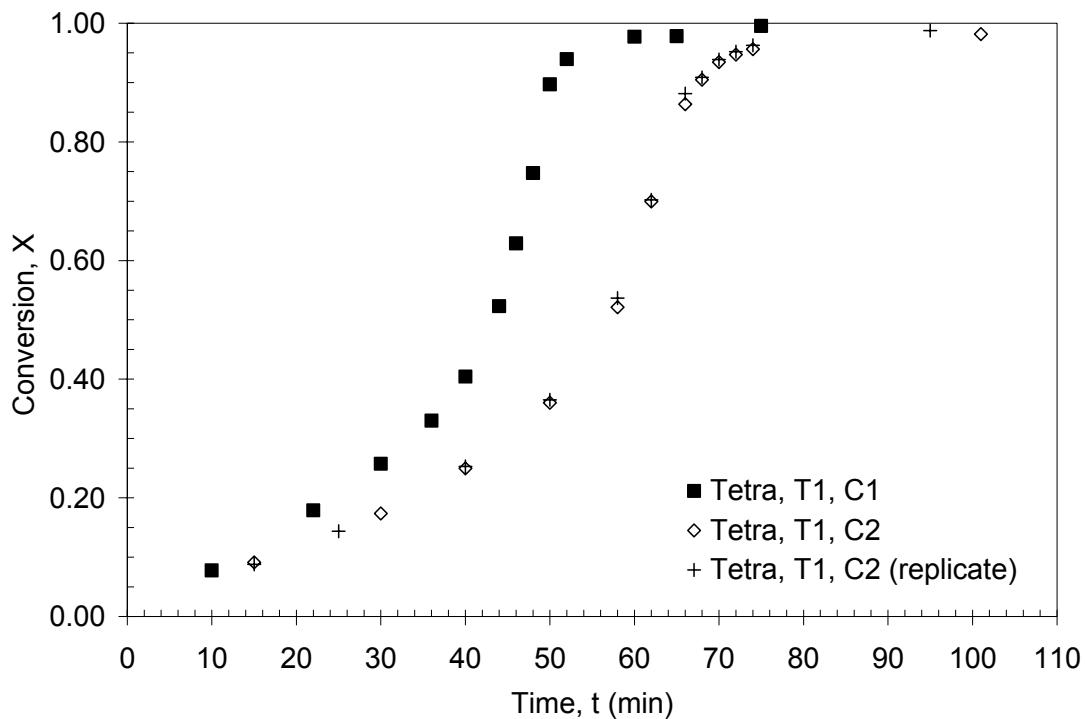


Figure 4.4. Monomer conversion as a function of time for the polymerization of MMA with JWEB50 at C_1 (1×10^{-3} M) and C_2 (5×10^{-4} M).

Analogous results were found for the monofunctional initiator, as doubling the initiator concentration increased the rate by $\sim\sqrt{2}$, decreased molecular weight averages and had no discernible effect on polydispersity. Similar observations were made for the polymerization of styrene with JWEB50 and TBEC (5).

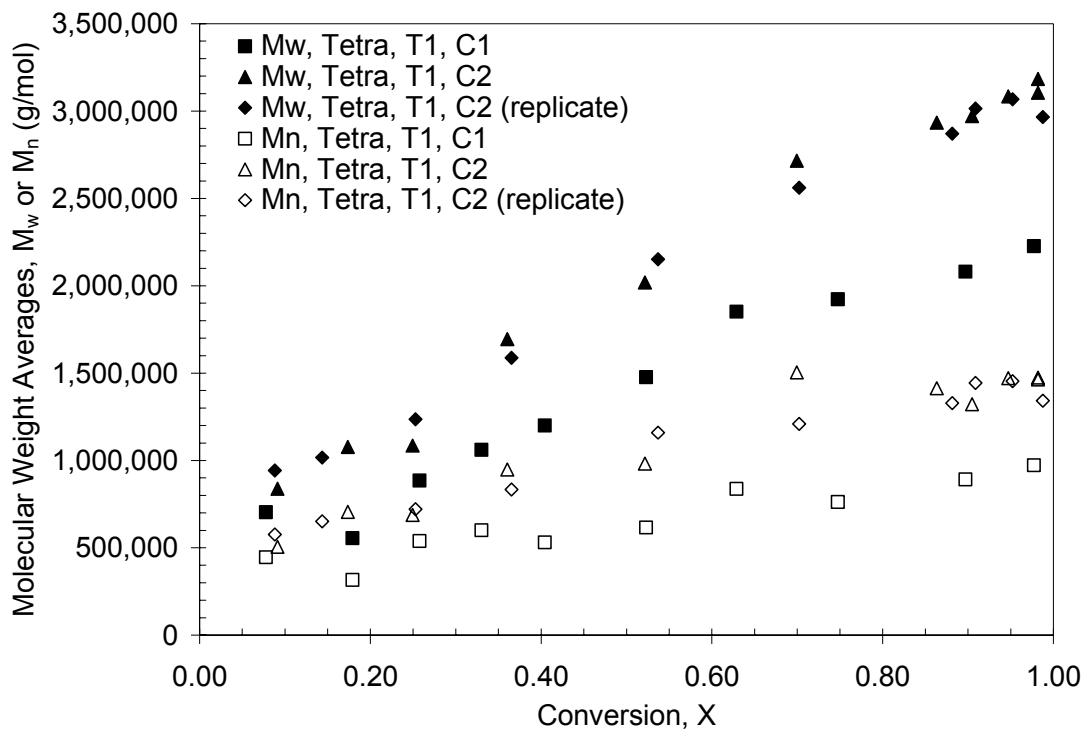


Figure 4.5. Molecular weight averages as a function of conversion for the polymerization of MMA with JWEB50 at C_1 (1×10^{-3} M) and C_2 (5×10^{-4} M).

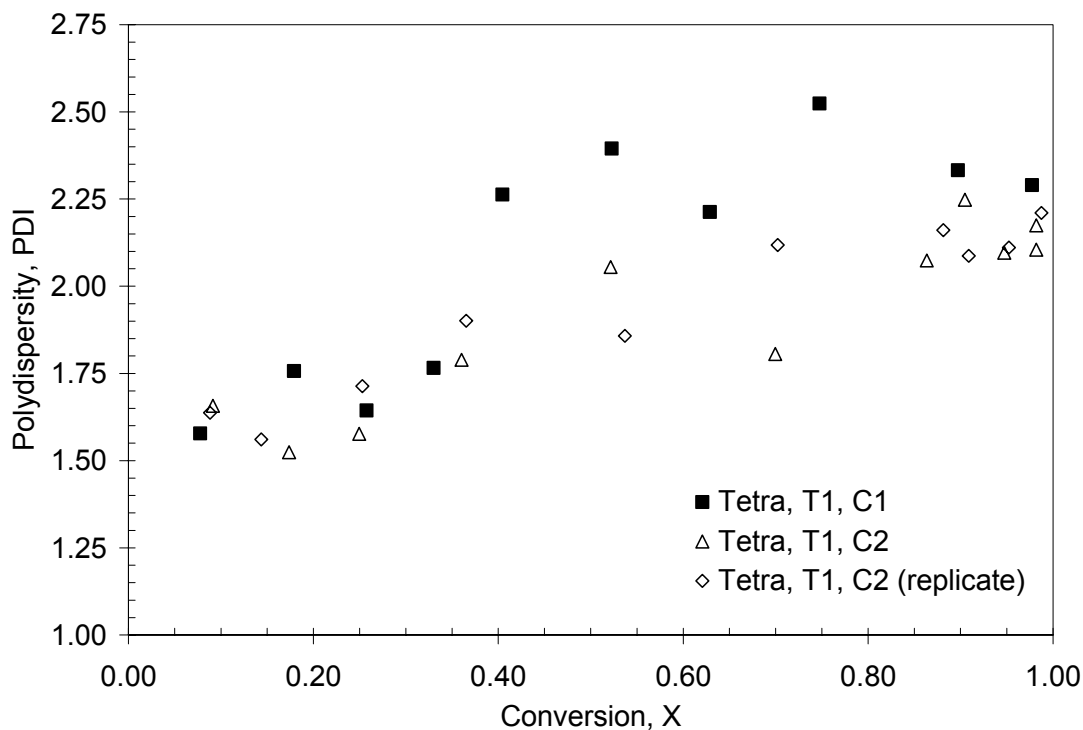


Figure 4.6. Polydispersity as a function of conversion for the polymerization of MMA with JWEB50 at C_1 (1×10^{-3} M) and C_2 (5×10^{-4} M).

4.3.3 Initiator Functionality

One of the major objectives of this study was to compare the tetrafunctional initiator to a suitable monofunctional initiator and evaluate the effect of initiator functionality on the rate of polymerization and molecular weight. Figure 4.7 compares conversion versus time data for the polymerization of MMA with JWEB50 to the polymerization with TBEC. Initiator concentrations and the reaction temperature for each run are at the same level (T_2 and C_2). The plot shows that the tetrafunctional initiator produces a higher rate of polymerization. Estimates for the rate show that the use of JWEB50 (rate at low $X = 0.0033 \text{ min}^{-1}$, rate at mid to high $X = 0.019 \text{ min}^{-1}$) caused the rate to approximately double compared to the rate obtained with TBEC (rate at low $X = 0.0018 \text{ min}^{-1}$, rate at mid to high $X = 0.010 \text{ min}^{-1}$). This same result was observed for comparisons made at the other three conditions (T_1 and C_1 , T_2 and C_1 , T_1 and C_2).

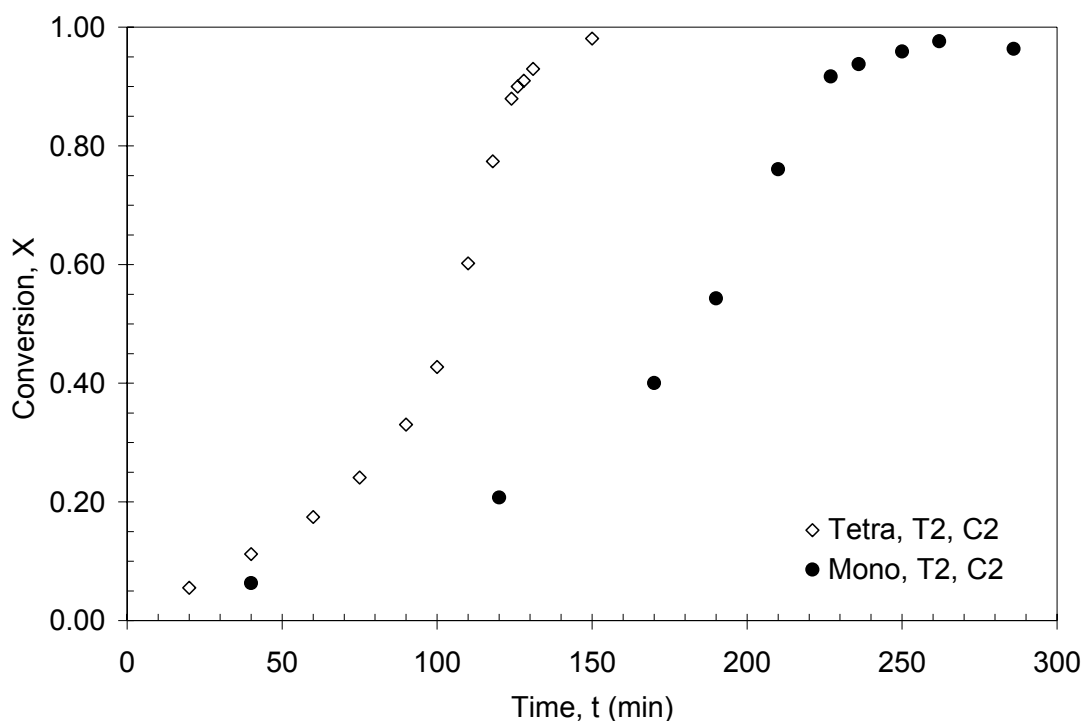


Figure 4.7. Monomer conversion as a function of time for the polymerization of MMA: comparing Tetra to Mono at T_2 (100°C) and C_2 ($5 \times 10^{-4} \text{ M}$).

This observation can be explained by examining the decomposition of both initiators. For every molecule of the tetrafunctional initiator, its full decomposition produces one tetra-radical and four mono-radicals, giving a total of eight radical sites. The full decomposition of the monofunctional initiator, however, generates only two mono-radicals for a total of two radical sites. As a result, one tetrafunctional initiator molecule has the radical generating potential of four monofunctional initiator molecules and because the rate of polymerization is proportional to the square root of the initiator concentration, we would expect to see a factor of 2 between the rates. Again, this reasoning assumes that the tetrafunctional initiator's labile groups are decomposing and reacting in a way similar to the monofunctional functional groups.

In order to further compare the rate of polymerization obtained with JWEB50 to the rate produced with TBEC, runs were completed where the concentration of the monofunctional initiator was four times that of the tetrafunctional. The conversion versus time results for this comparison are shown in Figure 4.8. It can be seen from the data that when TBEC is used at a concentration four times that of JWEB50, the two runs produce similar trends as the curves nearly overlap. Identical results were obtained for the comparisons made at the other three conditions.

The fact that the conversion results for the tetrafunctional initiator are quite comparable to those of the monofunctional initiator at a concentration four times as great is an indication that the functional groups of JWEB50 are decomposing and behaving similarly to those of TBEC.

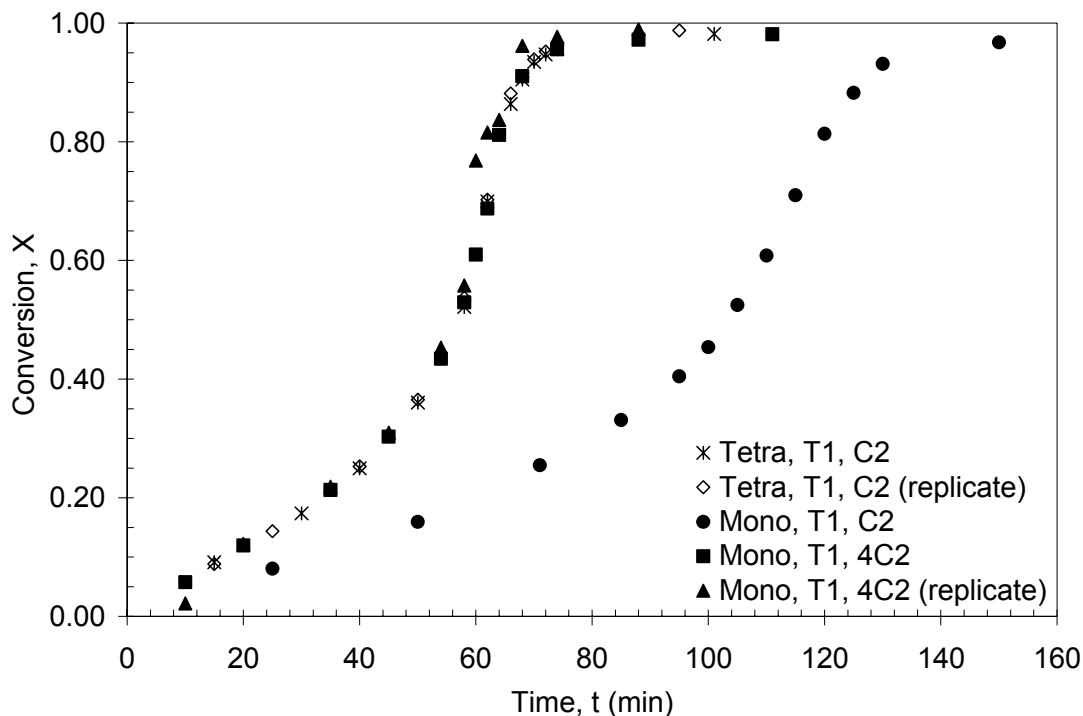


Figure 4.8. Monomer conversion as a function of time for the polymerization of MMA at T_1 (110°C): comparing Tetra at C_2 (5×10^{-4} M), Mono at C_2 (5×10^{-4} M) and Mono at $4C_2$ (2×10^{-3} M).

One of the potential advantages of multifunctional initiators is their ability to increase the rate of polymerization while maintaining or increasing the molecular weight compared to a monofunctional initiator. Looking at the molecular weight results (see Figure 4.9), it was observed that for the polymerization of MMA with JWEB50 there is a decrease in the molecular weight results compared to TBEC. In Figure 4.9 we find that the curve for JWEB50 at C_2 is significantly below the trend for TBEC at C_2 . In actual fact, the molecular weight results for JWEB50 at C_2 are much more similar to the trend for TBEC at $4C_2$. However, the curve for JWEB50 at C_2 is slightly above that of TBEC at $4C_2$, with the difference between the two curves becoming more apparent as conversion is increased. These observations were found for each of the other conditions examined in this study. Initiator functionality did not seem to have an effect on polydispersity as no noticeable trends were observed.

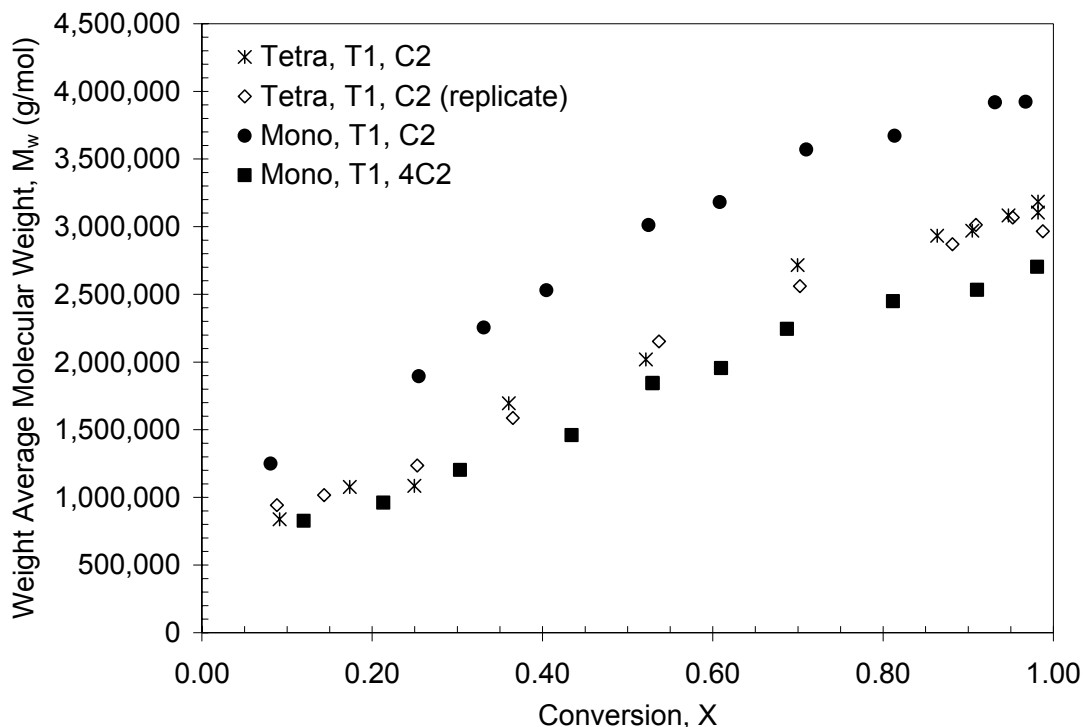


Figure 4.9. Weight-average molecular weights as a function of conversion for the polymerization of MMA at T_1 (110°C): comparing Tetra at C_2 ($5 \times 10^{-4} \text{ M}$), Mono at C_2 ($5 \times 10^{-4} \text{ M}$) and Mono at $4C_2$ ($2 \times 10^{-3} \text{ M}$).

The effect of initiator functionality on molecular weight for MMA is the opposite from what had been observed with the polymerization of styrene initiated by JWEB50 (5). In that study, it was found that JWEB50 gave a higher rate of polymerization and similar molecular weights compared to TBEC at the same initiator concentration. This result with MMA is somewhat unexpected as many sources, both industrial (2, 7) and academic (5, 8-15) have claimed that multifunctional initiators will increase the rate while either increasing or maintaining similar molecular weights. However, in those studies styrene is the only monomer that was investigated and the one study that did report on the use of MMA with a multifunctional initiator did not compare with a monofunctional counterpart (16).

One possible reason for the discrepancy between the behaviour of MMA and styrene with the tetrafunctional initiator is the difference between their modes of termination. Styrene is known to terminate predominantly by radical coupling while methyl methacrylate

radicals terminate mostly by disproportionation for the temperature range studied. If all of the tetra-radicals terminated by combination with the linear radicals, the star polymers would have a much higher molecular weight compared to tetra-radicals that terminated by disproportionation. That is, coupling of radicals could be what allows JWEB50 to produce higher rates but similar molecular weights compared to TBEC for polystyrene. In order to determine whether the differences observed between styrene and MMA with JWEB50 are due to their modes of termination, further experiments were completed. Since disproportionation is favoured by higher temperatures, a lower reaction temperature should result in a higher fraction of radicals terminating by coupling. Thus, several experiments were carried out at a lower temperature of 70°C. However, identical results were obtained when compared to the observations made at 110 and 100°C. At 70°C, it was observed that MMA initiated with JWEB50 produced polymer of a lower molecular weight when compared to MMA initiated with TBEC at the same concentration. From the literature, estimates of the rate constants for termination by combination (k_{tc}) and disproportionation (k_{td}) were obtained (17). It was determined that at 110°C, 90% of chains terminate by disproportionation while at 70°C the fraction decreases to 84%. Therefore, even by lowering the temperature from 110 to 70°C, disproportionation is still heavily favoured and as a result, no discernable difference can be seen between the observations at the two temperatures.

4.3.4 Detection of Branching

From the conversion versus time plots it was shown that the use of JWEB50 produced a rate of polymerization similar to TBEC at a concentration four times as high. This was an indication that JWEB50 should be fully decomposing in order to generate the same number of radicals as TBEC at a concentration of 4C. This would suggest that branched radicals did exist during the polymerization with JWEB50 and that star polymers were generated. As a result we would expect the polymer produced with JWEB50 to contain more branching than the polymer generated with TBEC.

Figures 4.10 and 4.11 provide SEC chromatograms of samples with increasing conversions for two runs: JWEB50 at T₁ and C₂ and TBEC at T₁ and 4C₂. The RI and

90° light scattering (LS) signals are shown in arbitrary units. When examining the low conversions samples for JWEB50 (Figure 4.10), the chromatograms do not show any shoulders or bimodality which might be an indication of a fraction of the polymer being significantly different in molecular weight, branching or both. As conversion increases, we find that the SEC traces broaden and the peaks shift to lower elution volumes indicating that the samples are increasing in molecular weight with conversion. Looking at the LS signal, a small shoulder does appear at lower elution volumes and increases with increasing conversion. Without further consideration, it might be argued that this could be the branched fraction expected from the use of JWEB50. However, when examining the traces for the monofunctional initiator (Figure 4.11), it can be seen that identical results are obtained and the use of TBEC also gives rise to a small shoulder that increases with conversion. The origin of this shoulder is due to the high molecular weight material produced when the autoacceleration effect begins in the bulk polymerization of MMA. As the reaction proceeds, the viscosity of the reaction mixture increases and with subsequent chain entanglements, termination becomes increasingly difficult due to diffusional limitations. Although propagation is also hindered, the effect is not as significant and it is found that $k_p/k_t^{1/2}$ increases causing an increase in the rate of polymerization (see Equation 4.2). A second consequence of the decrease in the rate of termination is that the molecular weight increases. As a result, a shoulder of high molecular weight polymer appears and increases with increasing conversion. Overall, a comparison of the SEC traces do not show any differences between polymer initiated with JWEB50 and TBEC.

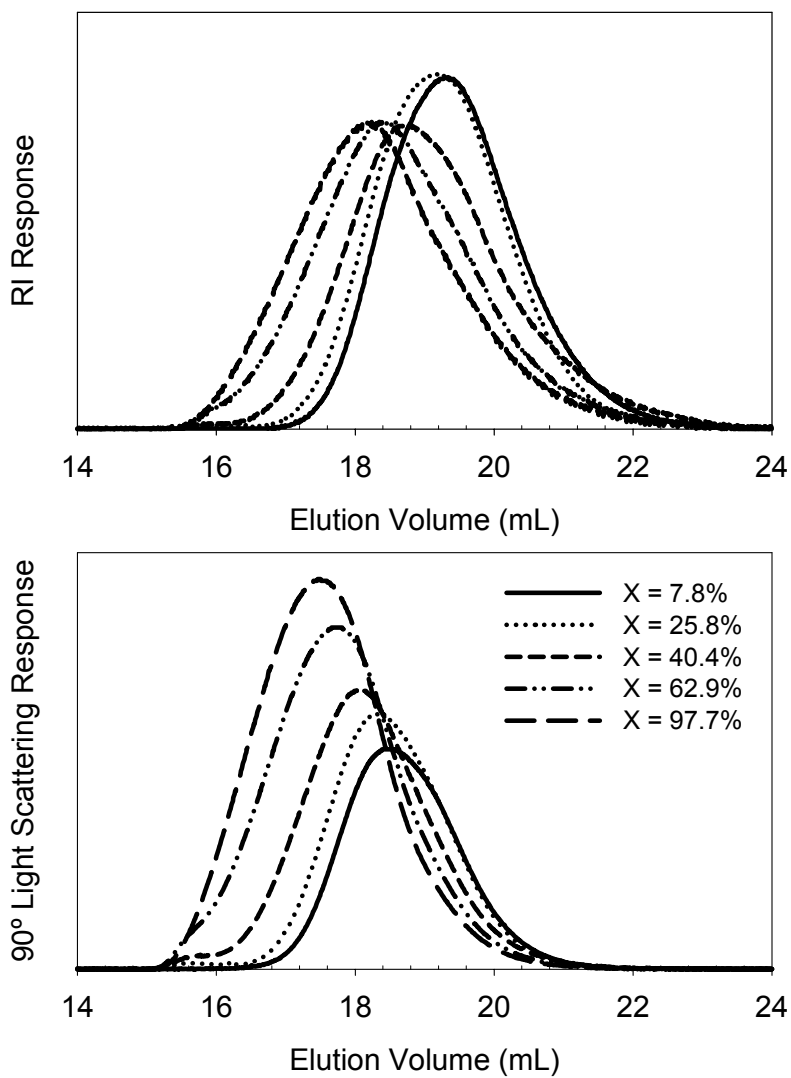


Figure 4.10. SEC chromatograms for polymer produced with Tetra at T_1 (110°C) and C_2 (5×10^{-4} M).

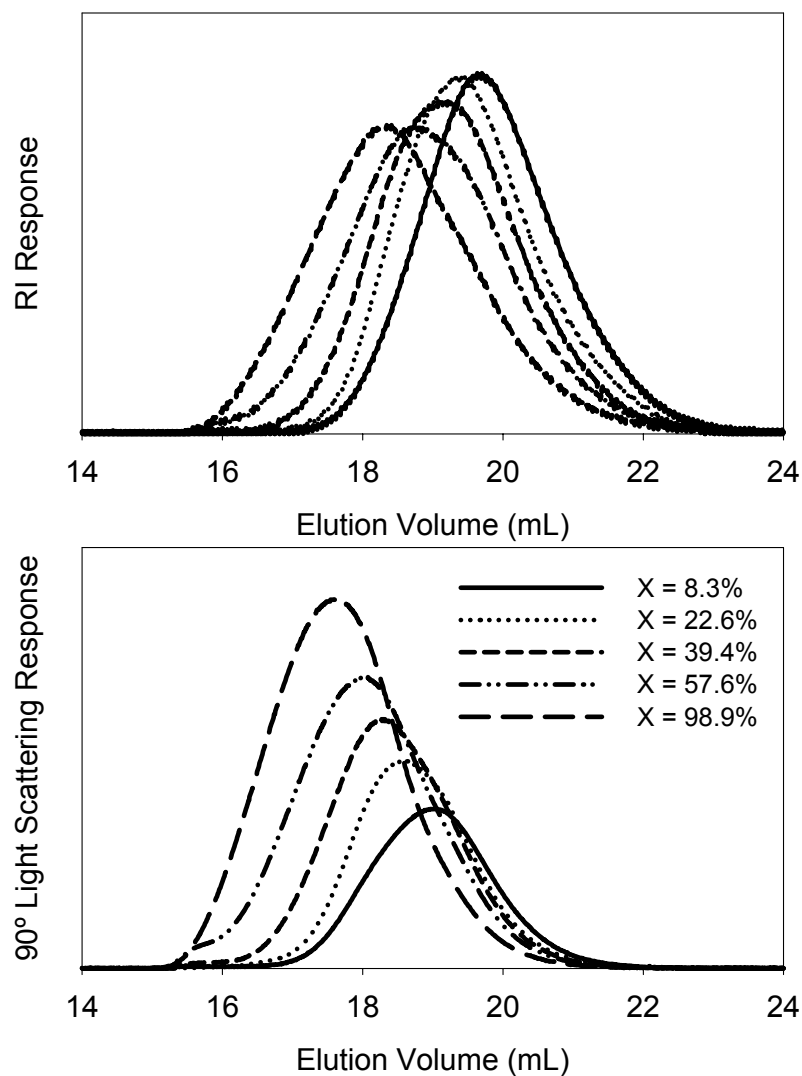


Figure 4.11. SEC chromatograms for polymer produced with Mono at T_1 (110°C) and $4C_2$ (2×10^{-3} M).

A better suited method for the detection of branched molecules other than comparing SEC chromatograms would be the examination of dilute solution polymer properties. A characteristic of branched molecules is that they have a smaller size compared to a linear analogue of identical molecular weight. As a result, the extent of branching can be determined by comparing the radius of gyration for the branched polymer relative to the linear. The radius of gyration describes the size of a polymer molecule in solution, regardless of its shape.

Light scattering experiments provide a direct measurement of the z-average radius of gyration for a polymer. However, for samples with a broad polydispersity, the z-average radius of gyration can be insensitive to branching. Because the z-average is more dependent upon the higher molecular weight fractions of the polymer, it is found that increasing polydispersity greatly increases the z-average. Thus, it has been found that the decrease in the z-average radius of gyration due to branching can be offset by a large polydispersity, making the determination of branching for a polydisperse sample impossible by classical light scattering measurements (18). Consequently, SEC must be used in combination with light scattering to obtain the molecular weight and radius of gyration for each “monodisperse” volume slice. From this, a distribution of the radius of gyration as a function of elution volume can be obtained. The radius of gyration can then be plotted as a function of molecular weight for two samples and any deviation in the curves would be an indication of branching.

Figure 4.12 shows a plot of the radius of gyration versus molecular weight typical of the results obtained in this study. It can be seen that the curve for the polymer sample produced by TBEC overlaps the curve for polymer sample initiated with JEWB50. Although the rate data would suggest that branched radicals are forming and hence branched molecules are generated, the radius of gyration plot indicates that samples produced with the tetrafunctional initiator are no more branched than the polymer generated with the monofunctional initiator. Therefore, either branched molecules are not being produced or SEC-MALLS is not a sensitive enough characterization method to detect any branching.

When JWEB50 fully decomposes, four fifths of the radicals generated are linear and as such, only a portion of the final polymer sample will be branched molecules. Therefore, the samples produced with JEWB50 can be considered to be a mixture of branched and linear polymers with more linear than branched molecules. As well, it has been shown that regardless of the care taken to purify the monomer or the technique employed, the presence of an impurity associated with MMA acts as a free radical initiator (19).

Impurities and the possibility of the thermal polymerization of MMA would further contribute to the number of linear chains.

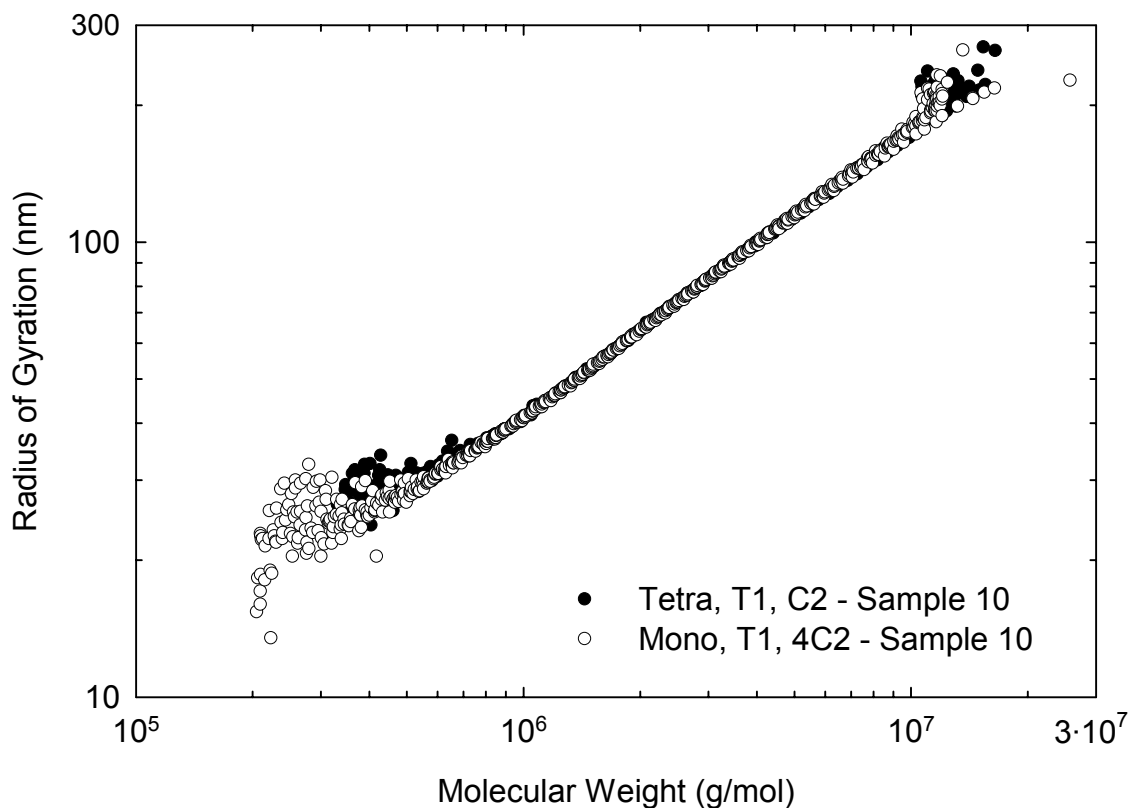


Figure 4.12. Radius of gyration as a function of molecular weight for PMMA samples from runs Tetra, T₁ (110°C), C₂ (5×10^{-4} M) and Mono, T₁ (110°C), 4C₂ (2×10^{-3} M) with similar weight-average molecular weights.

The limitation of SEC is that the separation of polymer molecules is based on their hydrodynamic size and not their molecular weight. For a blend of branched and linear polymer molecules, the fractionation will not always be complete as a linear and branched molecule can have the same hydrodynamic volume but different molecular weights. Hence, they will coelute and at a particular elution volume, the detector cell will contain linear and branched polymer molecules of differing molecular weights (20). Typically, it is assumed that the level of branching increases with increasing molecular weight and that the highest molecular weight fractions are branched (i.e., this is the only

portion of the distribution where branched molecules are not eluting with linear molecules). However, if this fraction of the distribution is too small, experimental error may hide any evidence of branching. Alternatively, it is possible that the branched molecules are not of higher molecular weight than the linear chains and therefore, there is always coelution of branched and linear chains (see Figure 4.13). As seen in Figure 4.12, this may be the case as there is no difference between the samples from TBEC and JWEB50 in the high molecular weight range.

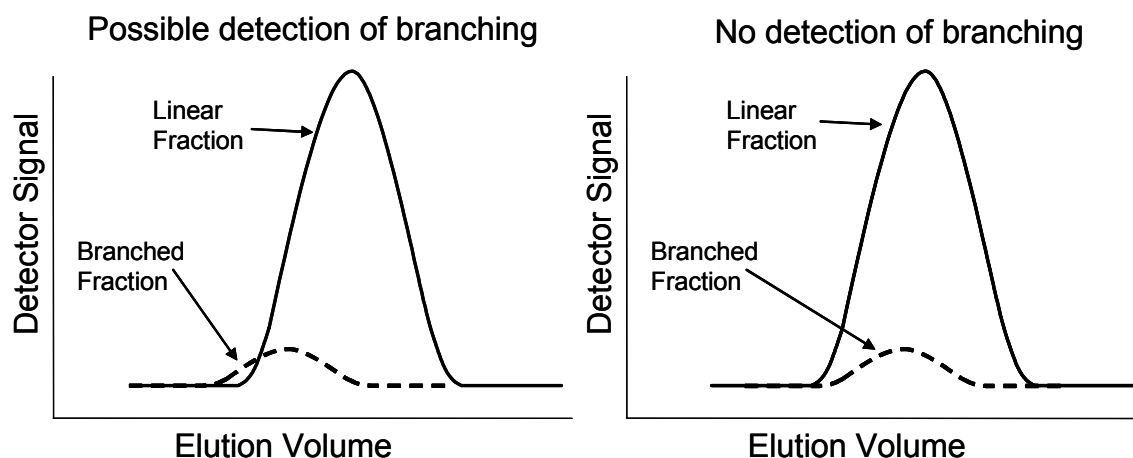


Figure 4.13. Chromatograms depicting the effect that the linear fraction in a polymer has on the detection of branching by SEC-MALLS.

These results are unlike those observed with styrene where branching was detected in the polystyrene samples produced with JWEB50. The detection of branching in styrene but not in MMA could also be attributed to the different modes of termination. Branched radicals terminating by radical coupling will be larger than those terminating by disproportionation. The fact that radical coupling occurs may cause the star polymers to have much higher molecular weights than the linear chains (produced either by monoradicals or thermal polymerization). As a result, a fraction of star polymers are obtained at elution volumes without or with a minimal number of linear chains such that branching is detected. However, with disproportionation, it could be that the star polymers are not significantly larger than the linear chains. As such, essentially all star molecules elute with linear chains and no evidence of branching is detected.

4.4 Conclusions

The effects of employing a novel tetrafunctional initiator (JWEB50) in the free radical polymerization of MMA were examined. The initiator's performance was evaluated with respect to the rate of polymerization, molecular weights and evidence of branching while temperature and initiator concentration were varied. As well, a comparison was made to a monofunctional initiator (TBEC) with a functional group of similar structure and thermal stability to those of the tetrafunctional initiator. The polymerization of MMA with JWEB50 follow expected conventional free radical polymerization trends with respect to temperature and initiator concentration.

When comparing JWEB50 and TBEC under identical conditions, it was found that the tetrafunctional initiator produced a higher rate of polymerization but lower molecular weight averages compared to the monofunctional initiator. However, when TBEC was employed at a concentration four times that of JWEB50, the two initiators generated similar rates and molecular weight averages. In addition, no direct evidence of branching for the polymerization of MMA was detected when examining radius of gyration versus molecular weight plots. The trends observed with MMA were found to be the opposite of those observed with styrene in a previous study (5).

Although SEC is a relatively fast and easy method to analyze polymers, the detection and characterization of branched molecules by dilute solution methods can be difficult. Alternatively, it is known that flow properties are more sensitive to branched molecules than dilute solution properties (21) and as such future work will investigate the rheological properties of polymers produced with JWEB50.

4.5 References

1. Odian, G. *Principles of Polymerization*; Wiley: Toronto, 1991.
2. Kamath, Vassanth R. and Harpell, Gary A. (Pennwalt Corporation). Free-radical polymerizations using mixed initiator systems at two thermally distinct polymerization stages. US Patent 4,129,703, **1978**.

3. Hadjichristidis, N., Pispas, S., Pitsikalis, M., Iatrou, H., Vlahos, C. Asymmetric star polymers: Synthesis and properties. *Advances in Polymer Science* **1999**, *142*, 71-127.
4. Kasehagen, L., Wicher, J., Brennan, J., Debaud, F., Suehisa, T. A New Multifunctional Peroxide Initiator for High Molecular Weight, High Productivity, and Long-Chain Branching. *ANTEC - Soc. Plast. Eng.* **2002**, *60* (2), 1837-1841.
5. Fityani-Trimmi, S., Dhib, R., Penlidis, A. Free Radical Polymerization of Styrene with a New Tetrafunctional Peroxide Initiator. *Macromolecular Chemistry and Physics* **2003**, *204*, 436-442.
6. Podzimek, S. The use of GPC coupled with a multiangle laser light scattering photometer for the characterization of polymers. On the determination of molecular weight, size, and branching. *Journal of Applied Polymer Science* **1994**, *54*, 91-103.
7. Sanchez, Jose, Yormick, Salvatore, Wicher, Jerome, and Malone, Kenneth George (Elf Atochem North America, Inc.). Poly(monoperoxy carbonates). US Patent 5,760,149, **1998**.
8. Choi, K. Y., Lei, G. D. Modeling of free radical polymerization of styrene by bifunctional initiators. *AIChE Journal* **1987**, *33* (12), 2067-2076.
9. Kim, K. J., Choi, K. Y. Modeling of free radical polymerization of styrene catalyzed by unsymmetrical bifunctional initiators. *Chemical Engineering Science* **1989**, *44* (2), 297-312.
10. Yoon, W. J., Choi, K. Y. Free radical polymerization of styrene with a binary mixture of symmetrical bifunctional initiators. *Journal of Applied Polymer Science* **1992**, *46*, 1353-1367.
11. Villalobos, M. A., Hamielec, A. E., Wood, P. E. Bulk and suspension polymerization of styrene in the presence of *n*-pentane. An evaluation of monofunctional and bifunctional initiation. *Journal of Applied Polymer Science* **1993**, *50*, 327-343.
12. González, I. M., Meira, G. R., Oliva, H. M. Synthesis of polystyrene with mixtures of mono- and bifunctional initiators. *Journal of Applied Polymer Science* **1996**, *59*, 1015-1026.
13. Dhib, R., Gao, J., Penlidis, A. Simulation of free radical bulk/solution homopolymerization using mono- and bi-functional initiators. *Polymer Reaction Engineering Journal* **2000**, *8*, 299-464.
14. Cavin, L., Rouge, A., Meyer, T., Renken, A. Kinetic modeling of free radical polymerization of styrene initiated by the bifunctional initiator 2,5-dimethyl-2,5-bis(2-ethyl hexanoyl peroxy)hexane. *Polymer* **2000**, *41*, 3925-3935.
15. Cerna, J. R., Morales, G., Eyler, G. N., Canizo, A. I. Bulk Polymerization of Styrene Catalyzed by Bi- and Trifunctional Cyclic Initiators. *Journal of Applied Polymer Science* **2002**, *83*, 1-11.
16. Holzinger, D., Kickelbick, G. Modified cubic spherosilicates as macroinitiators for the synthesis of inorganic-organic starlike polymers. *Journal of Polymer Science Part A-Polymer Chemistry* **2002**, *40* (21), 3858-3872.

17. Gao, J., Penlidis, A. A comprehensive simulator/database package for reviewing free-radical homopolymerizations. *Journal of Macromolecular Science-Reviews in Macromolecular Chemistry and Physics* **1996**, *C36* (2), 199-404.
18. Podzimek, S., Vlcek, T. Characterization of Branched Polymers by SEC Coupled with a Multiangle Light Scattering Detector. II. Data Processing and Interpretation. *Journal of Applied Polymer Science* **2001**, *82*, 454-460.
19. Clouet, G., Chaumont, P., Corpart, P. Studies on bulk polymerization of methyl methacrylate. I. Thermal polymerization. *Journal of Polymer Science: Part A: Polymer Chemistry* **1993**, *31*, 2815-2824.
20. Rudin, Alfred Measurement of Long-Chain Branch Frequency in Synthetic Polymers. In *Modern Methods of Polymer Characterization*; John Wiley & Sons: Toronto, 1991; 103-112.
21. Graessley, W. W. Effect of Long Branches on the Flow Properties of Polymers. *Accounts of Chemical Research* **1977**, *10* (9), 332-339.

CHAPTER 5 - COPOLYMERIZATION OF METHYL METHACRYLATE/STYRENE AND METHYL METHACRYLATE/ α -METHYL STYRENE

5.1 Introduction

The purpose of this chapter is to continue the kinetic investigation of a tetrafunctional peroxide initiator designed for free radical polymerization. Previously, the use of the tetrafunctional initiator in the bulk free radical polymerization of styrene (1) and methyl methacrylate (2) was completed. This study expands the work in the area by investigating comonomer systems such as styrene-MMA and α -methyl styrene(α -MS)-MMA. In the work presented herein the performance of the tetrafunctional initiator is evaluated on the basis of the rate of polymerization, polymer molecular weight and evidence of branching compared to a monofunctional counterpart.

5.2 Experimental

5.2.1 Reagent Purification

Monomers (styrene, methyl methacrylate, and α -methyl styrene) (Sigma-Aldrich Canada Ltd.) were washed three times with a 10 w/v % sodium hydroxide solution, washed three times with distilled water, dried over calcium chloride and distilled under vacuum. Solvents such as ethanol, dichloromethane and acetone used during the course of the experiment and both initiators (JWEB50 and TBEC) were used as received from suppliers without further purification.

5.2.2 Polymer Synthesis

Bulk polymerizations were completed in borosilicate glass ampoules (capacity ~4 mL) for a range of conversions. Monomers and initiator were weighed, mixed and pipetted into ampoules. Ampoules were then degassed by 4 vacuum-freeze-thaw cycles, sealed under vacuum and then immersed in a silicone oil bath. Ampoules were removed at

selected time intervals and placed in liquid nitrogen to quench the reaction. The ampoules were then thawed, weighed, opened and the contents poured into a flask containing ethanol and a radical inhibitor (hydroquinone) to prevent any further reactions. The weights of the empty ampoules were also recorded. For the higher conversion levels where the reaction mixture was more gel- or solid-like, the ampoules were not thawed before being opened. In these cases, a frozen piece of the reaction mixture was removed from the ampoule, weighed, allowed to dissolve in dichloromethane with hydroquinone and then precipitated with ethanol before being dried in a vacuum oven.

5.2.3 Polymer Characterization

Two size exclusion chromatographs (SEC) were used to characterize the polymer samples. The first setup (SEC1) is a Waters size exclusion chromatograph equipped with a multi-angle laser light scattering (MALLS) detector (DAWN DSP, Wyatt Technology Corp.) followed by a differential refractometer (2410 RI, Waters) in series. This SEC was maintained at 30 °C and used to determine molecular weight and radius of gyration estimates. It was equipped with one PLgel 10 µm guard column (50 x 7.5 mm) and three PLgel 10µm MIXED-B columns (300 x 7.5 mm) (Polymer Laboratories Ltd.). The laser operated at 633 nm and the light-scattering intensity was measured at 18 angles between 14 and 152°. Molecular weight and radius of gyration estimates were determined using Astra version 4.7 software (Wyatt Technology Corp.).

The second size exclusion chromatograph (SEC2) consists of Waters solvent delivery system and autosampler followed by Viscotek's quad detector equipped with a UV detector, low- and right-angle laser light scattering detectors (LALLS/RALLS), differential refractometer and viscometer in series. One PLgel 10 µm guard column (50 x 7.5 mm, Polymer Laboratories Ltd.) and three HR 5E columns (300 x 7.5 mm, Waters) were used with the detectors and columns maintained at 30 °C. The laser operated at 670 nm and the light-scattering intensity was measured at 7° (LALLS) and 90° (RALLS). Data analysis for this system was performed using OmniSEC version 3.0 (Viscotek).

Tetrahydrofuran (THF) (Caledon Laboratories Inc.) was filtered and used as the eluent at a flowrate of 1 mL/min for both SEC setups. The polymer was dissolved in THF to obtain concentrations of ~0.2 wt. % and the injection volume varied between 100 and 200 μ L. The second virial coefficient for the light-scattering equation was assumed to be negligible as very low concentrations of polymer were employed. Specific refractive index increment (dn/dc) values of 0.185 mL/g, 0.083 mL/g and 0.2056 mL/g were used in the light scattering analysis for polystyrene (PS), poly(methyl methacrylate) PMMA and poly(α -methyl styrene) (poly(α -MS)), respectively. In the case of copolymers, dn/dc values were determined from a weighted average based on copolymer composition. When using SEC2, copolymer composition was obtained from the UV signal while for SEC1 values were obtained from NMR.

A Bruker AVANCE 500 NMR spectrometer was employed for polymer composition analysis. Deuterated chloroform was used as the solvent and the measurements were taken at room temperature. The relative amounts of each monomer incorporated in the copolymer were estimated from absorption peaks of the spectra. In the case of MMA, the three protons in the $-\text{OCH}_3$ group were found at $\delta = 3.6$ ppm while for α -MS and Sty the five protons in the $-\text{C}_6\text{H}_5$ group were taken at 6.7-7.3 ppm.

5.2.4 Experimental Design

Tables 5.1 and 5.2 provide a list of the experiments completed with methyl methacrylate, styrene, α -methyl styrene and various comonomer mixtures. For the experiments listed in Table 5.1, the label starts with the feed type (S = styrene, M = methyl methacrylate, SM = 50/50 wt. % mixture of styrene and MMA), then the type of initiator (M = monofunctional, T = tetrafunctional), followed by the initiator concentration (C = 0.004 mol/L, 4C = 0.016 mol/L). For the block of runs which were conducted at the higher temperature, 120 is placed at the end of the label. A similar labeling code is used for the runs with α -MS as shown in Table 5.2.

Table 5.1. Styrene-methyl methacrylate experiment conditions.

Experiment	Styrene Feed Composition, wt. %	Temperature, °C	Initiator Type	Initiator Concentration, mol/L
S-MC	100	110	TBEC	0.004
S-M4C	100	110	TBEC	0.016
S-TC	100	110	JWEB50	0.004
M-MC	0	110	TBEC	0.004
M-M4C	0	110	TBEC	0.016
M-TC	0	110	JWEB50	0.004
SM-MC	50	110	TBEC	0.004
SM-M4C	50	110	TBEC	0.016
SM-TC	50	110	JWEB50	0.004
S-MC120	100	120	TBEC	0.004
S-TC120	100	120	JWEB50	0.004
M-MC120	0	120	TBEC	0.004
M-M4C120	0	120	TBEC	0.016
M-TC120	0	120	JWEB50	0.004

Table 5.2. α -Methyl styrene-methyl methacrylate experiment conditions.

Experiment	α -Methyl Styrene Feed Composition, wt. %	Temperature, °C	Initiator Type	Initiator Concentration, mol/L
aMS-MMA-MC	20	110	TBEC	0.004
aMS-MMA-M4C	20	110	TBEC	0.016
aMS-MMA-TC	20	110	JWEB50	0.004

5.3 Results and Discussion

5.3.1 Styrene-Methyl Methacrylate Copolymer

A total of nine experiments were completed in this section of the study with three experiments for styrene homopolymerization, three for MMA homopolymerization and three for the copolymerization of a 50-50 wt.% mixture. In each of these sets, two runs employed the mono- and tetrafunctional initiators at identical concentrations. Looking at the decomposition of the initiators (see Figures 3.1 and 3.2) it can be seen that each JWEB50 molecule has the ability to produce four times as many radical sites as one TBEC molecule. Therefore, a third run was also performed for each feed composition with the monofunctional initiator at a concentration four times that of the tetrafunctional

initiator. This would enable a comparison of the initiators at similar “potential” radical concentrations.

5.3.1.1 Conversion and Molecular Weight Results

Figure 5.1 presents conversion versus time data for the bulk polymerization of styrene with JWEB50 and TBEC. By selecting linear regions of the low conversion data, estimates of the rate of polymerization were determined from the slope. When both initiators are employed at identical concentrations, it was observed that JWEB50 produced a higher rate of polymerization (rate for JWEB50 = 0.0051 min^{-1} , rate for TBEC = 0.0026 min^{-1}) and a limiting conversion of ~98% was achieved in half of the time required for TBEC (time for JWEB50 = 220 min, time for TBEC = 419 min). However, when the monofunctional initiator is added at a concentration four times that of the tetrafunctional, we found that the two data sets overlapped. In other words, when JWEB50 is used at a concentration of 0.004 M it produces a rate of polymerization similar to the rate obtained with TBEC at a concentration of 0.016 M. This result would suggest that the tetrafunctional initiator’s labile groups are decomposing and reacting in a way similar to TBEC’s functional group.

Figure 5.2 is a plot of the weight-average molecular weight estimates for the three styrene homopolymerization runs. Results from both SEC setups are plotted and agree very well showing good reproducibility. When examining the molecular weight results, it can be seen that by increasing the concentration of the monofunctional initiator a polymer of lower molecular weight is produced. This is the dilemma facing polymer manufacturers where an increase in the rate of polymerization causes a noticeable decrease in the polymer molecular weight. Looking at the data for the tetrafunctional initiator, it can be seen that the molecular weights are comparable to those produced when the monofunctional initiator is used at the same concentration. These results are similar to what has previously been observed with multifunctional initiators and styrene: high rates of polymerization are obtained while maintaining or increasing the molecular weight (1, 3-12).

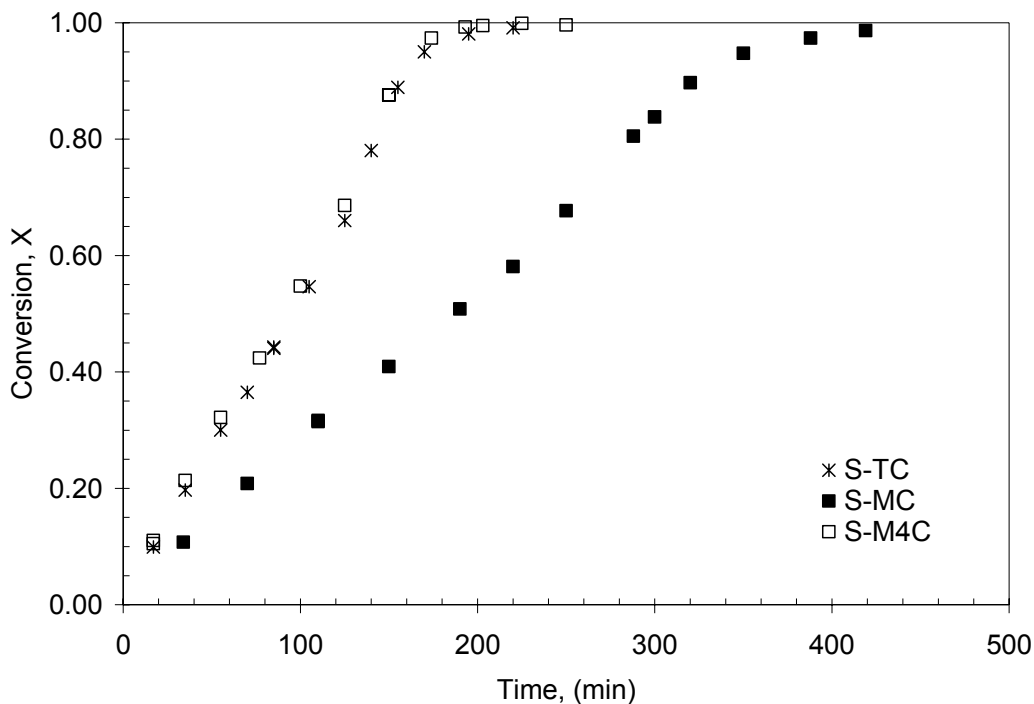


Figure 5.1. Monomer conversion as a function of time for the bulk polymerization of styrene at 110°C ($C = 0.004$ M, $4C = 0.016$ M).

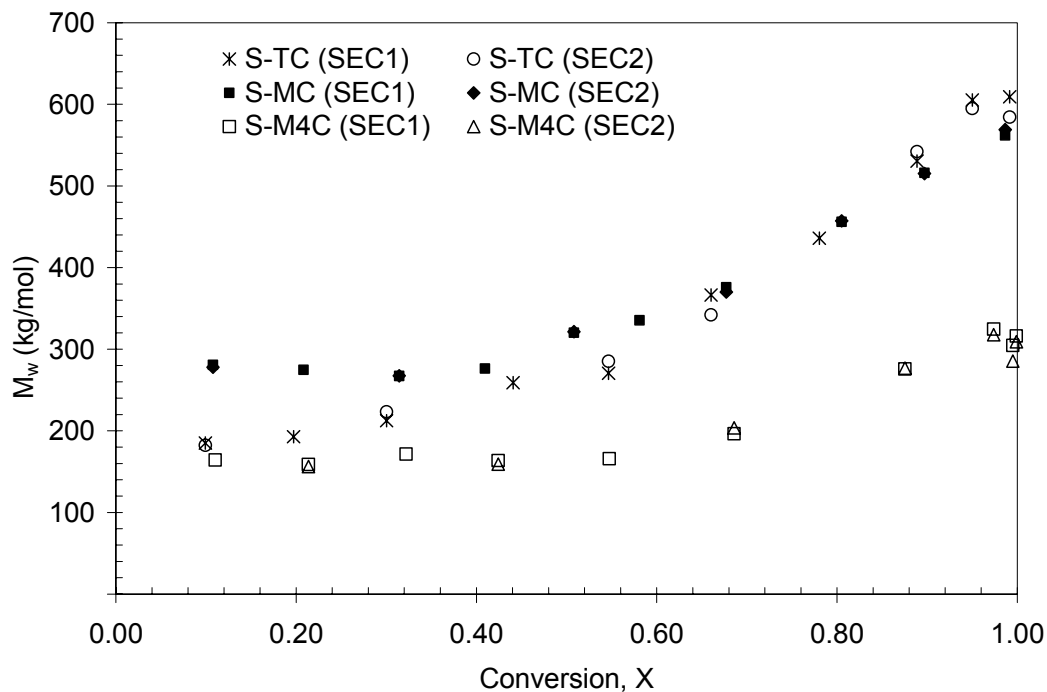


Figure 5.2. Weight-average molecular weight as a function of conversion for the bulk polymerization of styrene at 110°C ($C = 0.004$ M, $4C = 0.016$ M).

Figure 5.3 is a plot of the polydispersity results for the styrene experiments. The curves indicate that at low conversions each of the three conditions ($[JWEB50]_0 = 0.004$ M, $[TBEC]_0 = 0.004$ M, and $[TBEC]_0 = 0.016$ M) produce polymer with a similar polydispersity. However, at higher conversions it was found that the tetrafunctional initiator produced polymer with a somewhat broader molecular weight distribution. This effect is clearly shown when examining the evolution of the SEC traces as the reaction progresses. Figures 5.4 and 5.5 provide the chromatograms obtained from SEC1 for several samples from experiments S-TC and S-MC. The RI and 90° LS signals are shown in arbitrary units. For the case of the tetrafunctional initiator we find that as conversion increases a shoulder appears at lower elution volumes indicating a high molecular weight fraction. This shoulder can be seen in both the refractive index and the light scattering signals. This phenomenon is not seen when we examine the evolution of chromatograms for polymer produced with the monofunctional initiator.

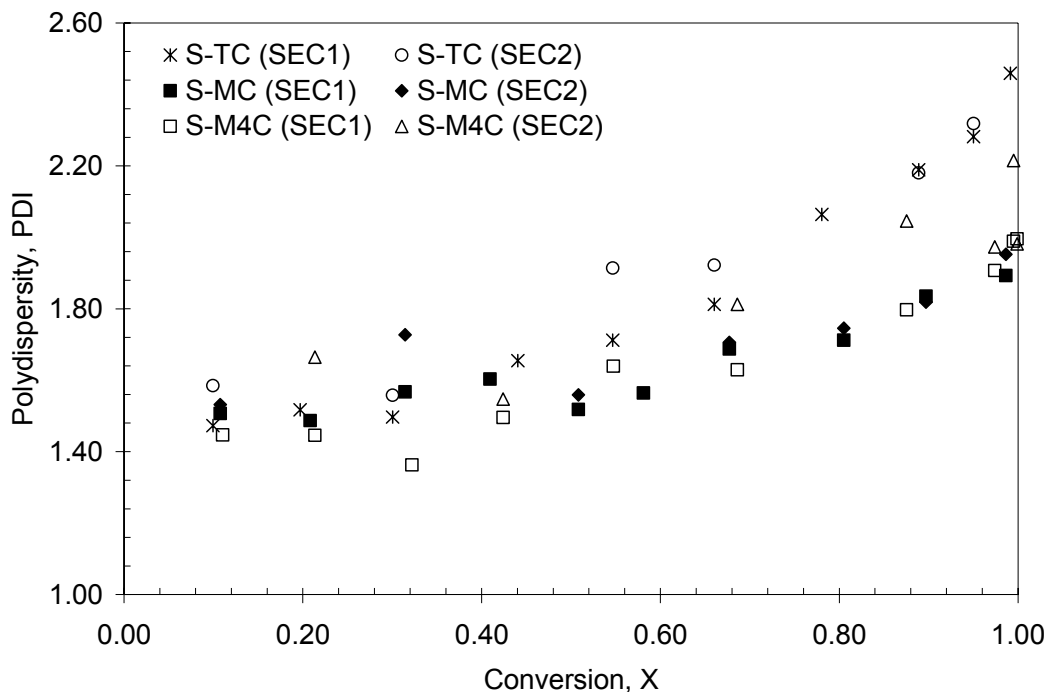


Figure 5.3. Polydispersity as a function of conversion for the bulk polymerization of styrene at 110°C ($C = 0.004$ M, $4C = 0.016$ M).

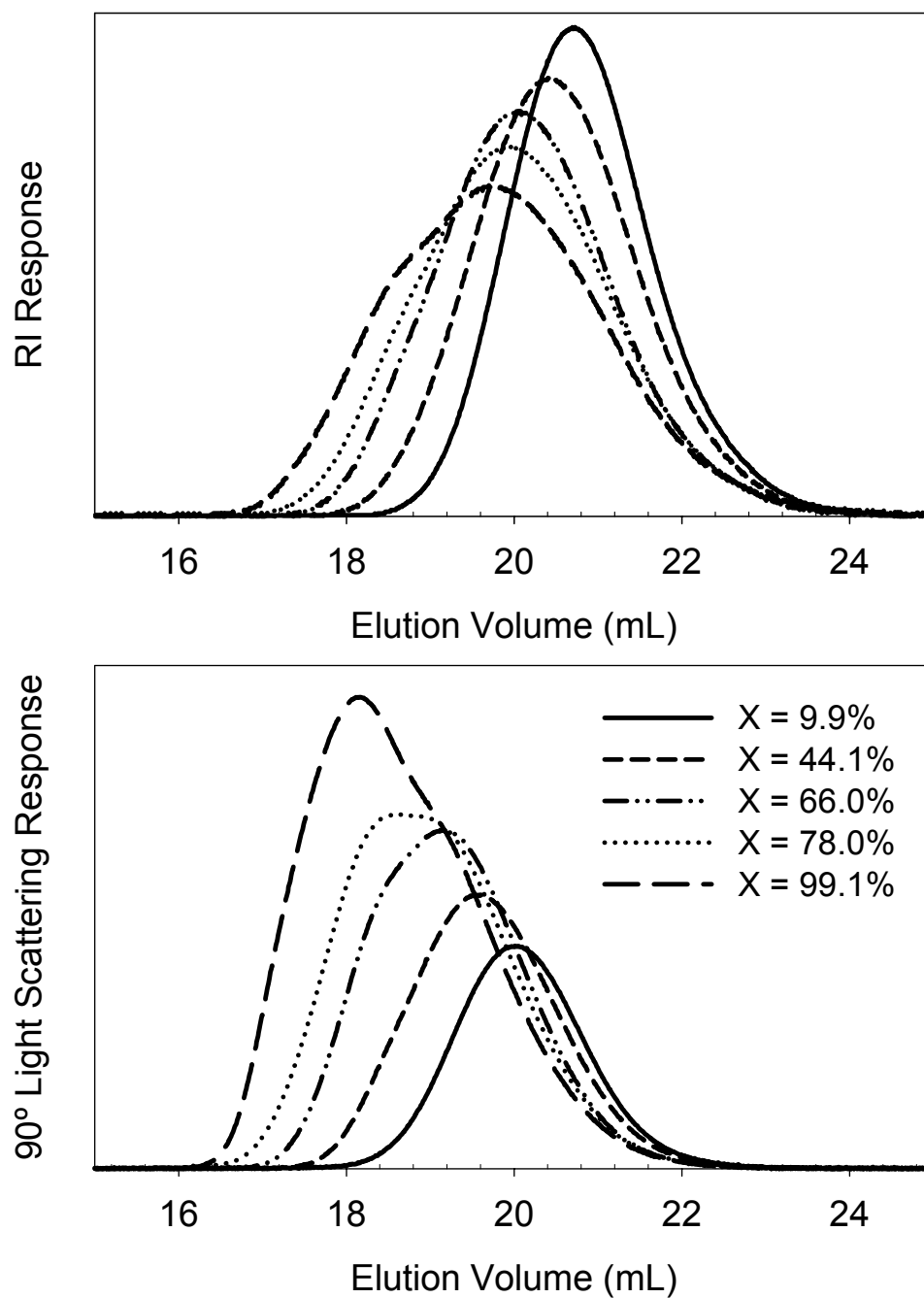


Figure 5.4. SEC chromatograms for polymer samples from experiment S-TC (from SEC1).

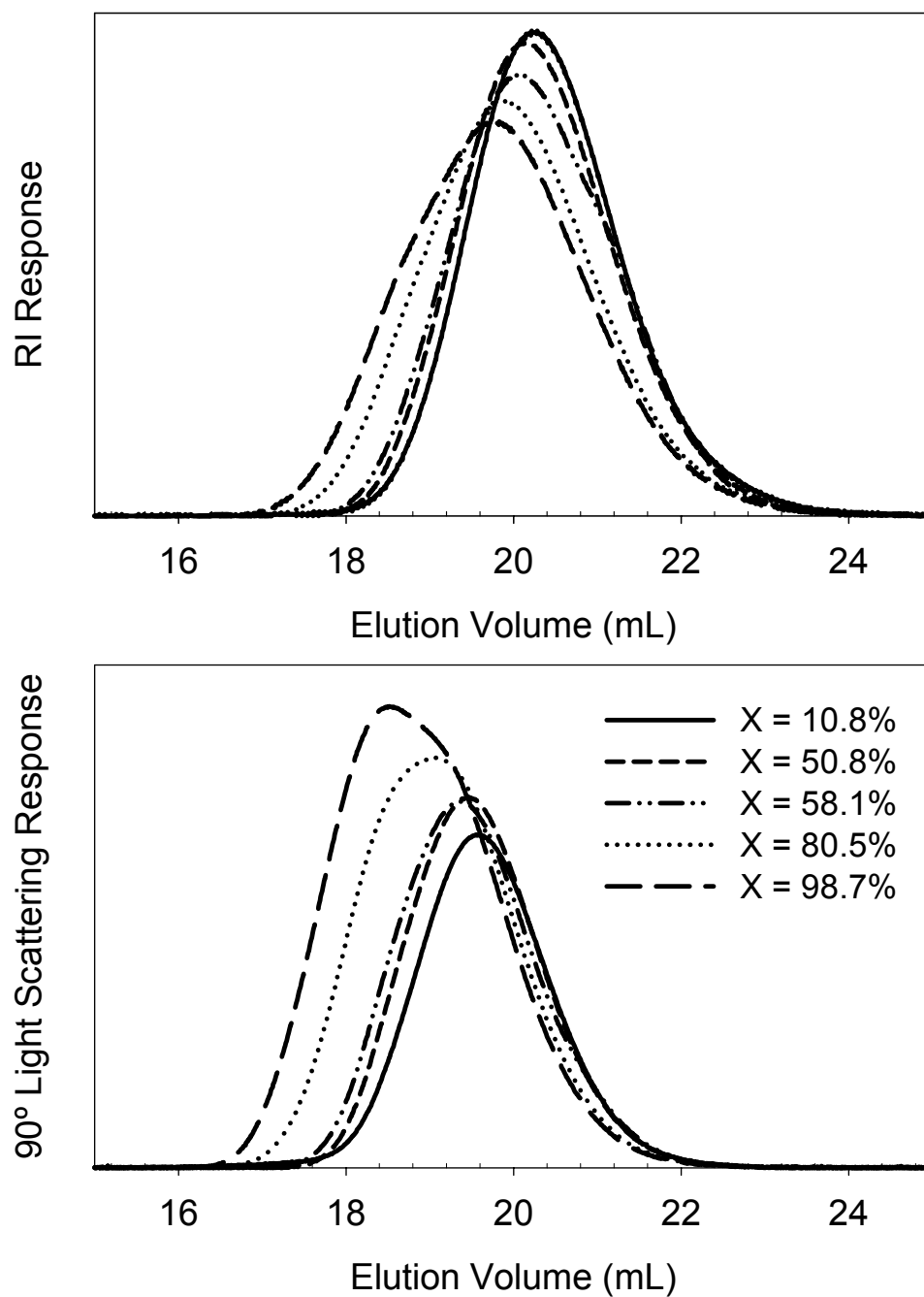


Figure 5.5. SEC chromatograms for polymer samples from experiment S-MC (from SEC1).

Conversion versus time results for the homopolymerization of MMA are shown in Figure 5.6. Again, it is observed that the tetrafunctional initiator produces a higher rate of polymerization compared to the monofunctional initiator when used at the same

concentration. Similar to the homopolymerization of styrene, the curve for JWEB50 overlaps that of TBEC at a concentration four times that of the tetrafunctional initiator. In contrast, when we examine the molecular weight results for MMA we do not find the same trends previously observed with styrene. Figure 5.7 presents the weight-average molecular weight estimates for the three MMA homopolymerization experiments. The data show that the polymer produced with the tetrafunctional initiator has molecular weights much lower than when the monofunctional initiator is employed at the same concentration. In fact, the results for JWEB50 are similar to the curve observed for TBEC at a concentration four times as high.

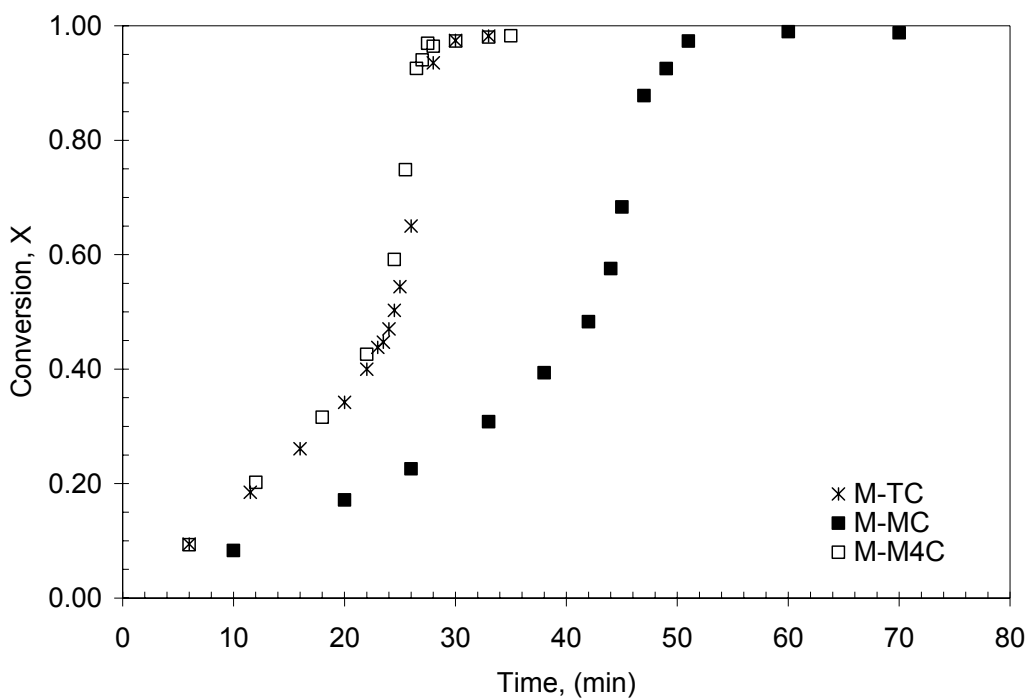


Figure 5.6. Monomer conversion as a function of time for the bulk polymerization of MMA at 110°C ($C = 0.004$ M, $4C = 0.016$ M).

In the case of MMA, differences between the polydispersity for polymer produced with the tetrafunctional initiator compared to the monofunctional counterpart were not observed. As well, a comparison between the SEC chromatograms for the PMMA samples did not show a high molecular weight shoulder for the polymer produced with

JWEB50. In fact, no discernible differences were observed between the SEC traces for polymer produced with JWEB50 compared to those samples initiated with TBEC.

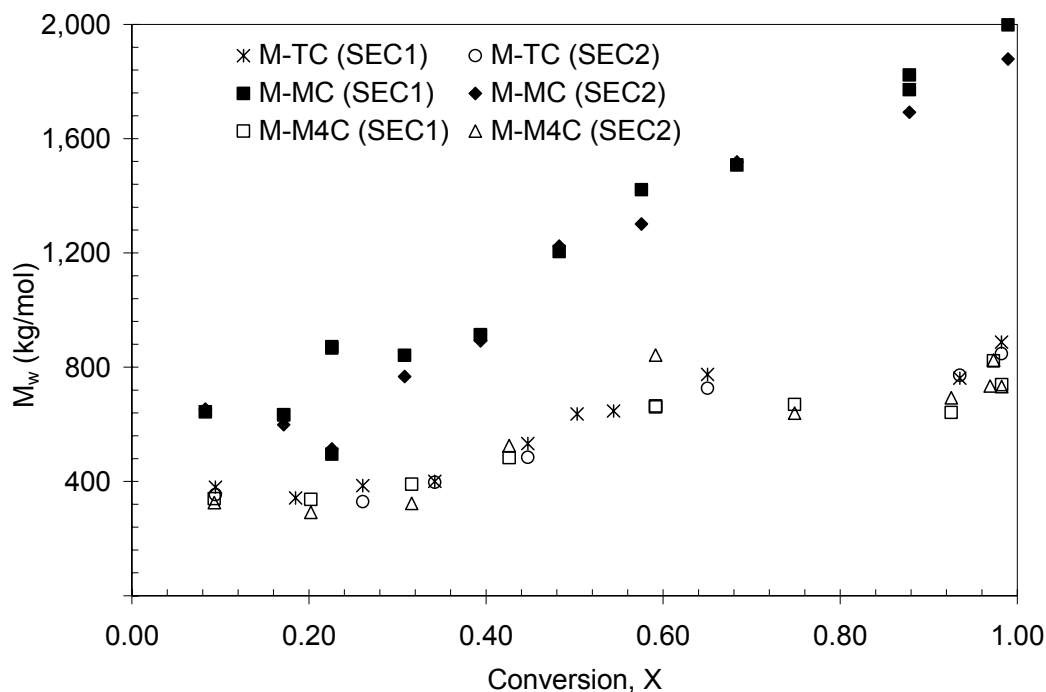


Figure 5.7. Weight-average molecular weight as a function of conversion for the bulk polymerization of MMA at 110°C ($C = 0.004$ M, $4C = 0.016$ M).

These observations with styrene and MMA are comparable to what has previously been reported (1, 2). With styrene, the tetrafunctional initiator would produce higher rates of polymerization while maintaining similar molecular weights compared to the monofunctional counterpart. However, this benefit was not observed with MMA and it was found that using the tetrafunctional initiator is equivalent to employing the monofunctional initiator at a concentration four times as high. The varying results between the two monomers have been attributed to their different modes of termination. For the temperature range studied, styrene is known to terminate predominately by radical coupling while in the case of methyl methacrylate radicals terminate mostly by disproportionation. Figure 5.8 provides an example of the influence the mode of termination will have on the degree of polymerization. We consider a theoretically simple situation where a tetra-radical has n monomer units for each arm and terminates

homopolymerizations of MMA and styrene, we observe that the tetrafunctional initiator yields a rate of polymerization similar to that of the monofunctional initiator at a concentration four times as high. Molecular weight results for this comparison are shown in Figure 5.10. The data show trends that are a mixture of what has been observed for the homopolymerization of styrene and methyl methacrylate. Initiating the polymerization with the tetrafunctional initiator has produced polymer with molecular weights in between those trends observed for the monofunctional initiator at the high and low concentrations (0.004 M and 0.016 M). The polydispersity of the polymer was calculated and no difference was observed between the three runs. Figure 5.11 shows the accumulated polymer composition as a function of conversion for the copolymerization experiments of styrene and MMA. As expected, the data indicate that the tetrafunctional initiator does not influence copolymer composition.

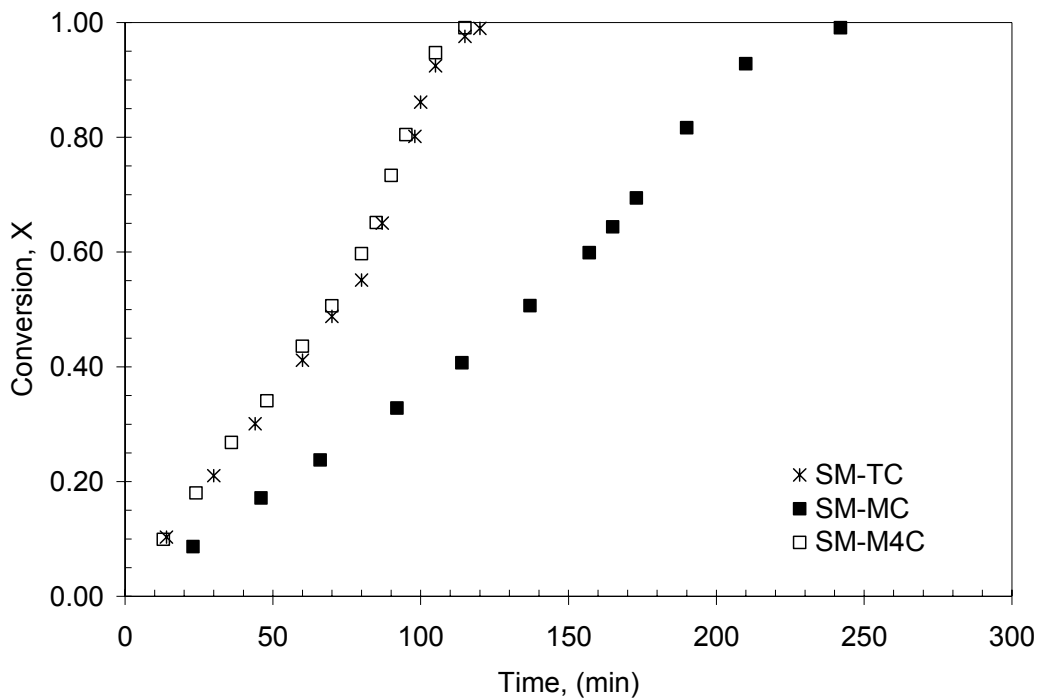


Figure 5.9. Monomer conversion as a function of time for the bulk copolymerization of styrene and MMA at 110°C ($C = 0.004$ M, $4C = 0.016$ M).

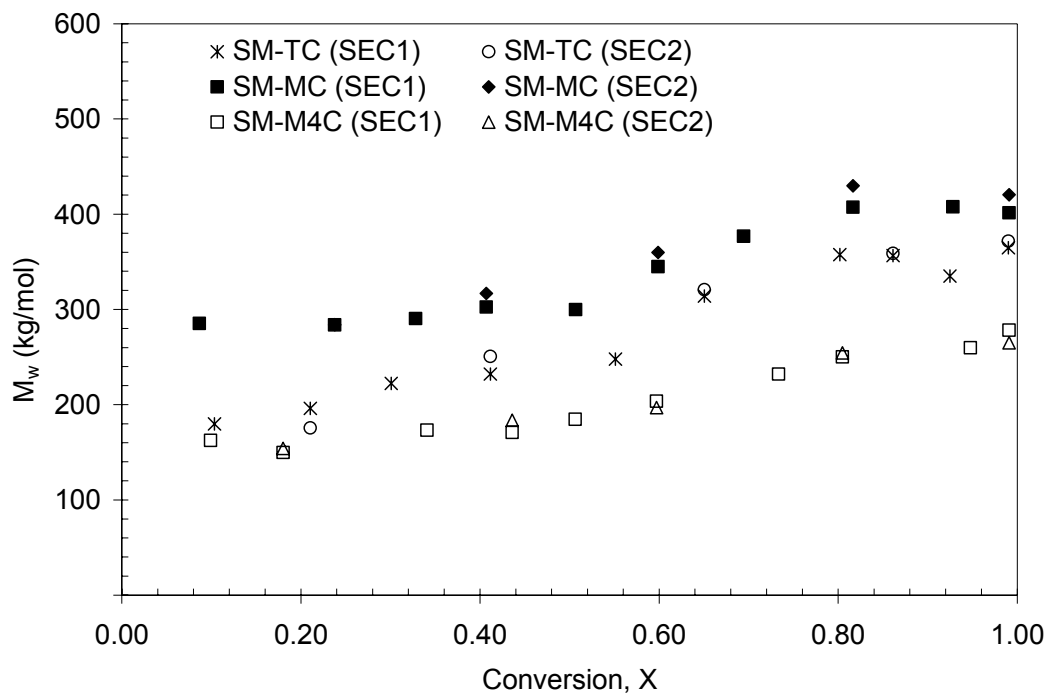


Figure 5.10. Weight-average molecular weight as a function of conversion for the bulk copolymerization of styrene and MMA at 110°C ($C = 0.004$ M, $4C = 0.016$ M).

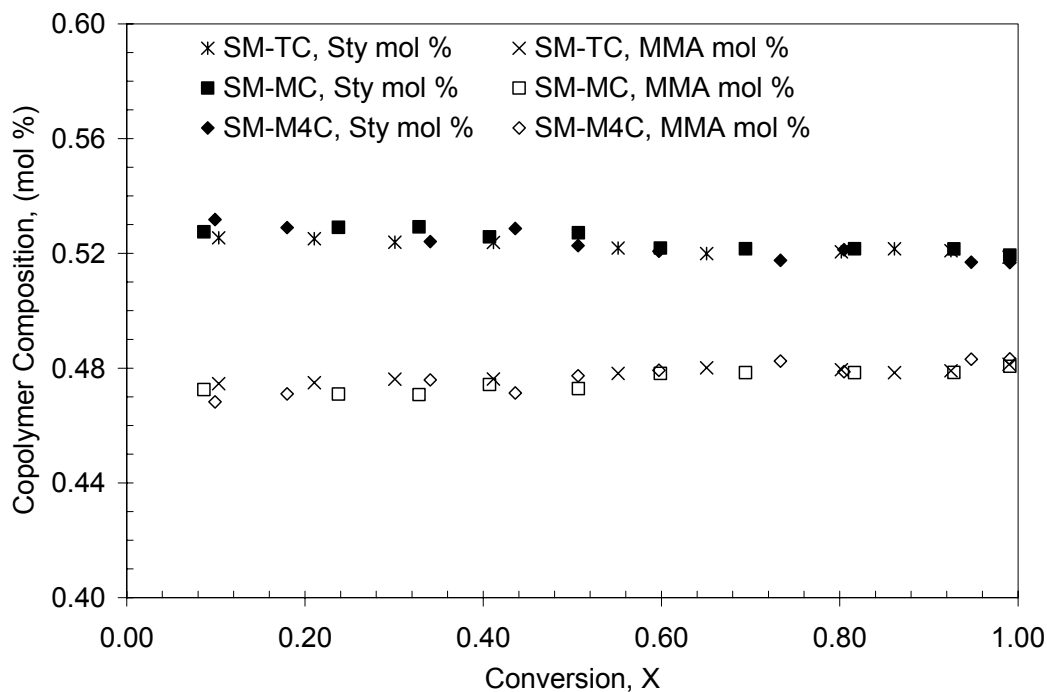


Figure 5.11. Copolymer composition as a function of conversion for the bulk copolymerization of styrene and MMA at 110°C ($C = 0.004$ M, $4C = 0.016$ M).

5.3.1.2 Evidence of Branching

The examination of dilute solution properties is a common method for discovering evidence of branching within a polymer sample and has been the subject of a variety of experimental and theoretical studies (13-17). One of the most fundamental properties that can be obtained from dilute solution methods is the size of a polymer molecule, normally measured as the mean-square radius:

$$\langle S^2 \rangle = \left\langle \frac{\sum_{i=1}^N r_i^2}{N} \right\rangle \quad 5.1$$

where the polymer molecule is separated into N small elements of identical mass and r_i is the distance of the i^{th} unit from the polymer molecule's centre of gravity. The angled brackets denote that the mean-square radius is averaged over all possible conformations. The term radius of gyration is commonly used when referring to a polymer molecule's size and is simply the square root of the mean-square radius:

$$R_g = \langle S^2 \rangle^{1/2} \quad 5.2$$

The influence of branching on the size of a polymer chain is that for a particular molecular weight, an increase in branching will decrease the radius of gyration. To assess the decrease in size due to branching, the mean-square radius of a branched polymer is compared to its linear analog of identical molecular weight. Quantitatively, this is expressed through the following contraction factor:

$$g = \frac{\langle S^2 \rangle_b}{\langle S^2 \rangle_l} = \frac{(R_g^2)_b}{(R_g^2)_l} \quad 5.3$$

where the subscript b denotes that it is the branched polymer and l is for the linear polymer of identical molecular weight. Values of g less than unity are an indication of branching.

The mean-square radius can be determined experimentally from static light scattering experiments through the angular dependence of the intensity of scattered light. However, when the sample is polydisperse, scattering experiments provide the *z*-average mean-square radius. A broad molecular weight distribution can undoubtedly impact polymer properties and it has been found that the influence of branching can be completely masked by a large polydispersity. As such, differences between results for an unfractionated branched sample and its linear counterpart will be indiscernible. Coupling a light scattering device with SEC is a method to overcome this problem. Assuming that SEC adequately fractionates the polymer sample, the LS detector cell should contain monodisperse fractions at any particular time and a distribution of the radius of gyration as a function of molecular weight can be obtained.

Figures 5.12 (a), (b) and (c) are radius of gyration plots for the three different styrene-MMA feed mixtures. The plots provide a comparison between polymer produced with the tetrafunctional initiator and polymer produced with the monofunctional initiator. In the case of the homopolymers, an extra curve is included for a polydisperse linear polystyrene standard (American Polymer Standards Corp.). The polystyrene data show that the broad standard and the polymer produced with the monofunctional initiator have identical curves for radius of gyration as a function of molecular weight. The results for these two samples show the expected linear trend in a double logarithmic plot as R_g is related to molecular weight by the following equation:

$$R_g = aM^b \quad 5.4$$

A value of 0.5 or greater for the exponent is expected for linear polymers in a good solvent. Using nonlinear regression, estimates of *a* and *b* were obtained for the broad molecular weight standard and the sample produced with the monofunctional initiator (see Table 5.3). These estimates are comparable to what has been previously reported in the literature (16, 18, 19).

When examining the data for the polymer produced with the tetrafunctional initiator, it can be seen that at low molecular weights the three curves overlap (Figure 5.12 (a)). This is an indication that in the low molecular weight range, the polymer produced with JWEB50 is linear. However, in the high molecular weight range, the data for the tetrafunctional initiator curves away and downwards from the data for the broad standard and for the polymer produced with TBEC. The fact that at a particular molecular weight, the polymer produced with JWEB50 has a lower radius of gyration than the polymer generated with TBEC is an indication that the former is more branched.

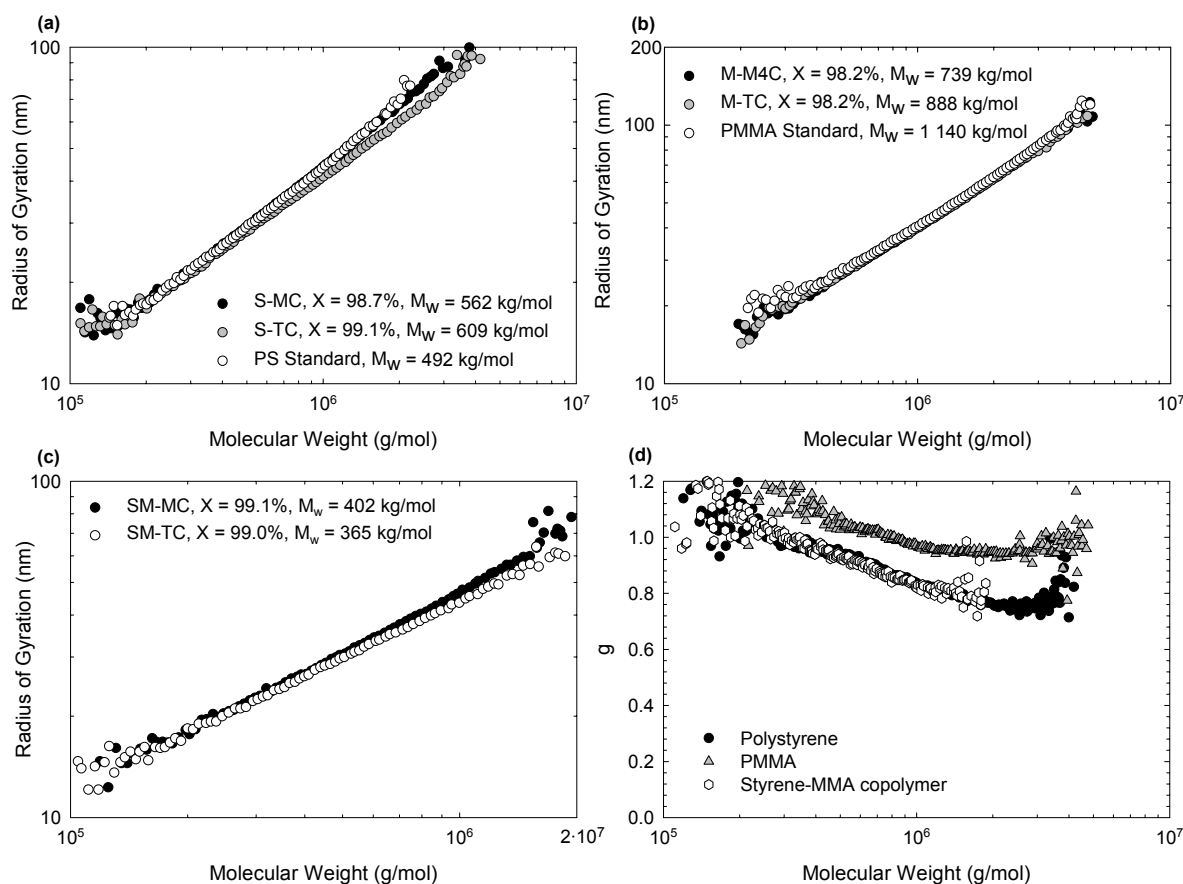


Figure 5.12. Radius of gyration and corresponding branching factor as a function of molecular weight: (a) polystyrene; (b) poly(methyl methacrylate); (c) styrene-methyl methacrylate copolymer; (d) g values for PS, PMMA and copolymer samples produced with the tetrafunctional initiator.

Table 5.3. Power law coefficients for radius of gyration-molecular weight relationship and Kuhn-Mark-Houwink-Sakurada coefficients.

Sample	a (nm)	b	K (dL/g)	α
S-MC (sample 14)	0.0103	0.606	1.38×10^{-4}	0.705
Broad PS	0.00987	0.609		
M-M4C (sample 14)	0.00616	0.636	1.55×10^{-4}	0.747
Broad PMMA	0.00501	0.652		
SM-MC (sample 12)	0.0103	0.610	1.16×10^{-4}	0.722

Figure 5.12 (b) provides the comparison for the poly(methyl methacrylate) samples. Unlike the case of polystyrene, deviations between the curves for the broad standard and the polymer samples produced with the tetra- and monofunctional initiators were not found. Based on these results we do not see any evidence of branching when the tetrafunctional initiator is employed with methyl methacrylate. This observation was somewhat unexpected. A comparison of the rate data for the two initiators suggested that the functional groups for the tetrafunctional initiator were fully decomposing and behaving similar to those of the monofunctional initiator. From this, we would expect that branched polymers had formed. If this was the case, then it could be that SEC-MALLS is not sensitive enough to detect low levels of branching in these samples.

A characteristic of SEC is that separation occurs based on hydrodynamic size. If the polymer sample contains a mixture of branched and linear chains, each with their own molecular weight distribution, it is possible for branched and linear molecules to have the same hydrodynamic size but differing molecular weights. When this occurs, the branched and linear polymer chains will not be separated by SEC. The detector cells will then no longer contain monodisperse fractions and the results will represent an average. As previously mentioned, the R_g estimate obtained from light scattering experiments is a z-average and the effect of polydispersity can counterbalance any reduction in R_g caused by branching.

Because JWEB50 was employed in a free radical process, the final polymer will have a branching distribution due to several factors including the structure of JWEB50, coupling of multi-radicals, and in a more general case, also due to chain transfer to polymer and terminal double bond polymerization, with each fraction having its own molecular weight distribution. However, revisiting the example shown in Figure 5.8 may explain why branching is not seen with MMA. In the case of styrene, the fact that radicals terminate predominantly by coupling means that the tetra-chains have the potential to grow much larger than the linear chains. As well, radical coupling helps reduce the number of linear chains compared to radicals terminating by disproportionation. These two factors would help branching to be detected because the branched chains would be significantly larger than the linear chains and the fraction of linear chains would be smaller, thus limiting coelution.

The radius of gyration plot for the styrene-MMA copolymer data is shown in Figure 5.12 (c). The results are a combination of what was seen with the homopolymers. The data for the polymer produced with the tetrafunctional initiator only curve slightly away from the linear sample. Using the relationship given by equation 5.4 and the parameters in Table 5.3, the branching factor, g , for each of the three samples produced with JWEB50 has been calculated and the results are shown in Figure 5.12 (d). Noise in the detector signals in the low molecular weight and low radius of gyration range contributes to the scatter in the data and to the values of g being greater than unity. The data indicate that the PMMA sample is not branched while the PS and copolymer samples show similar levels of branching.

In addition to the LS results, the viscometer can provide similar information about branching as it allows for the determination of the polymer intrinsic viscosity, $[\eta]$, and its appropriate contraction factor:

$$g' = \frac{[\eta]_b}{[\eta]_l} \quad (5)$$

where the intrinsic viscosity values are for branched and linear polymers of identical molecular weight. Coupled with SEC, the viscometer produces a Kuhn-Mark-Houwink-Sakurada (KMHS) plot for each sample (see Figures 5.13 (a), (b) and (c)). The KMHS plots show similar trends to those observed with the radius of gyration plots. Evidence of branching was detected for PS and the styrene-MMA copolymer produced with the tetrafunctional initiator. However, in the case of PMMA no discernible difference was detected between polymer produced with the monofunctional and tetrafunctional initiators. In order to estimate values of g' , the KMHS coefficients were obtained from nonlinear regression and used to calculate the intrinsic viscosity of the linear polymer (see Table 5.3). The estimates of K and α are similar to those reported in the literature (14, 16, 20).

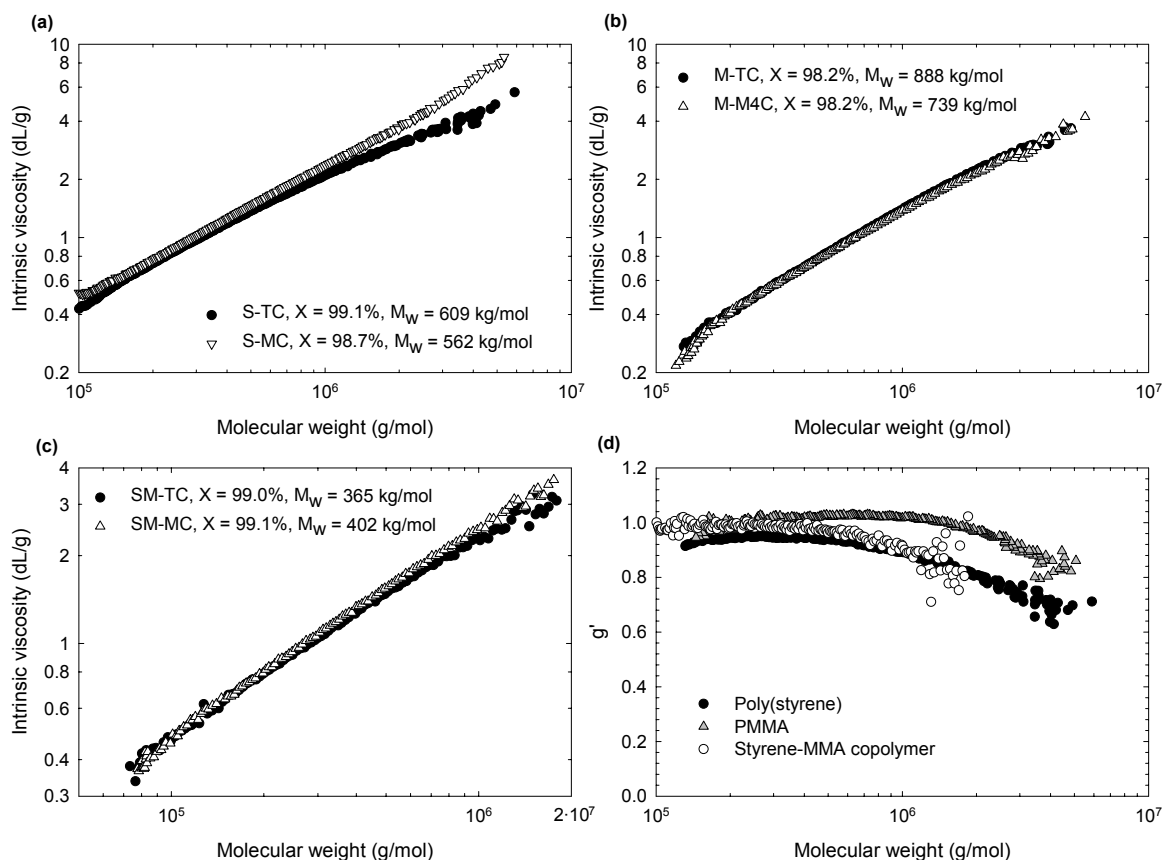


Figure 5.13. Intrinsic viscosity and corresponding branching factor as a function of molecular weight: (a) polystyrene; (b) poly(methyl methacrylate); (c) styrene-methyl methacrylate copolymer; (d) g' values for PS, PMMA and copolymer samples produced with the tetrafunctional initiator.

Figure 5.13 (d) provides a plot of g' as a function of molecular weight for the three samples produced with the tetrafunctional initiator. One point to note is the results indicate that the PMMA sample could be slightly branched in the very high molecular weight range. However, this sample is no more branched than the PMMA sample produced with TBEC as both their KMHS plots overlap (see Figure 5.13 (b)). In fact, the g' curve for the PMMA sample produced with TBEC (not shown) and the curve for the sample produced with JWEB50 completely overlap, thus indicating that both samples have the same level of branching. A certain (low) amount of branching can be generated with a monofunctional initiator because of the nature of the free radical polymerization. For example, terminal double bonds formed by radicals terminating through disproportionation might eventually be consumed and form trifunctional branches.

5.3.1.3 Effect of Longer Reaction Times

In several of the experiments for the homopolymerization of styrene, it was observed that at low and mid conversions, both initiators produced polymer of similar molecular weight. However, towards the end of the reaction it was found that the polymer molecular weights were increasing more with the tetrafunctional initiator than with the monofunctional initiator. As a result, a final block of experiments with styrene and MMA were completed to study the use of the tetrafunctional initiator at longer reaction times. It was found in the polymerization of styrene with JWEB50 that the molecular weight increased further even though full conversion had been reached. Figure 5.14 shows the weight-average molecular weight results for the homopolymerization of styrene at 120 °C where each of the samples analyzed had reached a conversion of 99% or greater. The molecular weight data show an increasing trend for the polymerization initiated with the tetrafunctional initiator. However, in the case of the monofunctional initiator, it was found that the molecular weight of the polymer did not change over time (note that at 600 minutes three data points are plotted for three different samples). Figure 5.15 provides chromatograms for three samples produced with JEWB50 for various reaction times. The curves show that the high molecular shoulder increases with time even though full conversion has been reached. Looking at the data for the

homopolymerization of MMA a different trend was observed. The tetrafunctional initiator did not cause the polymer molecular weight to increase after the final limiting conversion had been reached (see Figure 5.16).

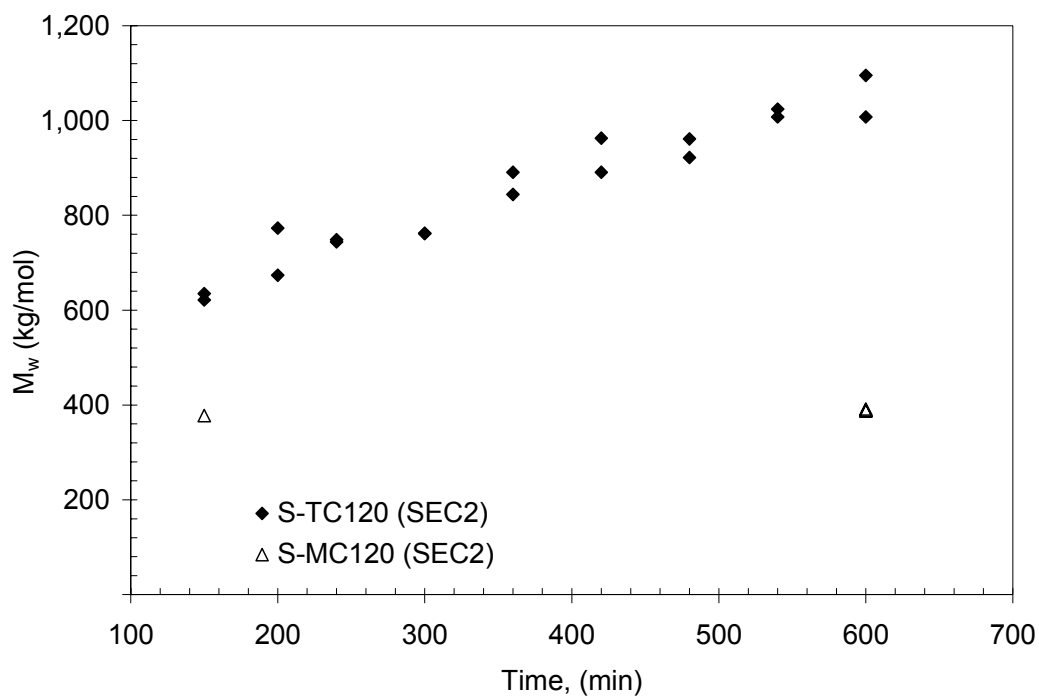


Figure 5.14. Weight-average molecular weight as a function of conversion for the bulk polymerization of styrene at 120°C (all samples are >99% conversion).

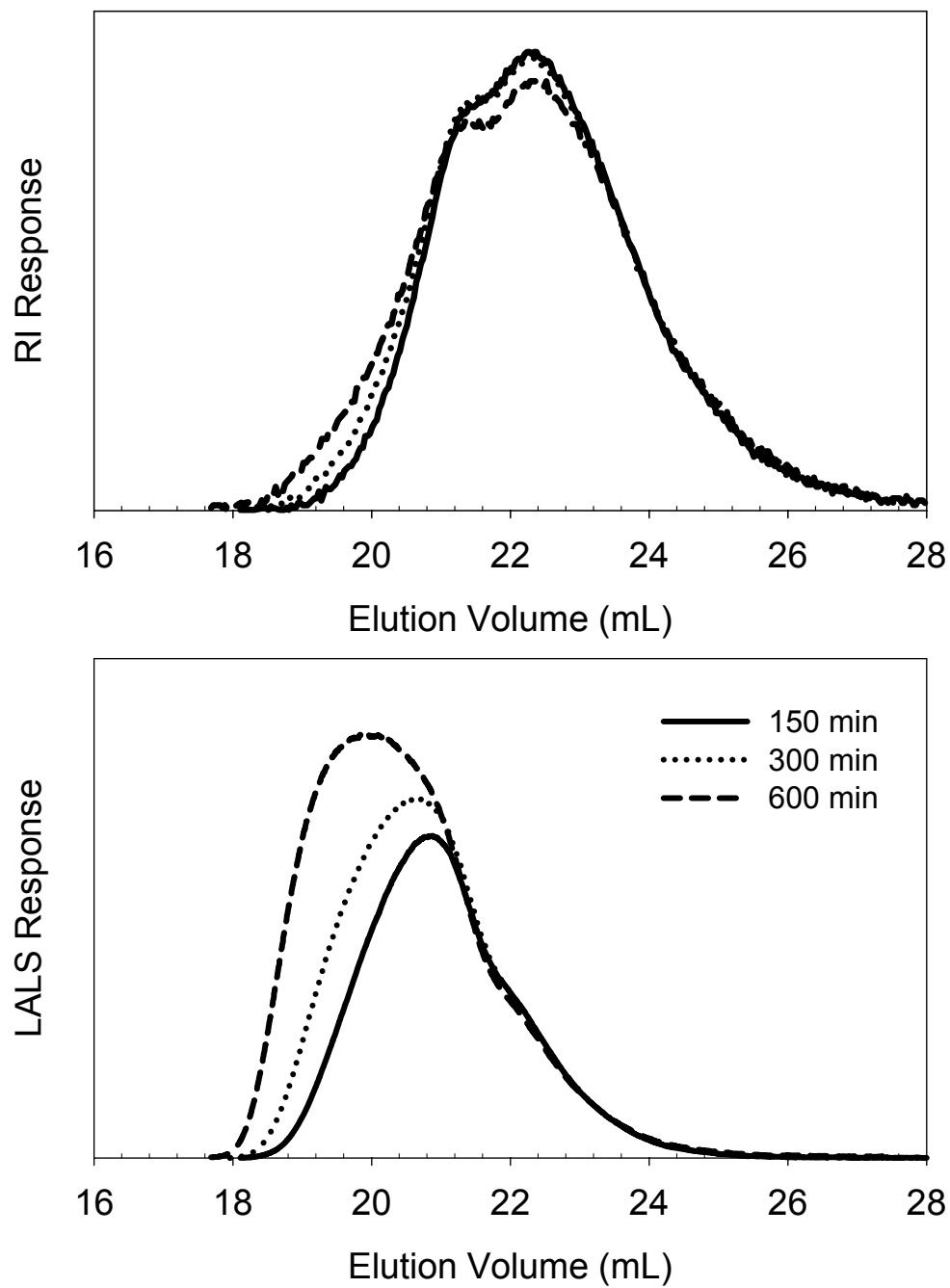


Figure 5.15. SEC chromatograms for polymer samples from experiment S-TC120 (from SEC2).

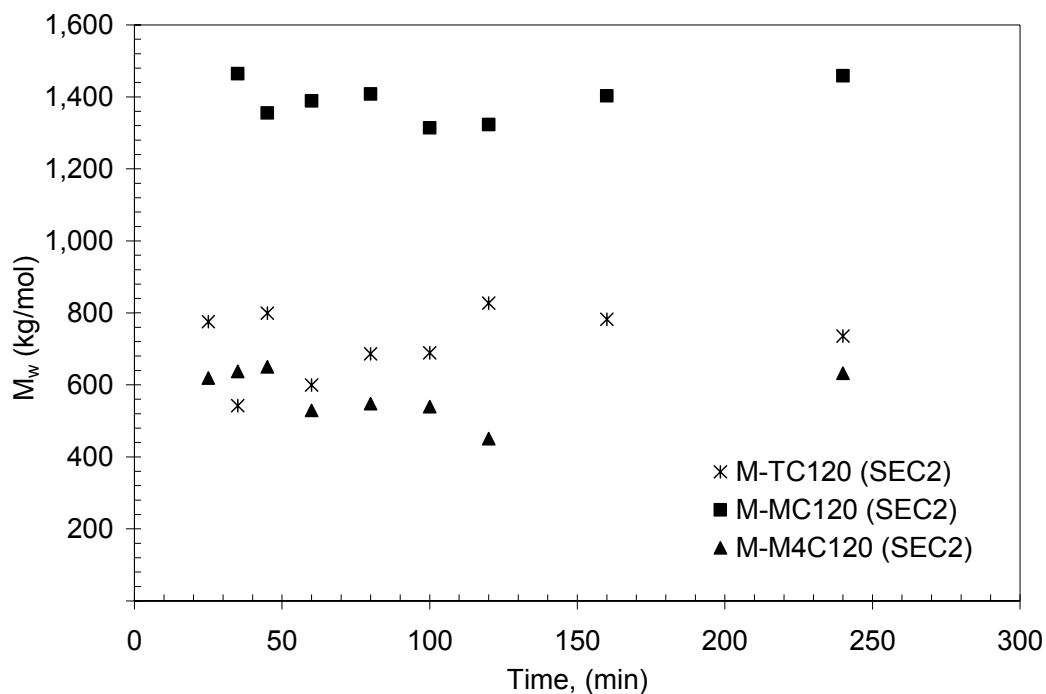


Figure 5.16. Weight-average molecular weight as a function of conversion for the bulk polymerization of MMA at 120°C (all samples are >99% conversion).

5.3.2 Methyl Methacrylate and α -Methyl Styrene Copolymer

Three experiments were performed with a comonomer feed mixture of α -methyl styrene and methyl methacrylate to examine the behaviour of the tetrafunctional initiator with a monomer that readily depropagates. α -MS is known to have a low ceiling temperature of 61°C for the pure monomer. Its use as a comonomer has several advantages including its ability to act similarly to a chain transfer agent and lower the polymer molecular weight, and its ability to increase the polymer glass transition temperature (poly(α -MS) T_g = 177°C compared to PS T_g = 100°C). However, the use of α -MS does have drawbacks as it can significantly lower the rate of polymerization. These features are evident when comparing the conversion and molecular weight data of the homopolymerization of MMA (see Figures 5.6 and 5.7) to the copolymerization of MMA with α -MS (see Figures 5.17 and 5.18). Looking at the experiments with TBEC as an example, the addition of 20 wt.% α -MS significantly extended the reaction times to reach a limiting conversion (~20

times longer) and molecular weights were noticeably reduced (full conversion: no α -MS, $M_w \approx 2 \times 10^6$; with α -MS, $M_w \approx 5 \times 10^5$).

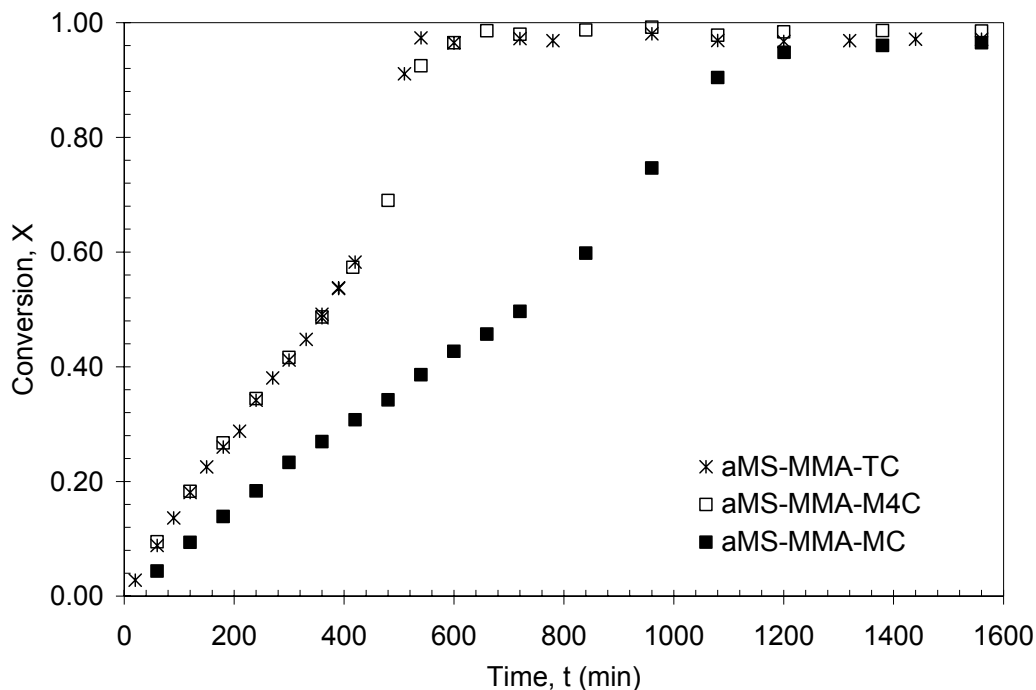


Figure 5.17. Monomer conversion as a function of time for the bulk copolymerization of α -methyl styrene and MMA at 110°C ($C = 0.004$ M, $4C = 0.016$ M).

When comparing the conversion, molecular weight and composition results for the α -MS-MMA experiments to those observed for the copolymerization of styrene and MMA, several similarities were observed. The conversion data again indicated that the tetrafunctional initiator produced a faster rate of polymerization compared to the monofunctional initiator and that similar rates can be obtained when the monofunctional initiator is employed at a concentration four times as great (see Figure 5.17). The molecular weight results showed that the use of JWEB50 produced polymer of similar molecular weight to when TBEC is used at the same concentration (see Figure 5.18). As well, the intrinsic viscosity data indicate that the polymer produced with the tetrafunctional initiator is more branched than the polymer produced with the monofunctional initiator (see Figure 5.19). An interesting point to note is that for the copolymerization of an equal feed mixture of styrene and MMA, we observed trends that

were halfway between those of pure styrene and pure MMA (i.e., JWEB50 produced polymer molecular weights that were bounded by the trends for TBEC). However, in the case of the copolymerization with α -MS, we do not see a combination of the trends found with styrene and MMA. In fact, with a small amount of α -MS, we see trends similar to those observed with pure styrene. Therefore, with the addition of α -MS, the polymerization of MMA with the tetrafunctional initiator produced high rates and high molecular weights compared to TBEC. Although not shown here for the sake of brevity, the copolymer composition was again not affected by initiator functionality.

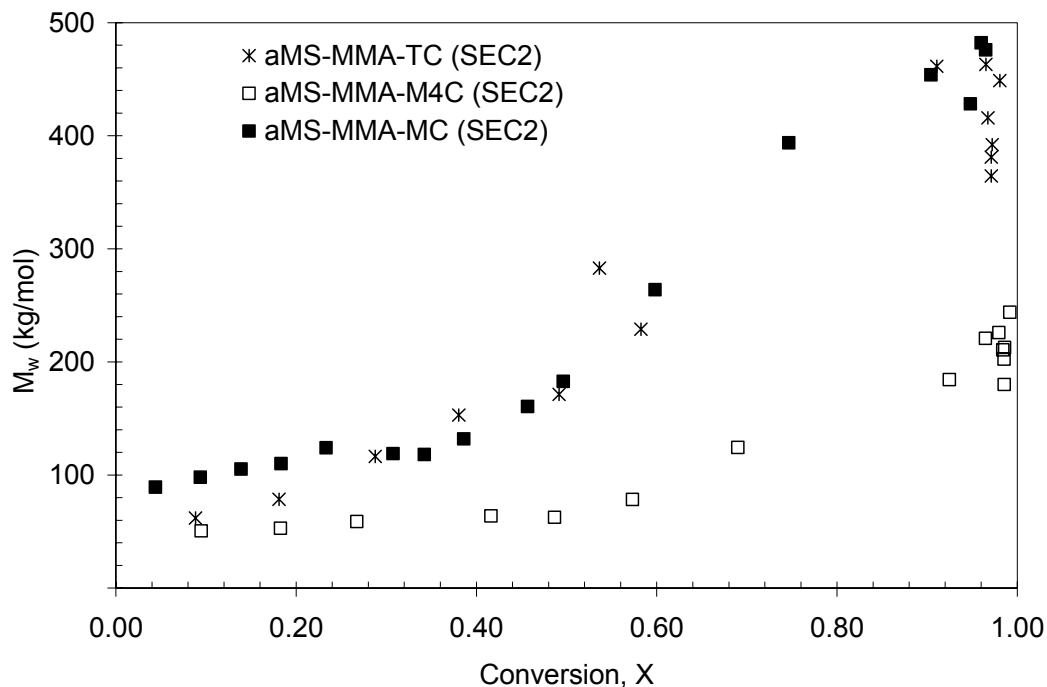


Figure 5.18. Weight-average molecular weight as a function of conversion for the bulk copolymerization of α -methyl styrene and MMA at 110°C ($C = 0.004$ M, $4C = 0.016$ M).

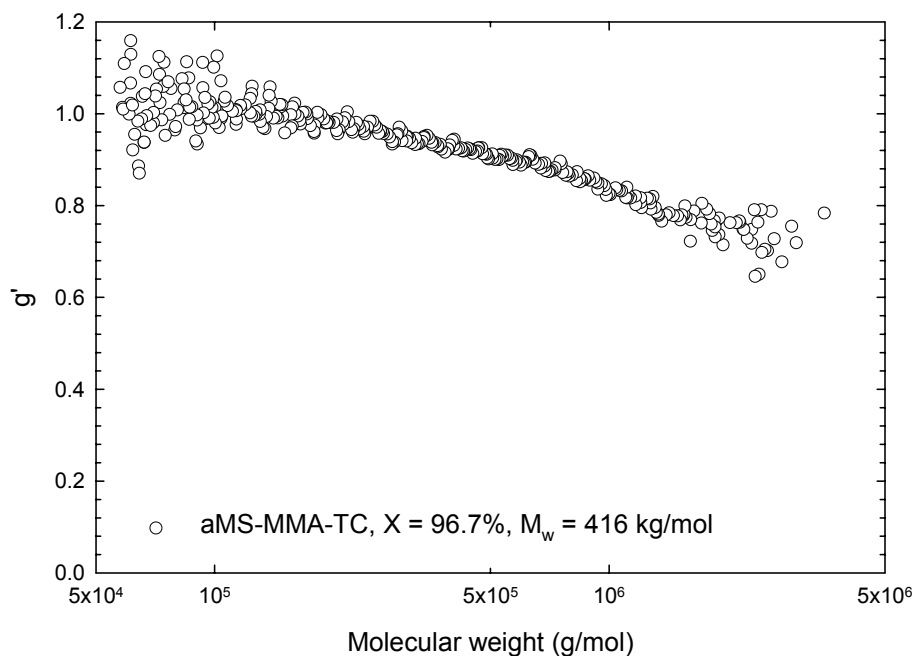


Figure 5.19. Intrinsic viscosity contraction factor as a function of molecular weight for polymer produced with the tetrafunctional initiator.

5.4 Conclusions

The use of JWEB50, a tetrafunctional peroxide initiator, in the bulk polymerization of various systems including styrene, MMA, styrene-MMA and α -MS-MMA was investigated. Comparisons with respect to the rate of polymerization and polymer molecular weight were made to TBEC, a monofunctional initiator with a functional group of similar structure and thermal stability to those of JWEB50. For every monomer and comonomer feed mixture studied, JWEB50 produced similar conversion-time data to that obtained with TBEC at a concentration four times as great. The results demonstrate that regardless of monomer type, the tetrafunctional initiator generates a higher rate of polymerization compared to its monofunctional counterpart.

Examination of the molecular weight results showed varying trends for the different feeds. In the case of styrene, JWEB50 produced molecular weight averages similar to those obtained with TBEC at the same concentration. As well, towards the end of the

polymerization, higher polydispersities were observed with JWEB50 and inspection of the SEC traces showed the appearance of a high molecular weight shoulder not seen when using the monofunctional initiator. Experiments completed at longer reaction times with styrene showed that even after the final limiting conversion had been obtained, the polymer molecular weights kept on increasing when JWEB50 was employed. This was not observed with the monofunctional initiator. In contrast, for the homopolymerization of MMA, JWEB50 was found to decrease the molecular weight to a level similar to the results for TBEC at a concentration four times as great. SEC traces for polymer generated with the two initiators did not show any differences. As well, the increase in molecular weight after a limiting conversion was reached with JWEB50 was not observed with MMA. When a similar set of experiments were conducted with a 50/50 mixture of styrene and MMA, the molecular weight results were a combination of the trends observed for the two homopolymer cases. JWEB50 was found to produce molecular weights in between those for TBEC at the high and low concentrations. Plots of radius of gyration, intrinsic viscosity and their corresponding branching factors showed samples produced with JWEB50 were more branched than those for TBEC in the case of styrene and its copolymers. No evidence of branching was found with MMA. With a relatively small addition of α -MS to MMA, the use of JWEB50 allowed high molecular weight polymer to be produced and evidence of branching was shown via g' estimates.

5.5 References

1. Fityani-Trimmi, S., Dhib, R., Penlidis, A. Free Radical Polymerization of Styrene with a New Tetrafunctional Peroxide Initiator. *Macromolecular Chemistry and Physics* **2003**, *204*, 436-442.
2. Scolah, M. J., Dhib, R., Penlidis, A. Free-radical polymerization of methyl methacrylate with a tetrafunctional peroxide initiator. *Journal of Polymer Science Part A-Polymer Chemistry* **2004**, *42* (22), 5647-5661.
3. Prisyazhnyuk, A. I., Ivanchev, S. S. Diperoxides with differing thermal stabilities of the peroxide group as initiators of radical polymerization and block copolymerization. *Polymer Science USSR* **1970**, *12* (2), 514-524.
4. Kamath, V. R. New initiators for PS offer big efficiencies. *Modern Plastics* **1981**, *58* (9), 106-110.

5. Simionescu, C. I., Comanita, E., Pastravanu, M., Dumitriu, S. Progress in the field of bi- and poly-functional free-radical polymerization initiator. *Progress in Polymer Science* **1986**, *12*, 1-109.
6. Choi, K. Y., Lei, G. D. Modeling of free radical polymerization of styrene by bifunctional initiators. *AIChE Journal* **1987**, *33* (12), 2067-2076.
7. Villalobos, M. A., Hamielec, A. E., Wood, P. E. Kinetic model for short-cycle bulk styrene polymerization through bifunctional initiators. *Journal of Applied Polymer Science* **1991**, *42*, 629-641.
8. González, I. M., Meira, G. R., Oliva, H. M. Synthesis of polystyrene with mixtures of mono- and bifunctional initiators. *Journal of Applied Polymer Science* **1996**, *59*, 1015-1026.
9. Cavin, L., Rouge, A., Meyer, T., Renken, A. Kinetic modeling of free radical polymerization of styrene initiated by the bifunctional initiator 2,5-dimethyl-2,5-bis(2-ethyl hexanoyl peroxy)hexane. *Polymer* **2000**, *41*, 3925-3935.
10. Dhib, R., Gao, J., Penlidis, A. Simulation of free radical bulk/solution homopolymerization using mono- and bi-functional initiators. *Polymer Reaction Engineering Journal* **2000**, *8*, 299-464.
11. Cerna, J. R., Morales, G., Eyler, G. N., Canizo, A. I. Bulk Polymerization of Styrene Catalyzed by Bi- and Trifunctional Cyclic Initiators. *Journal of Applied Polymer Science* **2002**, *83*, 1-11.
12. Kasehagen, L., Wicher, J., Brennan, J., Debaud, F., Suehisa, T. A New Multifunctional Peroxide Initiator for High Molecular Weight, High Productivity, and Long-Chain Branching. *ANTEC - Soc. Plast. Eng.* **2002**, *60* (2), 1837-1841.
13. Small, P. A. Long-Chain Branching in Polymers. *Adv. Polym. Sci.* **1975**, *18*, 1-64.
14. Ambler, M. R., McIntyre, D. Randomly Branched Styrene/Divinylbenzene Copolymers. II. Solution Properties and Structure. *J. Appl. Polym. Sci.* **1977**, *21*, 2268-2282.
15. Mays, J. W., Hadjichristidis, N. Dilute Solution Properties of Branched Macromolecules. *J. Appl. Polym. Sci. : Appl. Polym. Symp.* **1992**, *51*, 55-72.
16. Jackson, C., Chen, Y.-J., Mays, J. W. Dilute Solution Properties of Randomly Branched Poly(methyl methacrylate). *Journal of Applied Polymer Science* **1996**, *59*, 179-188.
17. Burchard, W. Solution Properties of Branched Macromolecules. *Adv. Polym. Sci.* **1999**, *143*, 113-194.
18. Podzimek, S. The Use of GPC Coupled with a Multiangle Laser Light Scattering Photometer for the Characterization of Polymers. On the Determination of Molecular Weight, Size, and Branching. *J. Appl. Polym. Sci.* **1994**, *54* (1), 91-103.
19. Terao, K. and J. W. Mays *European Polymer Journal* 2004; **40**, 1623-1627.
20. Fetters, L. J., Hadjichristidis, N., Lindner, J. S., Mays, J. W. Molecular Weight Dependence of Hydrodynamic and Thermodynamic Properties for Well-Defined Linear Polymers in Solution. *J. Phys. Chem. Ref. Data* **1994**, *23* (4), 619-640.

CHAPTER 6 - POLYMERIZATION OF BUTYL ACRYLATE AND VINYL ACETATE

6.1 Introduction

The potential advantages of multifunctional initiators in the free radical polymerizations of styrene have been documented by several groups (1, 2, 3, 4, 5, 6, 7). Studies have found that high rates of polymerization and high molecular weights were simultaneously possible by increasing an initiator's functionality (e.g., switching from a monofunctional to a difunctional initiator). Previous chapters have shown that these advantages depend greatly upon on the nature of the monomer being polymerized. Specifically, it has been shown in the polymerization methyl methacrylate (MMA) that a tetrafunctional initiator can be used to give a faster rate of polymerization; however, the molecular weight weights were lower when compared to its monofunctional counterpart. The most significant difference between the polymerization mechanism of styrene and MMA is their modes of termination. Styrene chains typically terminate by radical coupling while in the case of MMA, chains terminate predominately by disproportionation. The next step in our investigation of the behaviour of multifunctional initiators in various monomer systems is to examine polymerizations dominated by transfer reactions.

Butyl acrylate (BA) is an important acrylic monomer used in many commercial products such as latex paints, adhesives and coatings. Its polymerization mechanism is greatly influenced by transfer reactions, especially transfer to polymer. Propagating chain-end radicals have been found to either wrap around and abstract a hydrogen from an acrylate unit on its own backbone (backbiting or intramolecular chain transfer) or the radical may abstract a hydrogen from a nearby polymer chain (intermolecular chain transfer). In the case of the former, the transfer reaction involves the chain-end wrapping to form a six-membered ring and as a result, short cyclic branches are produced. However, when intermolecular chain transfer occurs, a tertiary radical may be formed at any point along the backbone resulting in long chain branching. Overall, transfer to polymer reactions

can lead to the formation of highly branched polymers and it is not uncommon to observe the formation of insoluble gel fractions early in the polymerization of butyl acrylate. Similarly, the polymerization mechanism of vinyl acetate (VAc) is greatly influenced by transfer reactions. It has been demonstrated that branching occurs in vinyl acetate as the results of reactions with both monomer and polymer (8) and that the formation of insoluble gel material is observed at very high conversions.

In this chapter, we extend our investigation of the behaviour of the tetrafunctional peroxide initiator, JWEB50, by examining its impact on the polymerization of butyl acrylate and vinyl acetate. A suitable monofunctional counterpart to the tetrafunctional initiator is used in order to evaluate the performance of JWEB50. Due to the nature of the polymerization of butyl acrylate to form significant amounts of gel, some runs were completed to investigate the use of a chain transfer agent (CTA) with each initiator.

6.2 Experimental

6.2.1 Reagent Purification

Butyl acrylate (Sigma-Aldrich Canada Ltd.) was washed three times with a sodium hydroxide solution (10 w/v %), washed three times with distilled water, dried over calcium chloride and distilled under vacuum. Vinyl acetate (Sigma-Aldrich Canada Ltd.) which is much more water soluble, was only purified by vacuum distillation. All other materials such as solvents and initiators were used as received from suppliers. Dodecanethiol was utilized as a chain transfer agent in certain experiments with butyl acrylate and hydroquinone was used to help quench the reaction and prevent additional polymerization. Both chemicals were used without further purification from suppliers.

6.2.2 Polymer Synthesis

Experiments were carried out in borosilicate glass ampoules (capacity ~4 mL) where a solution of reagents (monomer, initiator and in some cases CTA) was prepared and pipetted into ampoules. Ampoules were then degassed by vacuum-freeze-thaw cycles, sealed under vacuum and immersed in a silicone oil bath. Ampoules were removed at

selected time intervals and placed in liquid nitrogen to quench the reaction. Due to the fact that the samples were typically in a gel-like state, the removal of residual monomer was not possible using conventional methods. As such, after thawing and weighing the ampoules, they were broken and placed in stoppered flasks containing toluene and an inhibitor (hydroquinone). Approximately one day later, the broken pieces of the ampoule were then removed from the flask, cleaned and weighed. The polymer solutions were then precipitated in ethanol and dried in a vacuum oven. In the polymerization of vinyl acetate, dichloromethane was used as the solvent to dissolve the polymer and petroleum ether as the nonsolvent to precipitate.

6.2.3 Polymer Characterization

Gel content was determined for poly(butyl acrylate) (PBA) samples using Soxhlet extraction. Prior to the extraction procedure, the paper thimbles were placed inside the Soxhlet apparatus, refluxed with toluene for one hour, dried under vacuum and then weighed. This was done to help reduce any error associated with the loss in weight of the paper thimble before and after the extraction of soluble material from the polymer. In the extraction process, toluene was refluxed over approximately 1 gram of polymer for 8 hours. The thimble and insoluble polymer were removed from the setup, dried under vacuum and then weighed to allow for the calculation of the gel content. The soluble fraction of the polymer (sol fraction) was recovered from the solvent reservoir and analyzed with SEC.

Molecular weight averages and molecular weight distributions for poly(butyl acrylate) samples were determined using a Waters size exclusion chromatograph (SEC) followed by a refractive index (RI) detector (2410 RI, Waters) and a multi-angle laser light scattering (MALLS) detector (DAWN DSP, Wyatt Technology Corp.) in series. Poly(vinyl acetate) (PVAc) samples were characterized with a different SEC setup equipped with low- and right-angle laser light scattering detectors (LALLS/RALLS), differential refractometer and viscometer in series (Viscotek). For both systems, the columns (one PLgel 10 μm guard column and three PLgel 10 μm MIXED-B columns (Polymer Laboratories Inc.)) and detectors were maintained at 30°C. The mobile phase

was filtered with tetrahydrofuran (THF) (HPLC Grade, Caledon Laboratories Inc.) at a flowrate of 1 mL/min. Polymer solutions of approximately 0.2 wt. % were prepared and injected at volume of 100 μ L. PBA samples were filtered prior to injection with 0.45 μ m filters while 0.20 μ m filters were used for the PVAc samples (GHP Acrodisc GF, Waters). The MALLS wavelength was 633 nm and the light-scattering intensity was measured at 18 angles between 14 and 152°. The LALS used a wavelength of 670 nm and the light scattering was measured at 7°. Specific refractive index increments of 0.063 mL/g and 0.055 mL/g were used for poly(butyl acrylate) and poly(vinyl acetate) in THF.

6.2.4 Experimental Design

Table 6.1 lists the various polymerizations of butyl acrylate and vinyl acetate carried out in this study. Unlike our previous work with styrene and methyl methacrylate, only selective experiments were chosen. In the case of BA, a comparison between initiators of equal concentrations and not “potential” radical concentrations (i.e., employing the monofunctional initiator at a concentration four times that of the tetrafunctional initiator) was performed. For the work with VAc, the run with JWEB50 was compared to two experiments with TBEC: one at equivalent initiator concentration and another at comparable “potential” radical concentrations.

Table 6.1. Butyl acrylate and vinyl acetate experiment conditions.

Experiment	Initiator Type	Temperature, °C	Initiator Concentration, mol/L	CTA Concentration, wt. %
BA-M1	TBEC	80	0.0005	0
BA-T1	JWEB50	80	0.0005	0
BA-M2	TBEC	80	0.0005	0.05
BA-T2	JWEB50	80	0.0005	0.05
BA-M3	TBEC	80	0.0005	0.5
BA-T3	JWEB50	80	0.0005	0.5
VAC-M	TBEC	100	0.0005	0
VAC-4M	TBEC	100	0.0020	0
VAC-T	JWEB50	100	0.0005	0

6.3 Results and Discussion

6.3.1 Butyl Acrylate

Figure 6.1 is a plot of conversion versus time for the bulk BA polymerization experiments. Looking at the data for each experiment a curved profile is observed with an initial sharp rise in conversion and a leveling off as the reaction progresses.

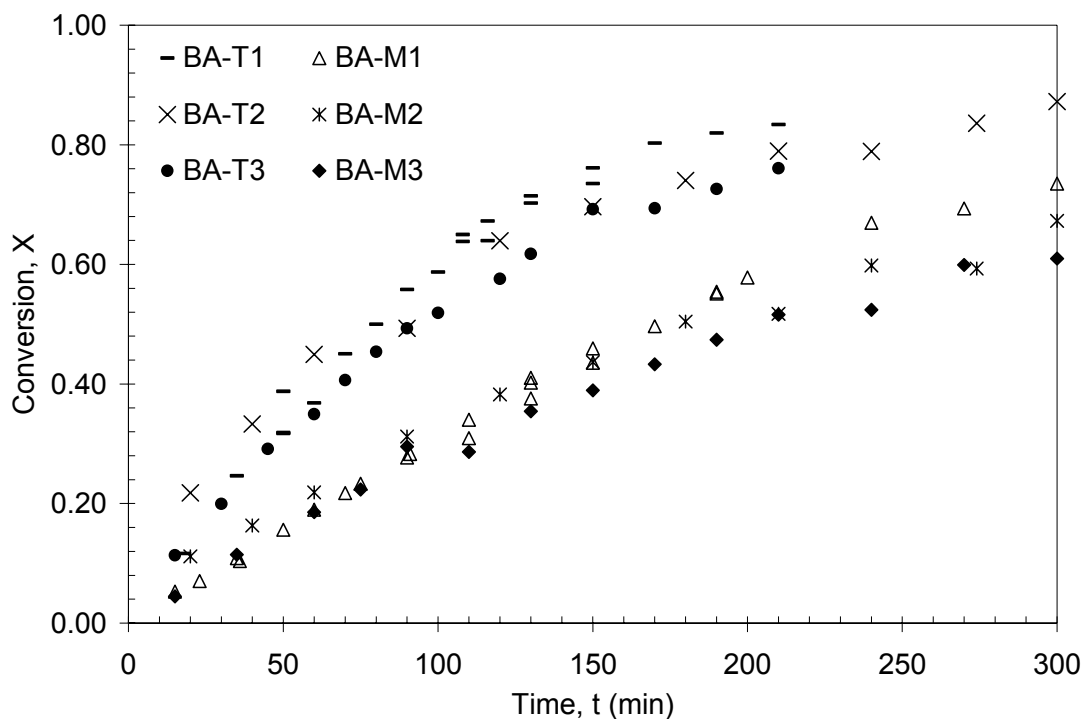


Figure 6.1. Monomer conversion as a function of time for the bulk polymerization of butyl acrylate at 80°C.

For each of the three CTA concentration levels (0, 0.05 and 0.5 wt%), the data show that the tetrafunctional initiator requires less time to reach a particular conversion when compared to the monofunctional initiator at the same initiator concentration. For the comparison without CTA, the initial rate of polymerization was estimated by the slope of the conversion-time data at low conversion. The ratio of the rate of polymerization for the tetrafunctional initiator (0.0056 min^{-1}) to the rate with the monofunctional initiator (0.0028 min^{-1}) was determined to be approximately 2. From theory it is known that the rate of polymerization is proportional to the square root of the initiator concentration. A

ratio of two between rates implies that using the tetrafunctional initiator is equivalent to employing the monofunctional initiator at a concentration four times as great. This observation corresponds well with the fact that the tetrafunctional initiator has the potential to generate four times as many radical sites per molecule of initiator compared to its monofunctional counterpart. These results suggest that JWEB50 is decomposing fully and that its radical sites are behaving similar to those of TBEC.

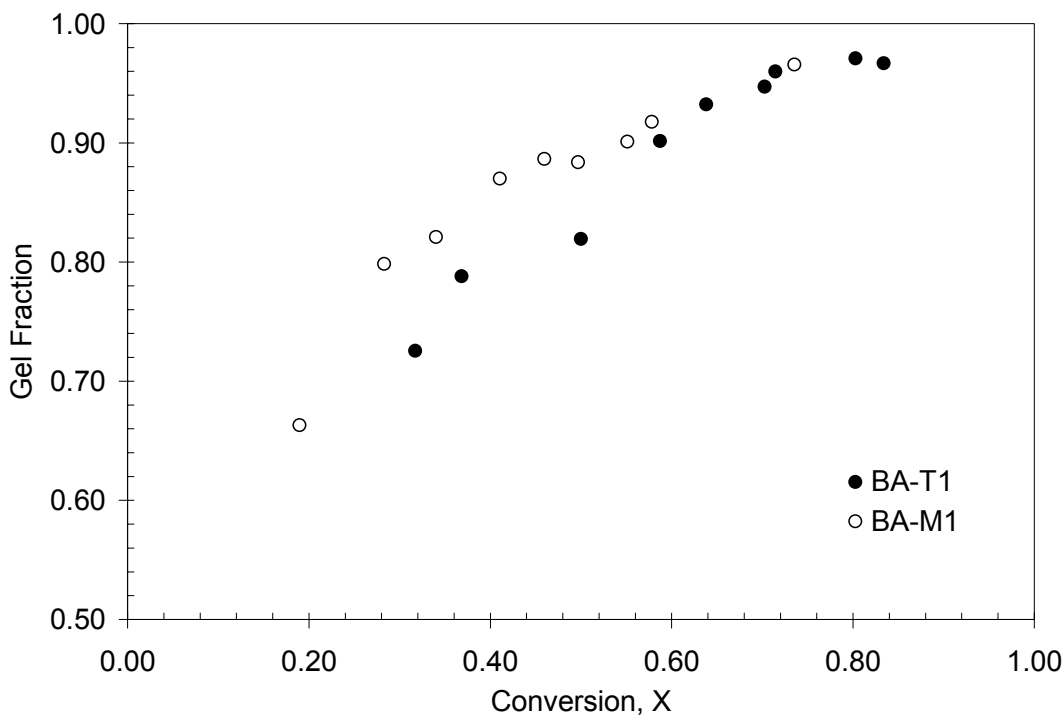


Figure 6.2. Gel fraction as a function of conversion for butyl acrylate experiments with no chain transfer agent.

The BA runs without CTA invariably produced polymer with a certain amount of gel material. Using a Soxhlet extractor, the gel fraction of polymer samples was determined. Figure 6.2 illustrates the effect of initiator functionality on the amount of gel produced. The gel content in the polymer samples increased with monomer conversion until roughly 70% conversion was achieved where the two initiators produced polymer with ~95% gel. A difference between the gel content of polymer produced with the two initiators can be seen at lower conversions. The tetrafunctional initiator produced polymer with a lower

gel fraction compared to its monofunctional counterpart. This observation was unexpected as it was thought that the tetrafunctional initiator would lead to higher gel content compared to the monofunctional initiator. The unexpected outcome might very well be an experimental artifact.

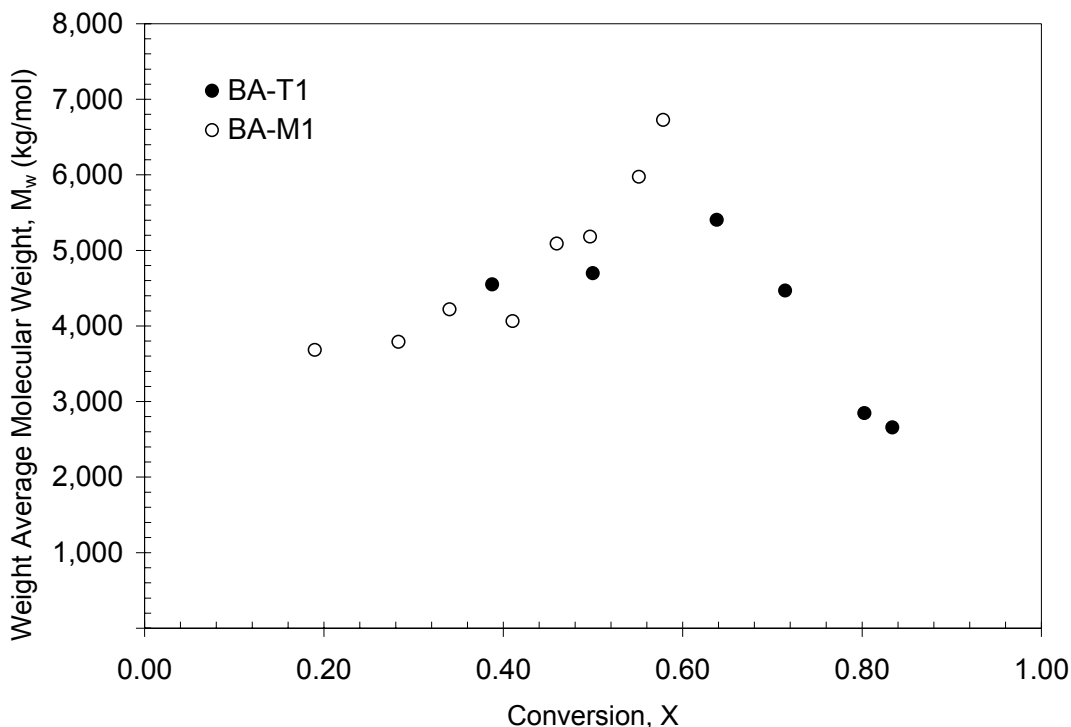


Figure 6.3. Weight average molecular weight of soluble material extracted from poly(butyl acrylate) samples.

Molecular weight data for the soluble material extracted from PBA samples are presented in Figure 6.3. The samples were of extremely high molecular weight and the shape of the chromatograms indicated that the limit of the columns had been reached. In cases where the detector cell contains a polydisperse fraction (i.e., incompletely separation by the columns), light scattering will provide a weight average molecular weight estimate. Thus the weight average molecular weight of the entire sample can still be used while the other averages and polydispersity are not valid. The data in Figure 6.3 indicate that the molecular weight of the soluble fraction increases with conversion up to a certain point. At conversions greater than 60% and a corresponding gel fraction of >90%, the molecular

weight of the soluble fraction begins to decrease. At this point, it is most likely the growth of the gel fraction that begins to incorporate the uncross-linked chains and reduces the sol molecular weight.

From the data in Figure 6.1 it can be seen that the addition of dodecanethiol had a slight effect on the rate of polymerization. The trends show that with increasing CTA concentration, the conversion-time trends are slightly lowered. Experimental error does, however, make it difficult to firmly state such a conclusion. The effect of dodecanethiol on molecular weight and gel fraction was quite evident. Weight average molecular weight estimates for the four experiments run with CTA are shown in Figures 6.4 and 6.5. Prior to injection into the SEC, samples were filtered. A comparison of the polymer mass injected to the mass estimated from the RI signal showed no differences. This result along with the observation that the samples could be filtered without applying significant pressure was taken as an indication that the samples did not contain insoluble microgels. At both CTA levels, molecular weight curves for the tetrafunctional and monofunctional initiator coincided well. A significant effect on the molecular weight was observed when increasing the CTA concentration. At the higher concentration, both initiators produced polymer molecular weights starting at approximately 50 000 g/mol and increasing with conversion to an upper limit of 80 000 g/mol. While at the lower CTA concentration, polymer molecular weights were much higher and increased dramatically after 50% conversion was reached.

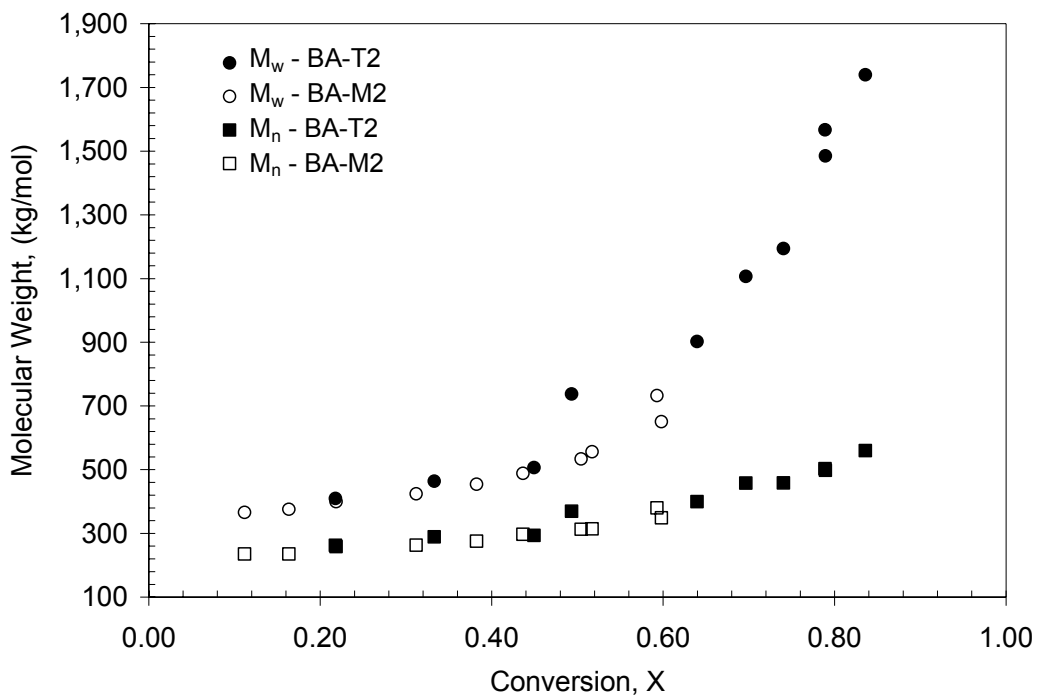


Figure 6.4. Molecular weight averages as a function of conversion for the bulk polymerization of butyl acrylate with [CTA] = 0.05 wt.%.

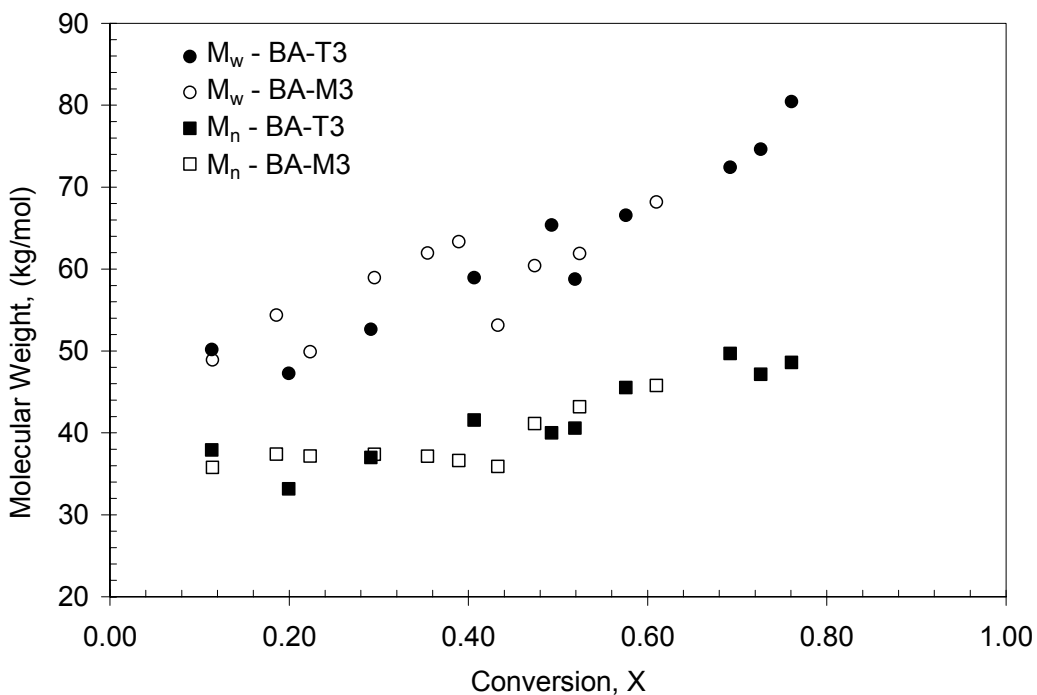


Figure 6.5. Molecular weight averages as a function of conversion for the bulk polymerization of butyl acrylate with [CTA] = 0.5 wt.%.

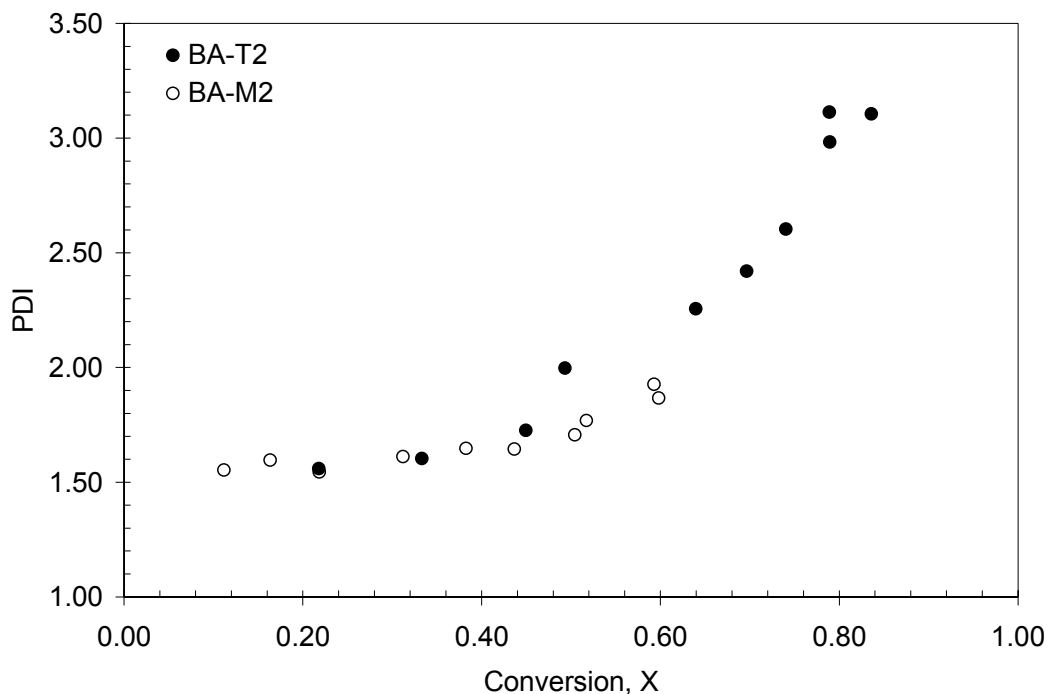


Figure 6.6. Polydispersity index as a function of conversion for the bulk polymerization of butyl acrylate at 80°C (SEC1).

The PDI values at the higher CTA concentration were determined to be similar for both initiators and remained constant for the course of the reaction. Figure 6.6 provides the polydispersity index values for the two experiments completed at the lower CTA concentration. From low to mid conversions where the molecular weight estimates do not vary considerably, it was found that the PDI values remained fairly constant. After reaching ~50% conversion, polymer with much broader molecular weight distributions is produced and the PDI is found to noticeably increase. These results would suggest that at the higher CTA concentration, transfer to CTA is the dominant factor controlling molecular weight for the entire course of the reaction. While at the lower CTA concentration, the data indicates that transfer to CTA is the controlling factor up until ~50% conversion where enough dodecanethiol has been consumed such that transfer to polymer and monomer becomes significant. Although radius of gyration plots for the poly(butyl acrylate) samples are not shown here, the results were examined in order to

determine the extent of branching. A comparison of R_g data between polymer samples produced with JWEB50 and TBEC did not show any differences.

6.3.2 Vinyl Acetate

Conversion versus time trends for the bulk polymerization of vinyl acetate initiated with JWEB50 and TBEC are shown in Figure 6.7. The curves show that the tetrafunctional initiator produced a faster rate of polymerization compared to the monofunctional initiator at an equivalent initial concentration of initiator. However, when employed at a concentration four times that of JWEB50, the polymerization with TBEC reached a limiting conversion faster than JWEB50. Using the linear portion of the conversion versus time data, the initial rate of polymerization was estimated for the three cases. JWEB50 produced an initial rate of polymerization of 0.0152 min^{-1} while TBEC generated a rate of 0.017 and 0.0081 min^{-1} for the high and low concentrations. A ratio of the rates for TBEC at the high (0.0020 mol/L) and low (0.0005 mol/L) concentrations leads to a value of 2.1. This ratio agrees well with theory as the rate of polymerization scales with the square root of the initiator concentration. The ratio of the initial rate of polymerization produced with JWEB50 to the rate generated by TBEC at the same concentration level is 1.9. Unlike other monomer systems (e.g., styrene (5), MMA (9), and styrene/MMA (10)), it appears that the tetrafunctional initiator does not produce an identical rate of polymerization as the monofunctional initiator when both are used at equivalent potential radical concentrations. The difference in conversion curves observed with VAc may be due to differences in the initiator efficiency. It is known that the initiator efficiency is dependent upon monomer type and a lower efficiency for JWEB50 compared to TBEC in the bulk polymerization of vinyl acetate would lead to slower rates (11). However, further experiments need to be completed to see if this trend can be replicated with vinyl acetate before any conclusions can be made.

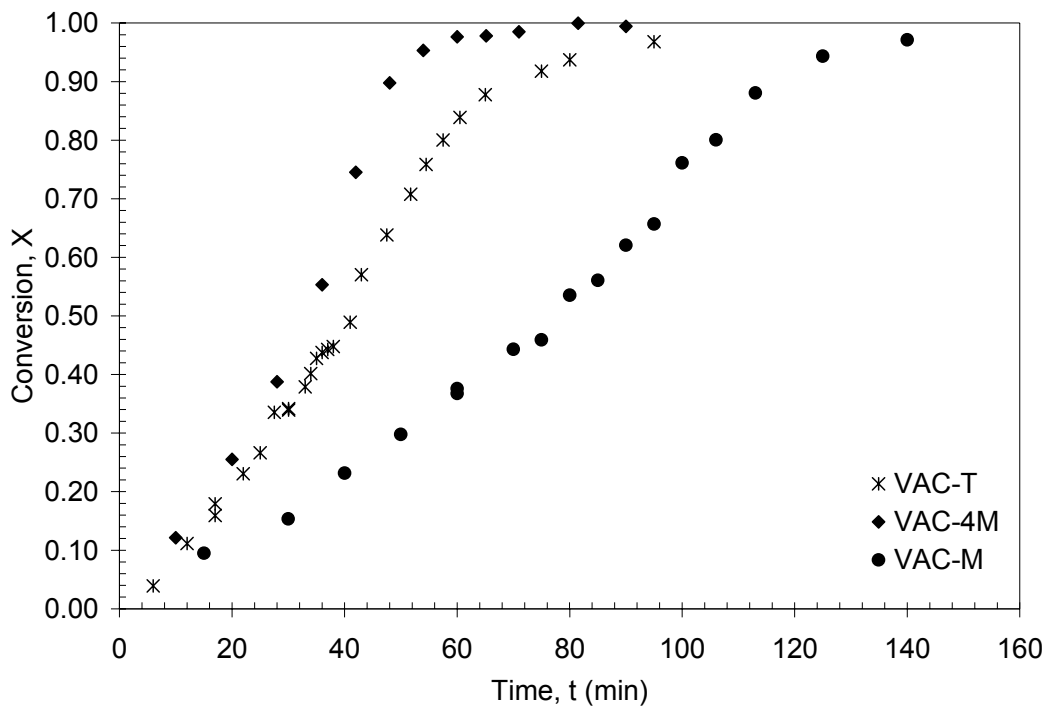


Figure 6.7. Conversion as a function of time for the bulk polymerization of vinyl acetate at 100°C.

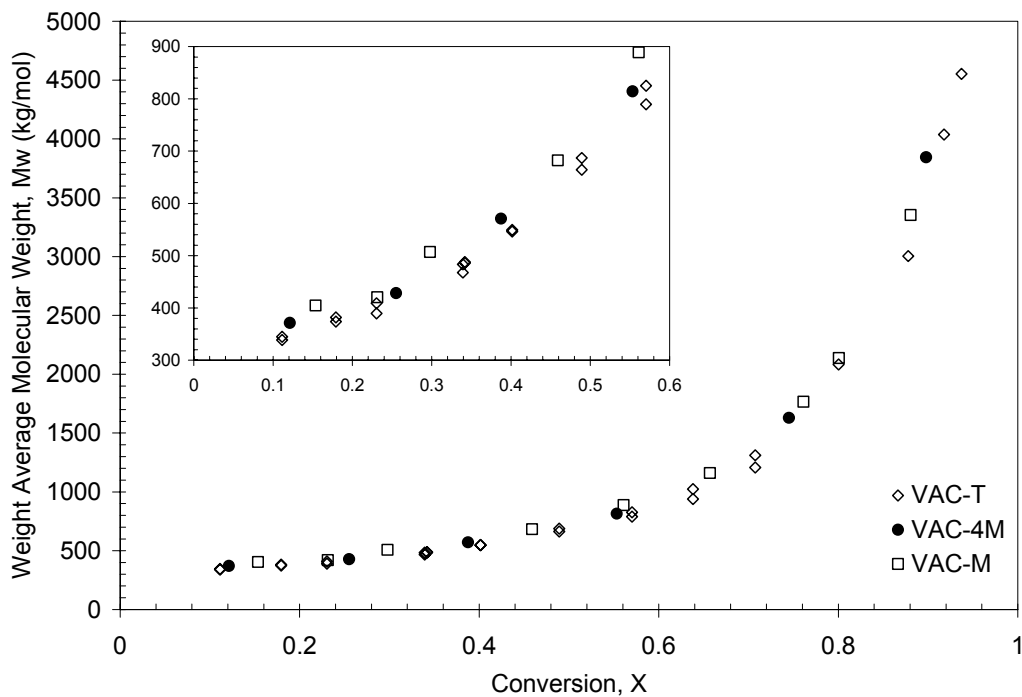


Figure 6.8. Weight average molecular weight as a function of conversion for the bulk polymerization of vinyl acetate at 100°C. Insert: weight average molecular weight for less than 60% conversion.

Weight average molecular weight results are shown in Figure 6.8 for the three vinyl acetate experiments. The data for each experiment show similar trends with molecular weights starting near 300 kg/mol and increasing dramatically with conversion towards 4000 kg/mol and above. The polymerization of vinyl acetate is characterized by high rates of transfer to monomer and polymer. As the act of either transfer reaction leads to a branched molecule, very high molecular weights are obtained as higher conversions are reached. The data in Figure 6.8 shows that the effect of initiator functionality and even initiator concentration has very little effect on molecular weight. In order to see if there is a difference between curves at lower conversions, the insert of Figure 6.8 is scaled for 60% conversion. At low conversion and hence low polymer concentrations, the extent of transfer to polymer is less of a factor. The molecular weight data for the polymerization with TBEC at 0.0005 mol/L appear to be slightly higher than the other two runs; however, given the error of GPC a firm statement cannot be made. The data suggests that transfer to monomer and polymer control the molecular weight more so than changes in initiator concentration and functionality. Although not shown here, plots of number average molecular weight or polydispersity as a function of conversion do not display any differences between the three experiments. As well, intrinsic viscosity versus molecular weight data for samples of similar conversion from the three experiments showed similar levels of branching.

Due to the importance of transfer reactions in the polymerization of vinyl acetate, the formation of gel material would not be unexpected. Unlike the PBA samples, all of the poly(vinyl acetate) samples dissolved and no swollen material was ever observed. However, it was suspected that the PVAc samples might contain soluble microgels. In each run, the very high conversion samples could not pass through the 0.2 μm filter. For VAC-T, the highest conversion sample that could be filtered was 93.7% while for VAC-4M and VAC-M, a maximum conversion of 89.8% and 88.1% were reached. The limits for the experiments with the monofunctional initiator are similar and further investigation would be needed to state whether the difference is statistically significant. However, the maximum filterable conversion for the run with JWEB50 is noticeably higher than the

values for the monofunctional runs. The trend would suggest that higher conversions are needed for JWEB50 to produce the same level of gel material as TBEC.

Comparing the mass injected to the mass calculated from the RI signal showed that no mass was lost either to the disposable filters (prior to injection), the inline filters or the guard column. In order to further test the samples that did pass through the disposable filters, a selected number of poly(vinyl acetate) samples were injected without prior filtration. Several phenomena occurred that would suggest the evidence of highly branched molecules including large negative peaks in the inlet pressure of the detector, spiking of the pump pressure, and extremely noisy data. These observations indicate that the samples which could be filtered did contain a low amount of highly crosslinked material.

6.4 Conclusions

The experiments in this study were chosen as a selective investigation on the use of a tetrafunctional initiator with monomer systems dominated by transfer reactions. Experimental results have shown that the tetrafunctional initiator, JWEB50, can produce a faster rate in the polymerization of both butyl acrylate and vinyl acetate compared to TBEC. A comparison of the initial rate of polymerization for butyl acrylate suggests that the tetrafunctional initiator is fully decomposing and that the radical sites are behaving similar to those of TBEC. In the case of vinyl acetate, this trend was not seen. The results showed that for the monofunctional initiator a factor of two was observed between rates when the initiator concentration was doubled. However, a factor of two was not found when varying initiator functionality. The experiments for both monomers lead to the production of highly branched polymer. Without the presence of a CTA, the bulk polymerization of butyl acrylate inevitably produced insoluble gel material. Results from Soxhlet extraction indicated that JWEB50 produced lower levels of gel material. When a CTA was used, the molecular weight results were dominated by the CTA concentration and initiator concentration and functionality did not have an impact. In the polymerization of vinyl acetate, a similar observation was found and no discernable difference could be seen between the molecular weight versus conversion results of

samples produced with JWEB50 and TBEC. As well, the filtration of samples prior to injection into the SEC indicated that while polymer produced with JWEB50 could be filtered, samples of similar conversion generated with TBEC could not. The polymerization results of butyl acrylate and vinyl acetate suggest that the use of JWEB50 leads to less highly branched material compared to a monofunctional initiator. This implication is contrary to what would be expected. Studies of conversion versus time data for JWEB50 and TBEC imply that the tetrafunctional initiator is fully decomposing. As such, additional branching due to the structure of the JWEB50 would be expected. However, further experiments including the replication of Soxhlet extractions should be performed before a definite conclusion can be made.

6.5 References

1. Ivanchev, S. S. New Views on Initiation and Radical Polymerization in Homogeneous and Heterogeneous Systems. *Polymer Science USSR* **1979**, *20* (9), 2157-2181.
2. Choi, K. Y., Lei, G. D. Modeling of free radical polymerization of styrene by bifunctional initiators. *AIChE Journal* **1987**, *33* (12), 2067-2076.
3. Villalobos, M. A., Hamielec, A. E., Wood, P. E. Kinetic model for short-cycle bulk styrene polymerization through bifunctional initiators. *Journal of Applied Polymer Science* **1991**, *42*, 629-641.
4. Cavin, L., Rouge, A., Meyer, T., Renken, A. Kinetic modeling of free radical polymerization of styrene initiated by the bifunctional initiator 2,5-dimethyl-2,5-bis(2-ethyl hexanoyl peroxy)hexane. *Polymer* **2000**, *41*, 3925-3935.
5. Fityani-Trim, S., Dhib, R., Penlidis, A. Free Radical Polymerization of Styrene with a New Tetrafunctional Peroxide Initiator. *Macromolecular Chemistry and Physics* **2003**, *204*, 436-442.
6. Cerna, J. R., Morales, G., Eyler, G. N., Canizo, A. I. Bulk Polymerization of Styrene Catalyzed by Bi- and Trifunctional Cyclic Initiators. *Journal of Applied Polymer Science* **2002**, *83*, 1-11.
7. González, I. M., Meira, G. R., Oliva, H. M. Synthesis of polystyrene with mixtures of mono- and bifunctional initiators. *Journal of Applied Polymer Science* **1996**, *59*, 1015-1026.
8. Wheeler, O. L., Lavin, E., Crozier, R. N. Branching Mechanisms in the Polymerization of Vinyl Acetate. *Journal of Polymer Science* **1952**, *9* (2), 157-169.
9. Scolah, M. J., Dhib, R., Penlidis, A. Free-radical polymerization of methyl methacrylate with a tetrafunctional peroxide initiator. *Journal of Polymer Science Part A-Polymer Chemistry* **2004**, *42* (22), 5647-5661.
10. Scolah, M. J., Dhib, R., Penlidis, A. Use of a Novel Tetrafunctional Initiator in the Free Radical Homo- and Copolymerization of Styrene, Methyl

Methacrylate and α -Methyl Styrene. *Journal of Macromolecular Science Pure and Applied Chemistry* **2005**, *A42* (4), 403-426.

11. Odian, G. *Principles of Polymerization*; Wiley: Toronto, 1991.

CHAPTER 7 - DETECTION OF BRANCHING IN POLYSTYRENE AND POLY(METHYL METHACRYLATE)

7.1 Introduction

The characterization of branched polymers has been the focus of innumerable studies since their existence was postulated roughly seventy years ago (1, 2). Much of the fundamental understanding of branching and its influence on dilute solution and rheological properties began with specific molecular architectures such as stars and combs (see (3-7) for reviews). However, many commercially important polymers are produced by random polymerization processes and as such, have a distribution in both molecular weight and branching. This polydispersity in molecular weight and branching is the cause of difficulties in the characterization of such polymers and has led to a number of investigations on the detection of branching (8-13).

Even today, the detection of long-chain branching (LCB) is seen by some as one of the most challenging and long standing unsolved problem in polymer science (14). The importance of such a problem lies in the fact that these branched molecules can have a tremendous impact on the rheological properties even at extremely low concentrations. Spectroscopic and chemical methods relying on the differences in chemical structure that branching introduces, namely more end-groups or the existence of branch points, can be used to quantitatively determine the amount of branching without the need of a linear reference. The main limitation of these methods is that rarely are the differences between branch points or end-groups and normal repeat units significant enough to be detected for very low concentrations of LCB that still influences the polymer's rheological properties (9).

Similar to spectroscopic methods, chromatographic techniques such as size exclusion chromatography (SEC) are widely used in the detection of LCB. It has been shown when examining the average solution properties of a polymer that the effects of branching can

be masked by the polydispersity. For this reason, fractionation methods in combination with various detectors are used to measure either the radius of gyration (R_g) or intrinsic viscosity ($[\eta]$) and in turn, allow the calculation of the corresponding contraction factors (g or g') as a function of molecular weight. Difficulties can arise as some chromatographic techniques fractionate samples by size and not molecular weight or branching. For example, in size exclusion chromatography (SEC), polymer molecules are separated based on a hydrodynamic volume. In the case of a polydisperse sample having both molecular weight and branching distributions, it is possible for branched and linear molecules having identical hydrodynamic volumes but differing molecular weights to coelute (12, 15). Typically, the analysis of branched polymers with SEC assumes that the extent of branching increases with molecular weight because of the randomness of the polymerization reaction. As a result, partial separation of the branched chains does occur.

Because the flow behaviour of polymers is tremendously susceptible to the presence of long-chain branching, rheological methods are seen as the most sensitive and in some instances, a last means of detecting branching. A comprehensive method for the quantitative determination of LCB by rheological tests does not exist as the degree, length and structure of branching affect the rheological behaviour of a polymer in various ways. The situation is even further complicated by variations in molecular weight distribution. In most studies, linear and branched materials are analyzed and a comparison of the linear viscoelastic properties such as the zero-shear viscosity or compliance is used to provide evidence of branching. Others have attempted to quantify the degree of branching by various rheological indices or models (14, 16, 17). Additional methods of detecting branching by rheological methods include the loss angle (18) or Van Gurp plot (19), thermorheological behaviour (17, 20) and extensional rheology (21, 22) (see Section 2.3.2.3 for further discussion). The dilemma with these rheological tests is that the absence of any difference between the behaviour of linear and branched materials does not preclude the existence of branching. For example, higher values of the flow activation energies can be attributed to LCB. However, the reverse is not always true as the presence of LCB does not necessarily enhance the activation energy (17, 23).

In the previous chapters we have reported on the use of a tetrafunctional peroxide initiator (JWEB50) in the free radical polymerization of styrene and methyl methacrylate (MMA). The results of this work showed that higher rates of polymerization can be obtained with the tetrafunctional initiator compared to a monofunctional counterpart (TBEC) of similar thermal stability. However, the impact on molecular weight depends upon monomer type. With styrene, JWEB50 produced similar molecular weights to those obtained with TBEC while for MMA, much lower molecular weights compared to TBEC were measured. In this study, samples of polystyrene and poly(methyl methacrylate) produced with JWEB50 are characterized by SEC, field-flow fractionation (FFF) and rheological experiments in a effort to detect evidence of branching.

7.2 Experimental Methods

7.2.1 Materials

Polymer samples were produced from the bulk homopolymerization of styrene and methyl methacrylate initiated with a tetrafunctional peroxide initiator, JWEB50 (Atofina Chemicals Inc.). For comparisons purposes, “linear” material was produced with a monofunctional initiator (tert-butylperoxy 2-ethylhexyl carbonate, TBEC). Details of the polymerization can be found in elsewhere (24-26).

7.2.2 Characterization

7.2.2.1 Size Exclusion Chromatography

Molecular weight, radius of gyration and intrinsic viscosity distributions were measured using two SEC setups. The first system was equipped with a multi-angle laser light scattering detector (DAWN DSP, Wyatt Technology Corp.) followed by a differential refractometer (2410 RI, Waters) in series. The second SEC employed Viscotek’s quad detector comprised of a UV detector, low- (7°) and right-angle (90°) laser light scattering detectors (LALLS/RALLS), differential refractometer and viscometer in series. The MALLS wavelength was 633 nm while the laser wavelength of Viscotek’s detector system was 670 nm. Although the specific refractive increment (dn/dc) is function of the

laser wavelength, the difference between values at two wavelengths was assumed to be negligible. Thus, dn/dc values of 0.185 mL/g and 0.083 mL/g were used for polystyrene and poly(methyl methacrylate). Analysis of data from the first SEC setup was performed with Astra v4.7 software (Wyatt Technology Corp.) while OmniSEC v3.0 (Viscotek) software was employed for the second system. Both SEC setups were equipped with one PLgel 10 μ m guard column (50 x 7.5 mm) and three PLgel 10 μ m MIXED-B columns (300 x 7.5 mm) (Polymer Laboratories Ltd.). All columns and detectors were maintained at 30 °C. Tetrahydrofuran (THF) (Caledon Laboratories Inc.) was filtered and used as the eluent at a flowrate of 1 mL/min. Polymer solutions of approximately 0.2 wt. % were prepared and left for 12-24 hours to fully dissolve. Injection volumes between 100 and 200 μ L were used.

7.2.2.2 Thermal Field Flow Fractionation

Field-flow fractionation is a set of techniques used in the separation of polymer materials. FFF is similar to SEC with the exception that the column is replaced by a channel, void of any stationary phase where flow inside the channel is laminar. Retention, and in turn separation, is caused by an externally generated field applied perpendicular to the direction of flow. As the name implies, thermal FFF (ThFFF) uses a thermal gradient to separate molecules of varying size. When a thermal gradient is applied to the channel, dissolved polymer molecules are forced towards the cold wall by a process known as thermal diffusion (thermophoresis) (27). A build-up of molecules near one wall of the channel produces a concentration gradient and leads to mass diffusion of polymer molecules away from the cold wall. Fractionation of the polymer samples is then achieved as the thermal diffusion coefficient is independent of molecular weight while the mass diffusion constant is not (28).

Polystyrene and poly(methyl methacrylate) samples were analyzed with thermal field-flow fractionation by Postnova analytics (Salt Lake City, Utah, USA). Injection volumes ranged from 50 to 100 μ L of 1.5 mg/mL polymer solutions in THF. Evaporative light scattering (ELSD MK III, Varex) and static light scattering (PN3010-SLS, Postnova analytics) detectors measured the concentration and molecular weight of the eluting

species. An initial temperature gradient of 63°C was chosen and decayed to 0°C by the end of each run with a flowrate of 0.19 mL/min.

7.2.2.3 Differential Scanning Calorimetry

A Q100 DSC (TA Instruments) was used to measure the glass transition temperature, T_g , of polymer samples. Polymer samples (approximately 10 mg) were sealed in aluminum pans and annealed at 200 °C for two minutes. The samples were then cooled to 40 °C and then scanned from 40 to 200 °C at a heating rate of 10°C/min. Replicates of scans and entire runs showed good reproducibility of the data. The glass transition temperature was selected as the mid-point change in the heat capacity for the transition region.

7.2.2.4 Rheological Analysis

Oscillatory shear experiments and shear creep tests were performed to examine the viscoelastic behaviour of polymer samples. Rheological data were collected using a TA Instruments AR 2000 rheometer equipped with a parallel-plate geometry and an environmental test chamber for temperature control. All experiments were completed under a nitrogen atmosphere to avoid any degradation or crosslinking reactions. Samples discs (25 mm in diameter and 2.5 mm in thickness) were formed by compression molding roughly 1 g of polymer and 10 mg of antioxidant (Irganox 1010) at 190 °C for several minutes. The linear viscoelastic region for each polymer was determined by conducting strain sweeps at 1 Hz. A series of frequency sweeps from 0.01 to 100 Hz were obtained for various temperatures in increments of 10 °C for each sample. Frequency sweeps were then replicated with a new sample in order to ensure good reproducibility of results. In the case of polystyrene, the temperature ranged from 160 to 220 °C while for PMMA, an interval of 190 to 250 °C was chosen. The upper temperature limits were selected to avoid the decomposition of polymer samples. In order to check whether degradation or crosslinking reactions occurred during the testing of samples, a frequency sweep at the lowest temperature was performed again. Good agreement with the original low temperature frequency sweep indicated that side reactions did not occur. As a second check, the molecular weight distribution of the samples after testing were determined by SEC and showed no evidence of degradation.

Creep experiments for polystyrene and poly(methyl methacrylate) were conducted at 220°C and 250°C, respectively. The linear viscoelastic region was determined by performing creep tests for a variety of shear stresses (29). The limit of this region was established by comparing creep compliances for the various shear stresses and locating the stress where curves no longer coincided.

Table 7.1. Molecular weight characterization of polystyrene and poly(methyl methacrylate) samples.

Sample	SEC-MALLS					SEC-LALS-Visc				
	M_n (kg/mol)	M_w (kg/mol)	M_w/M_n	K_{Rg} (nm)	ν	M_n (kg/mol)	M_w (kg/mol)	M_w/M_n	$K_{[\eta]}$ (dL/g)	α
PS-M	312	582	1.9	0.00855	0.62	316	579	1.8	9.54×10^{-4}	0.72
PS-T	264	628	2.4			282	629	2.2		
PMMA-M	455	854	1.9	0.00566	0.64	438	824	1.9	6.32×10^{-4}	0.73
PMMA-T	471	844	1.8			456	803	1.8		

Table 7.1. Continued.

Sample	ThFFF-ELSD-SLS		
	M_n (kg/mol)	M_w (kg/mol)	M_w/M_n
PS-M	438	540	1.2
PS-T	360	737	2.0
PMMA-M	576	859	1.5
PMMA-T	664	958	1.4

Table 7.2. Material properties for polystyrene and poly(methyl methacrylate) samples

Sample	T_g (°C)	η_0 (kPa·s)	J_e^0 (1/Pa)	G_N^0 (Pa)	τ_{0n} (s)	τ_{0w} (s)	τ_{0w}/τ_{0n}
PS-M	107	55	9.2×10^{-3}	1.8×10^5	0.29	510	1800
PS-T	105	14	1.6×10^{-2}	1.5×10^5	0.097	240	2500
PMMA-M	124	1340	1.7×10^{-4}	2.7×10^5	5.0	230	46
PMMA-T	124	708	1.4×10^{-4}	2.8×10^5	2.5	100	40

Note: T_{ref} for PS is 220°C and 250°C for PMMA.

7.3 Results and Discussion

7.3.1 SEC

Molecular weight averages and polydispersities for the polystyrene and poly(methyl methacrylate) samples analyzed in this study are reported in Table 7.1. The results from the two SEC setups show good agreement. Figures 7.1 and 7.2 provide plots of radius of gyration and intrinsic viscosity for the PS and PMMA samples. The trends for polystyrene show that at higher molecular weights, PS-T has smaller values for the radius of gyration and intrinsic viscosity compared to PS-M. The effect of branching on a polymer chain's size is well known. For identical molecular weights, a branched molecular will be more compact and have a smaller size compared to a linear molecular. Thus, the trends with polystyrene show that PS-T is more branched than PS-M. Looking at Figure 7.2, radius of gyration and intrinsic viscosity plots do not show any differences between poly(methyl methacrylate) samples. As such, there is no evidence of branching in PMMA-T compared to its corresponding M sample. The contraction factors for the radius of gyration (g) and intrinsic viscosity (g') are plotted in parts (c) and (d) of Figures 7.1 and 7.2. In the determination of the contraction factors, nonlinear regression was used to fit power-law models to the linear portion of $\log R_g - \log M$ and $\log [\eta] - \log M$ data of PS-M and PMMA-M. The estimated parameters are given in Table 7.1 and are similar to published values (15, 30-32). An interesting point to note is that the intrinsic viscosity plots for both PS-M and PMMA-M show some curvature near the high molecular weight end. Due to the random nature of free radical polymerization, even with a monofunctional initiator it is possible for branches to be produced via transfer reactions.

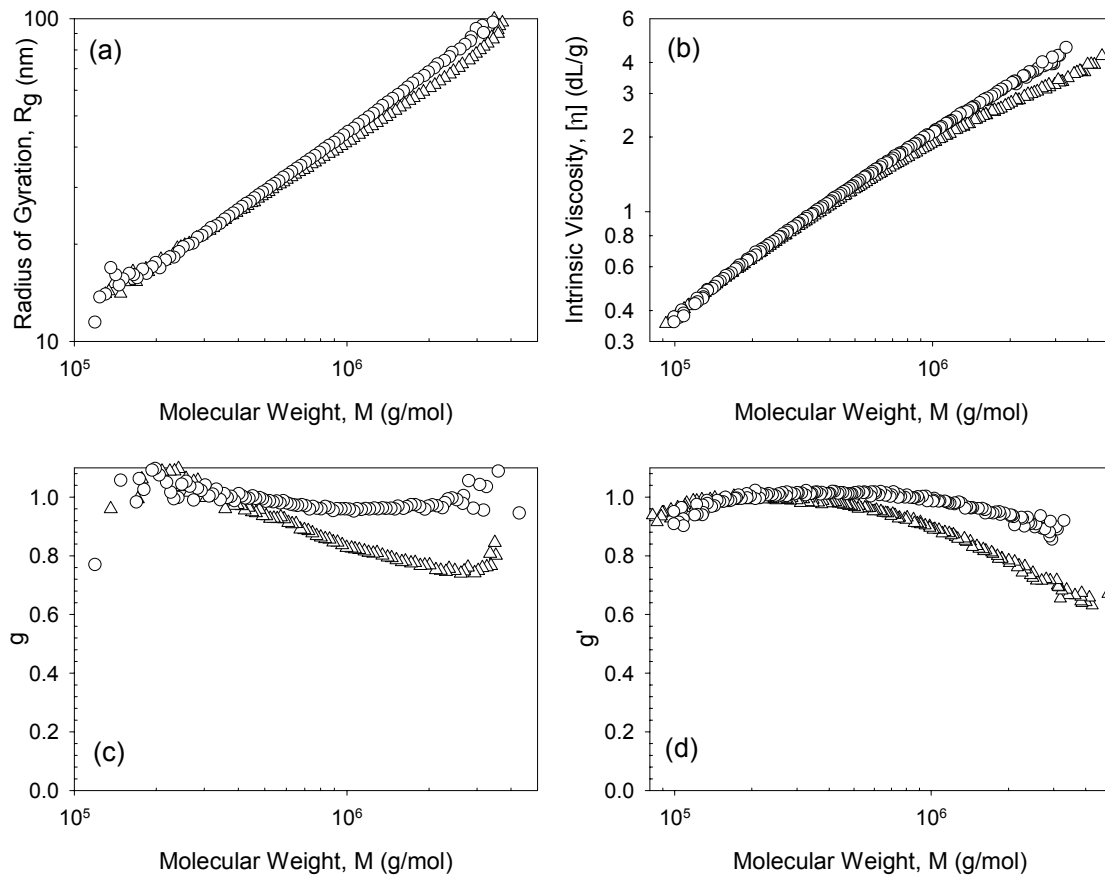


Figure 7.1. Plots of radius of gyration, intrinsic viscosity and their respective branching factors as a function of molecular weight for polystyrene samples (circles – PS-M; triangles – PS-T).

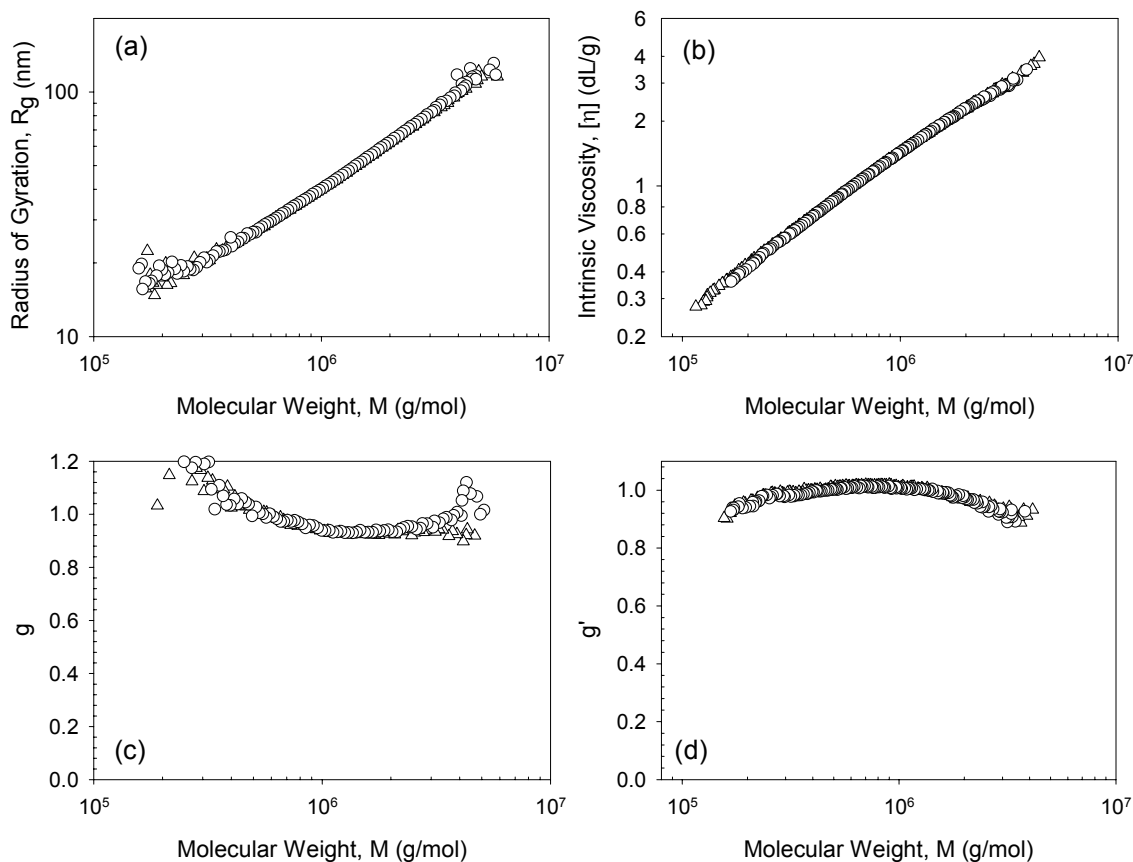


Figure 7.2. Plots of radius of gyration, intrinsic viscosity and their respective branching factors as a function of molecular weight for poly(methyl methacrylate) samples (circles – PMMA-M; triangles – PMMA-T).

Equations relating the number of branches per molecule and the radius of gyration contraction factor, g , have been developed and are listed in Table 2.1. The difficulty with applying these equations to randomly branched polymers is the decision of what type of branching exists. In free radical polymerization, transfer reactions typically lead to trifunctional branch points. However, due to the structure of the tetrafunctional initiator, the presence of tetrafunctional branch points will be introduced. The other dilemma that affects the choice of a proper equation is the assumption of whether samples fractionated by SEC are monodisperse or not (Equation 2.21 versus 2.23). There are examples of the use of either equation in published literature (33-35).

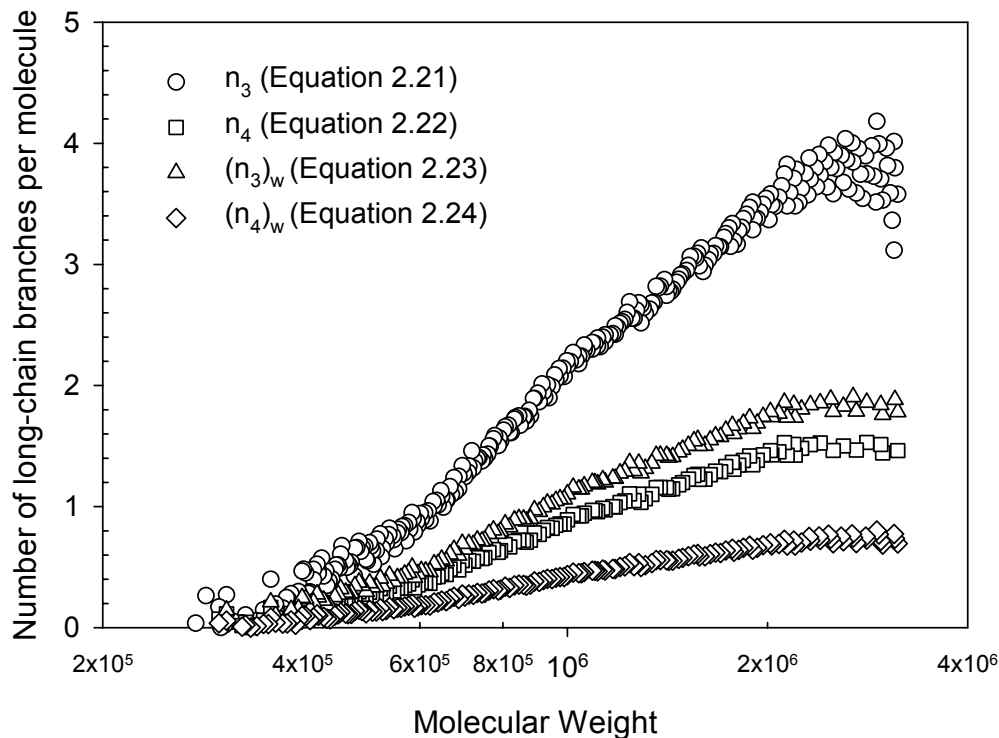


Figure 7.3. Number of long-chain branches per molecule as a function of molecular weight for PS-T. The subscript number denotes the type of branching (tri- or tetrafunctional) while the subscript w indicates a weight average.

Figure 7.3 is a plot of the number of long-chain branches as a function of molecular weight for PS-T. The data has been estimated from four cases: trifunctional versus tetrafunctional branching and fractionated versus unfractionated. All curves show the same trend of increasing number of LCB with increasing molecular weight. Estimates for the number of LCB are highest for trifunctional branching compared to tetrafunctional branching. For a particular molecular weight, a molecule with trifunctional branch points requires more branch points in order to obtain a similar g value for a molecule with tetrafunctional branching. The effect of polydispersity is to decrease the amount of branching estimated from the contraction factors. Figure 7.4 provides a comparison of the number of long-chain branches for PS-T and PS-M. Because the separation by SEC may not have been complete, equations assuming polydisperse fractions were used for the comparison. The data indicate that PS-M contains at most 0.25 and 0.10 branches per

molecule assuming trifunctional and tetrafunctional branching respectively. While for PS-T, the most highly branched (and highest molecular weight) fractions contain 1.8 and 0.80 branches. However, as PS-M was produced with a monofunctional initiator it is unlikely these samples contain chains with tetrafunctional branching.

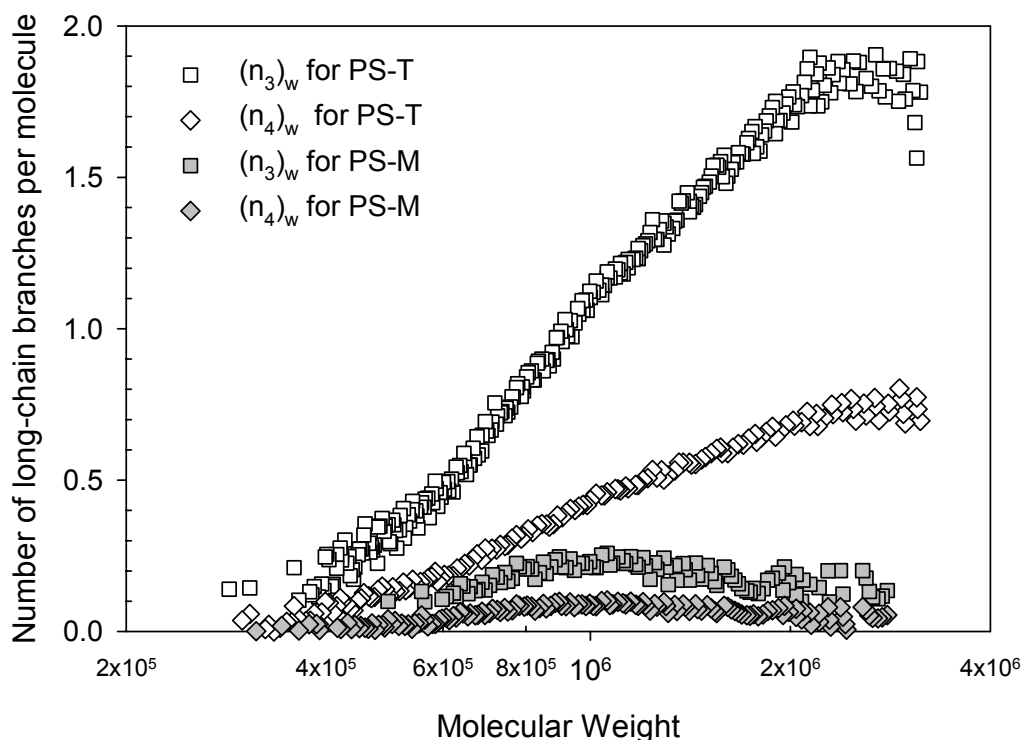


Figure 7.4. Number of long-chain branches per molecule as a function of molecular weight for PS-T and PS-M samples. The subscript number denotes the type of branching (tri- or tetrafunctional) while the subscript w indicates a weight average.

7.3.2 ThFFF

Molecular weight and polydispersity estimates obtained from ThFFF are listed in Table 7.1. The molecular weight results indicate that samples produced with the tetrafunctional initiator have higher molecular weights compared to the samples generated with the monofunctional initiator. This trend was not observed with either of the SEC systems. The weight average molecular weight estimates obtained from ThFFF for the M series samples are similar to those reported with the two SEC setups while those for the T series are not. A definitive reason for the discrepancy between the two characterization

methods is not apparent. Each setup was able to accurately estimate the molecular weight of several polystyrene and poly(methyl methacrylate) standards of narrow molecular weight distribution (Polymer Laboratories Ltd.) indicating that all three systems should produce similar results. Also, this discrepancy cannot be attributed to the type of detector because each of the chromatographic setups employed a light scattering detector which provides an absolute estimate of the molecular weight. Because the ThFFF results agreed well with the SEC systems for the characterization of the PS-M, PMMA-M and standards of known molecular weight, it would be reasonable to conclude that the inconsistency is not due to differences in the techniques. It is possible for polymer samples to have a significant amount of molecular weight heterogeneity and thus, greatly influence the variability in molecular weight estimates (36). Although unlikely, it may be that the higher molecular weight results from ThFFF are due to disparity in the piece of samples used for injection. As each of the SEC results is the average of two samples, injected twice, it is more likely that the difference between molecular weights observed with ThFFF is erroneous. Another discrepancy between the results obtained from SEC and ThFFF, is the breadth of the molecular weight distribution. The polydispersity data from the ThFFF analysis is much lower than those estimates from SEC. Past work has shown the resolving power of ThFFF to be comparable or superior to that of SEC (37-39). However, this statement assumes that an optimal set of experimental conditions have been used because the separation in ThFFF is highly dependent on such variables as flowrate and the temperature decay program.

7.3.3 DSC

Glass transition temperatures are reported in Table 7.2 for the polystyrene and poly(methyl methacrylate) samples. No significant difference exists between the samples produced with either initiator. Except for highly branched structures where the ratio of chain ends to the molecular weight becomes very high, the glass transition temperature of a branched polymer should be identical to that of its linear analog (40). The T_g values reported in Table 7.2 agree well with those published in the literature (41).

7.3.4 Rheology

7.3.4.1 Oscillatory Shear Experiments

The rheological properties of polymers are typically highly temperature dependent. As such, oscillatory shear experiments have been performed for various temperatures to gain a better insight into the behaviour of the polymers analyzed in this study. By means of a relation known as time-temperature superposition (TTS), curves for viscoelastic properties at several temperatures can be combined to form a single master curve. Before commencing an explanation of the principles of TTS, the concept of relaxation times and the relaxation spectrum is introduced.

The time or frequency dependence of the modulus (G) and compliance (J) can be mimicked by the behaviour of certain mechanical models with a number of elastic and viscous elements. A spring can be used to imitate the behaviour of an elastic element while a dashpot (piston moving in oil) is applicable to a viscous element. Figure 7.5 represents a Maxwell element with a spring and dashpot attached in series. If the spring is assigned the rigidity of G_i and the dashpot is responsible for the viscosity, η_i then the relaxation time of a particular element is defined as $\tau_i = \eta_i/G_i$. The viscoelastic behaviour of polymers cannot simply be represented by only one element. Thus, a group of Maxwell elements acting in parallel is needed where a discrete spectrum of relaxation times exists with each time τ_i being associated with a spectral modulus and viscosity. If the number of elements in the model is increased without limit, the result is a continuous spectrum. For such a model, each infinitesimal contribution to a viscoelastic function is associated with relaxation times lying between τ and $\tau + d\tau$. Past work has shown that linear time may be used but a logarithmic time scale is far more convenient. Thus the relaxation spectrum is defined as $H d \ln \tau$ which is the contribution to the rigidity for those relaxation times found between $\ln \tau$ and $\ln(\tau + d\tau)$. $H d \ln \tau$ can be thought of as a measure of the strength of a relaxation mechanism for an interval of relaxation times (42).

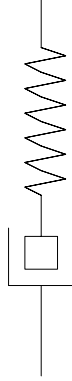


Figure 7.5. Maxwell element.

When H is known, various viscoelastic functions may be calculated, including the relaxation, storage and loss modulus (from which other viscoelastic functions can easily be determined):

$$G(t) = G_e + \int_{-\infty}^{\infty} H(\tau) e^{-t/\tau} d \ln \tau \quad 7.1$$

$$G'(\omega) = G_e + \int_{-\infty}^{\infty} H(\tau) \left(\frac{(\omega\tau)^2}{1 + (\omega\tau)^2} \right) d \ln \tau \quad 7.2$$

$$G''(\omega) = \int_{-\infty}^{\infty} H(\tau) \left(\frac{\omega\tau}{1 + (\omega\tau)^2} \right) d \ln \tau \quad 7.3$$

where G_e is a constant that is zero for viscoelastic liquids and non-zero for viscoelastic solids.

The underlying principle of TTS is that the relaxation spectrum obtained from data at different temperatures can be made to superimpose into a single curve by vertical (H , relaxation strength axis) and horizontal (τ , relaxation time axis) shifts (43). If a certain set of relaxation times $\tau_1(T_0)$, $\tau_2(T_0)$, $\tau_3(T_0)$, ... were obtained at a reference temperature of T_0 , then changing the temperature to a value of T would alter the relaxation times to $\tau_1 a_T$, $\tau_2 a_T$, $\tau_3 a_T$, ... In general, the effect of changing the temperature is given by the following:

$$b_T H\left(\frac{\tau}{a_T}, T\right) = H(\tau, T_0) \quad 7.4$$

where a_T and b_T are the horizontal (frequency) and vertical (modulus) shift factors that vary with temperature. One of the earliest models to predict horizontal shift factors as a function of temperature is the Williams-Landel-Ferry (WLF) equation:

$$\log a_T = \frac{-c_1(T - T_0)}{c_2 + T - T_0} \quad 7.5$$

where c_1 and c_2 are constants for the reference temperature T_0 . Although introduced as an empirical expression, the physical significance of the WLF equation is described by Ferry (42). The WLF equation has been found to be valid for temperatures near the glass transition temperature, from T_g to $T_g + 100^\circ\text{C}$. Above these temperatures and for relatively narrow temperature ranges, shift factors are typically fit to an Arrhenius type model:

$$a_T = \exp\left(\frac{E_a}{R} \left(\frac{1}{T} - \frac{1}{T_0}\right)\right) \quad 7.6$$

where E_a is sometimes referred to as the activation energy for flow.

Vertical shift factors are typically smaller and less influenced by temperature compared to horizontal shift factors. As such, most studies neglect vertically shifting modulus curves. According to the Rouse model, the vertical shift factor is related to temperature by the following (44):

$$b_T = \frac{\rho_0 T_0}{\rho T} \quad 7.7$$

where ρ_0 and ρ are the polymer densities at temperatures T_0 and T . Vertical shift factors generated from the above equation do not work well for every polymer but a more general equation is not available (20, 45). In some cases, an Arrhenius model has been fit to the vertical shift factors (43).

According to the work of Shroff and Mavridis (43), horizontal and vertical shift factors can be determined independently from experimental data by plotting specific viscoelastic functions. The storage modulus, loss modulus and loss tangent shift with temperature according to following:

$$b_T G'(a_T \omega, T) = G'(\omega, T_0) \quad 7.8$$

$$b_T G''(a_T \omega, T) = G''(\omega, T_0) \quad 7.9$$

$$\tan \delta(a_T \omega, T) = \tan \delta(\omega, T_0) \quad 7.10$$

Noting that the shifting of the loss tangent is independent of the vertical shift factor, viscoelastic functions can be redefined in terms of the loss tangent. The most significant results are those for the frequency and complex modulus.

$$\omega(\tan \delta, T) = \frac{1}{a_T} \omega(\tan \delta, T_0) \quad 7.11$$

$$G^*(\tan \delta, T) = \frac{1}{b_T} G^*(\tan \delta, T_0) \quad 7.12$$

These equations show that plots of the loss tangent versus frequency should produce curves separated by only the horizontal shift factor while the vertical shift factor can be independently determined from plots of the loss tangent versus the complex modulus. As previously stated, the vertical shift factor is typically ignored. For most cases, this is not a problem because the vertical shift factor is very close to unity with an activation energy

of approximately zero. However, Shroff and Mavridis have shown theoretically and experimentally for some materials that ignoring b_T factors will introduce a stress (or modulus) dependence on the horizontal activation energy (43). That is, different horizontal activation energies are required for each temperature in order to produce a smooth master curve.

Horizontal shift factors for the samples analyzed in this study are plotted in Figure 7.6. The reference temperature was arbitrarily chosen as the maximum measurement temperature for the two sets of samples (220°C for PS and 250°C for PMMA). For each polymer sample oscillatory shear experiments were replicated with a new sample disc. In the case of polystyrene, the replicated data agrees well, showing good reproducibility for these measurements. Looking at the data for the PMMA samples, the agreement is not quite as good but still adequate. The WLF equation was fit to the experimental horizontal shift factors and the parameter estimates are reported in Table 7.3. 95% joint probability contour regions (JCR) are shown for the WLF parameters in Figures 7.7 and 7.8.

When looking at the horizontal shift factors for the polystyrene samples, PS-T and PS-M have similar a_T values close to the reference temperature of 220 °C (see Figure 7.6 (a)). However, for lower temperatures, a noticeable difference can be seen between the two sets of data as the PS-M data require larger horizontal shift factors compared to PS-T. This divergence leads to different estimates of the WLF parameters for the two sets of polystyrene data. The 95% joint probability contour plots indicate that the estimates from the two sets of data are statistically different as no parts of the contour regions overlap (see Figure 7.7). The shape of the contours indicates that estimates of c_1 and c_2 are highly correlated. For the PMMA samples, the horizontal shift data in Figure 7.6 (b) indicates that there is a slight difference between the results for PMMA-M and PMMA-T and different WLF constants are estimated for each sample. The JCR plots in Figure 7.8 show that there is more uncertainty in the parameter estimates for the poly(methyl methacrylate) samples compared to the polystyrene samples. This was expected as there is more scatter in the PMMA data. The joint probability contour regions for the WLF parameters of PMMA-M and PMMA-T do not overlap, however, they are quite close.

The difficulty in dealing with the WLF equation is that the parameters are highly correlated, shown by the elliptical contours that almost approach the shape of a line. As a result, any increase (or decrease) in c_1 , must be followed by an increase (or decrease) c_2 and vice versa.

Table 7.3. Model parameters for horizontal shift factors.

Sample	c_1	c_2 (K)	T_0 (K)	Horizontal E_a (kJ/mol)
PS-M	3.7	160	493	140 ± 6
PS-T	4.5	191	493	136 ± 4
PMMA-M	12.6	373	523	183 ± 3
PMMA-T	15.8	441	523	192 ± 3

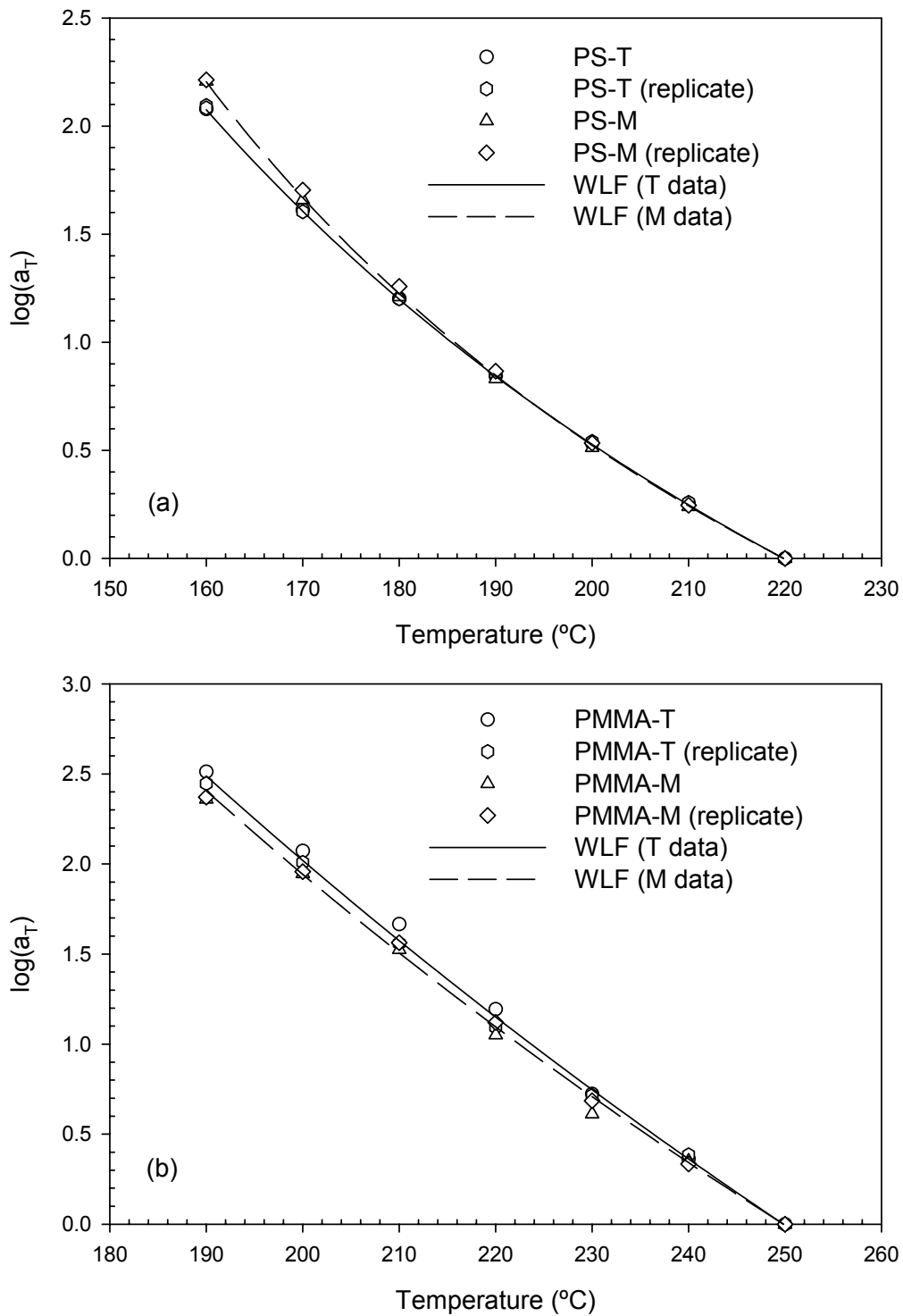


Figure 7.6. Logarithm of horizontal shift factors as a function of temperature for polystyrene and poly(methyl methacrylate) samples.

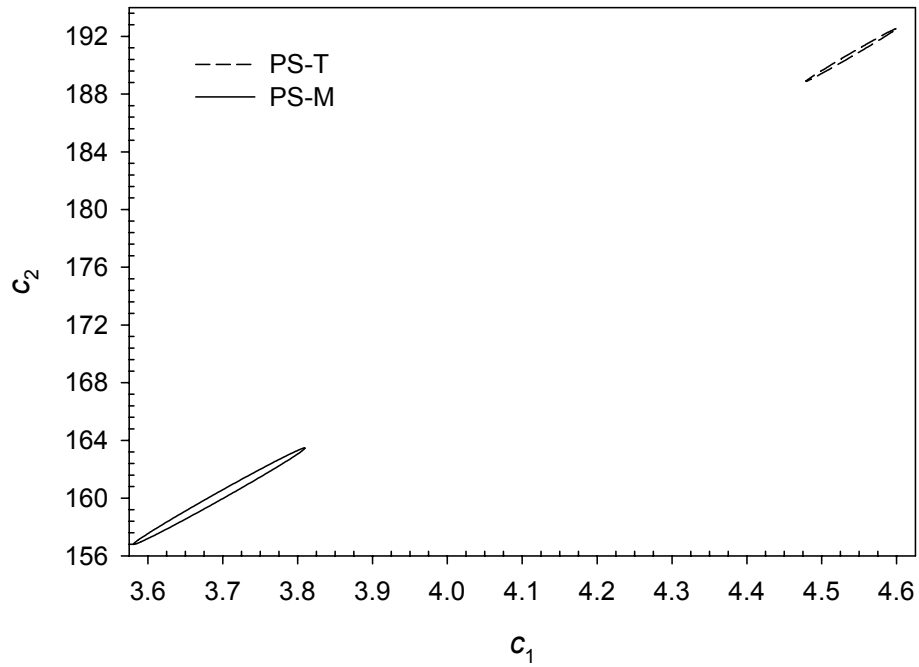


Figure 7.7. 95% Joint probability contour regions for WLF parameters estimated from polystyrene data.

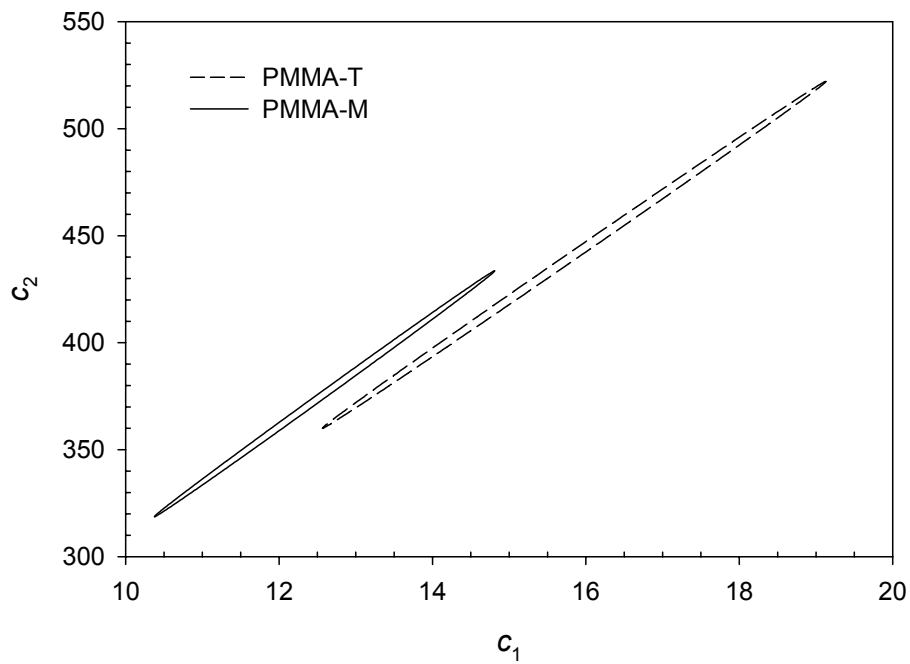


Figure 7.8. 95% Joint probability contour regions for WLF parameters estimated from poly(methyl methacrylate) data.

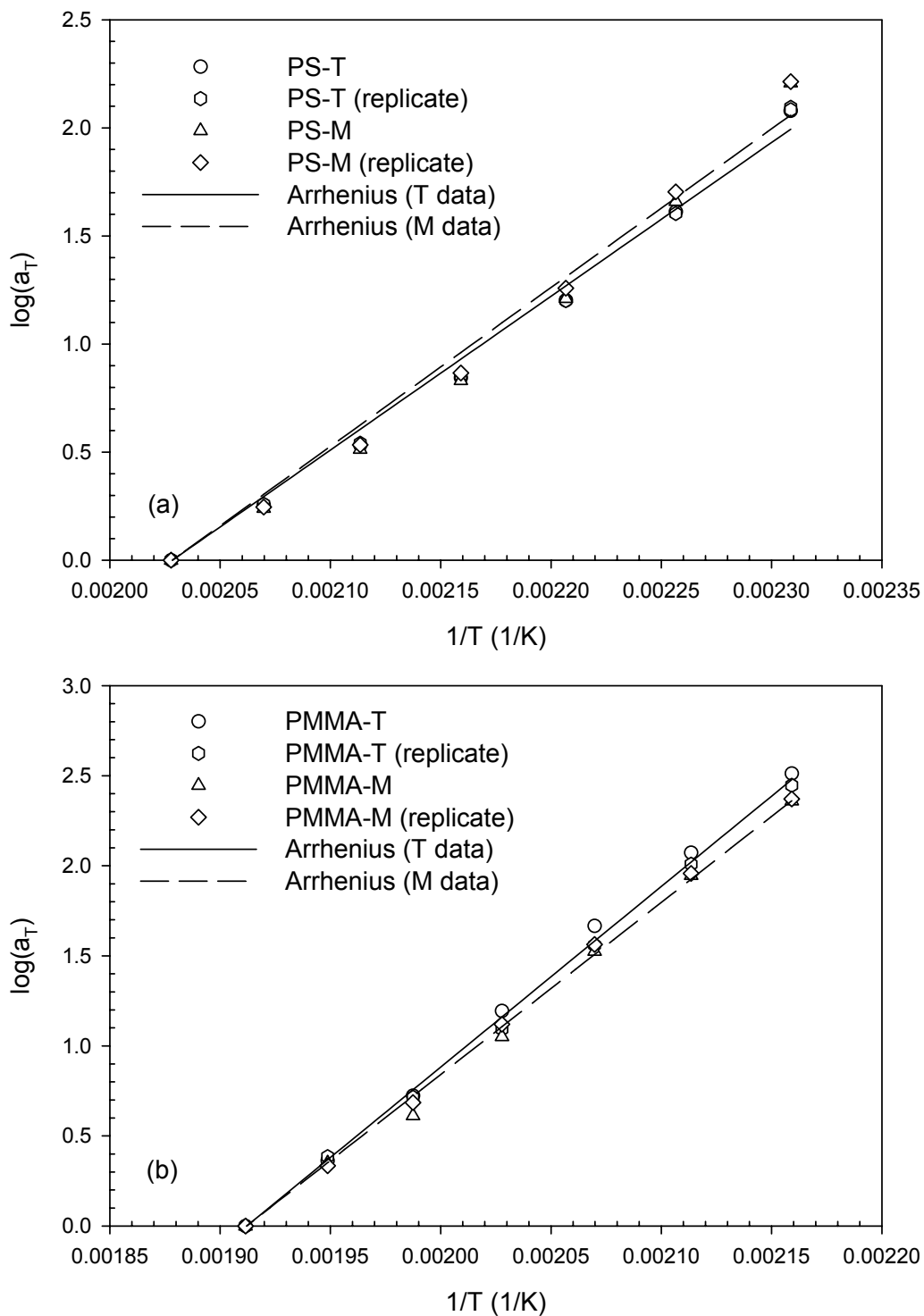


Figure 7.9. Logarithm of horizontal shift factors as a function of inverse temperature for polystyrene and poly(methyl methacrylate) samples.

The Arrhenius model given in Equation 7.6 was also fit to the horizontal shift factors. The horizontal activation energies and a 95% confidence interval are given in Table 7.3 while the model predictions are shown in plots of $\log(a_T)$ as a function of $1/T$ (see Figure 7.9). For the polystyrene samples, the 95% confidence intervals of the activation energies were found to overlap and thus, would indicate that there is no statistical difference between the two set of data. When looking at the model predictions for PS-M and PS-T in Figure 7.9 (a), it can be seen that there are indications of a model lack of fit. In a plot of $\log(a_T)$ versus $1/T$, each of the polystyrene data sets has some curvature that an Arrhenius model cannot account for. Although not shown here, plots of the residual error versus $1/T$ showed a parabolic shape which also provided evidence of lack of fit. These results along with the fact that the sum of squared residuals is lower for the WLF model compared to the Arrhenius model, indicate that the WLF equation is a better model for the polystyrene data. This can be reasoned based on the fact that the WLF equation has been found to be valid between T_g and $T_g + 100^\circ\text{C}$. For PS-M and PS-T, this range would encompass $\sim 105\text{-}207^\circ\text{C}$. Apart from the highest temperature of 220°C , the polystyrene data was collected within this interval. The Arrhenius model has been found to provide a better fit for temperatures above $T_g + 100^\circ\text{C}$. In contrast to the trends found with polystyrene, the activation energies for the PMMA did show a statistical difference where PMMA-T was found to have a higher E_a value. Model predictions using the Arrhenius model agreed well with the experimental poly(methyl methacrylate) data which in this case, did not show curvature in plots of $\log(a_T)$ versus $1/T$ (see Figure 7.9 (b)). The Arrhenius model performed better with the PMMA data compared to the PS data because more of the PMMA data was collected outside the range of the WLF equation's applicability.

As discussed in Section 2.3.1.3.3, the relationship between branching and the horizontal activation energy is not well known. It is generally accepted that a higher activation energy can be attributed to long-chain branching; however, the presence of long-chain branching does not always lead to an enhancement in E_a . As such, activation energies estimated for the PMMA samples, indicate that PMMA-T is more branched than PMM-M. Polystyrene samples showed no differences in their E_a estimates and thus, it cannot

be stated from this method whether PS-T or PS-M is more branched. This is in contrast to the results found from SEC-MALLS-Visc where a difference between samples was detected with polystyrene and not with poly(methyl methacrylate).

Although not reported here, plots of the vertical shift factor did not show any significant differences when comparing PS-T to PS-M and PMM-T to PMMA-M. Neither Equation 7.7 nor an Arrhenius model could adequately fit the b_T data as both models showed a significant lack of fit.

The fact that smooth master curves could be generated for various viscoelastic functions (see Figures 7.10 and 7.11) and that horizontal shift factors followed the WLF equation, proves that the application of TTS for the samples studied is valid. Therefore, no evidence of thermorheological complexity was observed. Storage and loss moduli master curves are plotted in Figures 7.10 and 7.11. In the case of polystyrene, curves for PS-T and PS-M show distinct differences. Looking at the moduli for high frequencies, both curves begin at similar values. Because of the temperature range chosen and the limit of the experimental apparatus, the data does not extend into the glassy region (which would be for higher frequencies or lower temperatures). For polydisperse polymers, the plateau region is not clearly defined and there is no clear transition to the terminal zone (see Figure 3.5, curve C as an illustration). Moving to lower frequencies, the curve for PS-T is below that of PS-M. Because many factors such as molecular weight, polydispersity and branching influence the storage and loss moduli curves, it is difficult to assign a divergence between curves to any one factor. When examining the master curves for the poly(methyl methacrylate) data (Figure 7.11), very little difference can be seen between samples PMMA-T and PMMA-M. For the storage modulus, both curves have the same shape except that the data for PMMA-T is slightly lower in the low frequency range. In the case of the loss modulus, it is difficult to discern any difference between the two samples due to the scatter in the data. However, similar to the storage modulus, PMMA-T moduli are lower than PMMA-M at the very low frequency range.

The zero-shear viscosity and steady-state shear compliance can be calculated from dynamic moduli obtained in the terminal region according to the following equations (42):

$$\eta_0 = \lim_{\omega \rightarrow 0} \frac{G''(\omega)}{\omega} \quad 7.13$$

$$A_G = \eta_0^2 J_e^0 = \lim_{\omega \rightarrow 0} \frac{G'(\omega)}{\omega^2} \quad 7.14$$

In the terminal region, the storage and loss modulus should become proportional to ω^2 and ω , respectively. In the case of the polystyrene samples, the dynamic data only just reaches the terminal zone while data for poly(methyl methacrylate) does not. To obtain data in the terminal region, either lower frequencies or higher temperature would be needed. Lower frequencies could not be readily achieved due to the limits of the experimental apparatus. Running the samples at higher temperatures was also not possible due to the likelihood of thermal degradation. Between 200 and 300°C, the thermal degradation of unstabilized polystyrene generates a decrease in molecular weight but volatile products are not produced until temperatures above 300°C are reached (46). For unstabilized poly(methyl methacrylate), minor thermal degradation begins as early as 165°C with the scission of head-to-head linkages followed by two major steps of degradation at 270 and 350°C (47). Stabilization of PMMA almost completely reduces the effect of the first and second degradation steps but has no effect on the third (48). There is a third option to obtain curves over a wider range of frequencies. Because linear viscoelastic functions are interrelated, data from various experimental tests can be combined to generate curves that span a greater frequency range. Thus, creep test were performed and the viscoelastic functions were converted to dynamic data.

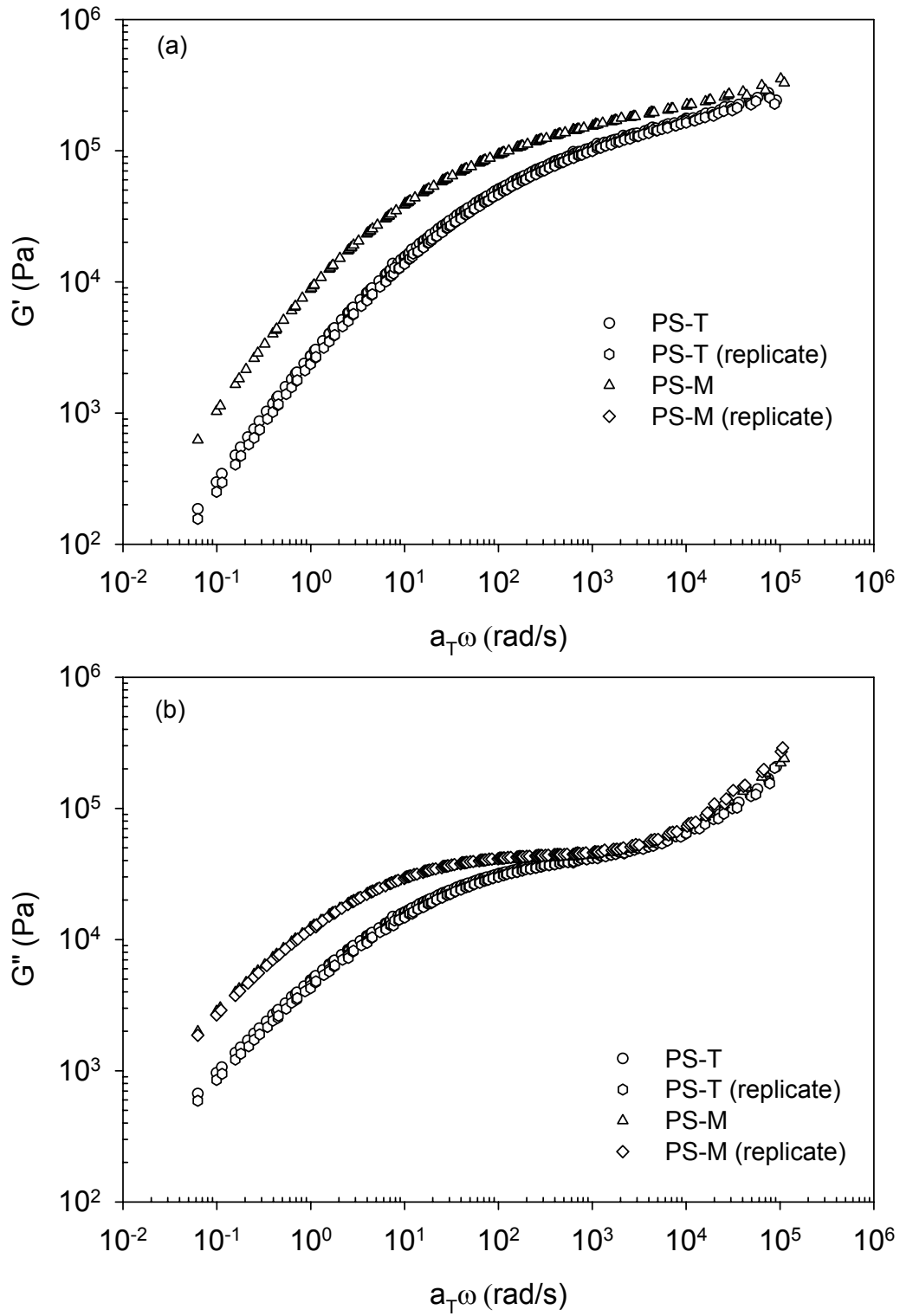


Figure 7.10. Storage and loss moduli master curves at 220°C for polystyrene samples.

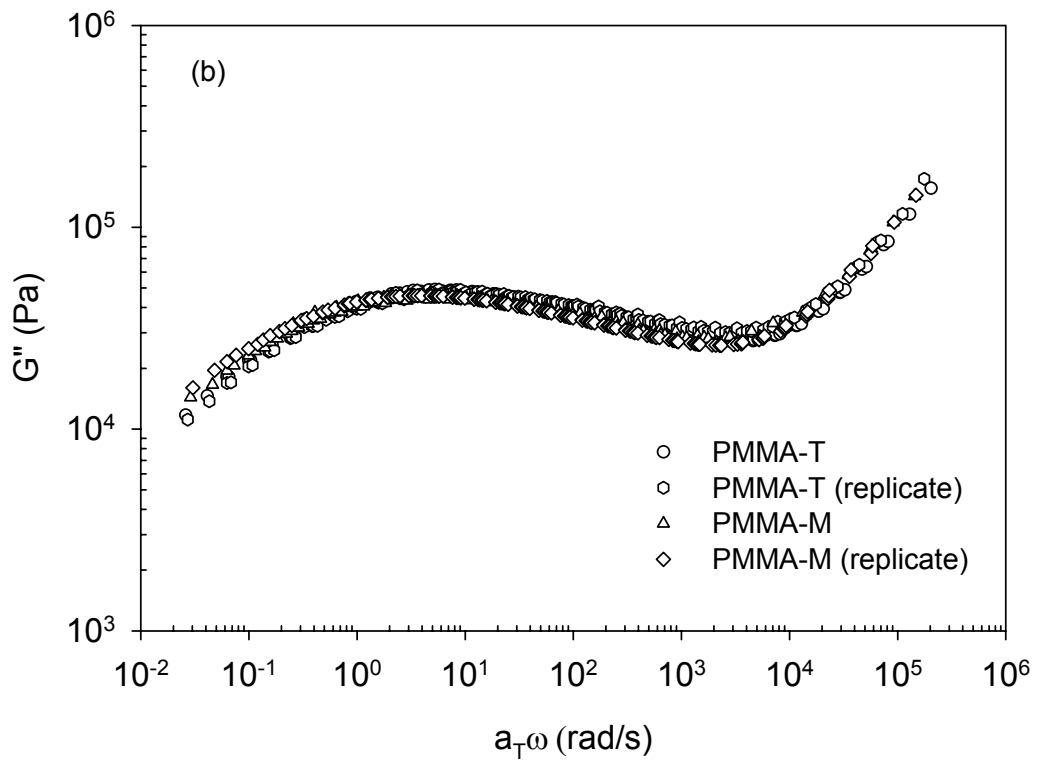
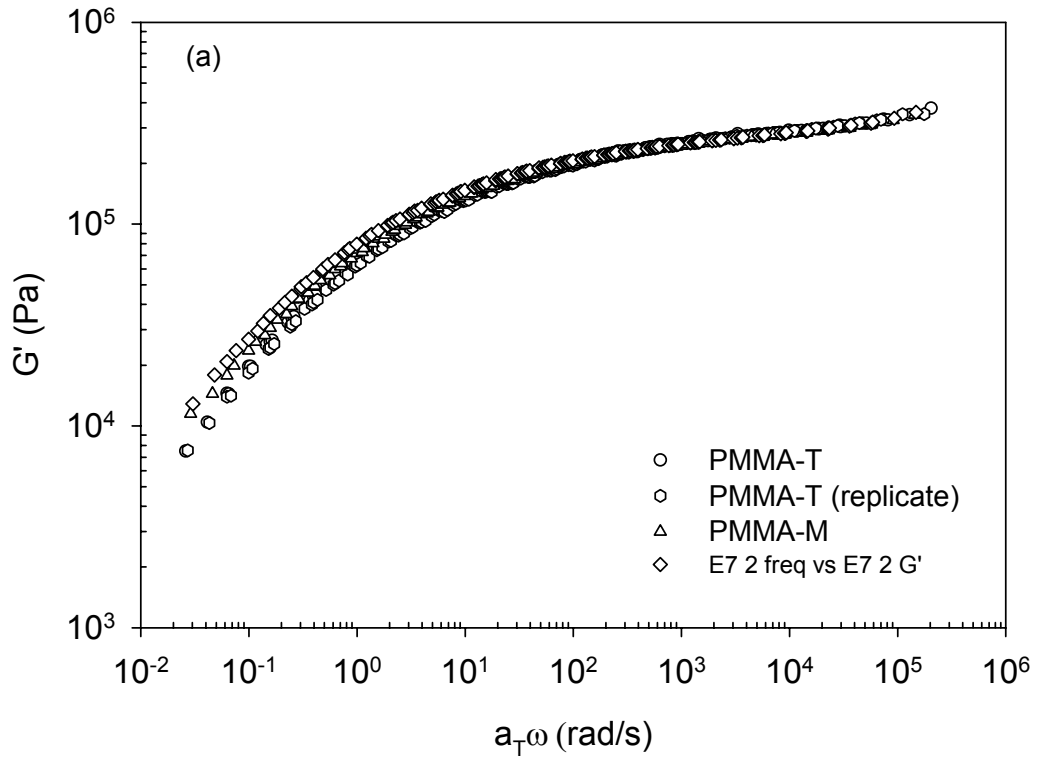


Figure 7.11. Storage and loss moduli master curves at 250°C for poly(methyl methacrylate) samples.

7.3.4.2 Shear Creep Tests

Creeps experiments were completed for various shear stresses in order to determine the linear region. Figure 7.12 is a typical example of the results obtained at varying shear stresses. A low shear stress was initially chosen for the creep experiment and subsequent experiments (performed with a new disc) of increasing shear stress were completed. The limit of the linear region was determined by the stress at which the curve no longer coincided with those of lower stress. Looking at Figure 7.12, the data for a shear stress of 20 Pa generated compliances greater than the trends for 7, 10 and 15 Pa. Thus the limit of the linear region is between 20 and 15 Pa. Identical results were found for the other polystyrene sample. In the case of the poly(methyl methacrylate) samples at a temperature of 250°C, a shift in compliance values was observed at a shear stress of 50 Pa. Although creep compliances are typically plotted on a log scale, differences observed on a linear scale were not apparent in log-log plots.

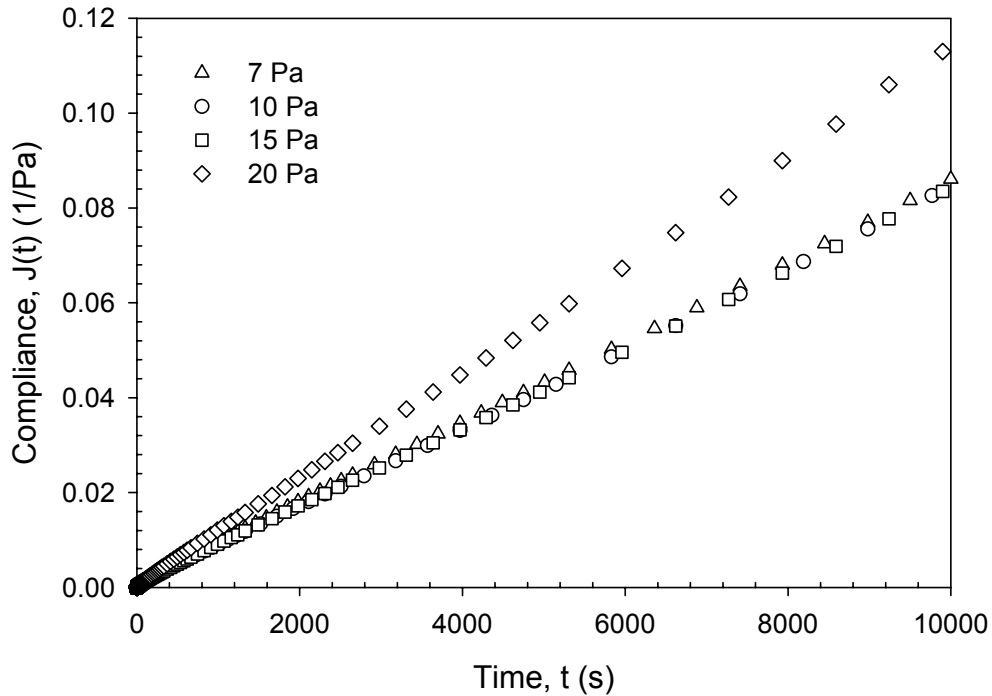


Figure 7.12. Shear compliance as a function of time for sample PS-M at varying shear stress and 220°C.

Except for sample PMMA-T, creep experiments were replicated three times and showed good agreement. The results of these experiments are shown in Figure 7.13. Note that for both polystyrene and PMMA, the M series has compliances lower than their corresponding T sample. Molecular weight, polydispersity and branching are all factors that influence the shear creep compliance. Because the PMMA samples have fairly similar molecular weight averages and polydispersities, the difference between compliance curves can be attributed to the effect of branching. However, in the comparison of polystyrene samples, there is a slight difference in molecular weight averages and polydispersity that prevents attributing the difference in trends solely to the effect of branching.

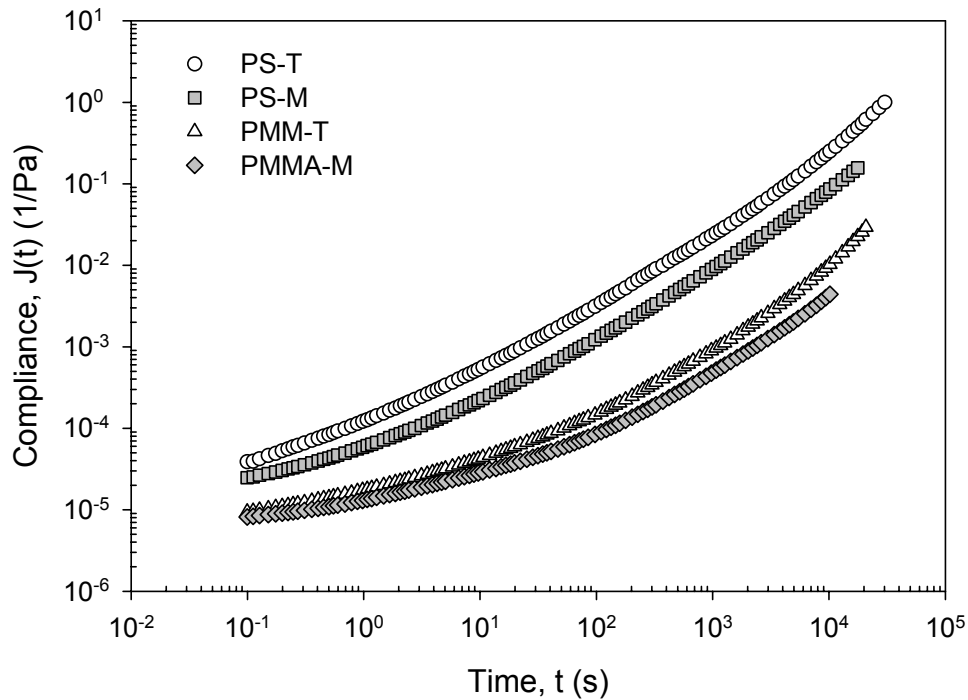


Figure 7.13. Shear creep compliance versus time for polystyrene samples at 220°C and poly(methyl methacrylate) samples at 250°C.

The zero-shear viscosity and steady-state shear compliance were determined from the creep data and are reported in Table 7.2. For both types of polymer, the T series has a lower zero-shear viscosity compared to the M series samples. The effect of LCB on the zero-shear viscosity depends upon the type and length of branching and both reductions

and enhancements in η_0 have been observed (see Section 2.3.1.3.1). The introduction of branching leads to a decrease in a polymer's molecular size and in turn, fewer molecular entanglements. However, when the branch length is sufficiently long, the overall number of entanglements will increase. Assuming that the general trend for linear polymers applies in that the zero-shear viscosity scales with molecular weight to the power of 3.4, the difference in M for the samples analyzed will not significantly affect η_0 ($\eta_{0T}/\eta_{0M} \propto (M_T/M_M)^{3.4}$: for PS, ratio ≈ 1.3 and for PMMA, ratio ≈ 0.92). Any differences in polydispersity can also be disregarded as the molecular weight distribution does not have a major influence on the zero-shear viscosity (35). Thus, the results indicate that both PS-T and PMMA-T are more branched than their corresponding M samples. Based on the structure of the tetrafunctional initiator, branching would be introduced in the form of star polymer chains. The results indicate that the reduction in size of a star polymer compared to a linear chain, which in turn leads to fewer entanglements is a significant factor. The trend in zero-shear viscosity suggests that the star arms are not sufficiently long enough to increase the overall number of entanglement.

When examining the zero-shear recoverable compliance data, there is not such an obvious trend. The PS-T sample exhibits a much larger elasticity compared to PS-M while the steady-state shear compliance of PMMA-T is lower than the value for PMMA-M. Similar to the effect of LCB on the zero-shear viscosity, the presence of branching can either increase or decrease J_e^0 . When looking at the results in Table 7.2, it is difficult to state a definite conclusion because the zero-shear recoverable compliance is highly sensitive to the polydispersity, especially to small amounts of very high molecular weight material (16, 49). A broader molecular weight distribution produces a much higher J_e^0 as shown by the following relation (49):

$$J_e^0 \propto \frac{M_{z+1}M_{z+2}}{M_w M_z} \quad 7.15$$

Chromatograms of PS-T showed a high molecular weight fraction that led to a larger polydispersity compared to PS-M. From the results, it appears that the high molecular weight fraction led to a larger value of the steady-state shear compliance and masked any effects of long-chain branching. A similar trend for the poly(methyl methacrylate) was observed. PMMA-M has a broader molecular weight distribution and a slightly larger J_e^0 compared to PMMA-T.

7.3.4.3 Combining Dynamic and Creep Viscoelastic Data

Theoretically, viscoelastic data obtained from one type of experiment can be converted into another. For example, it is possible to take time-dependent creep data, convert it to frequency-dependent data and thus, obtain viscoelastic functions over a wider frequency range. The general equations that relate the stress relaxation modulus $G(t)$, storage modulus $G'(\omega)$, loss modulus $G''(\omega)$, creep compliance $J(t)$, storage compliance $J'(\omega)$, loss compliance $J''(\omega)$, continuous relaxation spectrum $H(\tau)$ and continuous retardation spectrum $L(\tau)$ are given by equations 7.1-7.3 and 7.15-7.19.

$$J(t) = J_g + \int_{-\infty}^{\infty} L(\tau) \left(1 - e^{-t/\tau}\right) d \ln \tau + \frac{t}{\eta_0} \quad 7.16$$

$$J'(\omega) = J_g + \int_{-\infty}^{\infty} L(\tau) \left(\frac{1}{1 + (\omega\tau)^2}\right) d \ln \tau \quad 7.17$$

$$J''(\omega) = \int_{-\infty}^{\infty} L(\tau) \left(\frac{\omega\tau}{1 + (\omega\tau)^2}\right) d \ln \tau + \frac{1}{\omega\eta_0} \quad 7.18$$

$$H(\tau) = \frac{L(\tau)}{\left[J_g + \int_{-\infty}^{\infty} \frac{L(u)}{1 - u/\tau} d \ln u - \frac{\tau}{\eta_0} \right]^2 + \pi^2 L(\tau)^2} \quad 7.19$$

$$L(\tau) = \frac{H(\tau)}{\left[G_e - \int_{-\infty}^{\infty} \frac{H(u)}{\tau/u - 1} d \ln u \right]^2 + \pi^2 H(\tau)^2} \quad 7.20$$

where J_g is the instantaneous compliance. The relaxation or retardation spectrums cannot be measured directly from an experiment and must be calculated from materials functions (such as G or J as functions of time or frequency). The determination of either spectrum from the above equations requires the inversion of a Fredholm integral equation of the first kind and is known as an ill-posed problem (50). A software program (NLREG) using a nonlinear Tikhonov regularization method has been developed to solve this problem (51).

Utilizing NLREG, creep data in the form of $J(t)$ were used to determine the retardation spectrum for each of the samples. This spectrum was then employed to generate the compliance estimates as a function of frequency from which other viscoelastic functions could be determined. The complex, storage and loss compliances and moduli are related as follows:

$$G^* = \sqrt{(G'^2 + G''^2)} \quad 7.21$$

$$J^* = \sqrt{(J'^2 + J''^2)} \quad 7.22$$

$$J' = G' / G^{*2} \quad 7.23$$

$$J'' = G'' / G^{*2} \quad 7.24$$

$$J^* = 1 / G^* \quad 7.25$$

Figure 7.14 shows the complex compliance data generated by the conversion of the creep time-dependent data to frequency-dependent data. The results from the dynamic testing are also plotted. The two types of data coincide well in the mid-frequency well ($0.02 < \omega < 30$ rad/s) where the converted data (lines) overlaps the dynamic data (points). Combining the two data sets has now extended the frequency range by at least two decades. More importantly, it has provided data in the terminal region that was otherwise difficult to obtain with dynamic testing. For the polystyrene samples, the dynamic data was already sufficient enough to detect differences in the behaviour of PS-T compared to

PS-M. However, upon examination of the dynamic data for the set of poly(methyl methacrylate) samples, only a slight divergence between curves can be seen in the low frequency range ($0.02 < \omega < 0.1$ rad/s). With the aid of the converted creep data, the difference in complex compliance curves is much more obvious. Plots of the storage and loss modulus master curves based on the combination of dynamic and creep data for the polystyrene and poly(methyl methacrylate) samples are shown in Figure 7.15. At the lowest frequencies, the curves show that the well-known behaviour of the terminal region has been reached: $G' \propto \omega^2$ and $G'' \propto \omega$ (42). Differences between the PMMA samples are more apparent compared to plots of just the dynamic data (see Figure 7.11).

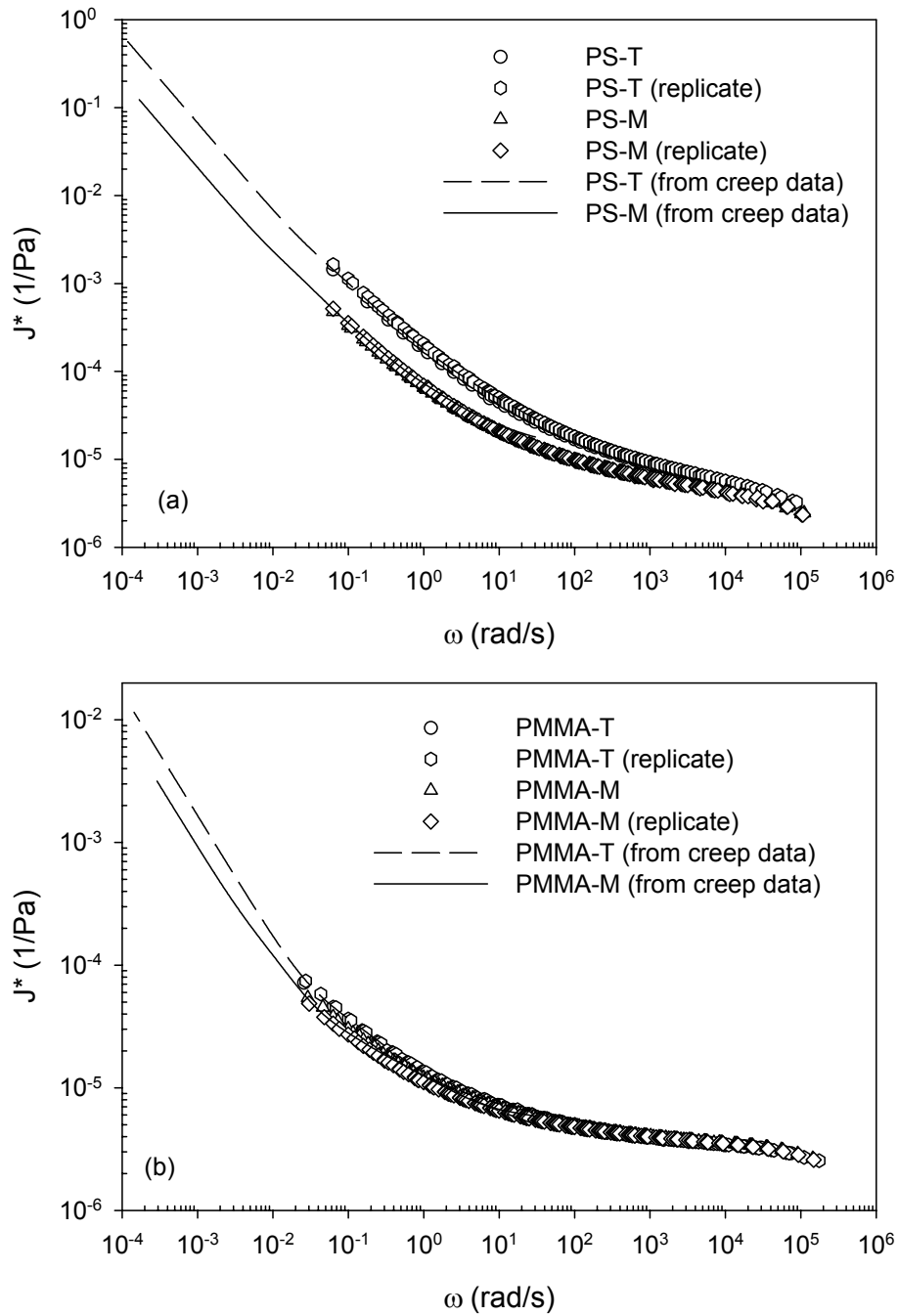


Figure 7.14. Complex compliance as a function of frequency for polystyrene samples at 220°C and poly(methyl methacrylate) samples at 250°C. Data points are master curves obtained from dynamic experiments while lines were generated by converted creep data.

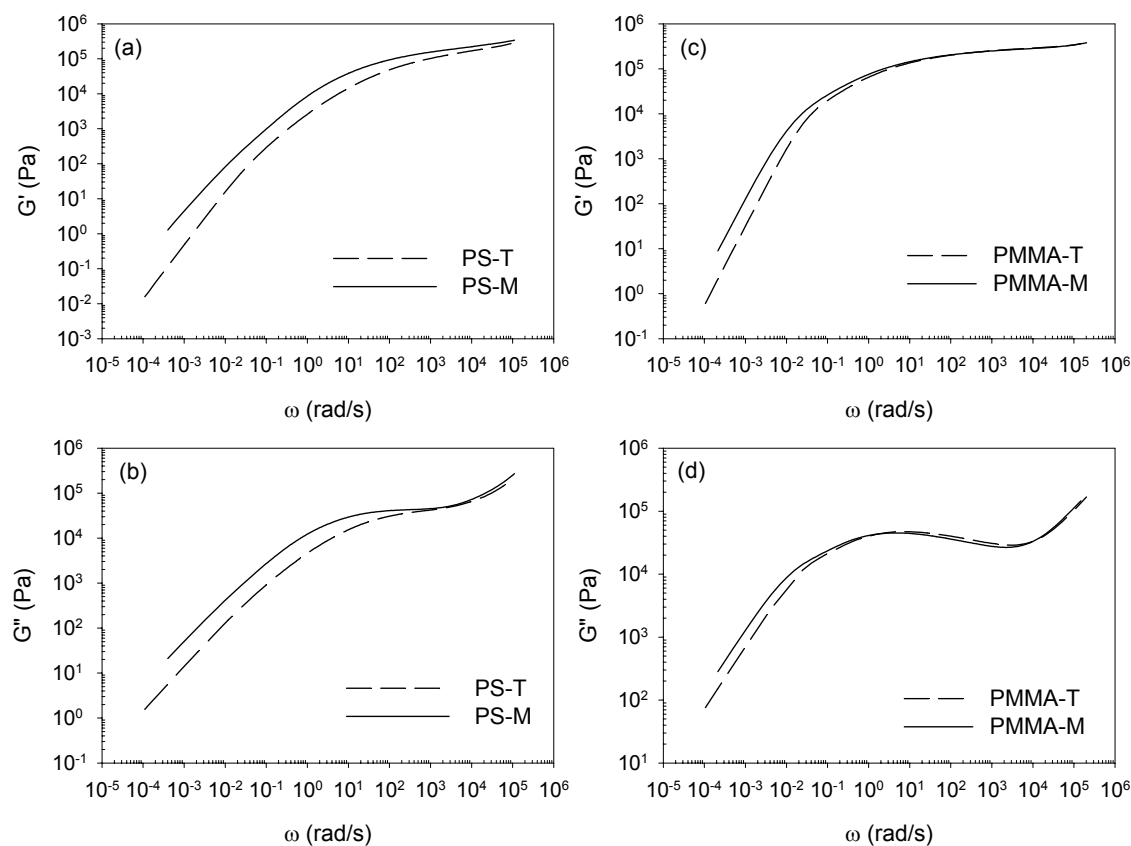


Figure 7.15. Storage and loss modulus master curves generated by combining dynamic and creep data for polystyrene at 220°C and poly(methyl methacrylate) at 250°C.

7.3.4.4 Detection of Branching

As described in Section 2.3.2.3, there are a number of methods available for the determination of long-chain branching in polymer samples. Already, examination of viscoelastic properties and the thermorheological behaviour of the samples have shown that the T series of samples is more branched than the M samples. Most of the rheological indices described in Section 2.3.2.3 are not suitable for the polymers analyzed in this study as they attempt to quantify low levels of LCB that produce a viscosity enhancement (and not a viscosity reduction) and that are not detected by SEC (i.e., $g \approx g' \approx 1$). In most cases, the indices are unable to differentiate between the effects of branching and molecular weight polydispersity and as such, they have not been calculated. However, there are two plots described in Section 2.3.2.3 that are useful in

the detection of branching: the Cole-Cole plot and the reduced Van Gorp-Palmen (rVPG) plot.

The Cole-Cole plot (G'' versus G') is independent of molecular weight and can be used to compare samples of similar polydispersity (16, 52). Plots of G'' versus G' for the PS and PMMA samples are shown in Figure 7.16. Similar to other methods the effects of molecular weight polydispersity and branching are indistinguishable and the differences between the Cole-Cole plots of PS-T and PS-M cannot be attributed to one factor. In contrast, the PMMA samples have similar molecular weight distributions and as a result, the divergence of the two trends at lower frequencies can be considered as evidence of branching. In a study of branched ethylene-propylene copolymers (EPM), higher levels of branching were found to produce smaller loss moduli for a particular value of G' (52). The EPM polymers also exhibited an increase in zero-shear viscosity with increasing levels of LCB. The opposite trend was found with PMMA where the curve for PMMA-T is above that of PMMA-M at lower frequencies and a viscosity reduction was found for PMMA-T.

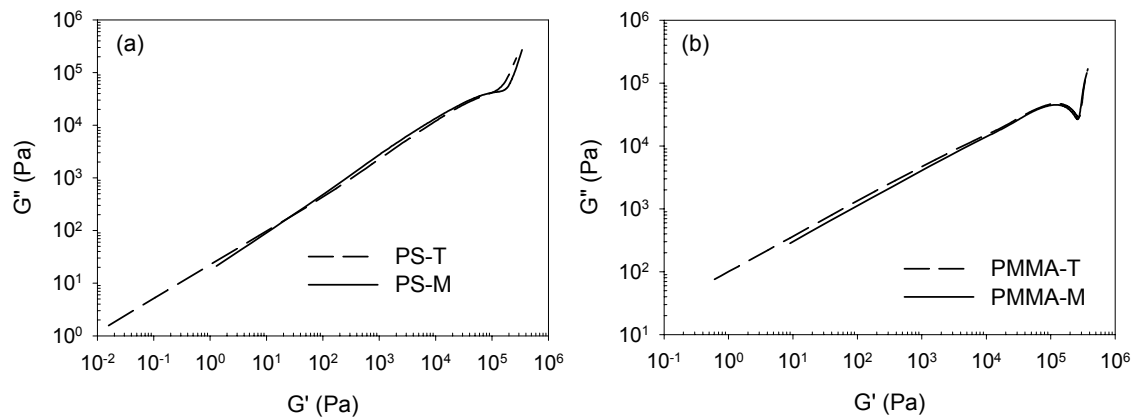


Figure 7.16. Cole-Cole plot for polystyrene and poly(methyl methacrylate) samples.

Reduced Van Gorp-Palmen plots are provided in Figure 7.17. G_N^0 is the plateau modulus and can be determined by applying the $\tan \delta$ minimum criterion (53, 54). The plateau modulus is defined as follows:

$$G_N^0 = G'(\omega_c) \quad 7.26$$

where ω_c is the frequency at which $\tan \delta$ reaches a minimum. In terms of the complex modulus, the expression can be redefined as follows:

$$G_N^0 = \lim_{\delta \rightarrow 0} |G^*(\delta)| \quad 7.27$$

As δ (or $\tan \delta$) tends towards zero, G' becomes significantly larger than G'' and the complex modulus approaches G' . Values of the plateau modulus for each of the samples are reported in Table 7.2 and are within the wide range of reported values for polystyrene and poly(methyl methacrylate) (42, 53-57). The curves shown in Figure 7.17 follow the general shape of the rvGP plot. The loss angle begins as a plateau at 90° and decreases with increasing values of the reduced modulus. For a linear polymer, an inflection point is passed and the loss angle reaches a minimum at $G_{\text{red}} = 1$. After this point, δ begins to increase. The effect of polydispersity is to produce a less steep drop in the loss angle while a higher molecular weight is seen by a lower minimum value of δ . The presence of branching causes a plateau or even a second minimum in the loss angle for $G_{\text{red}} < 1$. Looking at the polystyrene curves (see Figure 7.17 (a)), both sets of data have a similar shape except in the middle region of the reduced modulus. The data for PS-T does not show a smooth decrease in the loss angle towards its minimum as the results for PS-M do. Although it cannot be stated that this is a plateau, the change in shape can be attributed to the effects of branching. The influence of polydispersity is seen by the broader decrease in loss angle towards its minimum for PS-T compared to the PS-M curve. This trend suggests that PS-T has a broader molecular weight distribution which agrees with SEC data. When examining the minimum value of the loss angle, PS-M has a lower value compared to PS-T indicating that PS-M should be of a higher molecular

weight. This is contrary to the SEC data where PS-T was found to have a weight-average molecular weight of 628 kg/mol compared to PS-M with $M_w = 582$ kg/mol. The reason for this discrepancy is not known. Very little variation is found between the rvGP plots for the poly(methyl methacrylate) samples except for low values G_{red} (less than 0.05). The loss angle for PMMA-M begins to decrease at a smaller reduced modulus compared to PMMA-T suggesting that PMMA-M has a broader molecular weight distribution. This result agrees with the findings from SEC data (see Table 7.1).

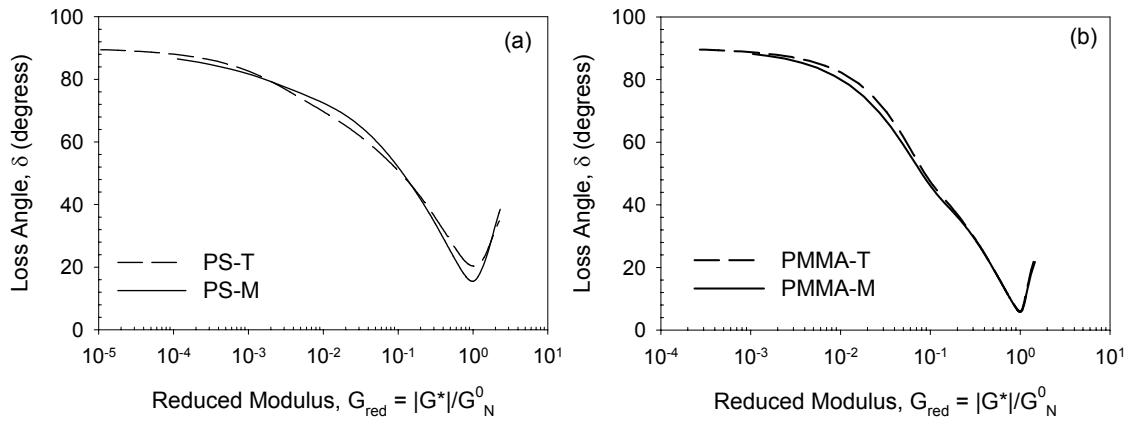


Figure 7.17. Reduced Van Gorp-Palmen plot for polystyrene and poly(methyl methacrylate) samples.

7.3.4.5 Relaxation Spectrum

Storage and loss modulus data generated by the combination of dynamic and creep data shown in Figure 7.15 were used to determine relaxation spectra with the computer program NLREG. The results are plotted in Figure 7.18 in the form of the relaxation strength as a function of relaxation time. The relaxation spectra are valid in a range of relaxation times corresponding to $\tau_{min} = (\omega_{max})^{-1}$ and $\tau_{max} = (\omega_{min})^{-1}$ where ω_{max} and ω_{min} are the maximum and minimum frequencies of the dynamic data (49). The shape of the spectra is comparable to expected trends for polymers with broad molecular weight distributions. At very small relaxation times, the relaxation strength is fairly large and decreases quickly during the transition zone. In the mid-relaxation region, H is relatively flat while in the terminal region, the relaxation strength approaches zero. Polymers of narrow molecular weight distribution show a well-defined sharp decrease in H in the

terminal region while polydisperse polymers exhibit a less abrupt drop in the relaxation strength. Examining the relaxation spectra for the polystyrene samples, it can be seen that in the mid range of relaxation times ($10^{-5} < \tau < 10^{-3}$), the two samples have similar relaxation strengths. For very low relaxation times ($\tau < 10^{-5}$), there may be a significant divergence between the curves; however, it is outside the range of validity for the relaxation spectrum ($\tau_{\min} = 1/\omega_{\max} = 10^{-5}$). The maxima observed at the short-time end of the spectrum for PS-M and other undulations can be attributed to experimental scatter and numerical artifacts (53). At times, the NLREG program attempts to fit the experimental data exactly but at the expense of introducing meaningless maxima and minima (58). As a solution, the number of experimental data points used in the creep conversion process was reduced and the number of relaxation times calculated was kept to 10 points per decade. Both steps were found to considerably reduce the undulations in the relaxation spectra. Significant differences between the relaxation spectrum of PS-T and PS-M can be seen from the mid relaxation times onwards. The curve for PS-T begins to decrease at shorter times than PS-M and corresponds to PS-T having a lower zero-shear viscosity. Relaxation spectra for PMMA-T and PMMA-M are shown in Figure 7.18 (b). The curves show the same general trend where H decreases sharply into a slight minimum and then drops to zero in the terminal region. Both samples have similar spectra until the terminal region is reached where the relaxation strength of PMMA-T begins to drop at a smaller relaxation time. Because the samples analyzed in this study have broad molecular weight distributions, the onset of the terminal region is not sharply defined and a terminal relaxation time is not easily identified. However, other measures of the relaxation spectrum can be defined such as the number- and weight-average terminal (longest) relaxation times:

$$\tau_{0n} = \frac{\eta_0}{G_N^0} \quad 7.28$$

$$\tau_{0w} = \eta_0 J_e^0 \quad 7.29$$

Estimates of τ_{0n} and τ_{0w} are given in Table 7.2. Both PS-M and PMMA-M show much higher values of the number- and weight-average terminal relaxation times. Since

branching in PS-T and PMMA-T has been found to significantly reduce η_0 , this has produced lower terminal relaxation times.

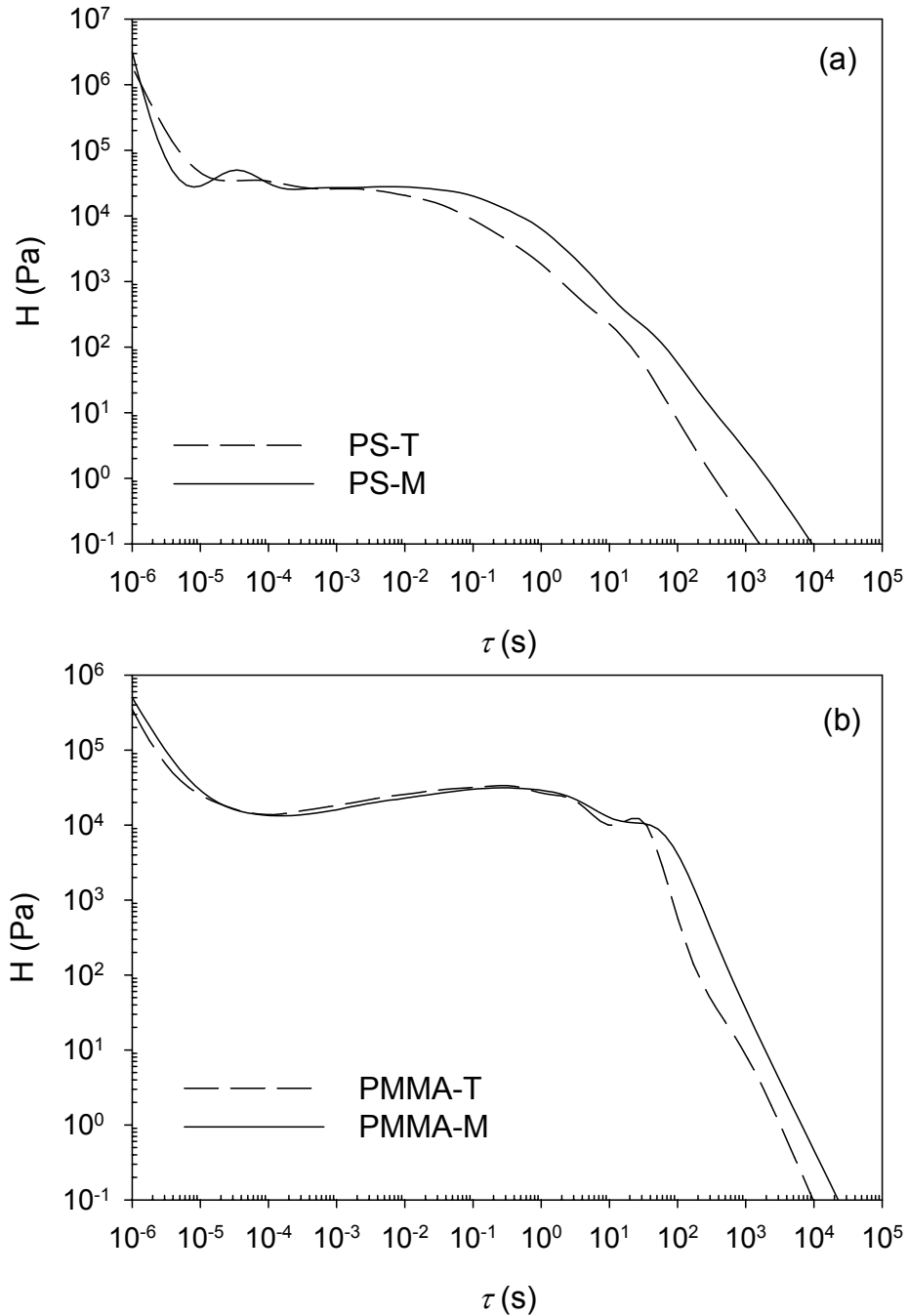


Figure 7.18. Relaxation spectra for polystyrene and poly(methyl methacrylate) samples.

7.3.4.6 Viscosity and the Cox-Merz Rule

When investigating dynamic and steady-flow viscosity measurements, Cox and Merz observed that curves of viscosity as a function of shear rate overlapped complex viscosity versus frequency data (59). Their empirical correlation was expressed as:

$$\eta(\dot{\gamma}) = |\eta^*(\omega)| \quad 7.30$$

where $\dot{\gamma}$ is the shear rate and η^* is the complex viscosity. The Cox-Merz rule has been found to be extremely useful. More often than not, viscoelastic data is collected in the linear region, typically due to the ease of running such experiments; however, the processing of polymers is typically performed in the nonlinear region. Use of the Cox-Merz correlation allows data from the linear region to be used in the study of nonlinear viscoelastic behaviour. The application of this empirical rule has been found to be valid for several polymers including those containing branched chains (60). Assuming that it can be used for the polymers analyzed in this study, viscosity-shear rate relations can be fit to the experimental data. Figure 7.19 is a log-log plot of viscosity as a function of shear rate for the samples analyzed in this study. In general, at low shear rates, the viscosity profile is relatively flat meaning that the viscosity is insensitive to variations in shear rate. The limit of this region is found as the shear rate tends towards zero and is referred to as the Newtonian or the zero-shear viscosity. With increasing shear rate, the viscosity begins to sharply decrease. This behaviour, known as shear thinning, occurs when polymer chains begin to disentangle and slip past one another. Because of this slippage, polymer chains can orient themselves in the direction of flow and thus, lead to a lower viscosity. The rate and onset of shear thinning are of considerable importance during polymer processing. Because the dependence of viscosity on shear rate in a log-log plot is very close to being linear in the shear thinning region, an empirical power law is typically proposed to describe the behaviour:

$$\eta = K\dot{\gamma}^{-(1-n)} \quad 7.31$$

where K is the consistency index and n is rate index. This model is only valid for high shear rates and cannot account for the zero-shear viscosity. A model better able to account for the viscosity profile over a wider range of shear rates is the generalized Cross-Carreau model:

$$\eta = \frac{\eta_0}{\left(1 + \left(\frac{\eta_0 \dot{\gamma}}{\tau^*}\right)^a\right)^{\frac{1-n}{a}}} \quad 7.32$$

where τ^* , a and n are the unique parameters of a polymer sample. τ^* characterizes the shear-stress level at which the viscosity transitions between the two asymptotic limits (Newtonian and power-law regions). n corresponds to the power-law index in Equation 7.31 while a allows the model to better fit the transition region and characterizes the breadth between the two limiting behaviours. The Cross model corresponds to $a = 1-n$ and allows for a broad transition region while the Carreau model uses $a = 2$ which produces a much narrower transition. The breadth of the shift between the Newtonian and power-law regions has been found to be greatly influenced by the polydispersity (61). Polymers with a narrow molecular weight distribution have a sharp transition while a broader molecular weight distribution leads to a broader shift. As such, the Carreau model predicts the viscosity-shear rate behaviour of narrow MWD polymers while the Cross model is better suited to polydisperse polymers. From the different model types regressed to the data, both the Carreau and Cross models showed a lack of fit and as such, the results are not reported (with the Carreau being the worst). The generalized Cross-Carreau model performed much better than the other models and the model predictions are shown in Figure 7.19. Parameter estimates for the polystyrene and poly(methyl methacrylate) samples are reported in Table 7.4. Although not shown here, joint probability contour regions were examined for the various parameter estimates and found to be extremely small and more circular in shape than elliptical. The latter finding indicates that the parameter estimates are not highly correlated. Comparison of JCR plots within polymer type showed no overlap at a significance level of 95%, indicating that there exists a significant statistical difference between parameters estimates of PS-T

versus PS-M and PMMA-T versus PMMA-M. Estimates of the zero-shear viscosity from the Cross-Carreau model are similar to the values obtained from creep data (see Table 7.2) and show the same trend where samples PS-T and PMMA-T have lower values of η_0 compared to their corresponding M samples. When examining estimates of τ^* , it appears that the transition between the Newtonian and power-law regions occurs at lower shear-stress levels for the T series of samples. However, it is difficult to directly compare values of τ^* as samples have varying zero-shear viscosities. A characteristic time for this transition can be defined as the ratio of η_0/τ^* . It can be seen from the ratios listed in Table 7.4 that the T samples have a lower characteristic time for the transition to shear thinning. In terms of the data plotted in Figure 7.19, this result implies that the onset of shear thinning occurs at higher shear rates for the T samples. As well, PS-T and PMMA-T have higher values of the exponent n . Based on the power-law model given by Equation 7.31, larger values of the rate index result in smaller absolute values of the exponent (i.e., $\uparrow n \rightarrow \downarrow(1-n)$) and thus, the decrease in viscosity with increasing shear rate is not as steep. In other words, a larger rate index indicates less shear thinning. Differences in the viscosity profile of each sample are more clearly observed by plotting a reduced viscosity (η/η_0) versus shear rate as presented in Figure 7.20. Curves for PS-T and PMMA-T begin to deviate from unity at higher shear rates and exhibit less of a dependence on shear rate in the power-law region compared to their M counterparts.

The shift in the transition region to higher shear rates has been attributed to long chain branching (62, 63). Mendelson et al. quantitative expressed the relation between branching in low-density polyethylene (LDPE) and the onset of shear thinning by the following (62):

$$\dot{\gamma}_{cr} = A(gM_w)^{-b} \quad 7.33$$

where A and b are constants and $\dot{\gamma}_{cr}$ is defined as the shear rate where $\eta = 0.95\eta_0$. Higher branching densities in LDPE would result in lower contraction factors and in turn, higher shear rates for the onset of non-Newtonian flow. It has been reasoned that for

relatively short branches or high branching densities, the probability of chain entanglement is reduced because of a branch chain's smaller molecular size. A linear polymer of similar molecular weight but greater molecular size is more readily entangled. In the flow region, molecular entanglements will constrain translational motion such that the linear polymer has a higher zero-shear viscosity. In contrast, branches of appreciable length or sparse branching can lead to considerable more entanglements and act as permanent constraints that prevent translational motion. A polymer with such branching will have a higher zero-shear viscosity compared to its linear analog. When the branches are large enough to cause more entanglements, the flow region, where uncoupling begins, will shift to longer times or lower frequencies (shear rates). The explanation is that longer times are needed for the coordinated motions of uncoupling to take place. When the branches are not sufficiently long enough to increase the number of entanglements, slippage occurs at much shorter times or higher frequencies (shear rates). In the first situation, the zero-shear viscosity of the branched polymer will be reached at a lower shear rate compared to the corresponding linear polymer while for the latter case, the Newtonian region will be reached at higher shear rates.

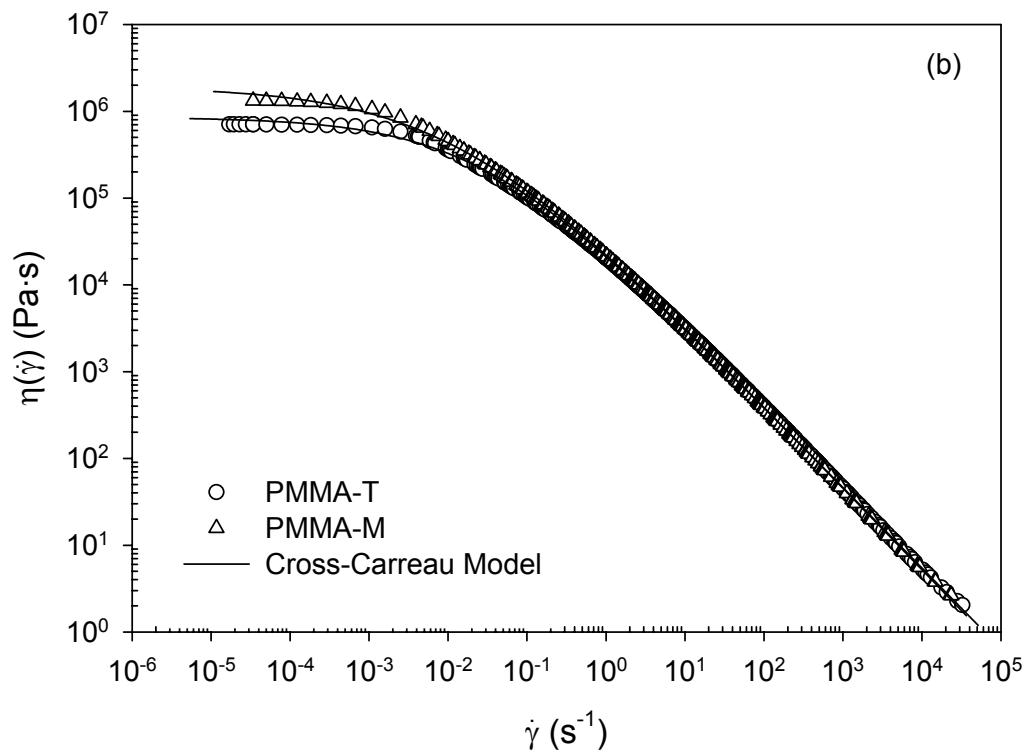
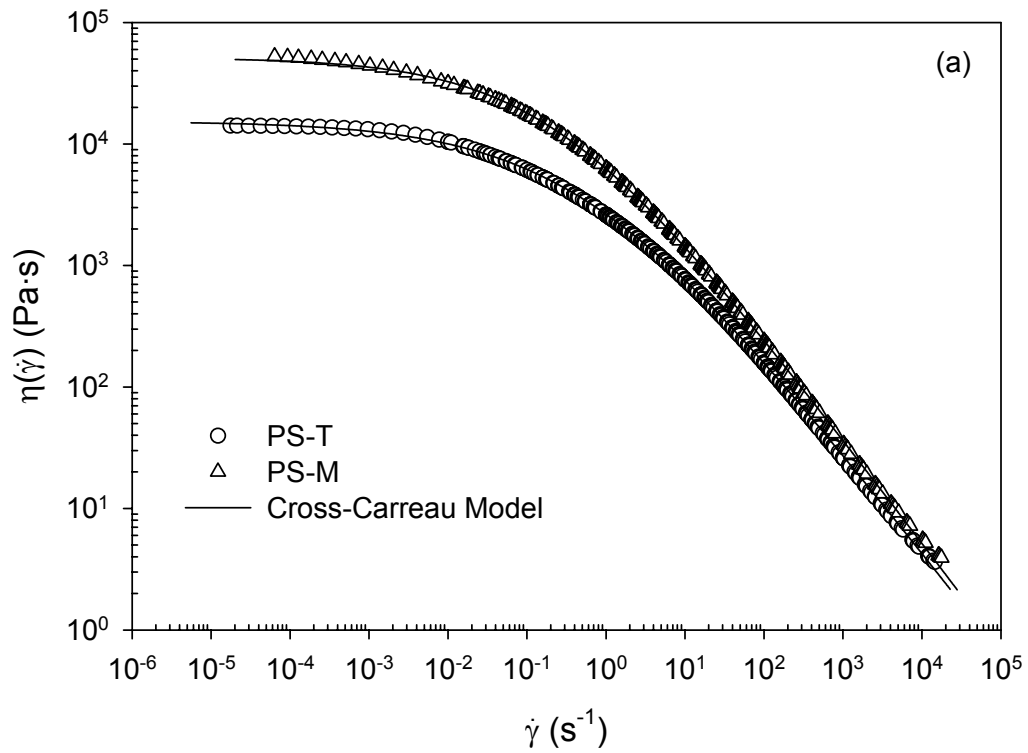


Figure 7.19. Viscosity versus shear rate for polystyrene and poly(methyl methacrylate) samples. Parameters for the Cross-Carreau model are given in Table 7.4 for sample.

Table 7.4. Cross-Carreau model parameters.

Sample	η_0 (kPa·s)	τ^* (kPa)	a	n	η_0/τ^* (s)
PS-M	51.3	11.9	0.433	0.139	4.31
PS-T	15.4	9.27	0.377	0.162	1.66
PMMA-M	1920	24.9	0.407	0.0551	77.1
PMMA-T	850	22.3	0.476	0.0700	38.1

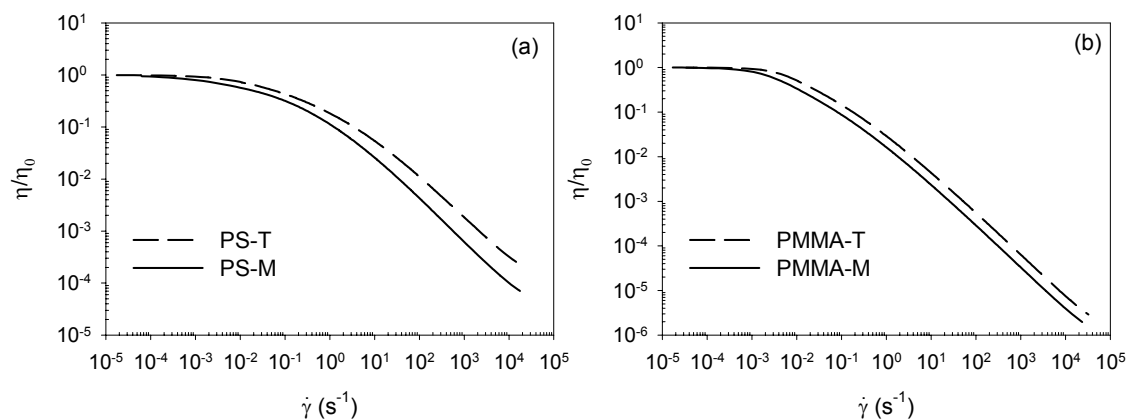


Figure 7.20. Reduced viscosity as a function of shear rate for polystyrene and poly(methyl methacrylate) samples.

7.4 Conclusions

Polystyrene and poly(methyl methacrylate) samples produced by free radical polymerization with either a tetrafunctional (PS-T and PMMA-T) or monofunctional (PS-M and PMMA-M) initiator were characterized by dilute solution and rheological methods. In the case of polystyrene, SEC analysis with multi-angle laser light scattering and viscometry revealed smaller radii of gyration and intrinsic viscosities for the sample produced with the tetrafunctional initiator. This reduction in molecular size confirmed that PS-T contained higher levels of branching than PS-M. In contrast, no differences were observed in R_g and $[\eta]$ plots for the comparison of PMMA samples.

Oscillatory shear experiments were performed at varying temperatures. The application of TTS was found to be valid for both sets of polystyrene and poly(methyl methacrylate) samples. The WLF equation was found to fit the horizontal shift factors of the polystyrene samples extremely well and a different set of parameters estimates were calculated for PS-T compared to PS-M. In the analysis of the poly(methyl methacrylate) data, an Arrhenius model provided a better fit compared to the WLF equation. Examination of the activation of viscous flow indicated that PMMA-T had a higher E_a value and the enhancement has been attributed to the presence of long-chain branching. Activation energies for the polystyrene samples were not determined to be statistically different. However, the Arrhenius model showed a clear lack of fit to the polystyrene data and thereby, resulted in higher confidence intervals for the PS activation estimates.

Viscoelastic functions measured during oscillatory shear experiments showed differences between the T and M samples due to branching (and in the case of polystyrene, molecular weight and MWD). Dynamic data did not adequately reach the terminal region in order to calculate the zero-shear viscosity or steady-state recoverable compliance. As such, shear creep tests were performed. Lower values of the zero-shear viscosity were observed for the T samples and indicated the presence of branching. Differences in the steady-state recoverable compliance could not be attributed solely to the effect of branching because of polydispersity effects.

Using a rheological software package, creep time-dependent data were converted to frequency-dependent functions. Combined with the data collected from the oscillatory experiments, viscoelastic functions were extended over several decades. Relaxation spectra were determined from the combined data and indicated that the terminal region began at lower relaxation times for samples produced with the tetrafunctional initiator. The Cox-Merz rule was applied and the resulting viscosity-shear rate data were fit to a generalized Cross-Carreau model. PS-T and PMMA-T showed lower zero-shear viscosities, higher shear rates for the transition between the Newtonian and power-law region, and less shear thinning compared to PS-M and PMMA-M. All three observations are indications that the set of T samples are more branched than the M series.

In the end, it has been shown that samples produced with the tetrafunctional initiator are more branched than their counterparts produced with a monofunctional initiator. Detection of branching by fractionation and the examination of dilute solution properties was found to be a less time and effort intensive method. The characterization by SEC-MALLS-Viscometry also required less material for testing compared to rheological methods. However, it was unable to detect the low levels of branching seen in PMMA-T that influenced the polymer's rheological behaviour. The results obtained from viscoelastic data suggest that the branch lengths are not adequately long enough to increase the number of entanglements. This behaviour is similar to that observed with low-density polyethylene (62-64).

7.5 References

1. Staudinger, H., Schulz, G. V. Highly polymerized compounds. CXXVI. Comparison of Osmotic and Viscosimetric Molecular-Weight Determinations of Polymer-Homologous Series. *Ber.* **1935**, *68B*, 2320-2335.
2. Flory, P. J. Mechanism of Vinyl Polymerizations. *J. Am. Chem. Soc.* **1937**, *59*, 241-253.
3. Bywater, S. Preparation and Properties of Star-branched Polymers. *Advances in Polymer Science* **1979**, *30* (2), 89-116.
4. Roovers, J. Dilute Solution Properties of Regular Star Polymers. *Plast. Eng.* **1999**, *53*, 285-341.
5. Burchard, W. Solution Properties of Branched Macromolecules. *Adv. Polym. Sci.* **1999**, *143*, 113-194.
6. Graessley, W. W. Effect of Long Branches on the Flow Properties of Polymers. *Acc. Chem. Res.* **1977**, *10*, 332-339.
7. Watanabe, H. Viscoelasticity and Dynamics of Entangled Polymers. *Prog. Polym. Sci.* **1999**, *24*, 1253-1403.
8. Graessley, W. W. Detection and Measurement of Branching in Polymers. In *Characterization of Molecular Structure*; 1968; 371-388.
9. Small, P. A. Long-Chain Branching in Polymers. *Adv. Polym. Sci.* **1975**, *18*, 1-64.
10. Roovers, J. Branched Polymers. In *Encyclopedia of Polymer Science and Engineering*; 1983; 478-499.
11. Shiga, S. Modern Characterization of Long-Chain Branching. *Polymer-Plastics Technology and Engineering* **1989**, *28* (1), 17-41.

12. Rudin, Alfred Measurement of Long-Chain Branch Frequency in Synthetic Polymers. In *Modern Methods of Polymer Characterization*; John Wiley & Sons: Toronto, 1991; 103-112.
13. Vega, J., Aguilar, M., Peon, J., Pastor, D., Martinez-Salazar, J. Effect of long chain branching on linear-viscoelastic melt properties of polyolefins. *E-Polymers* **2002**,
14. Janzen, J., Colby, R. H. Diagnosing Long-Chain Branching in Polyethylenes. *J. Molecul. Struct.* **1999**, 485-486, 569-584.
15. Jackson, C., Chen, Y.-J., Mays, J. W. Dilute Solution Properties of Randomly Branched Poly(methyl methacrylate). *Journal of Applied Polymer Science* **1996**, 59, 179-188.
16. Shroff, R., Mavridis, H. New Measures of Polydispersity from Rheological Data on Polymer Melts. *J. Appl. Polym. Sci.* **1995**, 57 (13), 1605-1626.
17. Shroff, R. N., Mavridis, H. Long-Chain Branching Index for Essentially Linear Polyethylenes. *Macromolecules* **1999**, 32, 8454-8464.
18. Wood-Adams, P., Dealy, J. M., deGroot, A. W., Redwine, O. D. Effect of Molecular Structure on the Linear Viscoelastic Behavior of Polyethylene. *Macromolecules* **2000**, 33 (20), 7489-7499.
19. Trinkle, S., Walter, P., Friedrich, C. Van Gurp-Palmen Plot II - Classification of Long Chain Branched Polymers by their Topology. *Rheol. Acta* **2002**, 41 (1-2), 103-113.
20. Wood-Adams, P., Costeux, S. Thermorheological Behavior of Polyethylene: Effects of Microstructure and Long Chain Branching. *Macromolecules* **2001**, 34 (18), 6281-6290.
21. Wood-Adams, P. M., Dealy, J. M. Using Rheological data to Determine the Branching Level in Metallocene Polyethylenes. *Macromolecules* **2000**, 33, 7481-7488.
22. Kasehagen, L. J., Macosko, C. W. Nonlinear Shear and Extensional Rheology of Long-Chain Randomly Branched Polybutadiene. *J. Rheol.* **1998**, 42 (6), 1303-1327.
23. Kasehagen, L. J. and C. W. Macosko *J.Rheol.* 1996; **40** (4), 689-709.
24. Fityani-Trimmi, S., Dhib, R., Penlidis, A. Free Radical Polymerization of Styrene with a New Tetrafunctional Peroxide Initiator. *Macromolecular Chemistry and Physics* **2003**, 204, 436-442.
25. Scoriah, M. J., Dhib, R., Penlidis, A. Free-radical polymerization of methyl methacrylate with a tetrafunctional peroxide initiator. *Journal of Polymer Science Part A-Polymer Chemistry* **2004**, 42 (22), 5647-5661.
26. Scoriah, M. J., R. Dhib, and A. Penlidis *Journal of Macromolecular Science Pure and Applied Chemistry* 2005; **A42** (4), 403-426.
27. Schimpf, M. E. and J. C. Giddings *Journal of Polymer Science Part B-Polymer Physics* 1989; **27** (6), 1317-1332.
28. Giddings, J. C. The field-flow fractionation family: underlying principles. In *Field-Flow Fractionation Handbook*; John Wiley: New York, 2000; 3-30.
29. Gabriel, C. and H. Münstedt *Rheol. Acta* 1999; **38**, 393-403.
30. Podzimek, S. The Use of GPC Coupled with a Multiangle Laser Light Scattering Photometer for the Characterization of Polymers. On the Determination of

- Molecular Weight, Size, and Branching. *J. Appl. Polym. Sci.* **1994**, *54* (1), 91-103.
31. Terao, K. and J. W. Mays *European Polymer Journal* 2004; **40**, 1623-1627.
 32. Fetters, L. J., Hadjichristidis, N., Lindner, J. S., Mays, J. W. Molecular Weight Dependence of Hydrodynamic and Thermodynamic Properties for Well-Defined Linear Polymers in Solution. *J. Phys. Chem. Ref. Data* **1994**, *23* (4), 619-640.
 33. Grinshpun, V., Rudin, A., Russell, K. E., Scammell, M. V. Long-Chain Branching Indexes from Size-Exclusion Chromatography of Polyethylenes. *J. Polym. Sci. , Part B: Polym. Phys.* **1986**, *24* (5), 1171-1176.
 34. Foster, G. N., Hamielec, A. E., MacRury, T. B. The Molecular Weight and Branching Distribution Method. *ACS Symposium Series* **1980**, *138*, 131-148.
 35. Gabriel, C., Münstedt, H. Influence of Long-Chain Branches in Polyethylenes on Linear Viscoelastic Flow Properties in Shear. *Rheol. Acta* **2002**, *41* (3), 232-244.
 36. D'Agnillo, L., Soares, J. B. P., Penlidis, A. A hierarchical data analysis of a replicate experiment in polyethylene synthesis with high-temperature gel permeation chromatography. *Polymer Reaction Engineering* **1999**, *7* (2), 259-281.
 37. Gunderson, J. J., Giddings, J. C. Chemical-Composition and Molecular-Size Factors in Polymer Analysis by Thermal Field-Flow Fractionation and Size Exclusion Chromatography. *Macromolecules* **1986**, *19* (10), 2618-2621.
 38. Dammert, R., Jussila, M., Vastamaki, P., Riekkola, M. L., Sundholm, F. Determination and comparison of molar mass distributions of substituted polystyrenes and block copolymers by using thermal field-flow fractionation, size exclusion chromatography and light scattering. *Polymer* **1997**, *38* (26), 6273-6280.
 39. Schimpf, M. E. Polymer analysis by thermal field-flow fractionation. *Journal of Liquid Chromatography & Related Technologies* **2002**, *25* (13-15), 2101-2134.
 40. Roovers, J. Branched Polymers. In *Encyclopedia of Polymer Science and Engineering*; John Wiley: New York, 1983; 478-499.
 41. Brandrup, J.; Immergut, E. H.; Grulke, E. A. *Polymer Handbook*; Wiley: New York, 1999.
 42. Ferry, J. D. *Viscoelastic Properties of Polymers*; John Wiley & Sons, Inc.: Toronto, 1980.
 43. Mavridis, H., Shroff, R. N. Temperature Dependence of Polyolefin Melt Rheology. *Polym. Eng. Sci.* **1992**, *32* (23), 1778-1791.
 44. Rouse, P. E. A Theory of the Linear Viscoelastic Properties of Dilute Solutions of Coiling Polymers. *Journal of Chemical Physics* **1953**, *21* (7), 1272-1280.
 45. Carella, J. M., Graessley, W. W., Fetters, L. J. Effects of Chain Microstructure on the Viscoelastic Properties of Linear Polymer Melts: Polybutadienes and Hydrogenated Polybutadienes. *Macromolecules* **1984**, *17* (12), 2775-2786.
 46. McNeill, I. C., Zulficar, M., Kousar, T. A Detailed Investigation of the Products of the Thermal-Degradation of Polystyrene. *Polymer Degradation and Stability* **1990**, *28* (2), 131-151.

47. Kashiwagi, T., Inaba, A., Brown, J. E., Hatada, K., Kitayama, T., Masuda, E. Effects of Weak Linkages on the Thermal and Oxidative-Degradation of Poly(Methyl Methacrylates). *Macromolecules* **1986**, *19* (8), 2160-2168.
48. Nising, P., Zeilmann, T., Meyer, T. On the Degradation and Stabilization of Poly(Methyl Methacrylate) in a Continuous Process. *Chemical Engineering Technology* **2003**, *26* (5), 599-604.
49. Dealy, J.; Wissbrun, K. F. *Melt Rheology and its Role in Plastics Processing*; Van Nostrand Reinhold: New York, 1989.
50. Weese, J. A Regularization Method for Nonlinear Ill-Posed Problems. *Computer Physics Communications* **1993**, *77*, 429-440.
51. Honerkamp, J., Weese, J. A Nonlinear Regularization Method for the Calculation of Relaxation Spectra. *Rheologica Acta* **1993**, *32*, 65-73.
52. Harrell, E. R., Nakajima, N. Modified Cole-Cole Plot Based on Viscoelastic Properties for Characterizing Molecular Architecture of Elastomers. *Journal of Applied Polymer Science* **1984**, *29*, 995-1010.
53. Fuchs, K., Friedrich, C., Weese, J. Viscoelastic properties of narrow-distribution poly(methyl methacrylates). *Macromolecules* **1996**, *29* (18), 5893-5901.
54. Trinkle, S., Friedrich, C. Van Gurp-Palmen-Plot: A Way to Characterize Polydispersity of Linear Polymers. *Rheol. Acta* **2001**, *40* (4), 322-328.
55. Wu, S. Chain Structure and Entanglement. *Journal of Polymer Science: Part B: Polymer Physics* **1989**, *27*, 723-741.
56. Aharoni, S. M. Correlations Between Chain Parameters and the Plateau Modulus of Polymers. *Macromolecules* **1986**, *19* (2), 426-434.
57. Fetters, L. J., Lohse, D. J., Graessley, W. W. Chain dimensions and entanglement spacings in dense macromolecular systems. *Journal of Polymer Science Part B-Polymer Physics* **1999**, *37* (10), 1023-1033.
58. NLREG Manual. **2001**, *Version Rheology 2.2*
59. Cox, W. P., Merz, E. H. Correlation of Dynamic and Steady Flow Viscosities. *Journal of Polymer Science* **1958**, *28* (118), 619-622.
60. Wood-Adams, P. The effect of long chain branches on the shear flow behavior of polyethylene. *J. Rheol.* **2001**, *45* (1), 203-210.
61. Hieber, C. A., Chiang, H. H. Shear-Rate-Dependence Modeling of Polymer Melt Viscosity. *Polymer Engineering and Science* **1992**, *32* (14), 931-938.
62. Mendelson, R. A., Bowles, W. A., Finger, F. L. Effect of Molecular Structure on Polyethylene Melt Rheology. II. Shear-Dependent Viscosity. *J. Polym. Sci. , Part A-2* **1970**, *8*, 127-141.
63. Chartoff, R. P., Maxwell, B. Viscoelastic properties of branched polyethylene melts. *Journal of Polymer Science: Part A-2* **1970**, *8*, 455-465.
64. Doerpinghaus, P. J., Baird, D. G. Separating the effects of sparse long-chain branching on rheology from those due to molecular weight in polyethylenes. *Journal of Rheology* **2003**, *47* (3), 717-736.

CHAPTER 8 - MATHEMATICAL MODELLING OF TETRAFUNCTIONAL INITIATORS

8.1 Introduction

Mathematical modeling plays an important role in the understanding of polymerization processes. A comprehensive and accurate model is an invaluable tool, able to aid in several areas of science and engineering from selection of a suitable catalyst to process design and optimization. The modelling of free radical polymerization in either bulk, solution or emulsion is an immense field of research with too many references to list. With the relatively recent introduction of multifunctional initiators, a new area of modelling in free radical polymerizations has begun. The majority of experimental work and thus, modelling efforts, have focused on the use of difunctional initiators, specifically in the polymerization of styrene (1-6) (see Appendices A and B for bench-marking and optimization studies with difunctional initiators). However, other systems have been examined including the use of difunctional initiators in the production of low-density polyethylene (7), poly(vinyl chloride) (8) and high impact polystyrene (9). Experimental studies of initiators with functionalities higher than two in free radical polymerization are scarce (10-12) and the modelling of such systems is nonexistent. The purpose of this work is to construct a mathematical model to predict the behaviour of tetrafunctional initiators in free radical polymerizations and test the model's ability to simulate experimental data.

8.2 Model Development

In general, the free radical polymerization of vinyl monomers is comprised of chain initiation, propagation, termination and chain transfer reactions (see Section 2.1). Gao and Penlidis developed a model for the bulk and solution free radical homo- and copolymerization of monofunctional initiators (13, 14). Their work involved the review of over 500 references where models, model parameters, and experimental data were combined to construct a unified database for a variety of monomers, initiators, solvents

and chain transfer agents. The model and database are used in this study to predict the behaviour of the monofunctional initiator, TBEC, while only the database is employed in the simulation of the tetrafunctional initiator.

8.2.1 Polymerization Mechanism

The polymerization mechanism of a tetrafunctional initiator is significantly more complex than that of a monofunctional initiator. Deciding upon an adequate reaction scheme required various assumptions. The first key difference between a monofunctional initiator and those of higher functionality is that the latter can theoretically produce species with more than one radical site per molecule. In the modelling of difunctional initiators, groups have assumed that the formation of di-radical species, by either the simultaneous decomposition of two functional groups (from an initiator or dead polymer chain) or the decomposition of one functional group in a radical, can be considered negligible (4, 6). The argument is that in a radical's lifetime, the probability of it propagating and then terminating is much higher than the decomposition of a second functional site. The group of Choi (2, 3, 15-18) and those who have used their model (5, 8) have chosen, however, to include the effect of species with two active radical sites. A comparison of the two models has found no discernable difference and thus, validates the decision to neglect di-radicals (5). Employing a tetrafunctional initiator can theoretically lead to the production of not only di- but tri- and tetra-radicals. In order to reduce the complexity of the model, it was initially assumed that molecules could have at most two active radical sites. The validity of this assumption will be verified in the Section 8.3.3. The second and arguably most important complexity that arises from modelling a tetrafunctional initiator is that through successive decomposition, propagation and termination by combination reactions, species with more functional groups than the initiator originally possesses can be formed. For example, two radical chains with three undecomposed sites may terminate by combination and form a dead polymer chain with six functional groups. This polymer chain can then have one of its functional sites decompose and continue growing in size, branching and functionality. To propose a definite reaction scheme, the chain functionality distribution must be limited. Thus, it was assumed that no more than two star radicals could combine together and therefore, a

polymer molecule could have at most six undecomposed sites. A third assumption in the modelling the tetrafunctional initiator is that all functional groups have identical decomposition kinetics. In the study of unsymmetrical difunctional initiators, functional groups have obviously been found to have varying thermal stability due to differences in the structure of the labile group. In the case of symmetrical molecules, it has been argued that an induction effect may be present when the neighbouring functional group decomposes. However, the presence of such an effect is found to depend upon the length of the bridge between sites (19). As the bridge length is increased, the induction effect is lessened. The structure of the tetrafunctional initiator employed in this study is shown in Figure 8.1. The composition and structure of the R group is kept proprietary by the manufacturer. The molecular weight of the initiator is 965.0 g/mol and the four tert-butylperoxy carbonate groups comprise 532.5 g/mol of that total. Although quite simplified and arguably unrealistic, if we assume that the core of JWEB50 can be represented by linear hydrocarbons links attached to a single carbon atom, there are roughly seven CH₂ groups separating the functional groups from the initiator's center. Studies with a difunctional initiator having a bridge as short as four carbon atoms, have assumed that the decomposition of one site does not affect the stability of the other (15, 17, 18). Therefore, it is not unreasonable to assume that all peroxides groups in the polymerization with the tetrafunctional initiator have identical kinetics.

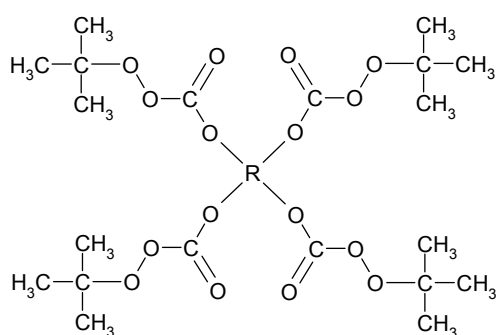


Figure 8.1. Molecular structure of tetrafunctional initiator, JWEB50.

A common assumption in the modelling of multifunctional initiators is that the functional groups on a dead or growing radical chain have the same efficiency as the initiator molecule. Because of the large number of differing species with functional groups, the

estimation of efficiencies for each type is not possible. As such, an efficiency factor independent of species type was assumed. Another important distinction between the modelling of multifunctional versus monofunctional initiator is the fate of functional groups. In a polymerization initiated with a monofunctional initiator, only a percentage (f) of the initiator successfully decomposes to form initiator radicals. $1-f$ of the time, the products of an initiator's decomposition are unreactive small molecules. If a functional group on a multifunctional initiator does not successfully decompose, it does not necessarily imply that the products will be unreactive small molecules. This is especially the case for polymer molecules with functional groups where neglecting reactions involving $(1-f)$ in the population balances can result in the apparent loss of polymer. From the literature it appears that the modelling of difunctional initiators ignores this effect (2-9). However, for initiators of higher functionality, the products of "wastage" reactions become more significant and as such, these reactions must be accounted for in the reaction scheme.

The proposed polymerization mechanism for a tetrafunctional initiator is given below beginning with a list of the main assumptions and possible species. Termination of radical chains by either combination or disproportionation is considered along with the thermal polymerization of styrene. Transfer reactions have been limited to monomer and solvent but the model can easily be altered to account for transfer to inhibitor or chain transfer agent. Transfer to polymer and terminal double bond polymerization formed by either transfer to polymer or termination by disproportionation have not included in the proposed mechanism.

Assumptions

1. No chain may have more than 2 active radical sites.
2. The maximum number of cores a chain may have is 2 (i.e., no more than two stars can couple together). As a consequence, the maximum number of undecomposed sites is six per molecule and chains with two cores can only terminate with linear chains.

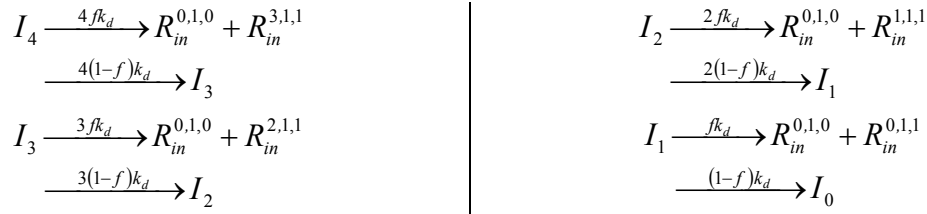
- The thermal stability of functional groups are not affected by the decomposition of neighbouring sites (i.e., all functional groups have identical decomposition kinetics).
- Initiator radicals, which are those radicals produced by initiator decomposition and exist before propagation has occurred, may have no more than 1 active site (i.e., the simultaneous decomposition of 2 or more sites on the initiator molecule does not occur).

Possible Species

$R_n^{u,a,c}$	Radical chain with u undecomposed sites, a active sites, c cores, and n total attached monomer units (total chain length): $0 \leq u \leq 6$; $1 \leq a \leq 2$; $0 \leq c \leq 2$; $n \geq 1$.
$P_n^{u,a,c}$	Dead polymer chain with similar indices except $a = 0$.
I_4	Initiator molecule
I_3, I_2, I_1	Products of an initiator's functional group wastage reaction
$R_{in}^{3,1,1}, R_{in}^{2,1,1}, R_{in}^{1,1,1}, R_{in}^{1,1,1}, R_{in}^{0,1,0}$	Star and linear initiator radicals
M	Monomer
S	Solvent

Reaction Mechanism

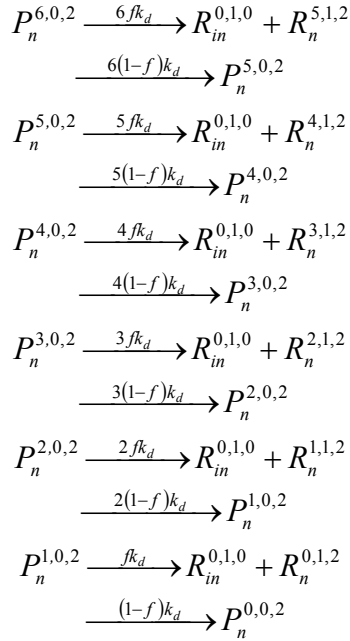
1. INITIATOR DECOMPOSITION



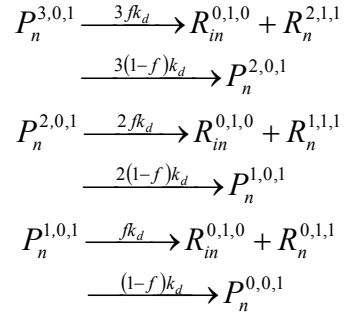
2. DECOMPOSITION OF UNDECOMPOSED SITES

a) Polymer

two cores

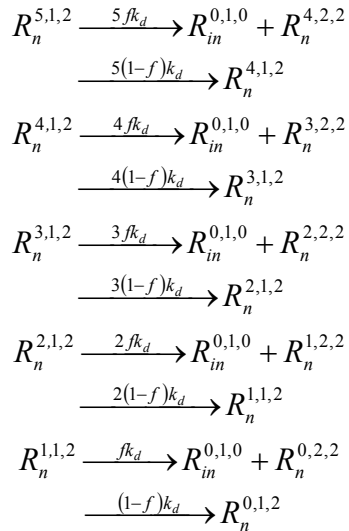


one core

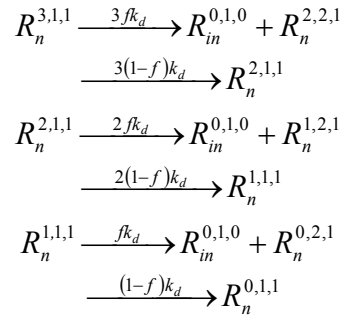


b) Radicals

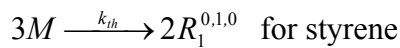
two cores



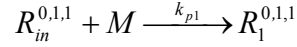
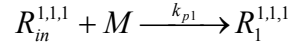
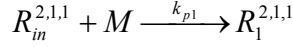
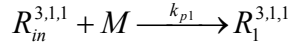
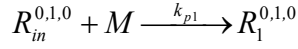
one core



3. THERMAL INITIATION

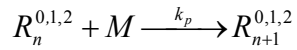
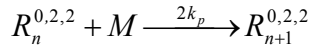
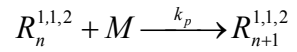
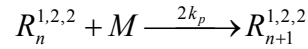
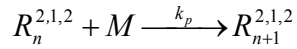
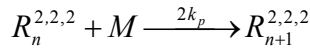
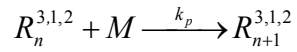
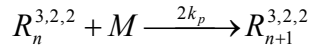
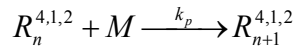
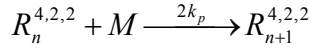
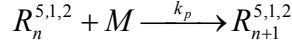


4. PRIMARY RADICAL FORMATION

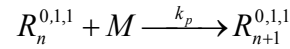
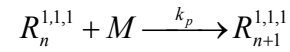
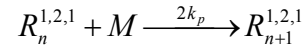
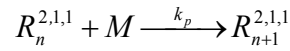
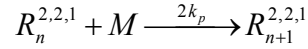
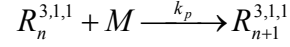


5. PROPAGATION

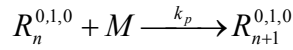
two cores



one core



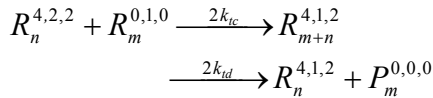
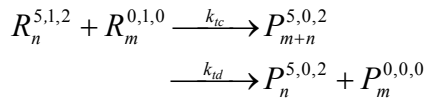
0 cores



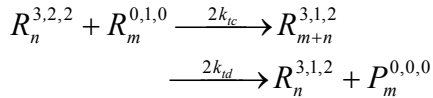
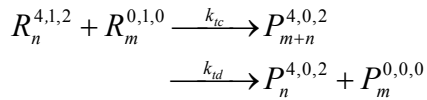
6. TERMINATION

a) Intermolecular

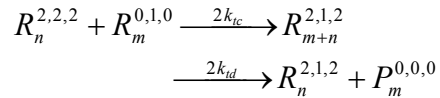
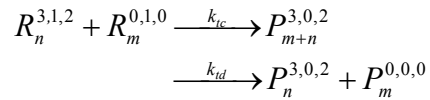
two cores, $u + a = 6$



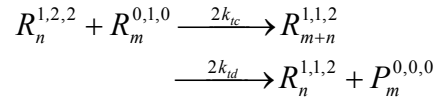
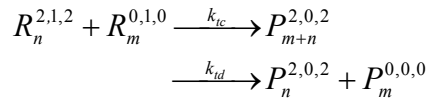
two cores, $u + a = 5$



two cores, $u + a = 4$



two cores, $u + a = 3$



two cores, $u + a = 2$

$$\begin{aligned} R_n^{1,1,2} + R_m^{0,1,0} &\xrightarrow{k_{tc}} P_{m+n}^{1,0,2} \\ &\xrightarrow{k_{td}} P_n^{1,0,2} + P_m^{0,0,0} \\ R_n^{0,2,2} + R_m^{0,1,0} &\xrightarrow{2k_{tc}} R_{m+n}^{0,1,2} \\ &\xrightarrow{2k_{td}} R_n^{0,1,2} + P_m^{0,0,0} \end{aligned}$$

two cores, $u + a = 1$

$$\begin{aligned} R_n^{0,1,2} + R_m^{0,1,0} &\xrightarrow{k_{tc}} P_{m+n}^{0,0,2} \\ &\xrightarrow{k_{td}} P_n^{0,0,2} + P_m^{0,0,0} \end{aligned}$$

one core, $u + a = 4$

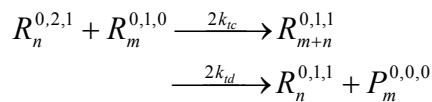
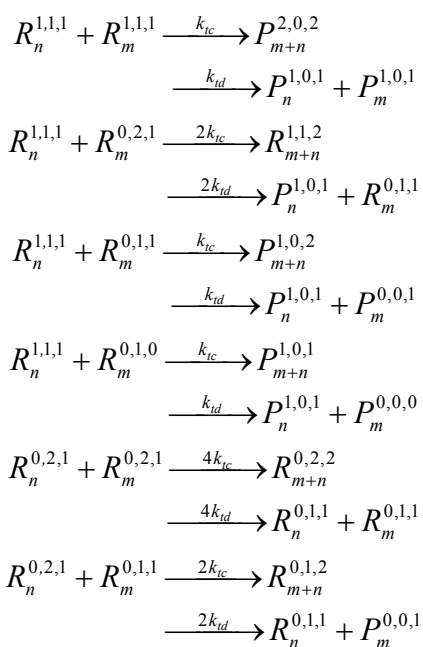
$$\begin{aligned} R_n^{3,1,1} + R_m^{3,1,1} &\xrightarrow{k_{tc}} P_{m+n}^{6,0,2} \\ &\xrightarrow{k_{td}} P_n^{3,0,1} + P_m^{3,0,1} \\ R_n^{3,1,1} + R_m^{2,2,1} &\xrightarrow{2k_{tc}} R_{m+n}^{5,1,2} \\ &\xrightarrow{2k_{td}} P_n^{3,0,1} + R_m^{2,1,1} \\ R_n^{3,1,1} + R_m^{2,1,1} &\xrightarrow{k_{tc}} P_{m+n}^{5,0,2} \\ &\xrightarrow{k_{td}} P_n^{3,0,1} + P_m^{2,0,1} \\ R_n^{3,1,1} + R_m^{1,2,1} &\xrightarrow{2k_{tc}} R_{m+n}^{4,1,2} \\ &\xrightarrow{2k_{td}} P_n^{3,0,1} + R_m^{1,1,1} \\ R_n^{3,1,1} + R_m^{1,1,1} &\xrightarrow{k_{tc}} P_{m+n}^{4,0,2} \\ &\xrightarrow{k_{td}} P_n^{3,0,1} + P_m^{1,0,1} \\ R_n^{3,1,1} + R_m^{0,2,1} &\xrightarrow{2k_{tc}} R_{m+n}^{3,1,2} \\ &\xrightarrow{2k_{td}} P_n^{3,0,1} + R_m^{0,1,1} \\ R_n^{3,1,1} + R_m^{0,1,1} &\xrightarrow{k_{tc}} P_{m+n}^{3,0,2} \\ &\xrightarrow{k_{td}} P_n^{3,0,1} + P_m^{0,0,1} \\ R_n^{3,1,1} + R_m^{0,1,0} &\xrightarrow{k_{tc}} P_{m+n}^{3,0,1} \\ &\xrightarrow{k_{td}} P_n^{3,0,1} + P_m^{0,0,0} \\ R_n^{2,2,1} + R_m^{2,2,1} &\xrightarrow{4k_{tc}} R_{m+n}^{4,2,2} \\ &\xrightarrow{4k_{td}} R_n^{2,1,1} + R_m^{2,1,1} \\ R_n^{2,2,1} + R_m^{2,1,1} &\xrightarrow{2k_{tc}} R_{m+n}^{4,1,2} \\ &\xrightarrow{2k_{td}} R_n^{2,1,1} + P_m^{2,0,1} \\ R_n^{2,2,1} + R_m^{1,2,1} &\xrightarrow{4k_{tc}} R_{m+n}^{3,2,2} \\ &\xrightarrow{4k_{td}} R_n^{2,1,1} + R_m^{1,1,1} \end{aligned}$$

$$\begin{aligned} R_n^{2,2,1} + R_m^{1,1,1} &\xrightarrow{2k_{tc}} R_{m+n}^{3,1,2} \\ &\xrightarrow{2k_{td}} R_n^{2,1,1} + P_m^{1,0,1} \\ R_n^{2,2,1} + R_m^{0,2,1} &\xrightarrow{4k_{tc}} R_{m+n}^{2,2,2} \\ &\xrightarrow{4k_{td}} R_n^{2,1,1} + R_m^{0,1,1} \\ R_n^{2,2,1} + R_m^{0,1,1} &\xrightarrow{2k_{tc}} R_{m+n}^{2,1,2} \\ &\xrightarrow{2k_{td}} R_n^{2,1,1} + P_m^{0,0,1} \\ R_n^{2,2,1} + R_m^{0,1,0} &\xrightarrow{2k_{tc}} R_{m+n}^{2,1,1} \\ &\xrightarrow{2k_{td}} R_n^{2,1,1} + P_m^{0,0,0} \end{aligned}$$

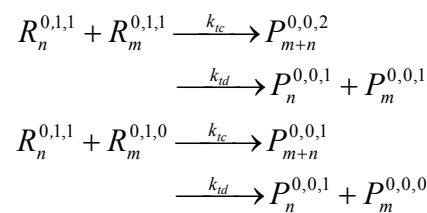
one core, $u + a = 3$

$$\begin{aligned} R_n^{2,1,1} + R_m^{2,1,1} &\xrightarrow{k_{tc}} P_{m+n}^{4,0,2} \\ &\xrightarrow{k_{td}} P_n^{2,0,1} + P_m^{2,0,1} \\ R_n^{2,1,1} + R_m^{1,2,1} &\xrightarrow{2k_{tc}} R_{m+n}^{3,1,2} \\ &\xrightarrow{2k_{td}} P_n^{2,0,1} + R_m^{1,1,1} \\ R_n^{2,1,1} + R_m^{1,1,1} &\xrightarrow{k_{tc}} P_{m+n}^{3,0,2} \\ &\xrightarrow{k_{td}} P_n^{2,0,1} + P_m^{1,0,1} \\ R_n^{2,1,1} + R_m^{0,2,1} &\xrightarrow{2k_{tc}} R_{m+n}^{2,1,2} \\ &\xrightarrow{2k_{td}} P_n^{2,0,1} + R_m^{0,1,1} \\ R_n^{2,1,1} + R_m^{0,1,1} &\xrightarrow{k_{tc}} P_{m+n}^{2,0,2} \\ &\xrightarrow{k_{td}} P_n^{2,0,1} + P_m^{0,0,1} \\ R_n^{2,1,1} + R_m^{0,1,0} &\xrightarrow{k_{tc}} P_{m+n}^{2,0,1} \\ &\xrightarrow{k_{td}} P_n^{2,0,1} + P_m^{0,0,0} \\ R_n^{1,2,1} + R_m^{1,2,1} &\xrightarrow{4k_{tc}} R_{m+n}^{2,2,2} \\ &\xrightarrow{4k_{td}} R_n^{1,1,1} + R_m^{1,1,1} \\ R_n^{1,2,1} + R_m^{1,1,1} &\xrightarrow{2k_{tc}} R_{m+n}^{2,1,2} \\ &\xrightarrow{2k_{td}} R_n^{1,1,1} + P_m^{1,0,1} \\ R_n^{1,2,1} + R_m^{0,2,1} &\xrightarrow{4k_{tc}} R_{m+n}^{1,2,2} \\ &\xrightarrow{4k_{td}} R_n^{1,1,1} + R_m^{0,1,1} \\ R_n^{1,2,1} + R_m^{0,1,1} &\xrightarrow{2k_{tc}} R_{m+n}^{1,1,2} \\ &\xrightarrow{2k_{td}} R_n^{1,1,1} + P_m^{0,0,1} \\ R_n^{1,2,1} + R_m^{0,1,0} &\xrightarrow{2k_{tc}} R_{m+n}^{1,1,1} \\ &\xrightarrow{2k_{td}} R_n^{1,1,1} + P_m^{0,0,0} \end{aligned}$$

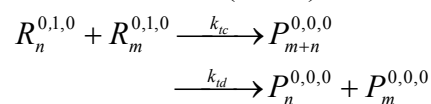
one core, $u + a = 2$



one core, $u + a = 1$

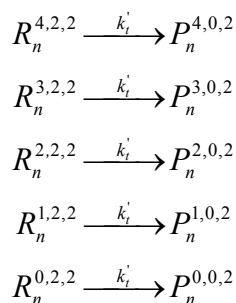


0 cores (linear)

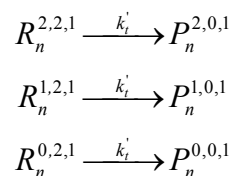


b) Intramolecular

two cores



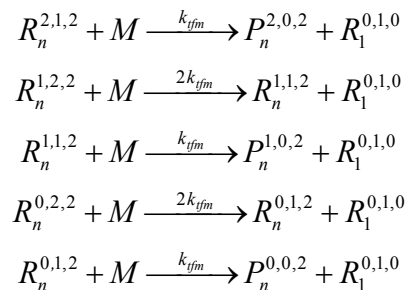
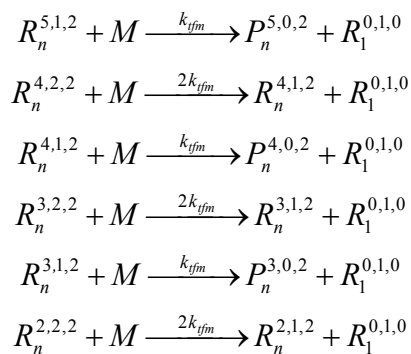
one core

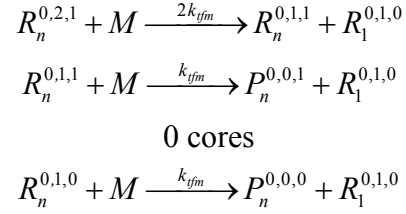
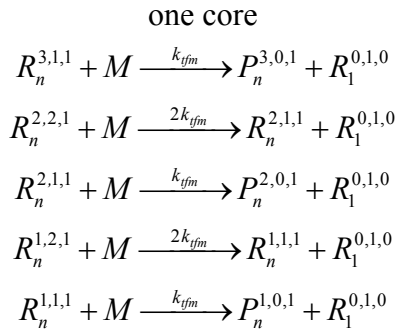


7. TRANSFER REACTIONS

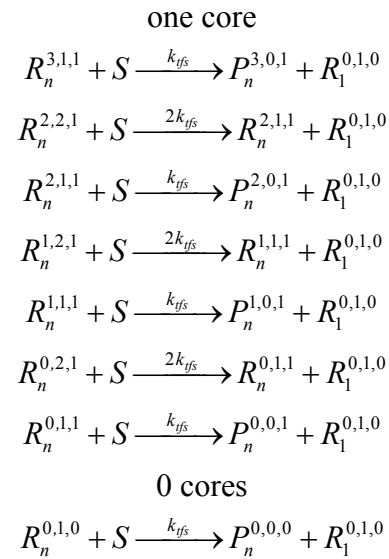
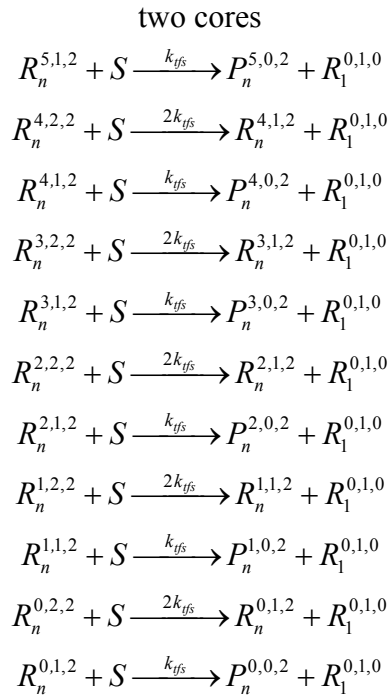
a) To monomer

two cores





b) To Solvent



Note that in the above mechanism a factor of u multiplies the decomposition rate constant to account for the increased possibility of a functional site decomposing. Similarly, a factor of a 2 or 4 is used for those reactions involving one or two di-radicals.

8.2.2 Mathematical Modelling

Modelling of the proposed polymerization mechanism was completed by performing mole balances on each species and using the method of moments. The derived equations were compared to a similar model developed specifically for the polymerization of styrene with a tetrafunctional initiator in a CSTR (20). The model presented herein was

found to reduce to the CSTR model following a few modifications (e.g., neglecting di-radicals, termination by disproportionation and intramolecular termination; and the addition of flow terms). Due to the large number of species, the formulation of population balances and the derivation of the respective moment equations are too lengthy to present here (see Appendix C). However, a discussion of the equations used in the determination of rate constants is presented.

The temperature dependency of the chemically-controlled rate constants are given by Arrhenius equations. As the polymerization progresses and conversion increases, the properties of the reaction medium change. With increasing polymer concentration, the properties of the medium change and certain reactions become diffusion controlled. A semi-empirical free volume theory is used to describe the diffusion-controlled regime (6, 13). The free volume of monomer, polymer and solvent are determined by the following equations:

$$V_{fm} = (0.025 + \alpha_m (T - T_{gm})) \frac{V_m}{V} \quad 8.1$$

$$V_{fp} = (0.025 + \alpha_p (T - T_{gp})) \frac{V_p}{V} \quad 8.2$$

$$V_{fs} = (0.025 + \alpha_s (T - T_{gs})) \frac{V_s}{V} \quad 8.3$$

where the subscripts of m , p and s refer to monomer, polymer and solvent; V is the total volume of the reaction medium; α is the free volume expansion coefficient; and T_g is the glass transition temperature. The free volume of each species changes throughout an isothermal reaction due to changes in their individual volumes (V_m , V_p , and V_s) and in turn, the total volume. A critical value for the onset of the diffusion-controlled regime is defined as K_{cr} :

$$K_{cr} = A_{cr} \exp\left(\frac{E_{cr}}{RT}\right) \quad 8.4$$

For each increment in the solution of the population and moment equations, a parameter, K , is calculated and compared to K_{cr} .

$$K = M_w^m \exp\left(\frac{A}{V_f}\right) \quad 8.5$$

where M_w is the weight-average molecular weight; V_f is the total free volume ($V_f = V_m + V_p + V_s$); and m and A are parameters dependent upon monomer type. As the reaction progresses, molecular weight will increase while the free volume will decrease. While K is less than K_{cr} , the termination rate constant is dominated by segmental diffusion. With increasing polymerization concentration, the reaction medium becomes a poorer solvent for the polymer. The coil size of propagating radical chains decreases and effectively, there is a higher concentration gradient across the coil. The segmental diffusion of the radical site out of the coil increases and in turn, produces an increase in the termination rate constant shown by the following:

$$k_t = k_{t0} (1 + \delta_c c_p \text{MW}) \quad 8.6$$

where k_{t0} is the chemically-controlled termination rate constant, δ_c is a segmental diffusion parameter, c_p is the polymer concentration and MW is the molecular weight of the monomer.

The increase in the termination rate constant is not seen throughout the entire reaction, however. With higher polymer concentrations, the reaction medium becomes more viscous and the mobility of radical chains decreases. This phenomena manifests itself as a sudden increase in conversion known as the “gel” or Trommsdorf-Smith-Norrish effect. In the kinetic model, the onset of this region is defined when K becomes equal to K_{cr} . At this point in the reaction, V_f and M_w are taken as being their critical values and the termination rate constant decreases accordingly:

$$k_t = k_{to} \left(\frac{M_{w_{cr}}}{M_w} \right)^n \exp \left(-A \left(\frac{1}{V_f} - \frac{1}{V_{f_{cr}}} \right) \right) \quad 8.7$$

where n and A are adjustable parameters. The propagation rate constant is similarly affected by a diffusion-controlled process and will start to decrease when the free volume is below some critical value of the monomer, $V_{f_{crM}}$.

$$k_p = k_{po} \exp \left(-B \left(\frac{1}{V_f} - \frac{1}{V_{f_{crM}}} \right) \right) \quad \text{for } V_f < V_{f_{crM}} \quad 8.8$$

k_{po} is the chemically-controlled propagation rate constant and B is a monomer specific parameter. Towards the end of the reaction, even the efficiency is no longer constant. At higher conversions, the efficiency begins to drop as initiator radicals are increasingly hindered from moving out of their cage due to the growing presence of larger molecules. The efficiency is expected to decrease dramatically when a critical free volume for the particular initiator is reached, $V_{f_{crEff}}$.

$$f = f_o \exp \left(-C \left(\frac{1}{V_f} - \frac{1}{V_{f_{crEff}}} \right) \right) \quad \text{for } V_f < V_{f_{crEff}} \quad 8.9$$

where f_o is the initial initiator efficiency and C is a constant.

8.3 Modelling Results

8.3.1 Determination of Model Parameters

Parameters used in the modelling of the polymerization of styrene and MMA were taken from Gao and Penlidis (13) and are listed in Table 8.1. Parameters related to the monofunctional initiator TBEC were also taken from Gao and Penlidis (13) and are listed in Table 8.2. The decomposition parameters for JWEB50 were obtained from

ATOFINA. Because previous experimental work had shown that the functional groups of the tetrafunctional initiator were decomposing and behaving similar to the sites of TBEC, the initiator efficiency for JWEB50 was taken to be the same as the value for TBEC (21-23).

From all of the constants used in the above equations, it was initially decided that only those associated with the initiator should be used in fitting the experimental data. These parameters include the critical free volume at which the efficiency becomes diffusion-controlled ($V_{f_{crEff}}$) and the strength of its decay in this region (C). It has been found that the parameter A is dependent upon initiator type and concentration and as such, was also estimated (6). Ordinary differential equations for the monofunctional and tetrafunctional models were solved using an Adams-Bashforth-Moulton solver in MATLAB. Parameter estimates were determined by fitting the model to the conversion data of one experiment. The remaining experiments were used in the model and parameter estimates validation. Nonlinear regression was performed where the sum of squares of errors was minimized using a trust-region method. The final results are reported in Table 8.3.

The parameter estimates of A determined in this work for the monofunctional initiator, TBEC, are similar to those used in the work of Gao and Penlidis ($A_{\text{styrene}} = 0.35$, $A_{\text{MMA}} = 1.1$) (13). Initially, the tetrafunctional model could not adequately predict the experimental conversion data, regardless of the chosen value of A . It was found that only by changing the parameter n (see Equation 8.7) to 0.5 could the model simulate the conversion versus time profiles satisfactory and in turn, allow the other parameters to be estimated. The effect of reducing n was to produce larger values of A for the tetrafunctional model.

Table 8.1. Database entries for styrene, methyl methacrylate and their polymers.

Entry	Styrene	MMA	Units
MW	104.12	100.12	g/mol
Monomer ρ	$0.924 - 0.000918 T$	$0.966471 - 0.001164 T$	kg/L, T in °C
Polymer ρ	$1.08 - 0.000605 T$	$1.19504 - 0.00033 T$	kg/L, T in °C
Monomer T_g	185	167	K
Polymer T_g	378	383	K
α_m	0.001	0.001	K ⁻¹
α_p	0.00048	0.00048	K ⁻¹
k_{po}	$1.302 \times 10^9 \exp\left(\frac{-7759}{RT}\right)$	$2.952 \times 10^7 \exp\left(\frac{-4353}{RT}\right)$	L/(mol·min)
k_{to}	$4.92 \times 10^{11} \exp\left(\frac{-3470}{RT}\right)$	$5.88 \times 10^9 \exp\left(\frac{-701}{RT}\right)$	L/(mol·min)
k ratio	0	$1.60926 \exp\left(\frac{-440}{RT}\right)$	
k_{ifm}	$5.14 \times 10^9 \exp\left(\frac{-15230}{RT}\right)$	$2.41 \times 10^9 \exp\left(\frac{-15541}{RT}\right)$	L/(mol·min)
k_{th}	$1.35 \times 10^7 \exp\left(\frac{-27450}{RT}\right)$	0	L/(mol·min)
K_{cr}	$9.44 \exp\left(\frac{3833}{RT}\right)$	$0.563 \exp\left(\frac{8900}{RT}\right)$	
$V_{f_{crM}}$	$0.3110 \exp\left(\frac{-1670}{RT}\right)$	$0.2709 \exp\left(\frac{-1590}{RT}\right)$	
δ_c	0.001	0.001	L/g
m	0.5	0.5	
n	1.75	1.75	
B	1	1	

Note: All activation energies in cal/mol. k ratio is the fraction of radical chains that terminate by disproportionation.

Examining the variables associated with the initiator efficiency, there appears to be little difference between TBEC and JWEB50. The monofunctional initiator has a somewhat lower critical free volume for the onset of a diffusion-controlled efficiency than the tetrafunctional initiator. It is quite difficult to state whether there are any real differences between $V_{f_{crE_{eff}}}$ of the two initiators. Both $V_{f_{crE_{eff}}}$ and C influence the shape of the conversion-time profile where the curve shifts from the autoacceleration region to the reaction's limiting conversion. The parameter estimates are sensitive to experimental error that changes the shape of this transition region and to which set of reaction data the model is being fit to.

The tetrafunctional model was found to be extremely insensitive to the rate constant for the termination by combination of two radical chains attached the same core (k_t'). Values ranging from 0 to 10^{20} made no noticeable difference in conversion or molecular weight results. Compared to the total termination constant for styrene and MMA at 100°C (4.6×10^9 and 2.3×10^9), the maximum of the test range for k_t' is nearly 11 orders of magnitude larger. It is unlikely that k_t' exceeds k_{to} by such an amount; however, a wide range was used in the sensitivity analysis to ensure that k_t' could be assumed to be zero. The reason for the model's insensitivity to k_t' is discussed further in the section on the validity of the model assumptions (see Section 8.3.3).

Table 8.2. Database entries for TBEC and JWEB50.

Entry	TBEC	JWEB50	Units
Functionality	1	4	
MW	246	965	g/mol
k_d	$3.389 \times 10^{15} \exp\left(\frac{-31500}{RT}\right)$	$1.494 \times 10^{17} \exp\left(\frac{-34300}{RT}\right)$	1/(min)
f_o	0.7	0.7	

Note: k_d data for JWEB50 obtained from ATOFINA; activation energy in cal/mol.

Table 8.3. Estimated parameters for monofunctional and tetrafunctional models.

Parameter	TBEC		JWEB50 ¹	
	Styrene	MMA	Styrene	MMA
A	0.42	1.1	0.58	1.8
$V_{f_{crEff}}$	0.069		0.084	
C	0.42		0.41	

Note: ¹ $n = 0.5$ was used in the tetrafunctional model (see Equation 8.7).

8.3.2 Validation of Model

Figure 8.2 compares the model predictions of the monofunctional initiator to experimental data for the bulk polymerization of styrene. The reactions at 110°C were completed during the course of this study while those at 100 and 90°C were obtained from the work of Fityani-Trimmi (24). The corresponding number- and weight-average molecular weight data are presented in Figures 8.3 and 8.4. The conversion and molecular weight results from the model agree well with the experimental data. The one exception appears to be for the molecular weight results at 90°C and 14 mmol/L of TBEC. The full conversion molecular weight averages from the model predictions and experimental data are quite similar; however, the model overpredicts the molecular weight data during most of the course of the reaction. Because the model successfully simulates the experimental data for all of the other reactions, it would suggest that the discrepancy, in this case, can be attributed to errors in the collected data. Conversion and molecular weight modelling results for polymerization of styrene initiated with the tetrafunctional initiator are compared to experimental data in Figures 8.5 and 8.6. The model predictions agree quite well with the collected data.

A similar comparison has been made with the monofunctional and tetrafunctional initiator in the bulk polymerization of methyl methacrylate at temperatures of 110 and 100°C. All MMA experimental data were taken from this study. Conversion versus time profiles are shown in Figure 8.7 while the molecular weight results are presented in Figures 8.8 and 8.9 for the polymerization of MMA initiated with TBEC. The

monofunctional model shows excellent agreement with the experimental data. Model predictions of conversion and experimental data for the tetrafunctional initiator are plotted in Figure 8.10. The corresponding number- and weight-average molecular weight results are shown in Figures 8.11. Modelling results show that the tetrafunctional model can accurately predict the behaviour of JWEB50 in the polymerization of MMA.

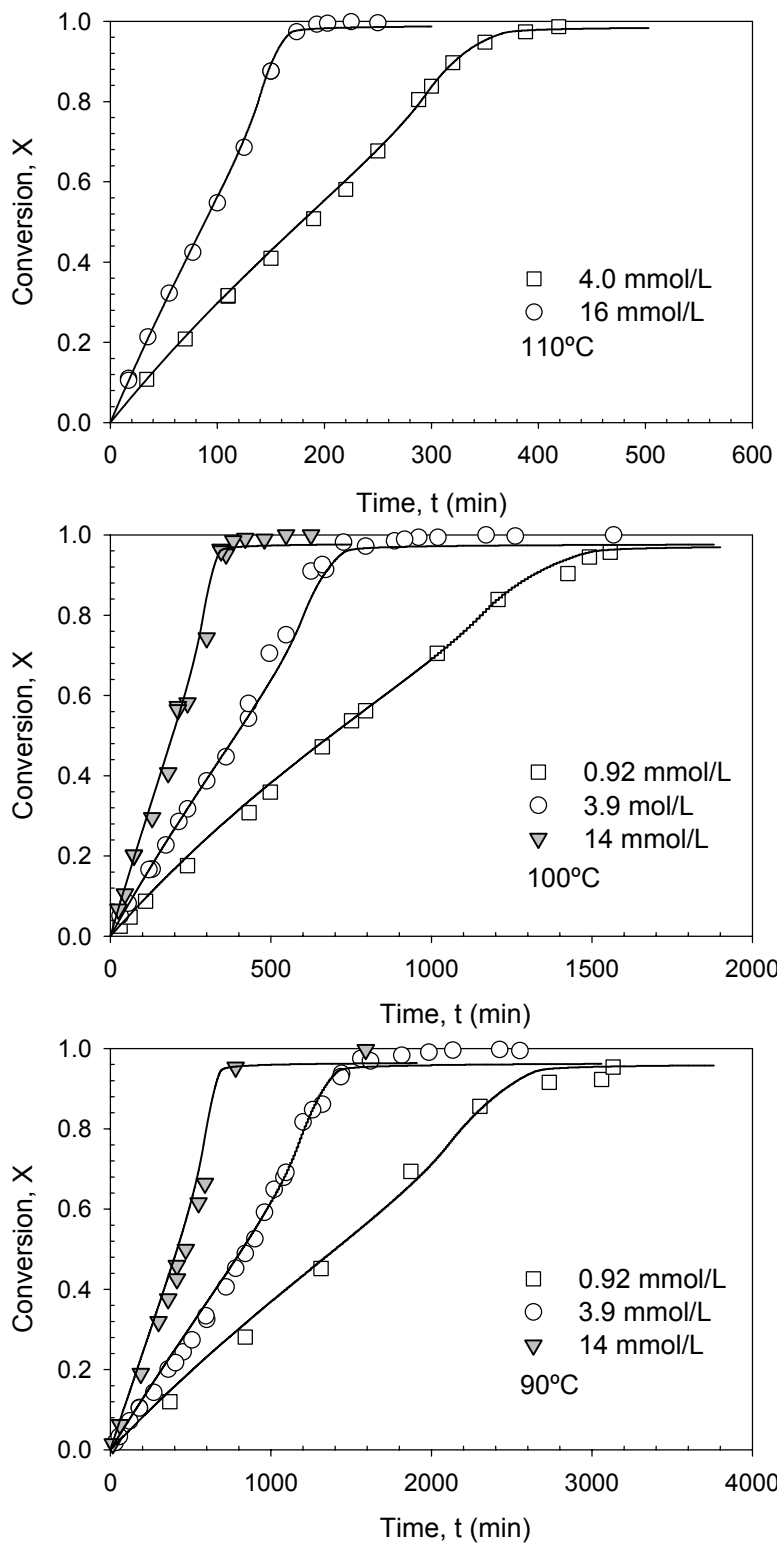


Figure 8.2. Conversion as a function of time for the bulk polymerization of styrene initiated with TBEC at varying concentrations and reaction temperatures.

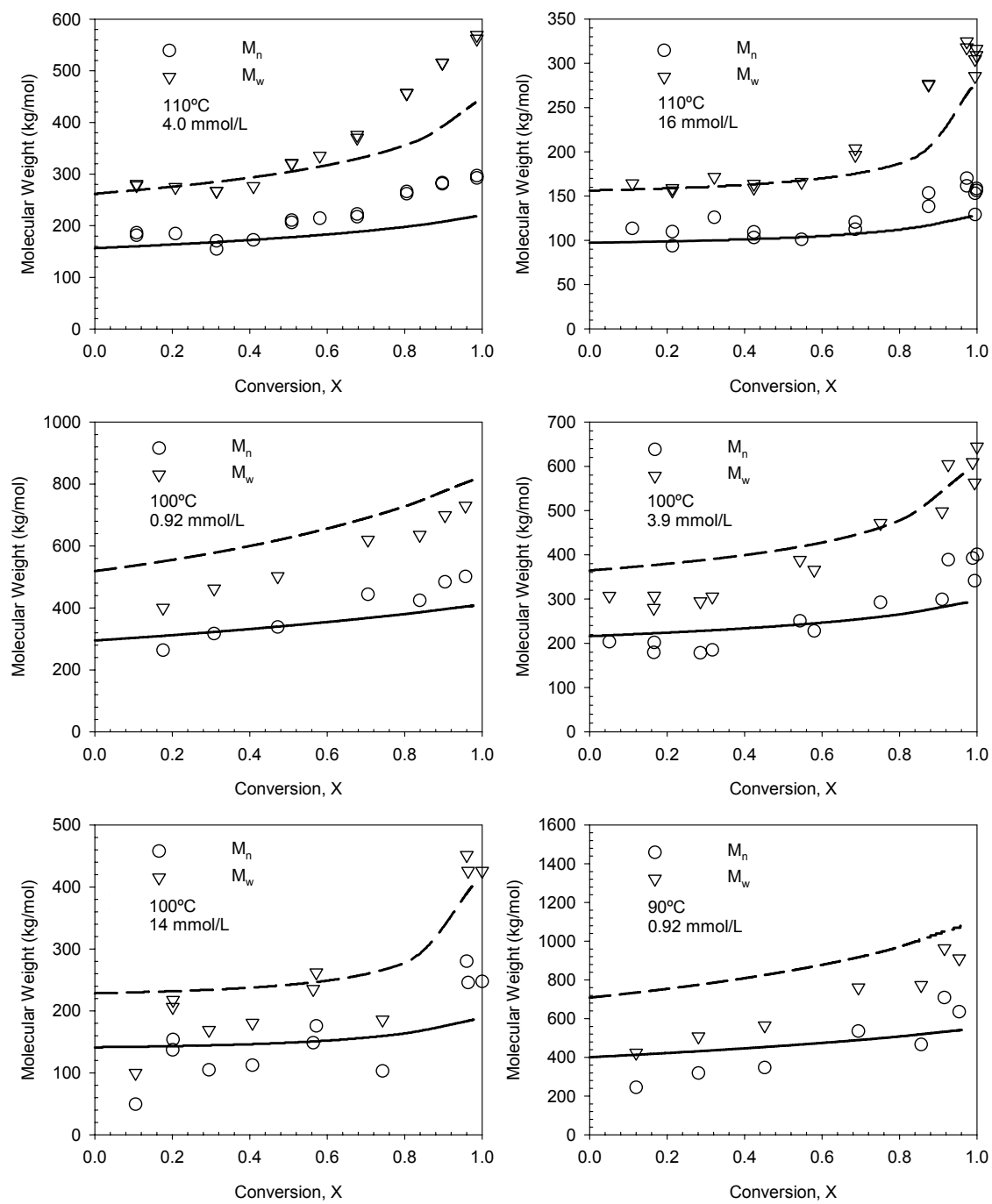


Figure 8.3. Molecular weight as a function of conversion for the bulk polymerization of styrene initiated with TEBC at varying concentrations and reaction temperatures.

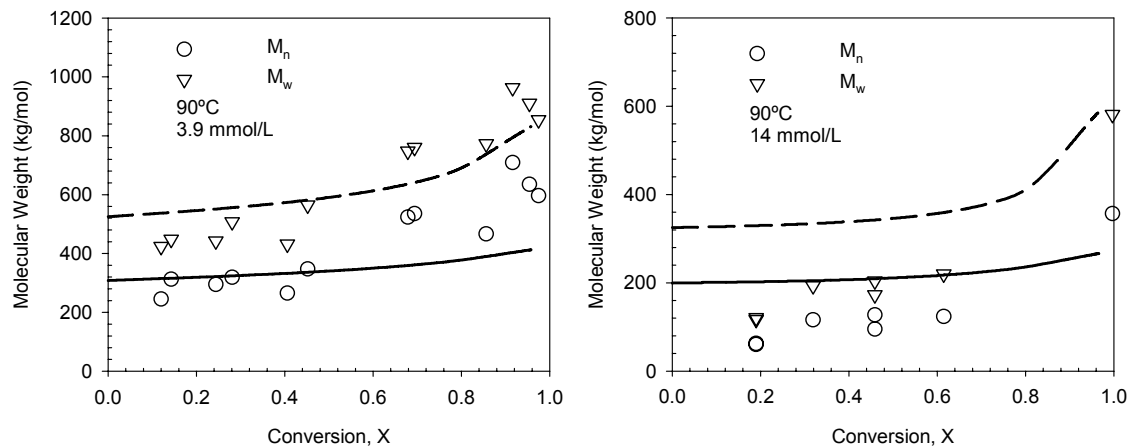


Figure 8.4. Molecular weight as a function of conversion for the bulk polymerization of styrene initiated with TEBC at varying concentrations and reaction temperatures (Figure 8.3 continued).

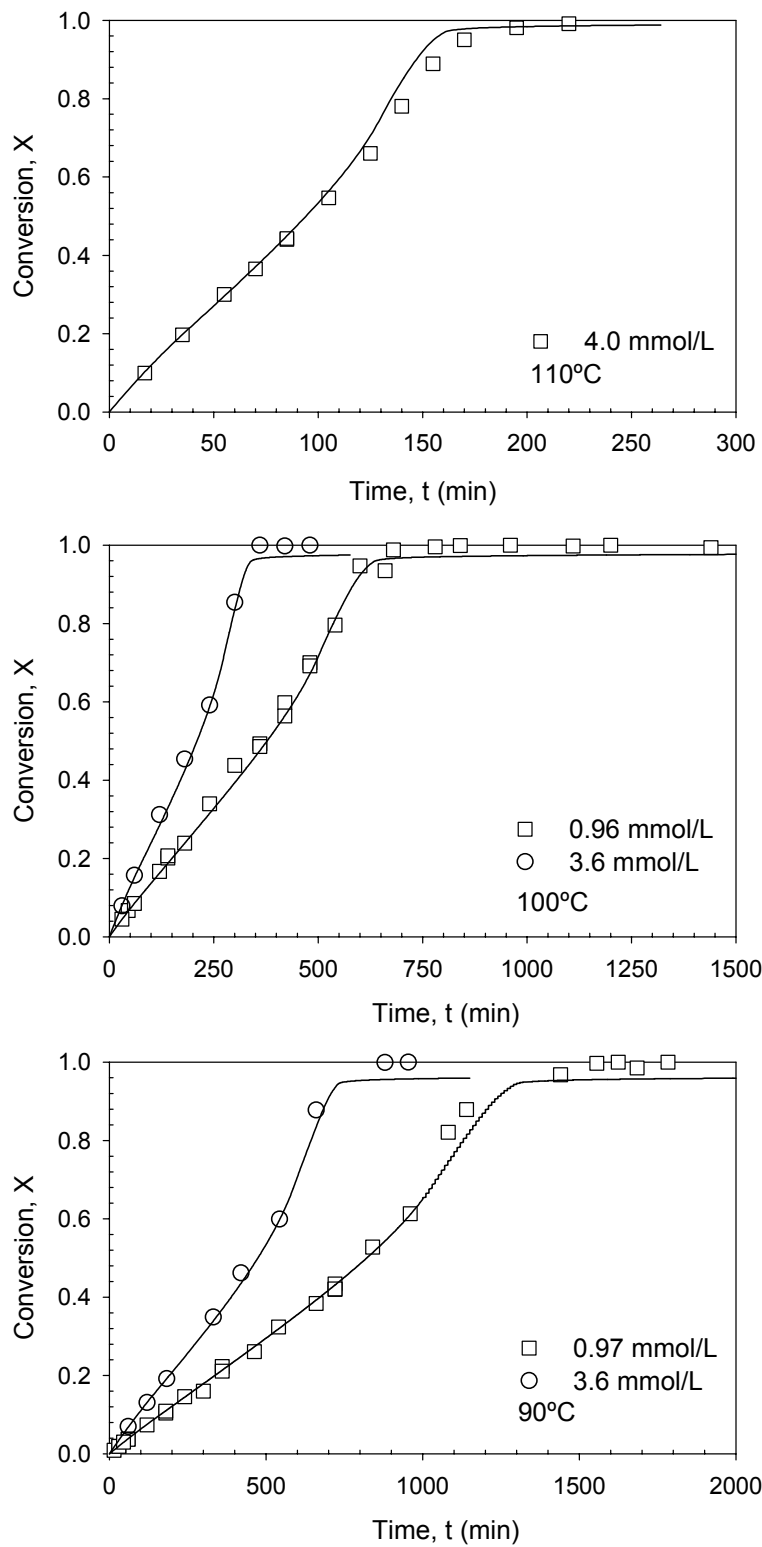


Figure 8.5. Conversion as a function of time for the bulk polymerization of styrene initiated with JWEB50 at varying concentrations and reaction temperatures.

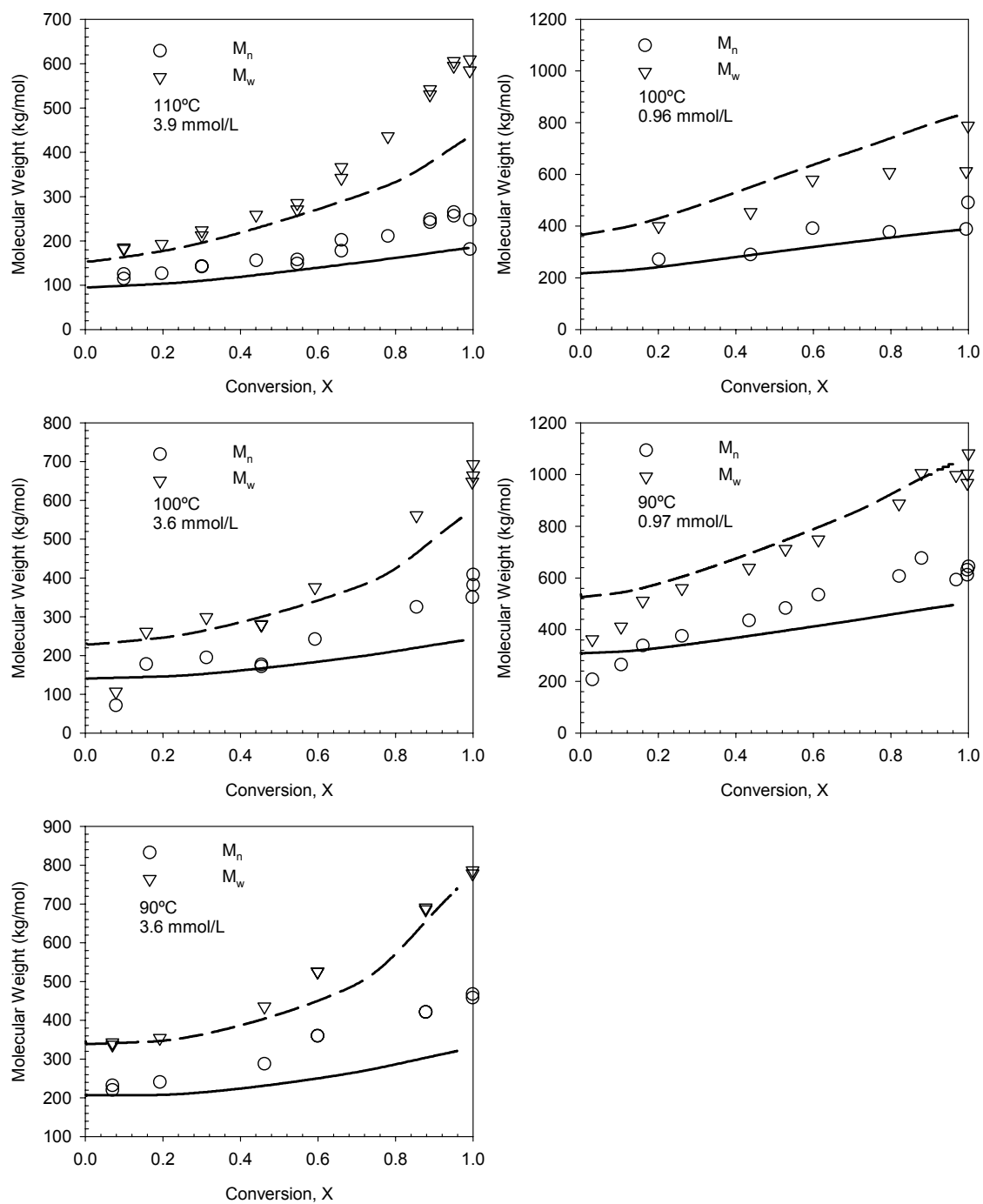


Figure 8.6. Molecular weight as a function of conversion for the bulk polymerization of styrene initiated with JWEB50 at varying concentrations and reaction temperatures.

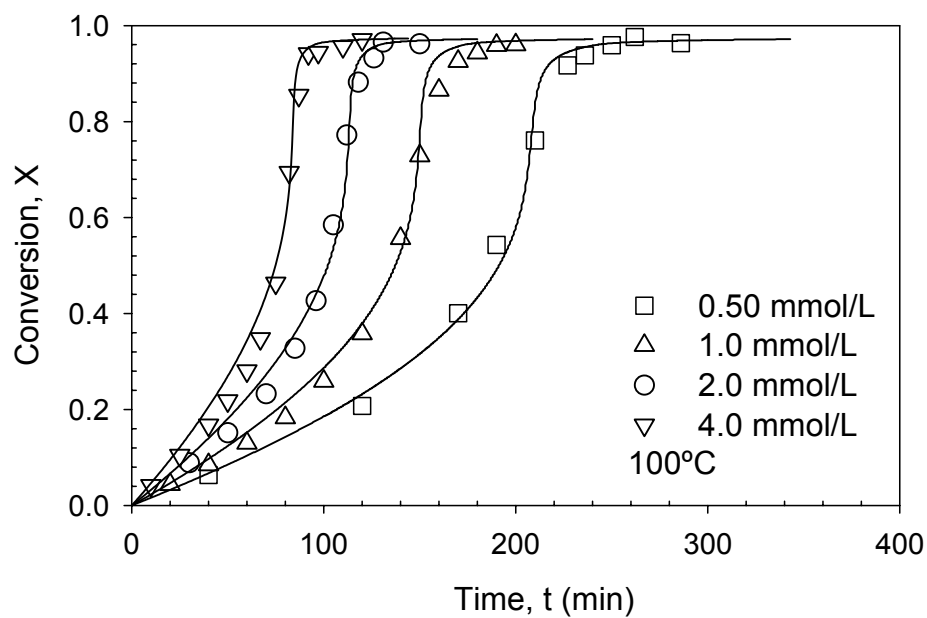
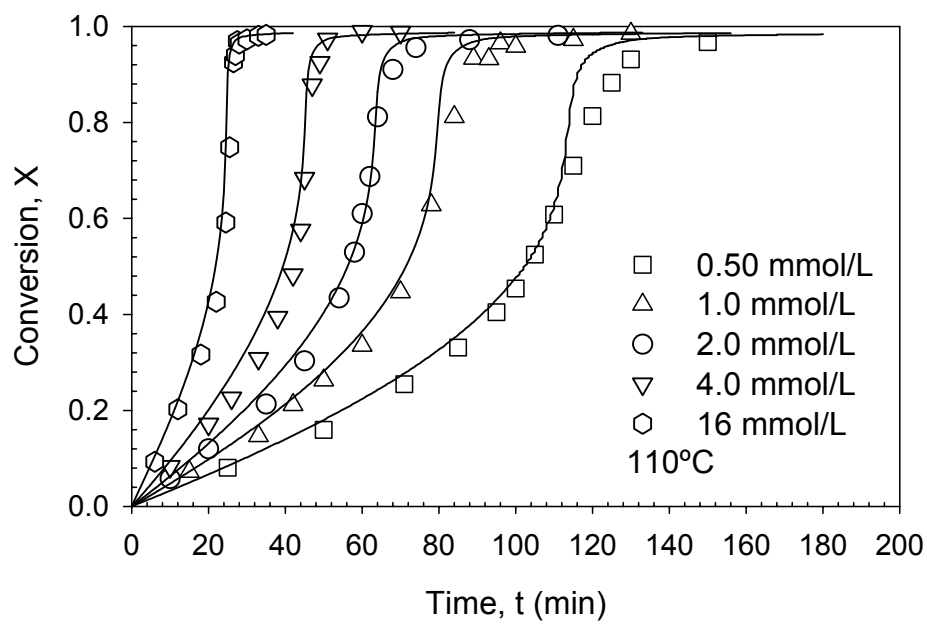


Figure 8.7. Conversion as a function of time for the bulk polymerization of MMA initiated with TBEC at varying concentrations and reaction temperatures.

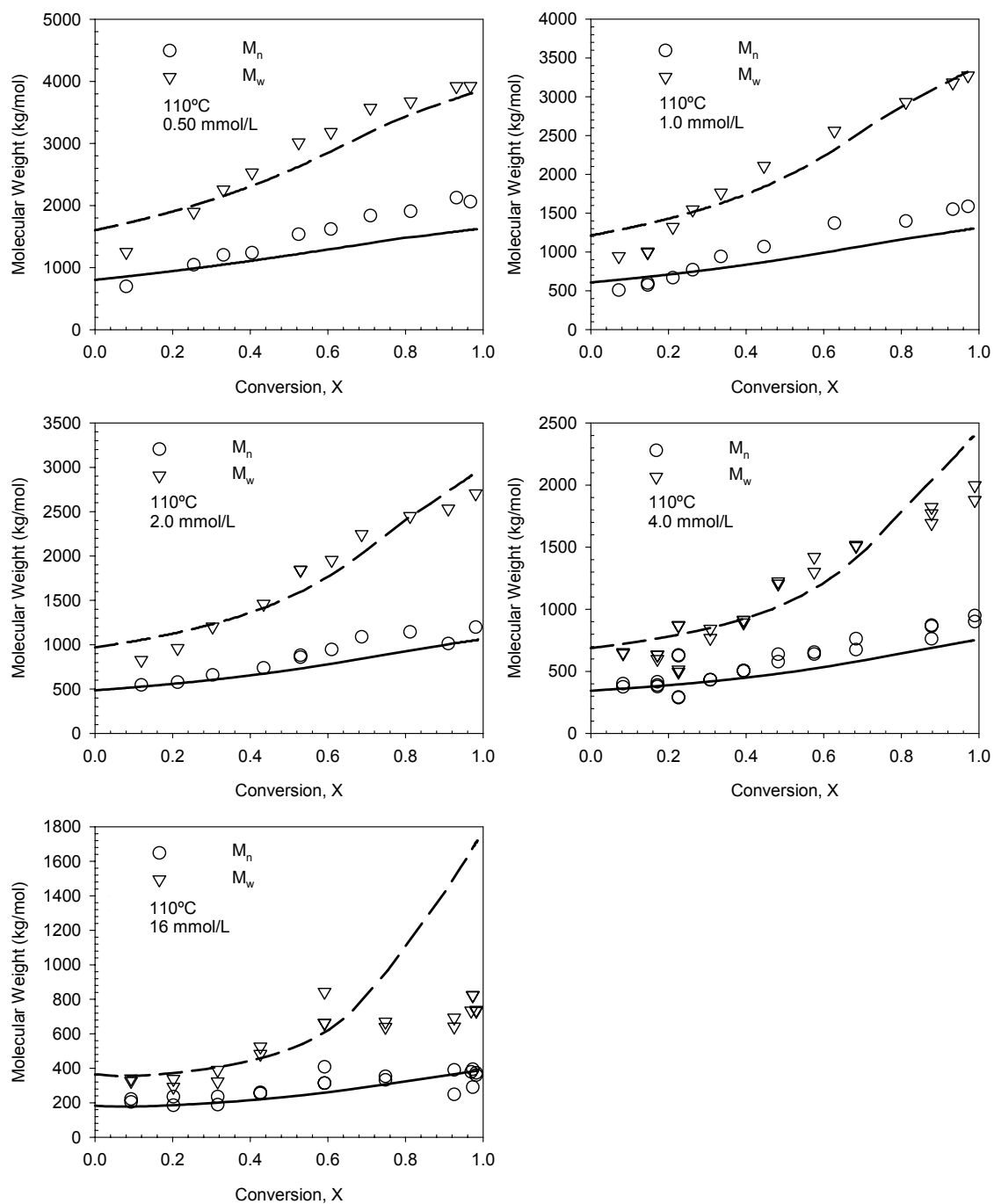


Figure 8.8. Molecular weight as a function of conversion for the bulk polymerization of MMA initiated with TBEC at varying concentrations and 110°C.

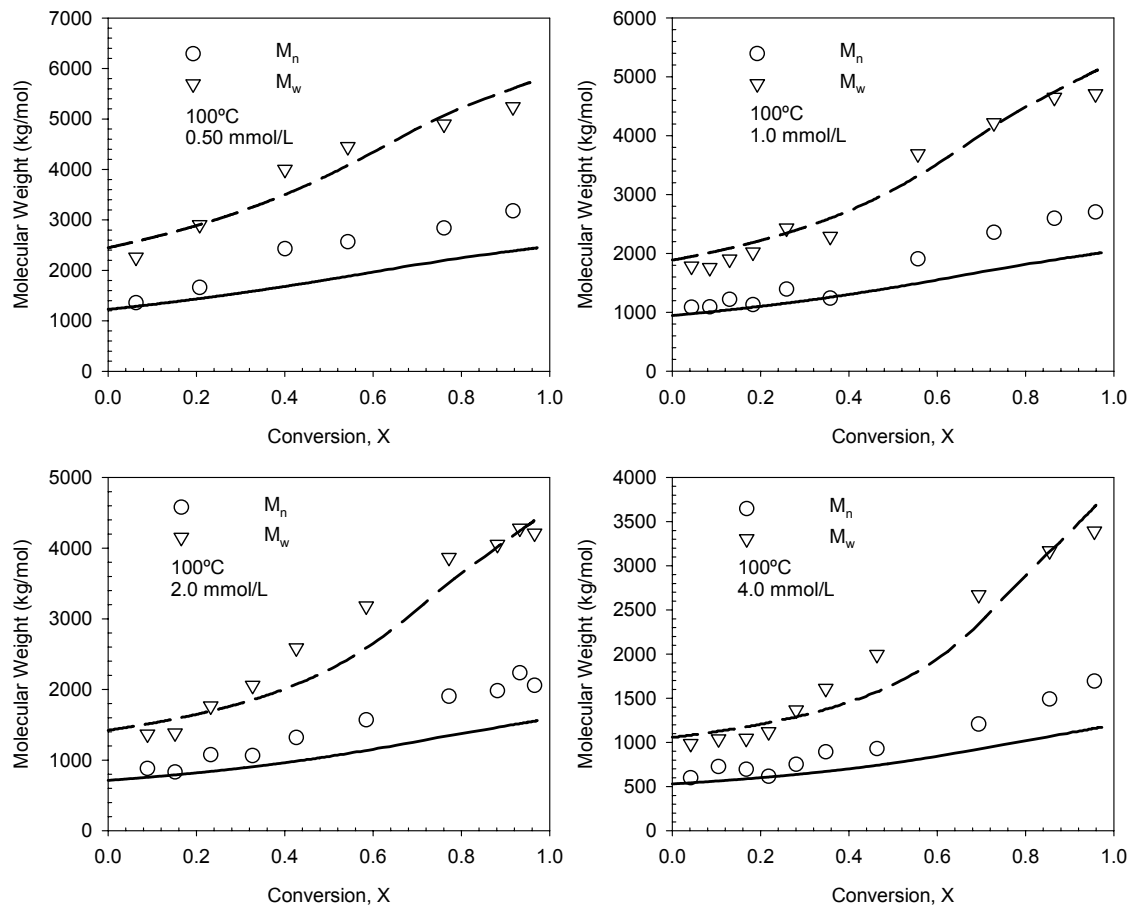


Figure 8.9. Molecular weight as a function of conversion for the bulk polymerization of MMA initiated with TBEC at varying concentrations and 100°C.

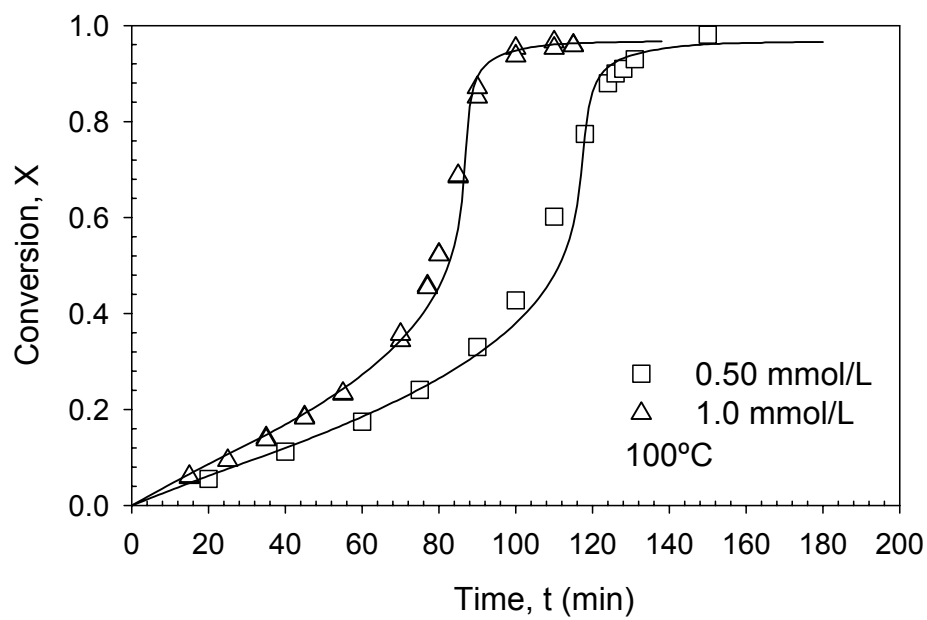
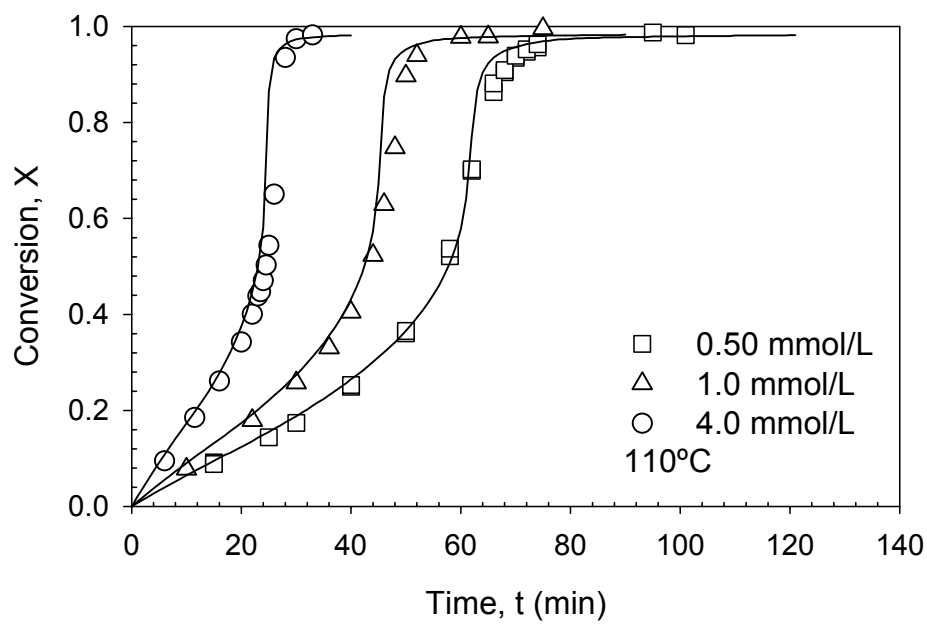


Figure 8.10. Conversion as a function of time for the bulk polymerization of MMA initiated with JWEB50 at varying concentrations and reaction temperatures.

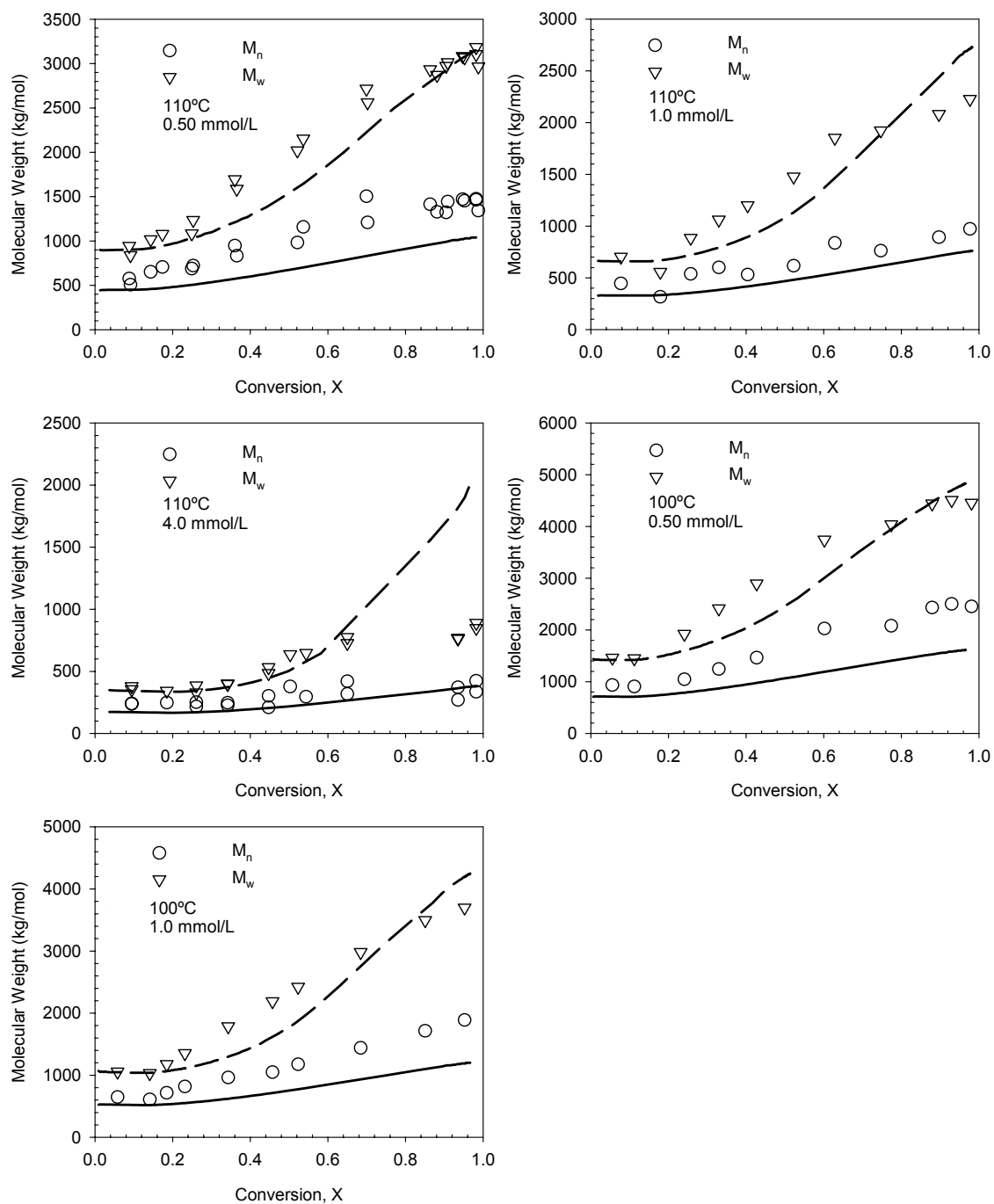


Figure 8.11. Molecular weight as a function of conversion for the bulk polymerization of MMA initiated with JWEB50 at varying concentrations and reaction temperatures.

8.3.3 Validation of Model Assumptions

The development of the tetrafunctional model made several assumptions with two of the major statements assuming that certain polymer species could be neglected. The first assumption states that there can be no more than two active radical sites per molecule while the second condition assumes that a species can have at most 6 undecomposed functional sites. The validity of these assumptions can be assessed by comparing the concentration of each species and examining their contribution to the polymerization.

Figure 8.12 is a plot of radical concentration versus time for the bulk polymerization of styrene. The solid curve represents the model predictions for the concentrations of all mono-radicals including linear, star (1 core) and coupled star (2 cores) chains while the dashed curve is the total di-radical concentration. Apart from differences in their shape, the major distinction between trends is that di-radical concentrations are 5 orders of magnitude smaller than mono-radical concentrations. Chains with a higher number of active sites such as tri- and tetra-radicals will be even less numerous. These results verify that neglecting tri- and tetra-radicals is a valid assumption and would suggest that even di-radicals could be ignored. These results help to explain the model's insensitivity to k_t' . With such relatively low concentrations, di-radicals are not a significant species in the modelling of multifunctional initiators and therefore, neither are their corresponding reactions.

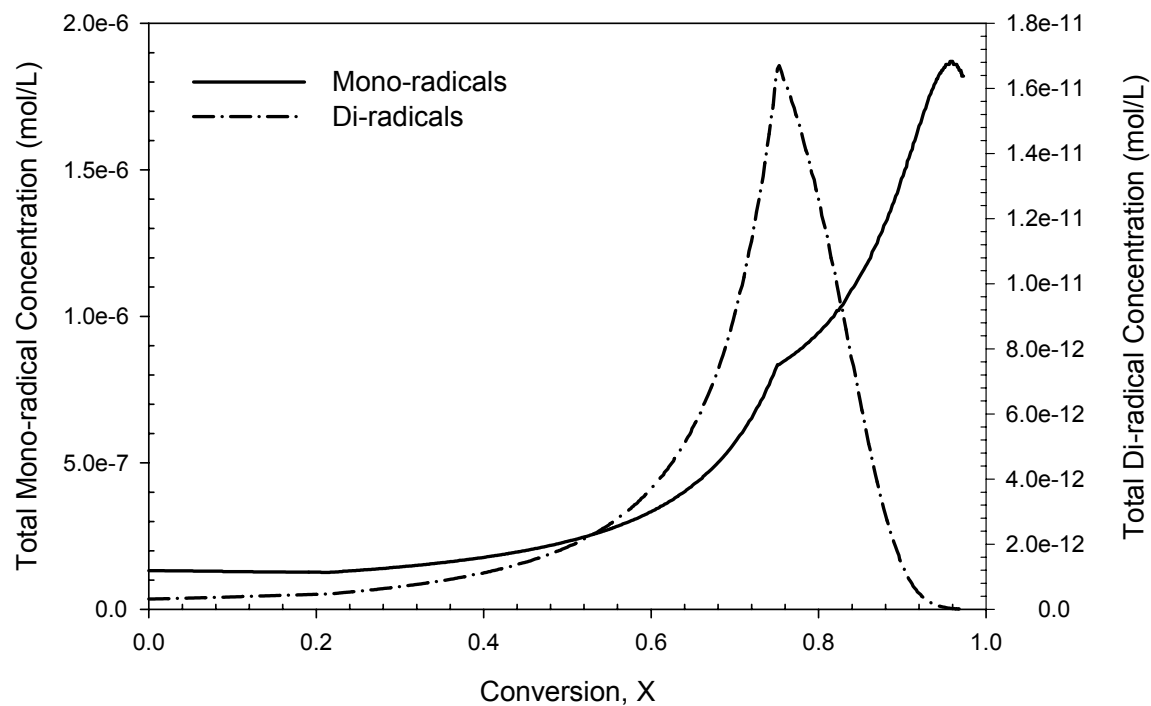


Figure 8.12. Mono- and di-radical concentrations as a function of conversion for the bulk polymerization of styrene (110°C, 4.0 mmol/L of JWEB50).

Contributions of the various chain structures to the total mono-radical concentrations in the bulk polymerization of styrene are presented in Figure 8.13. The trends show that the majority of mono-radicals are linear chains while star radicals are the second most abundant type of mono-radical. The concentration of coupled star mono-radicals is zero at the very beginning of the reaction, unlike that of the linear and star structures. This result is expected as linear and star mono-radicals are easily produced by the decomposition of an initiator molecule while coupled star radicals require several steps for their production (e.g., growth of star chains followed by the termination by combination of two star chains and then the decomposition of a functional site). Examination of the various types of polystyrene chain structures indicates that coupled star radicals are a noticeable fraction of the total number of mono-radicals and cannot be ignored. For a temperature of 110°C and an initial initiator concentration of 4.0 mmol/L, the fraction of mono-radicals that are coupled stars reaches a maximum of 18% during the course of the reaction. For lower temperatures and initiator concentrations, this maximum decreases but the contribution from this radical type is still significant (e.g., a

maximum of 5.0% for a reaction at 90°C and $[JWEB50]_0 = 0.97$ mmol/L). In the case of methyl methacrylate, termination is predominantly by disproportionation and coupling of stars is not as probable. The model predicts that under similar reaction conditions as styrene (110°C and $[JWEB50]_0 = 4.0$ mmol/L), only a maximum of 0.57% of mono-radicals will be coupled stars in the bulk polymerization of MMA.

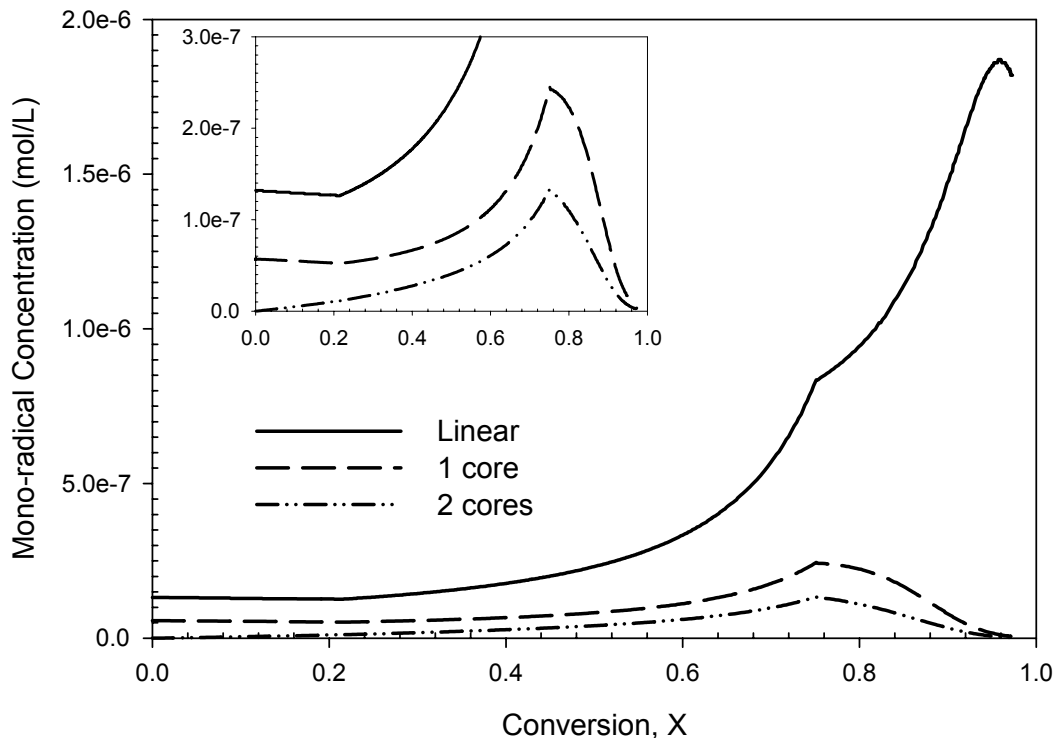


Figure 8.13. Mono-radical concentrations of linear, star (1 core) and coupled star (2 cores) chains as a function of conversion for the bulk polymerization of styrene (110°C, 4.0 mmol/L of JWEB50).

The trends seen with the various types of mono-radicals are also reflected by the concentration of polymer species. Figure 8.14 plots the concentration of linear, star and coupled star dead polymer chains as a function of time. Linear and star polymer chains have the highest concentrations; however, the concentration of coupled stars is significant enough that they cannot be ignored. An interesting trend shown in Figure 8.14 is that in the beginning of the reaction, star polymer chains are more abundant than linear chains. This phenomena is a result of termination by combination whereby linear radicals are

consumed by bimolecular coupling with star radicals. As the reaction progress a point is reached where linear polymer chains are the most abundant. This is due to several reasons including the generation of linear polymer as a result of thermal initiation and the termination of two linear radicals.

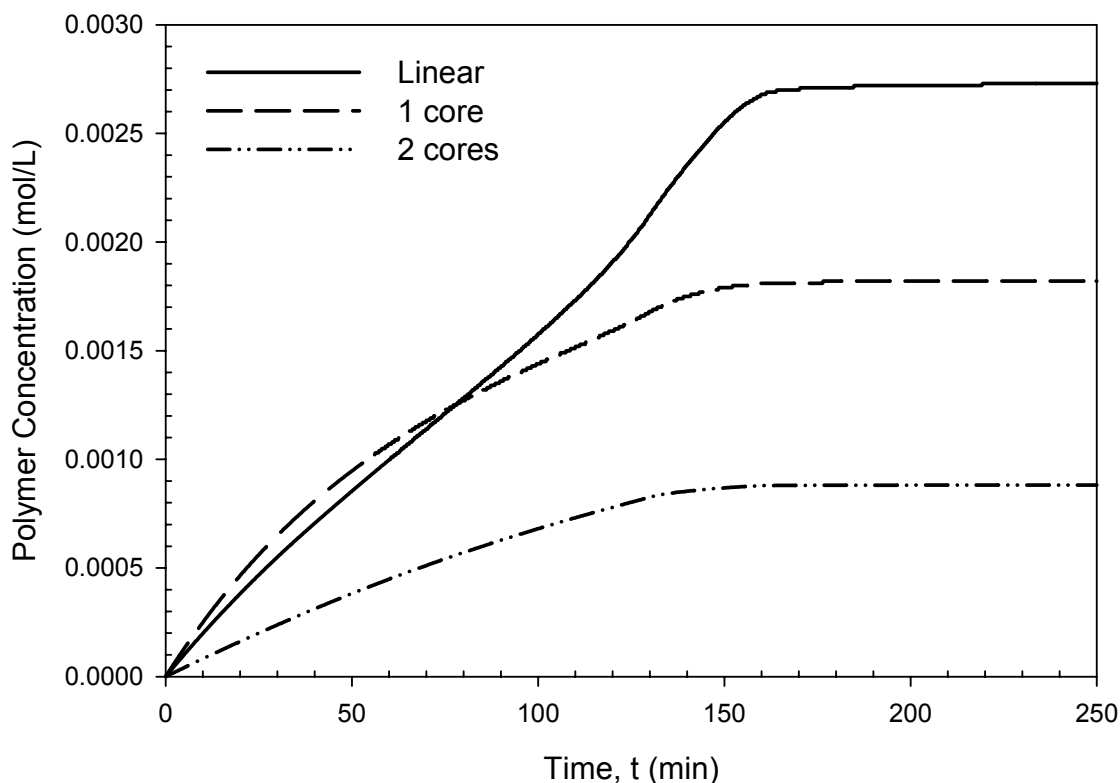


Figure 8.14. Concentration of linear, star (1 core) and coupled (2 cores) star polymer species for the bulk polymerization of styrene (110°C, 4.0 mmol/L of JWEB50).

In the end, the tetrafunctional model predicts that di-radicals concentrations are much lower than those of mono-radicals and in turn, their influence on the polymerization kinetics is minor. Thus, limiting the number of radicals per molecule to no greater than two appears to be a valid assumption. As for the second major assumption, the simulation results show that coupled stars are a notable fraction of the various polymer architectures (up to 18% for styrene at the highest temperature and initiator concentration). The concentration of polymers species with 1 or 2 cores and varying functionalities is shown in Figure 8.15. The data shows that for a large part of the

reaction, there is a significant concentration of coupled stars with 6 functional groups. With such high concentrations of coupled stars, it is plausible for species of even higher functionalities to be formed as the coupled stars can terminate by combining with each other or other stars. However, modification of the model to include species with higher functionalities would greatly increase the complexity of the model, even if di-radicals were ignored. As well, accounting for species of higher functionality would only be important for cases where termination is predominately due to bimolecular combination. For example, to include those species with 3 cores and up to 8 functional groups would introduce 9 more polymer species, 8 more mono-radicals and 7 more di-radicals.

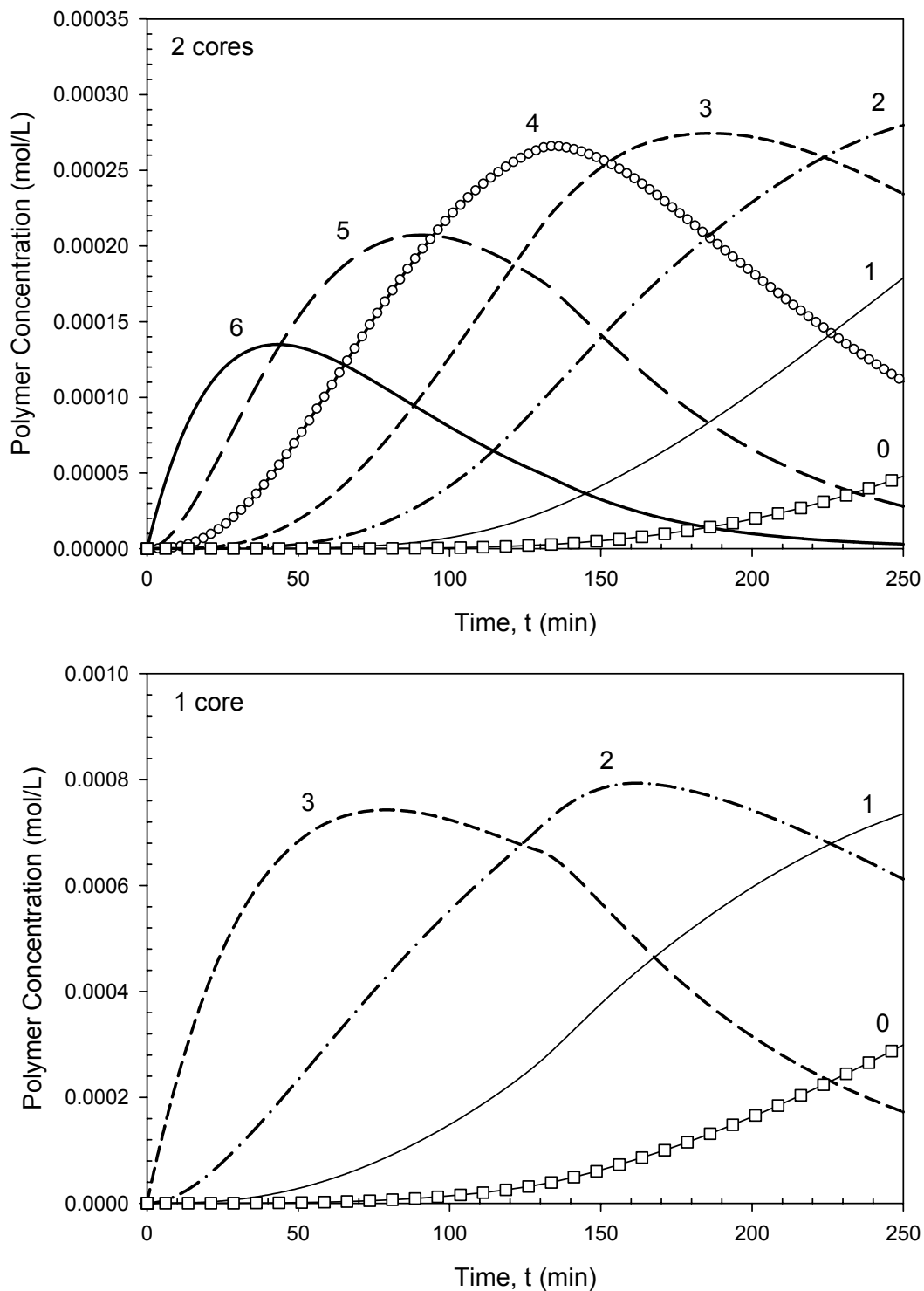


Figure 8.15. Concentration of polymer species with varying number of functional groups as a function of time for the bulk polymerization of styrene (110°C, 4.0 mol/L of JWEB50).

8.3.4 Case Studies

Through experimental work, the behaviour of the tetrafunctional initiator has been found to be dependent upon monomer type. The following case studies examine two reactions that characterize the polymerization of a monomer: termination and transfer reactions.

8.3.4.1 Mode of Termination

Studies with styrene and methyl methacrylate have both shown the benefits of using a multifunctional initiator where higher rates of production are obtained compared to monofunctional initiators. The impact on molecular weight, however, was found to vary between monomers. The polymerization of styrene initiated with a tetrafunctional initiator lead to molecular weights similar to those of the monofunctional initiator. In the case of MMA, the use of JWEB50 actually reduced the molecular weight compared to its monofunctional counterpart, TBEC. The varying behaviour of JWEB50 can be investigated using the tetrafunctional model.

Figure 8.16 shows the effect of the mode of terminations on molecular weight. Both data sets are for the bulk polymerization of styrene at 110°C and an initial initiator concentration of 1 mmol/L of JWEB50. The first case assumes that termination occurs only by combination while for the second simulation, disproportionation is the only possible mode of termination. In order to avoid thermal initiation masking any effects of varying the mode of termination, this option was turned off in the model. The molecular weight results plotted in Figure 8.16 clearly show that termination by combination produces polymer of much higher molecular weight compared to a system dominated by termination by disproportionation. This effect is seen with monofunctional initiators, however, the enhancement of molecular weight due to bimolecular coupling of radicals appears to have a larger influence with multifunctional initiators.

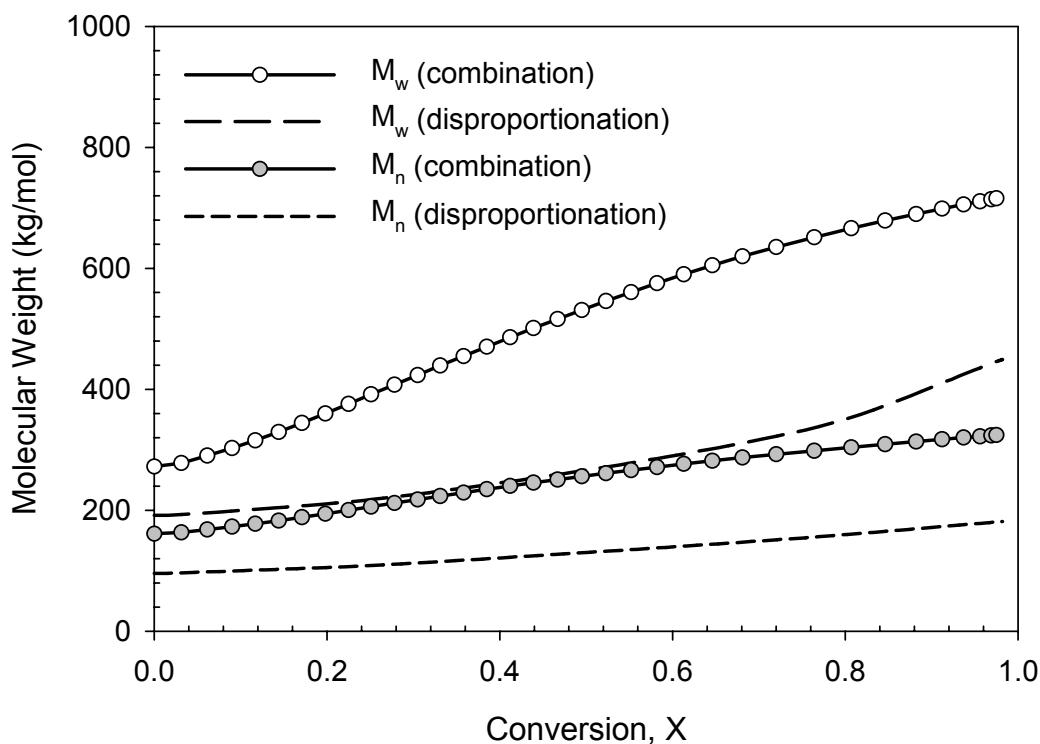


Figure 8.16. Number- and weight-average molecular weight for the bulk polymerization of styrene (110°C, 1 mmol/L of JWEB50).

The underlying difference between the two methods of termination can be seen when examining the mole fractions of the types of dead polymer and their corresponding chain lengths (see Figure 8.17). For both systems, linear chains are the most abundant type of polymer species and their molar fraction increases throughout the reaction. Single star chains are the next most common structure and both cases show similar fractions for this type of polymer. The main distinction between the two cases is found in the fraction of coupled stars. Termination by combination is the only process by which coupled stars can be formed and as such, they are not seen during the simulation where termination is dominated by disproportionation. In the termination by combination case, stars that have coupled together comprised a significant fraction of the dead polymer. For the reaction conditions of this case study, a maximum of 12% of dead polymer chains are coupled stars. This percentage is found to increase with temperature and initiator concentration. Without the existence of star coupling, we see the expected result that 80% of chains are linear and 20% are stars for full conversion.

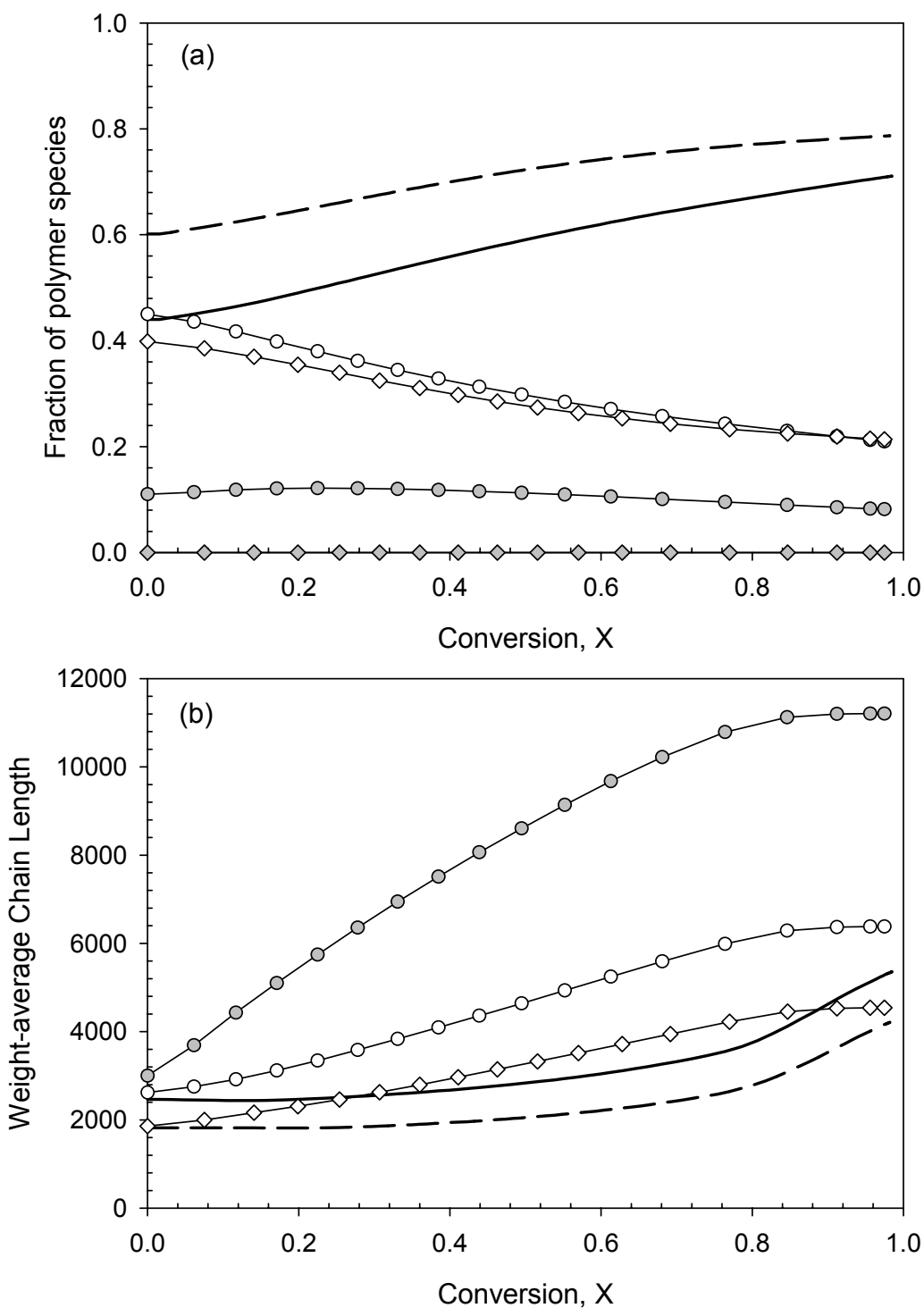


Figure 8.17. (a) Mole fraction of various polymer species. (b) Weight-average chain length. Identical conditions as reported in Figure 8.15. For combination data: solid line – linear, line and open circles – 1 core, line and grey circles – 2 cores. For disproportionation data: dashed line – linear, line and diamonds – 1 core, linear and grey diamonds – 2 cores.

Examining the concentration of each polymer species is only half of the solution as to why termination solely by combination significantly increases the overall molecular weight. The chain length of each species is the other factor that affects molecular weight results. Figure 8.17 (b) plots the weight-average chain length of linear, star and coupled star structures for both cases. For the case where termination proceeds solely by disproportionation, the chain length of coupled stars could not be determined as this species was never formed. Linear polymer chains produced by disproportionation have a lower chain length compared to linear chains formed by radical coupling. The same trend is observed for star polymers but the difference in chain lengths between the two cases is slightly greater. However, the most noticeable feature shown by this plot is the high chain lengths obtained by coupled stars. With a significant fraction of dead polymer being coupled stars, the overall molecular weight is dramatically increased. In the end, termination by combination enhances the chain length of linear and star polymer and also allows for the production of more highly branched species. For this reason, methyl methacrylate which is a monomer whose termination is dominated by disproportionation, does not exhibit the added benefits for molecular weight when employing a multifunctional initiator.

8.3.4.2 Transfer to Monomer

The influence of transfer reactions on the behaviour of a tetrafunctional initiator was investigated by varying the transfer to monomer rate constant. Weight-average molecular weight results are presented in Figure 8.18 for increasing transfer to monomer. As in the previous case study, thermal initiation has been removed from the model to avoid masking any effects. The plot shows the expected trend where higher rate constants lead to lower molecular weights.

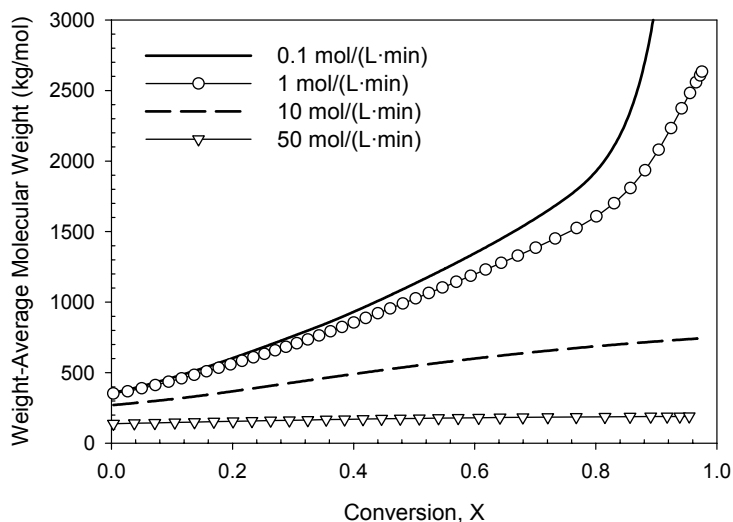


Figure 8.18. Weight-average molecular weight as a function of conversion for increasing transfer to monomer in the bulk polymerization of styrene (110°C, 1 mmol/L of JWEB50).

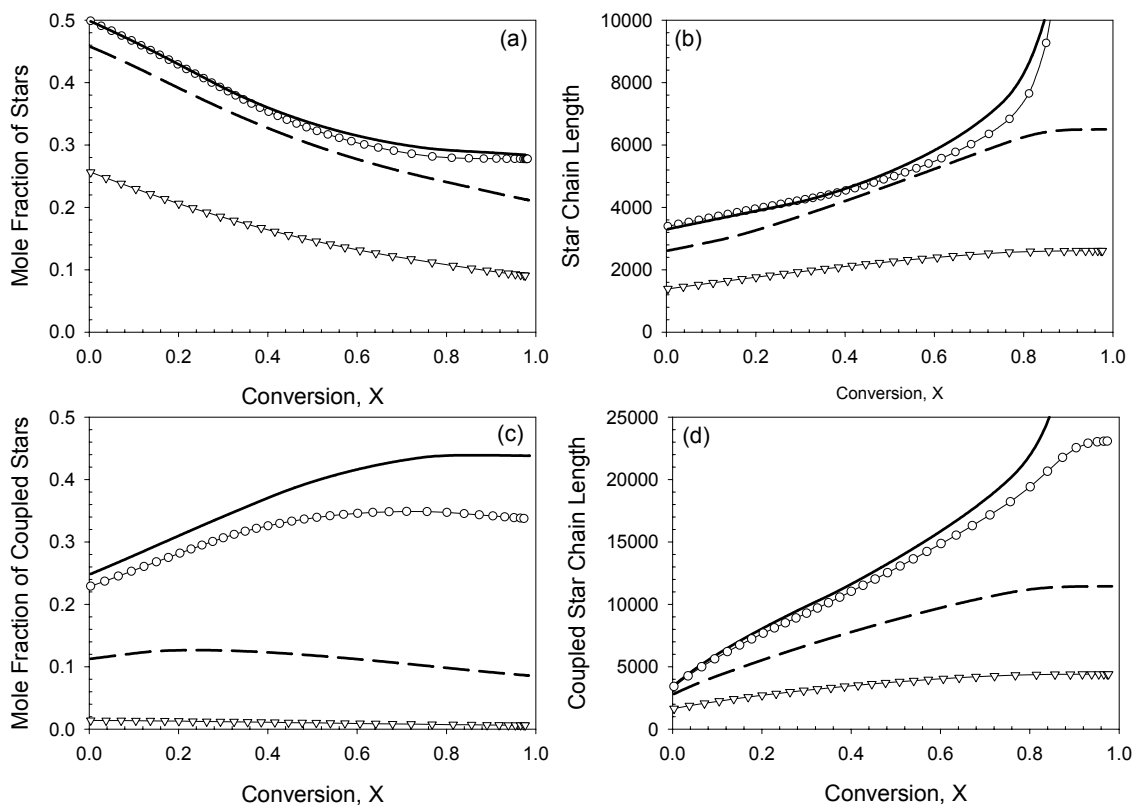


Figure 8.19. Mole fraction and chain length of star and coupled star polymer chains for increasing transfer to monomer in the bulk polymerization of styrene (110°C, 1 mmol/L of JWEB50). Solid line – 0.1 mol/(L·min), line and circles – 1 mol/(L·min), dashed line – 10 mol/(L·min), line and triangles – 50 mol/(L·min).

The more interesting phenomena can be seen when examining the concentration and chain length of the individual species. The mole fraction of star chains and the weight-average chain length of this polymer structure are plotted in Figures 8.19 (a) and (b). The curves indicate that with increasing transfer to monomer, the fraction of star chains decreases. Transfer reactions do not consume radicals and as the term implies, the radical site is simply transferred from one molecule to another. This process has no effect on linear molecules except to reduce their length. For star radicals, the impact is more significant as the free radical is passed from the star molecule to generate a linear radical. Therefore, the source of linear radicals is no longer merely the initiator and the number of linear chains dramatically increases. A second effect of high transfer to monomer rates can be seen in the concentration of coupled stars (see Figure 8.19 (c) and (d)). The fate of a radical is governed by the likelihood of either termination or transfer reactions and as k_{fm} is increased, transfer to monomer begins to dominate. The end result is that star radicals are more likely to transfer their radical activity before they have a chance to couple together. Therefore, the concentration of coupled stars decreases with increasing transfer to monomer. As shown in the case of $k_{fm} = 50 \text{ mol}/(\text{L}\cdot\text{min})$, the concentration of coupled stars is almost negligible. Comparing the concentration and length data, it appears that coupled stars are more strongly affected by increases k_{fm} than star chains.

8.4 Conclusions

A reaction mechanism for free radical polymerization initiated with a tetrafunctional was proposed and used in the development of a kinetic model employing the method of moments. The model accounts for reactions involving the “wastage” of a functional group (1- f) that produce initiator molecules or dead polymer chains. This detail has otherwise been ignored by modelling work of difunctional initiators found in the literature. The monofunctional and tetrafunctional models were fit to experimental data and provided estimates for free volume parameters associated with TBEC and JWEB50. Experimental work had shown that the functional groups of JWEB50 behave similar to those of TBEC and as a result, identical efficiencies were found for each initiator. Regression analysis indicated that the initiators have similar critical initiator free volumes

($V_{f_{crEff}}$) and diffusion-controlled constants (C). The only disparity between parameter estimates of the two models was observed for the diffusion-controlled termination equation (Equation 8.7). The tetrafunctional model require less of a dependence on the molecular weight term ($n_{tetra} = 0.5$ versus $n_{mono} = 1.75$) and a larger free volume constant ($A_{tetra} > A_{mono}$). Both the monofunctional and tetrafunctional models were used to simulate various polymerizations of styrene and methyl methacrylate. Conversion and molecular weight predictions agreed well with experimental data over a range of temperatures and initiator concentrations.

Two of the major assumptions employed in the development of the tetrafunctional model were examined. The first assumption stated that a molecule could have no more than two active radical sites. Results from the tetrafunctional model indicated that mono-radicals concentrations were several orders of magnitude greater than the concentration of di-radicals. Species with a greater number of active sites per molecule would have even lower concentrations and therefore, can be ignored. The second assumption involved truncating the functionality distribution at a maximum of 6 functional groups per chain. The statement implies that chains can have no more than two cores. The validity of the assumption was tested by examining the concentration of chains of varying architecture. In the case of MMA where termination by radical coupling is negligible and stars do not couple, the assumption is valid. Conversely, styrene radicals terminate solely by combination and the concentration of coupled stars can be quite substantial depending upon the reaction conditions. Higher temperatures and initiator concentrations increase the fraction of chains that are coupled stars. The results would suggest that the existence of species with more than simply two cores is plausible.

Experimental work with various monomers has shown that faster rates of polymerization can be obtained with a tetrafunctional initiator; however, only for certain monomers are their no effects on molecular weight. In order to explain these results, the effect of termination and transfer reactions on the behaviour of a tetrafunctional initiator was investigated. Simulation results showed that altering the dominant mode of termination from combination to disproportionation causes a drastic drop in molecular weight, more

so than would be expected for a monofunctional initiator. The reason behind such a decrease in molecular weight is because termination by disproportionation no longer allows for the formation of coupled stars. With termination occurring primarily by bimolecular coupling, coupled stars reach molecular weights much greater than linear and star chains and are produced in substantial amounts. Transfer reactions were found to have a similar impact on molecular weight and the concentration of the varying polymer structures. As the rate of transfer to monomer begins to increase, it competes with termination reactions. Instead of being able to terminate, radical sites on a star chain are transferred to a monomer molecule. The net effect is to produce more linear material and prevent star radicals from coupling. A decrease in the molecular weight of all species is observed but more importantly, the fraction of star chains drops and coupled stars are no longer formed.

Overall, the tetrafunctional model is able to accurately predict the behaviour of JWEB50. The model can be used to examine the effect of various reactions or conditions on the concentration and chain length of any specie in the polymerization mechanism. It is therefore, a useful tool in the understanding of a multifunctional initiator's behaviour in free radical polymerizations. Although not discussed in this work, the model is capable of simulating non-isothermal reactions and the polymerization of up to two monomers. The model has been designed for batch, bulk or solution mode but can be modified to account for flow terms with relatively minimal effort.

8.5 References

1. Prisyazhnyuk, A. I., Ivanchev, S. S. Diperoxides with differing thermal stabilities of the peroxide group as initiators of radical polymerization and block copolymerization. *Polymer Science USSR* **1970**, *12* (2), 514-524.
2. Choi, K. Y., Lei, G. D. Modeling of free radical polymerization of styrene by bifunctional initiators. *AIChE Journal* **1987**, *33* (12), 2067-2076.
3. Kim, K. J., Choi, K. Y. Modeling of free radical polymerization of styrene catalyzed by unsymmetrical bifunctional initiators. *Chemical Engineering Science* **1989**, *44* (2), 297-312.
4. Villalobos, M. A., Hamielec, A. E., Wood, P. E. Kinetic model for short-cycle bulk styrene polymerization through bifunctional initiators. *Journal of Applied Polymer Science* **1991**, *42*, 629-641.

5. Cavin, L., Rouge, A., Meyer, T., Renken, A. Kinetic modeling of free radical polymerization of styrene initiated by the bifunctional initiator 2,5-dimethyl-2,5-bis(2-ethyl hexanoyl peroxy)hexane. *Polymer* **2000**, *41*, 3925-3935.
6. Dhib, R., Gao, J., Penlidis, A. Simulation of free radical bulk/solution homopolymerization using mono- and bi-functional initiators. *Polymer Reaction Engineering Journal* **2000**, *8*, 299-464.
7. Dhib, R., Al Nidawy, N. Modelling of free radical polymerisation of ethylene using difunctional initiators. *Chemical Engineering Science* **2002**, *57* (14), 2735-2746.
8. Krallis, A., Kotoulas, C., Papadopoulos, S., Kiparissides, C., Bousquet, J., Bonardi, C. A comprehensive kinetic model for the free-radical polymerization of vinyl chloride in the presence of monofunctional and bifunctional initiators. *Industrial & Engineering Chemistry Research* **2004**, *43* (20), 6382-6399.
9. Estenoz, D. A., Leal, G. P., Lopez, Y. R., Oliva, H. M., Meira, G. R. Bulk Polymerization of Styrene in the Presence of Polybutadiene. The Use of Bifunctional Initiators. *Journal of Applied Polymer Science* **1996**, *62*, 917-939.
10. Menciloglu, Y. Z., Baysal, B. M. Synthesis and characterization of multifunctional initiators for preparation of four-branched polymers. *Die Angewandte Makromolekulare Chemie* **1992**, *200*, 37-47.
11. Holzinger, D., Kickelbick, G. Modified cubic spherosilicates as macroinitiators for the synthesis of inorganic-organic starlike polymers. *Journal of Polymer Science Part A-Polymer Chemistry* **2002**, *40* (21), 3858-3872.
12. Cerna, J. R., Morales, G., Eyler, G. N., Canizo, A. I. Bulk Polymerization of Styrene Catalyzed by Bi- and Trifunctional Cyclic Initiators. *Journal of Applied Polymer Science* **2002**, *83*, 1-11.
13. Gao, J., Penlidis, A. A comprehensive simulator/database package for reviewing free-radical homopolymerizations. *Journal of Macromolecular Science-Reviews in Macromolecular Chemistry and Physics* **1996**, *C36* (2), 199-404.
14. Gao, J., Penlidis, A. A comprehensive simulator database package for reviewing free-radical copolymerizations. *Journal of Macromolecular Science-Reviews in Macromolecular Chemistry and Physics* **1998**, *C38* (4), 651-780.
15. Choi, K. Y., Liang, W. R., Lei, G. D. Kinetic bulk styrene polymerization catalyzed by symmetrical bifunctional initiators. *Journal of Applied Polymer Science* **1988**, *35*, 1547-1562.
16. Kim, K. J., Liang, W. R., Choi, K. Y. Bulk free radical polymerization of styrene with unsymmetrical bifunctional initiators. *Industrial and Engineering Chemistry Research* **1989**, *28*, 131-138.
17. Yoon, W. J., Choi, K. Y. Free radical polymerization of styrene with a binary mixture of symmetrical bifunctional initiators. *Journal of Applied Polymer Science* **1992**, *46*, 1353-1367.
18. Yoon, W. J., Choi, K. Y. Kinetics of free radical styrene polymerization with the symmetrical bifunctional initiator 2,5-dimethyl-2,5-bis(2-ethyl hexanoyl peroxy)hexane. *Polymer* **1992**, *33* (21), 4582-4591.

19. Ivanchev, S. S. New Views on Initiation and Radical Polymerization in Homogeneous and Heterogeneous Systems. *Polymer Science USSR* **1979**, *20* (9), 2157-2181.
20. Kasehagen, L. Personal Communication, 2001.
21. Fityani-Trimmi, S., Dhib, R., Penlidis, A. Free Radical Polymerization of Styrene with a New Tetrafunctional Peroxide Initiator. *Macromolecular Chemistry and Physics* **2003**, *204*, 436-442.
22. Scoriah, M. J., Dhib, R., Penlidis, A. Free-radical polymerization of methyl methacrylate with a tetrafunctional peroxide initiator. *Journal of Polymer Science Part A-Polymer Chemistry* **2004**, *42* (22), 5647-5661.
23. Scoriah, M. J., R. Dhib, and A. Penlidis *Journal of Macromolecular Science Pure and Applied Chemistry* 2005; **A42** (4), 403-426.
24. Fityani-Trimmi, S. (2001). An Investigation into the Bulk Free Radical Polymerization of Styrene Using a Novel Tetrafunctional Initiator. University of Waterloo, 1-141.

CHAPTER 9 - CONTRIBUTIONS TO RESEARCH AND RECOMMENDATIONS

The use of a tetrafunctional initiator was systematically investigated for a variety of monomer systems for the first time. Experimental work showed that the benefits of a multifunctional initiator are limited by the polymerization characteristics of each specific monomer. Regardless of the homo- or copolymer system examined, it was observed that the tetrafunctional initiator could produce higher rates of polymerization due to the greater number of labile groups per initiator molecule. The second advantage of multifunctional initiators, claimed by work in the literature, is that these initiators are able to obtain high rates of production without sacrificing molecular weight. This advantage is the main motivation behind their use and has led to increased academic and industrial interest. The work presented herein has shown that this particular benefit of employing a multifunctional initiator is limited to certain monomer or comonomer feeds. The polymerization of methyl methacrylate with the tetrafunctional initiator, JWEB50, was found to produce lower molecular weight polymer compared to experiments run with the monofunctional initiator, TBEC. The addition of styrenic monomers such α -methyl styrene to the polymerization of MMA was shown to lessen the decrease in molecular weight.

A characterization study of polystyrene and poly(methyl methacrylate) samples produced with the tetrafunctional initiated was carried out to examine the effects of initiator functionality on polymer properties. Samples generated with the monofunctional initiator were used for comparison purposes. Using chromatographic and dilute solution methods, polystyrene produced with the tetrafunctional initiator was determined to contain significant levels of branched material compared to polystyrene generated with TBEC. In contrast, poly(methyl methacrylate) samples showed no evidence of branching. Rheological testing involved a combination of oscillatory and creep shear measurements in order to detect differences between samples. Evidence of branching using rheological

techniques was clearly observed for both polystyrene and poly(methyl methacrylate) samples produced with the tetrafunctional initiator.

Lastly, a reaction mechanism for polymerizations initiated with a tetrafunctional initiator was proposed and used in the development of a kinetic mathematical model. Unlike previous models for multifunctional initiators, the model formulated in this study correctly accounts for “wastage” reactions that lead to initiator or dead polymer molecules of lower functionality. The validity of two major model assumptions was tested. Based on model predictions, di-radical concentrations were found to be significantly smaller than those of mono-radicals. As a result, radicals with multiple active sites can safely be neglected in the model. Model predictions also show that depending upon the monomer type and the chosen reaction conditions, the coupling of star chains is considerable. Simulations show that it is these polymer species that allow the tetrafunctional initiator to generate such high molecular weights. Case studies examining the effects of termination and transfer reactions have shown that the concentration of coupled stars is highly dependent on the mode of termination (combination versus disproportionation) and the existence of significant transfer reactions.

Although a considerable amount of experimental work has already been completed in the investigation of JWEB50, other monomer systems could be examined. Selective experiments could be performed in the copolymerization of styrene or MMA and a divinyl monomer (such as divinyl benzene) with the tetrafunctional initiator. As well, the applicability of JWEB50 in other types of polymer related processes could be examined. JWEB50 could be employed in nitroxide mediated polymerizations to form well-defined 4-arm stars. The advantages of using the tetrafunctional initiator in the degradation of polypropylene could also be investigated.

As far as modelling efforts are concerned, there is still a great deal of work that remains to be done. Future development of the model should allow for more than two stars to couple. To offset the accompanying increase in complexity, the existence of di-radicals

could be ignored. Currently, the model has the ability to simulate copolymerization with a tetrafunctional initiator; however, certain parameters need to be estimated. In order to obtain reliable values of these parameters, a larger set of copolymerization experiments should be run. The model could also be modified to allow flow terms and non-isothermal operation. In addition, more complex steps would be to account for transfer to polymer, internal and terminal double bond polymerization, and depropagation.

APPENDIX A - BENCH-MARKING OF DIFUNCTIONAL INITIATORS

Before expanding the kinetic model proposed by Dhib et al. (1) to include tetrafunctional initiators, the simulator was compared to various sources of experimental data. This section presents the results of comparisons made between data taken from the open literature and an industrial source.

Open Literature

Cavin et al. examined the reaction kinetics of 2,5-dimethyl-2,5-bis(2-ethyl hexanoyl peroxy)hexane (Luperox 256) through the use of differential scanning calorimetry for several temperatures between 80 and 110 °C and at different initial initiator concentrations (2). Preliminary modelling results from our simulator do not agree well with the experimental data (see Figure B.1). In order to determine whether the model is at fault or if the discrepancy may be attributed to the experimental data, another data source was compared to the results of Cavin et al. (2). Villalobos et al. performed bulk polymerizations of styrene with Luperox 256 under similar conditions (3). Figure B.2 is a plot of conversion versus time for the polymerization of styrene at an initial initiator concentration of 0.01 M and at 80 °C. Note that the model agrees well with the data from Villalobos et al. (3). This suggests that the discrepancy between the model predictions and the results obtained by Cavin et al. (2) might be due to experimental error. If the reaction temperature is not well controlled, nonisothermality can be a significant factor. Small rises in the reaction mixture's temperature can cause large increases in the rate of polymerizations. Therefore, the experiments were simulated employing a linear ramp in the reactor temperature. For the three runs with initial initiator concentrations of 0.01 M, 0.02 M and 0.04 M, the slope of the temperature increase was 1, 1.5 and 2 °C per 50 minutes, respectively. Figure B.3 presents the modelling and experimental results for conversion versus time. The modelling profiles reproduce quite accurately the trends for conversion for each of the three initiator concentrations. The next plot (Figure B.4) shows the rate of polymerization as a function of conversion for the same experiments.

There is good agreement between the model predictions and experimental data until higher conversions are reached ($> 75\%$). Above this point, the model predicts a much larger rate of polymerization compared to the experimental data. This discrepancy can also be seen in the conversion data where the rate of polymerization is the slope of the curves in Figure B.3. Note that at high conversions the model is predicting a faster increase in conversion as time proceeds and hence, a higher rate of polymerization is observed.

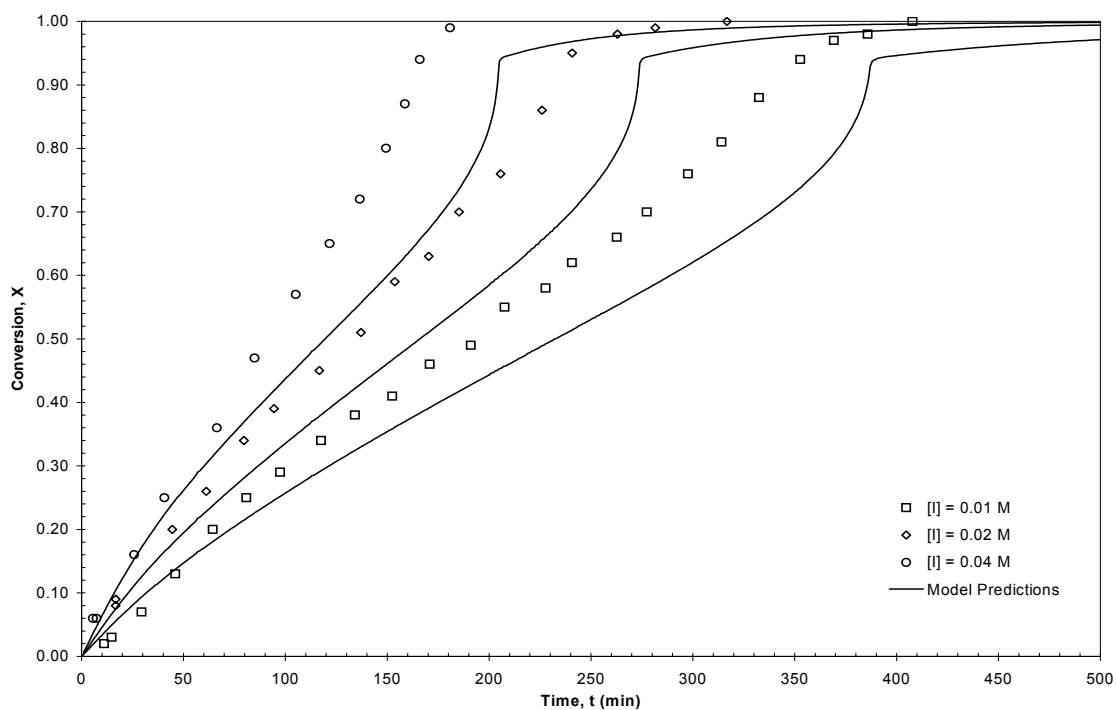


Figure A.1. Conversion as a function of time for the bulk polymerization of styrene initiated with Luperox 256 at 80 °C.

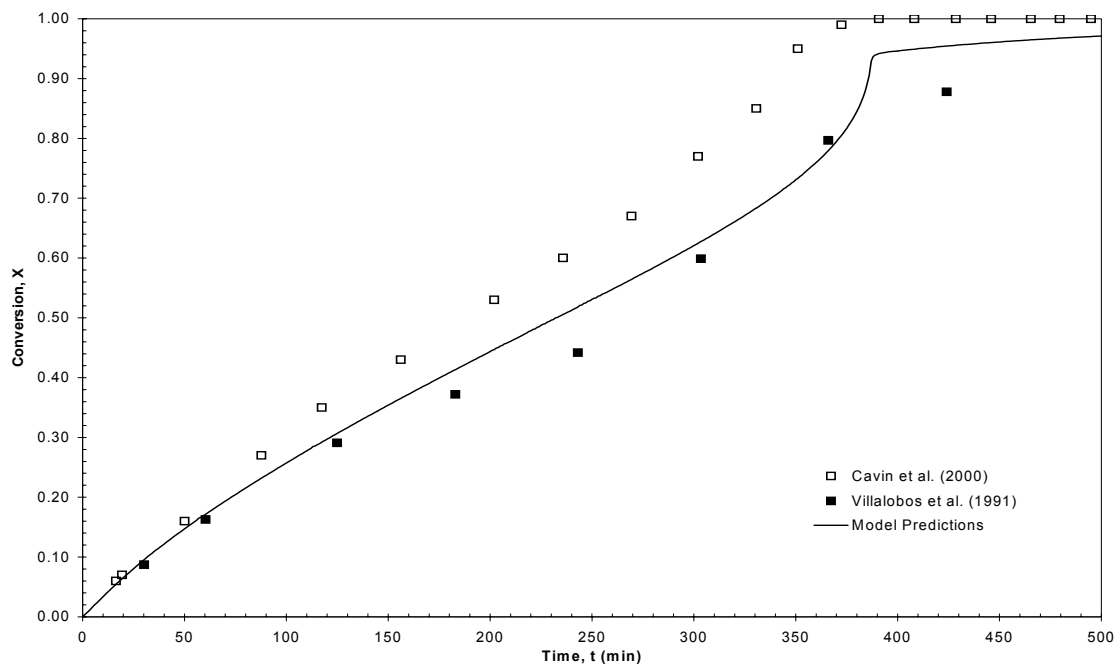


Figure A.2. Conversion as a function of time for the bulk polymerization of styrene initiated with Luperox 256 at an initial concentration of 0.01 M and a reactor temperature of 80 °C.

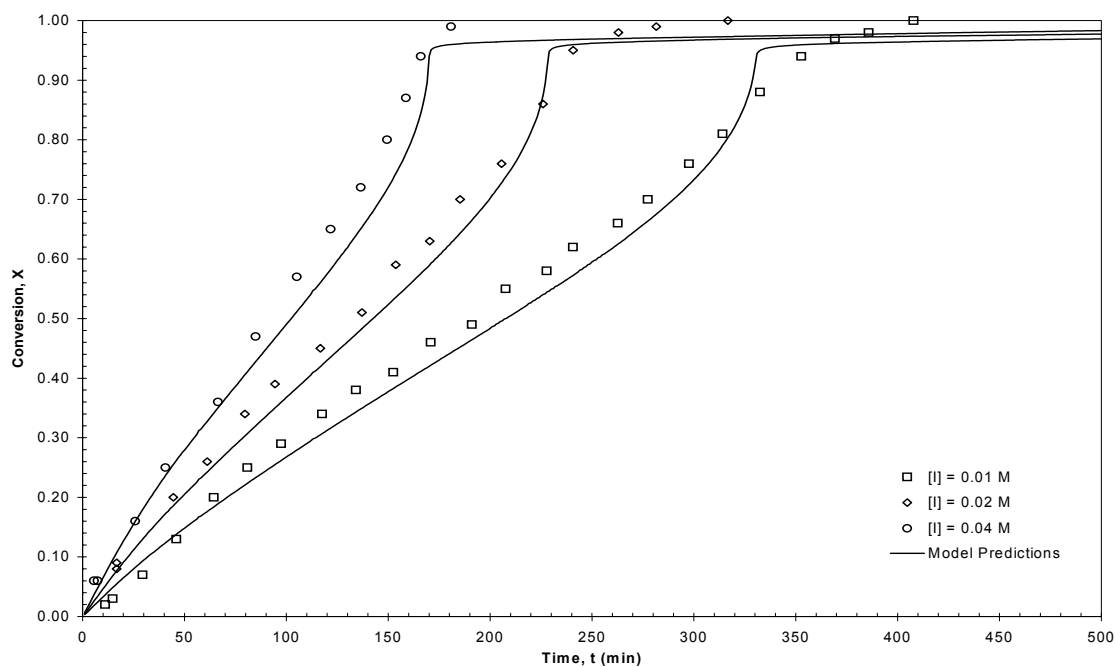


Figure A.3. Conversion as a function of time for the bulk polymerization of styrene initiated with Luperox 256 at $T_0 = 80$ °C. Model predictions are nonisothermal with a temperature rise of 1, 1.5 and 2 °C/min for $[I]_0 = 0.01$, 0.02, and 0.04 M, respectively.

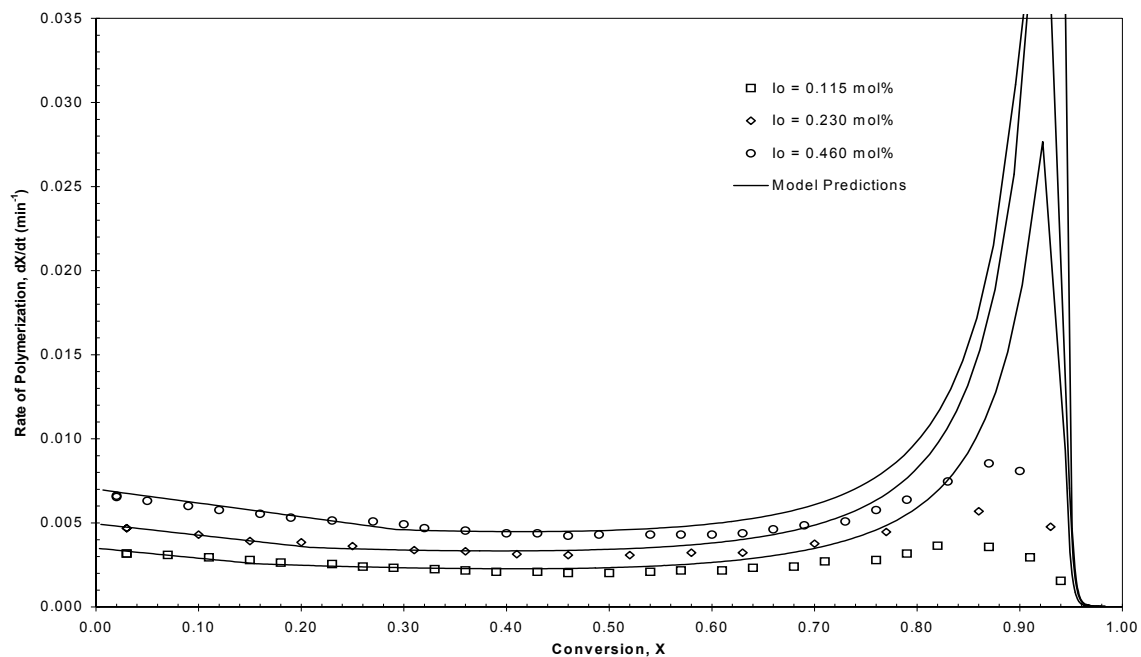


Figure A.4. Rate of polymerization as a function of conversion for the bulk polymerization of styrene initiated with Luperox 256 at $T_0 = 80 \text{ }^\circ\text{C}$. Model predictions are nonisothermal with a temperature rise of 1, 1.5 and 2 $^\circ\text{C}/\text{min}$ for $[I]_0 = 0.01, 0.02,$ and 0.04 M, respectively.

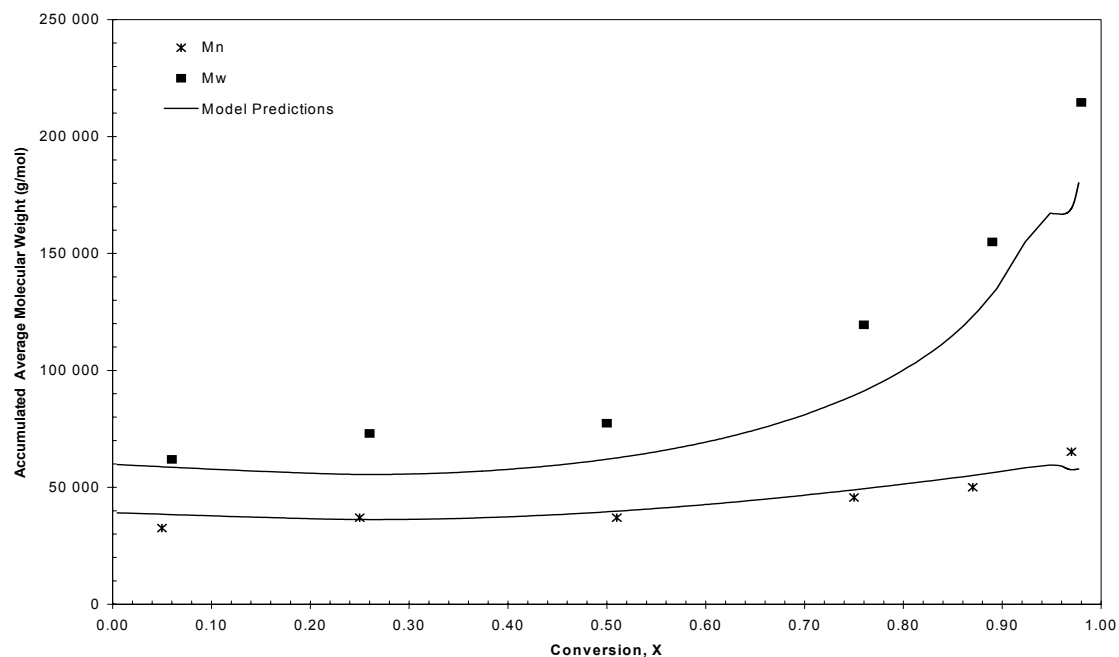


Figure A.5. Molecular weight averages as a function of conversion for the bulk polymerization of styrene initiated with $[\text{Luperox } 256]_0 = 0.02 \text{ M}$ at $T_0 = 80 \text{ }^\circ\text{C}$. Model predictions are nonisothermal with a temperature rise of 1 $^\circ\text{C}/\text{min}$.

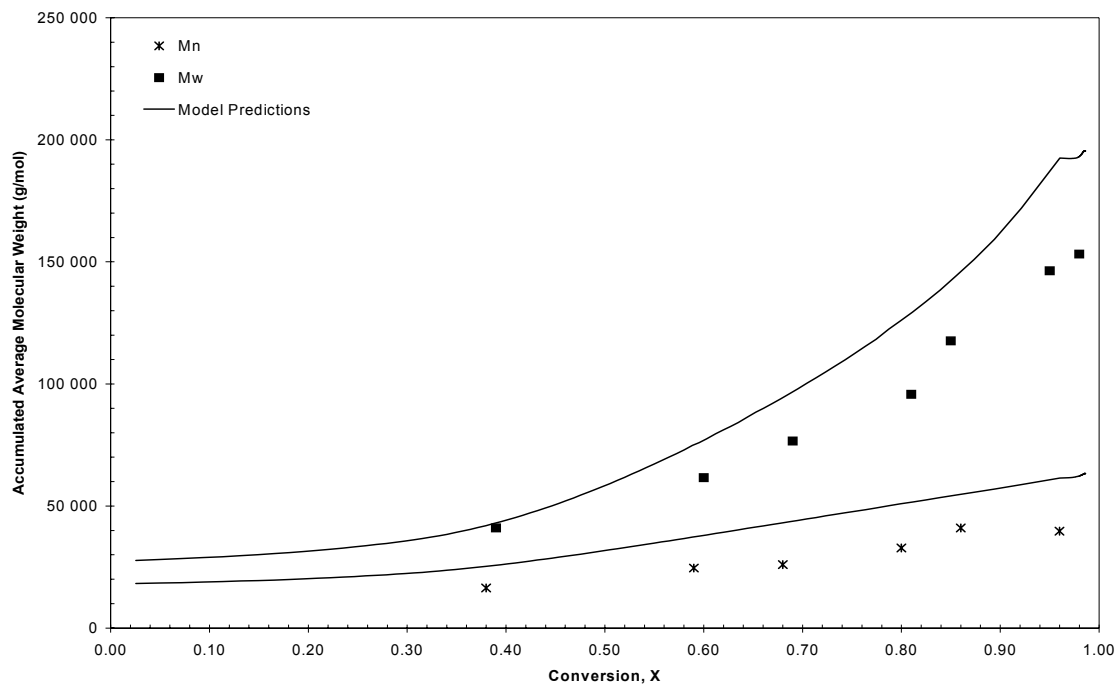


Figure A.6. Molecular weight averages as a function of conversion for the bulk polymerization of styrene initiated with $[Luperox\ 256]_0 = 0.02\ M$ at $T_0 = 100\ ^\circ C$.

Figures B.5 and B.6 are plots of number and weight-average molecular weights as a function of conversion for an initial initiator concentration of 0.02 M and temperatures of 80 and 100°C. There is reasonable agreement between the model and experimental data. Because the conversion versus time data were not included in the paper for the 100°C run, only the isothermal model predictions could be used. The isothermal model results are somewhat higher than the experimental results. However, the nonisothermal model predictions would give a better fit as increasing the temperature would decrease the predicted molecular weight averages.

Figure B.7 shows a graph of conversion as a function of time for an operating temperature of 110°C with nonisothermal model predictions. In this case, the model predictions agree well with the experimental data for approximately the first 60 minutes of the reaction. For the three runs with initial initiator concentration of 0.01 M, 0.02 M and 0.04 M, the temperature increase was 1, 1.5 and 2 °C per 20 minutes for the first 60 minutes. After 60 minutes, the model predictions do not agree well with the experimental

data unless a drastic temperature increase is used in the modelling. In order to determine what may be occurring near 60 minutes that may account for the sudden discrepancy between the model predictions and experimental results, the amount of initiator remaining as a function of time was determined. Figure B.8 is a plot of the percentage of initiator remaining in the system versus time. Note that at a temperature of 110°C, there is less than 0.01% of the initial initiator concentration at 50 minutes and any further production of polymer after this time would be the result of thermal polymerization.

The simulator package has been shown to accurately simulate the thermal polymerization of styrene. This is evident from the comparisons made to various academic and industry sources in the paper by Gao and Penlidis (4) (for a recent example of the simulation of thermal polymerization see Figure B.13 in this document). Because the simulator performs well when modelling the thermal polymerization of styrene, it suggests that the discrepancy in Figure B.7 may be attributed to experimental error.

As previously mentioned, Cavin et al. (2) employed a DSC to monitor the polymerization of styrene. At any particular time, the conversion can be calculated from the DSC thermograms by measuring the area between the curve and the baseline where the baseline is measured at the end of the reaction and extrapolated backwards. In order to use the thermograms, a calibration curve must be determined. A compound with a known latent heat of fusion is melted in the DSC and the area of the peak can be attributed to that release in heat.

A particular difficulty with DSC is the determination of the final conversion of the polymer sample so that the area under the DSC curve can be assigned to a certain total conversion. One method is to assume that 100% conversion has been reached (5). However, not all polymerizations reach complete conversion and if this assumption is incorrect, it would cause each experimental data point to be at a higher conversion value than expected. Another procedure is to take the final polymer sample and perform a temperature scan at a constant heating rate. As the temperature is increased, the residual monomer will begin to polymerize at a certain temperature and will continue to form

polymer as the temperature rises. This produces two thermograms: one for the isothermal polymerization (C1) and the other for the nonisothermal residual monomer polymerization (C2). The final conversion can then be calculated from the ratio of the C1's area over the sum of the areas of C1 and C2 (6, 7). However, this calculation is based on the assumption that all of the residual monomer has polymerized. If this is not the case, then the final conversion and every other data point will be overestimated. Other methods to determine the final conversion employ either a gas chromatograph or an ultraviolet spectrometer. Overall, extreme care must be taken in determining the final conversion as its value will affect each measurement. A second significant source of error that occurs in DSC experiments is weight loss. If the sample pan is not completely sealed, monomer can evaporate. Any loss in monomer will shift the conversion measurements to higher values. One group has reported typical weight losses of up to 6.3% (6). In each case, the sources of error associated with monitoring a polymerization with DSC will cause the conversion measurements to be higher than expected. As this is the trend shown in the figures, it may be likely that a combination of these errors along with the possibility of nonisothermality could be the reason for the discrepancy.

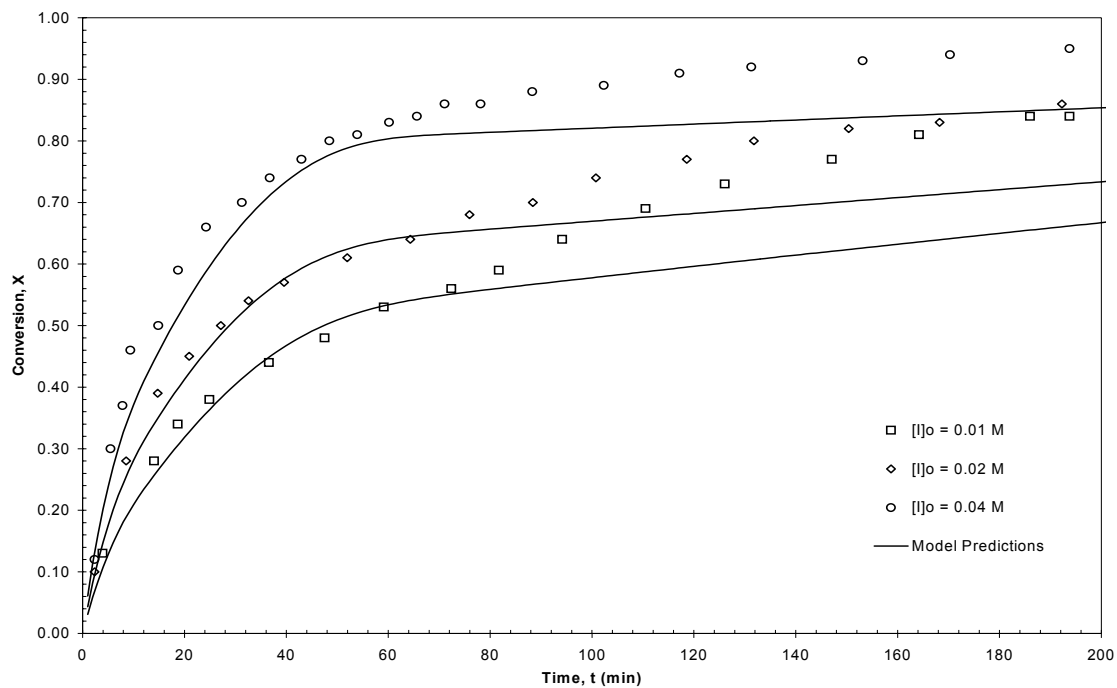


Figure A.7. Conversion as a function of time for the bulk polymerization of styrene initiated with Luperox 256 at 110 °C.

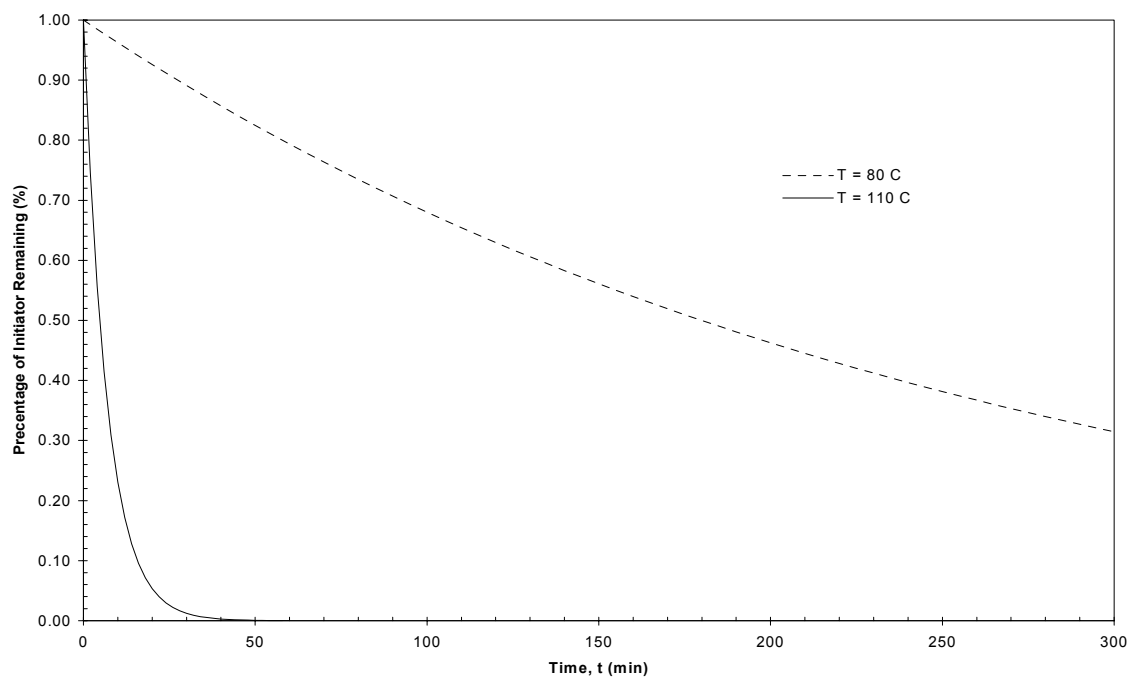


Figure A.8. Percentage of initiator remaining within the system as a function of time.

Atofina Industrial Data

Atofina is one of the major suppliers of initiators for the polymer industry. The company performs preliminary experiments with their initiators in order to supply customers with technical data. This section provides a comparison of their experimental data with the model predictions from the difunctional simulation package.

Tables B.1 and B.2 list the one-hour half-life temperatures for intermediate and low temperature peroxide initiators. The first set of data is what has been determined experimentally by Atofina and then reported in technical bulletins. The second dataset has been calculated from the parameters in the difunctional simulator's database. The good agreement between the two sets of data indicates that the database parameters for the dissociation of an initiator's reactive site are valid.

Table A.1. One-hour half-life temperature ($^{\circ}\text{C}$) for intermediate temperature peroxides.

Initiator	Luperox TBPB	Luperox 7M75	Luperox TBEC	Luperox 555M60	Luperox TAEC	Luperox 331M80
Functionality	Mono	Mono	Mono	Mono	Mono	Bi
Atofina	125	123	121	120	117	116
Database	121	123	121	120	117	116

Table A.2. One-hour half-life temperature ($^{\circ}\text{C}$) for low temperature peroxides.

Initiator	Luperox 80M75	Luperox 26	Luperox 575	BPO	Luperox 256	Luperox 665M50	Luperox DEC
Functionality	Mono	Mono	Mono	Mono	Bi	Mono	Mono
Atofina	102	95	92	92	91	84	83
Database	102	95	92	90	89	84	83

Figures B.10 to B.12 are plots of conversion versus time for a series of high temperature peroxides used in the polymerization of styrene. Figure B.13 presents conversion data for the thermal polymerization of styrene. Atofina has selected initiator concentrations so that some runs have the same concentration of radical generating sites. Note that at twice

the concentration of the difunctional initiators (Luperox 101 and 802), the monofunctional initiator (Luperox 500R) produces a similar rate of polymerization and approximately 100% conversion is attained in 300 minutes. The lines in the figures are model predictions generated by the simulator package. There is satisfactory agreement between the experimental data and modelling results and good agreement between datasets for the case of pure thermal polymerization. However, the model does not predict the conversion data very well for Luperox 500R (Figure B.12). The simulator does produce general trends that are similar to those shown by the experimental data but the conversions are underpredicted. There may be several reasons for the discrepancy between model and experimental data. It could be that the polymer samples were not dried sufficiently enough so that residual monomer contributed to the measurement of the conversion. This would account for why the experimental data are higher than model predictions. As well, Atofina may have used an initiator with a different purity than the one supplied to its customers. A lack of impurities that inhibit or retard polymer radicals would allow for a higher rate of polymerization and in turn, higher conversions. The database parameters may have been estimated based on an initiator that contains impurities and would predict a lower rate of polymerizations. This may occur when more than one company produces an initiator and each supplier produces a product with different concentrations and types of impurities. A third reason for the difference between the two sets of data could be that the experiments were run under non-isothermal conditions. Any increase in temperature as the reaction proceeds would increase the rate and produce a higher conversion.

Figures B.14 to B.19 show graphs of conversion versus time for the intermediate temperature peroxide initiators listed in Table B.2. The model predictions show trends similar to those exhibited by the experimental data and in most cases, the model is in satisfactory agreement with the experimental results. For Luperox TBPB and TBEC (Figures B.14 and B.16), the last conversion point at the lower temperature is much higher than predicted and does not fit with the expected trends. As previously mentioned, the source of error may be residual monomer in the sample and nonisothermality.

For the simulation of Luperox 331M80 (Figure B.19), there is good agreement between the experimental and modelling results for the higher temperature. However, at lower temperatures, the model underpredicts the experimental data.

Conversion versus time plots for low temperature peroxide initiators are shown in Figures B.20 to B.24. In most cases, the simulator reproduces the experimental trends well. For Luperox 256 (Figure B.24), the model and experimental data are in very good agreement for the lower temperature reaction. However, the model does not accurately reproduce the experimental data for the higher temperature experiment. The experimental results for the higher temperature run show that the rate of polymerization decreases at longer reaction times and indicate that the initiator is being depleted. Based on the good agreement between the model predictions for Luperox 256 and other experimental sources (e.g., Villalobos et al. (3), see Figure B.2) it might be likely that the discrepancy is due to experimental error.

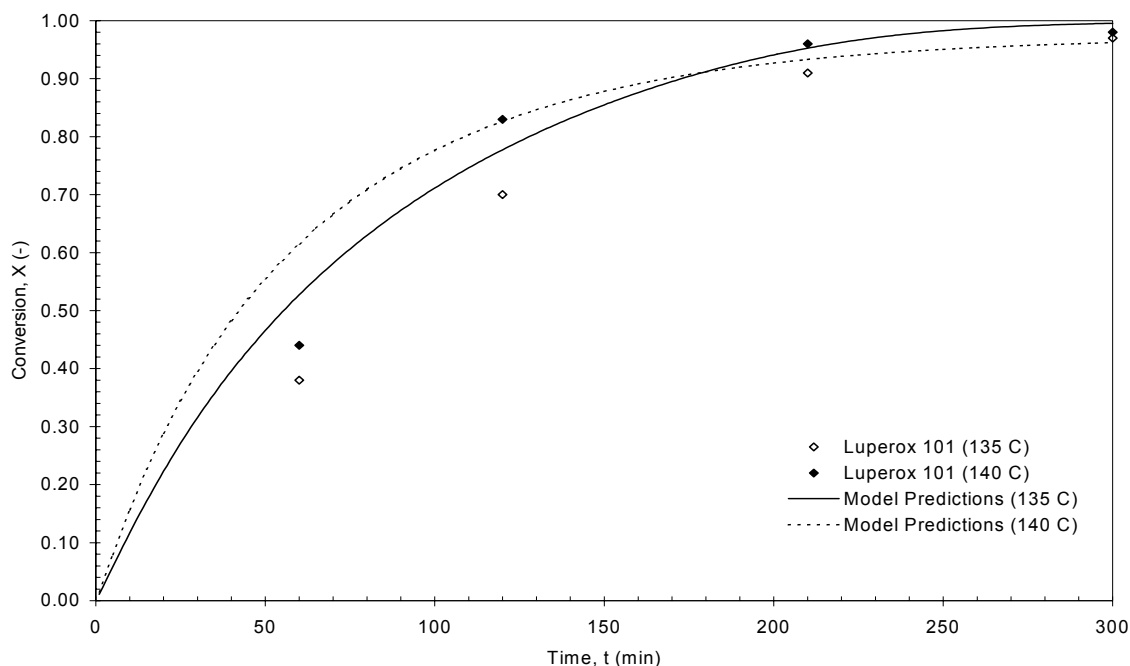


Figure A.9. Conversion as a function of time for the bulk styrene polymerization initiated by Luperox 101 (difunctional, $[I]_0 = 403 \text{ ppm} = 0.00125 \text{ M}$).

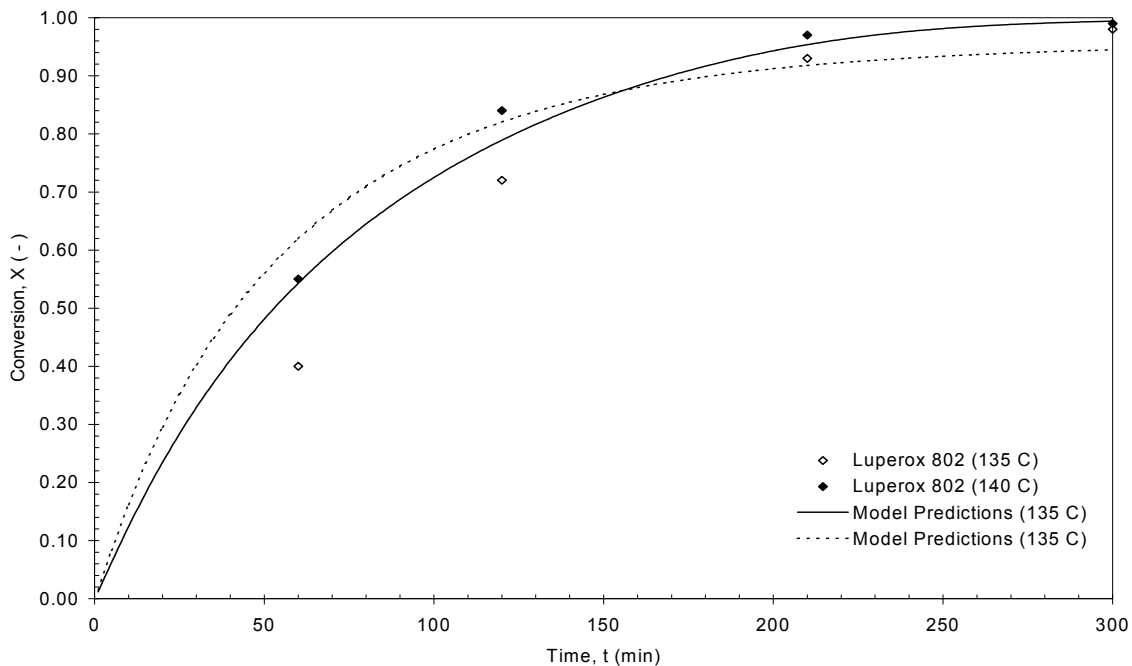


Figure A.10. Conversion as a function of time for the bulk styrene polymerization initiated by Luperox 802 (difunctional, $[I]_0 = 469 \text{ ppm} = 0.00125 \text{ M}$).

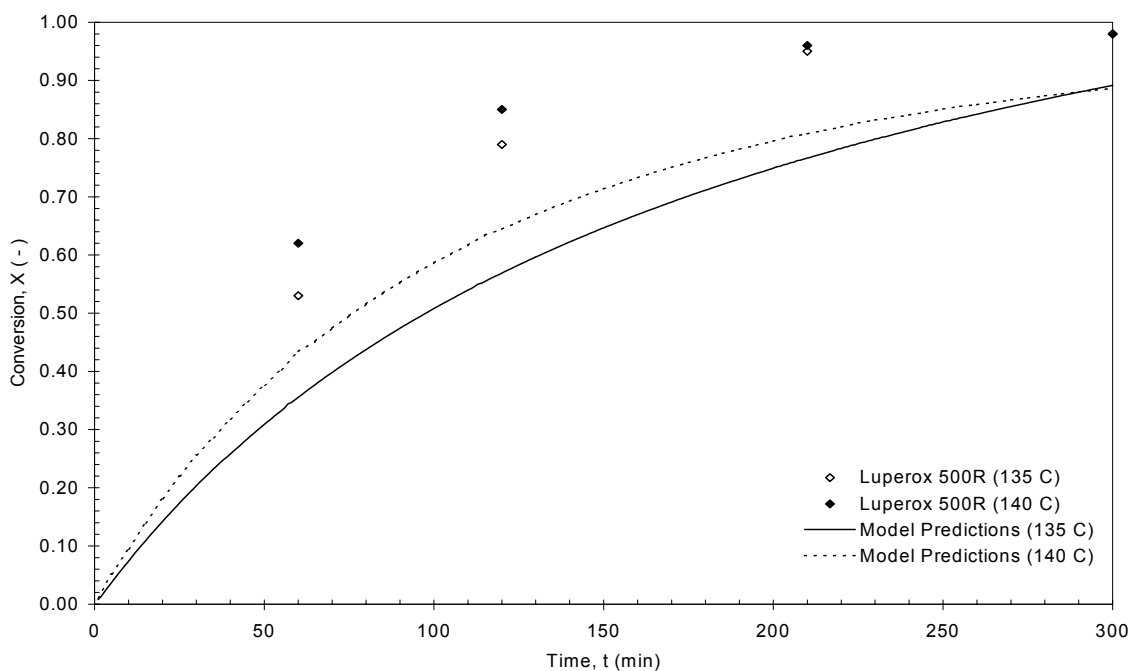


Figure A.11. Conversion as a function of time for the bulk styrene polymerization initiated by Luperox 500R (monofunctional, $[I]_0 = 750 \text{ ppm} = 0.00250 \text{ M}$).

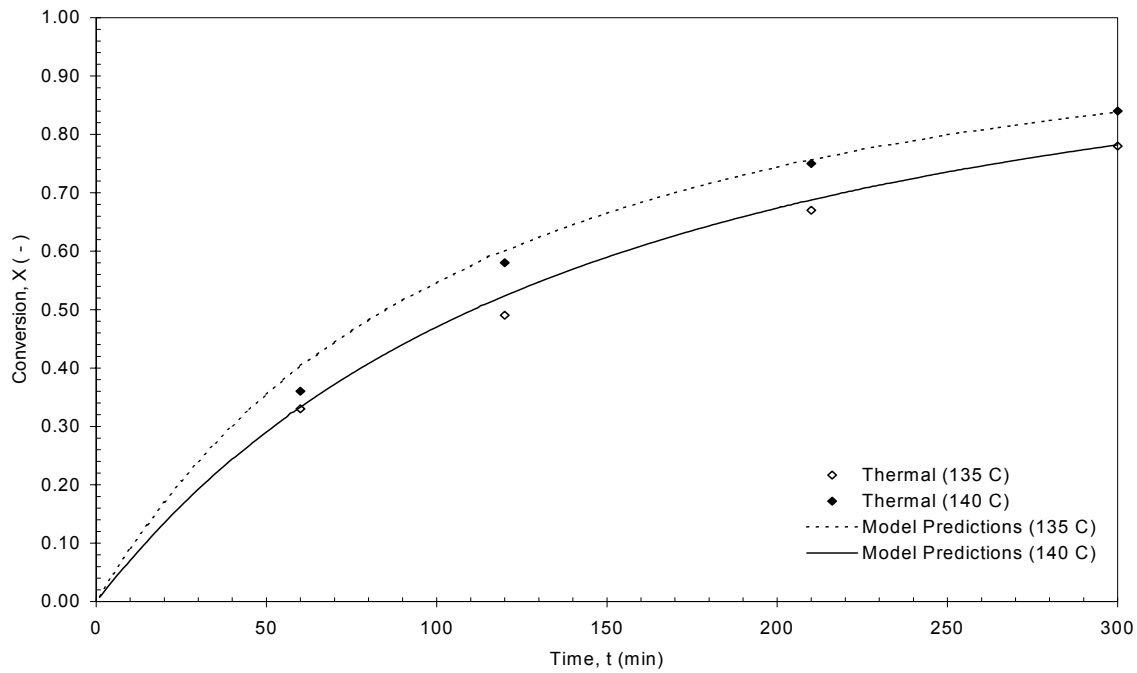


Figure A.12. Conversion as a function of time for the bulk thermal polymerization of styrene.

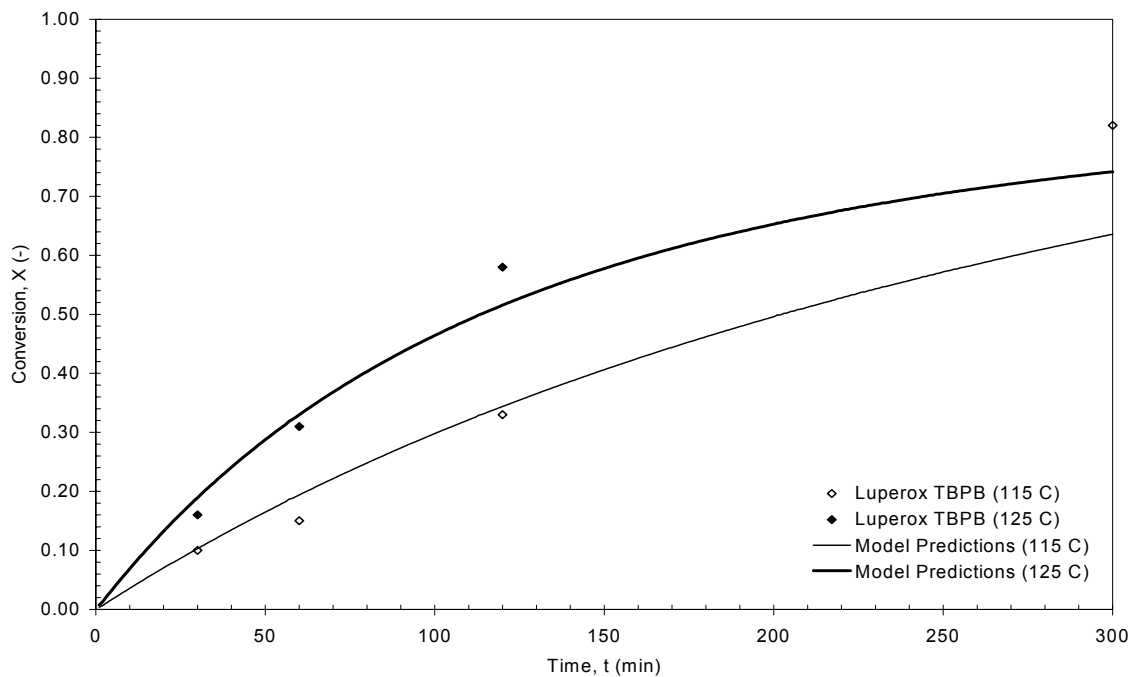


Figure A.13. Conversion as a function of time for the bulk styrene polymerization initiated by Luperox TBPB (monofunctional, $[I]_0 = 539 \text{ ppm} = 0.00250 \text{ M}$).

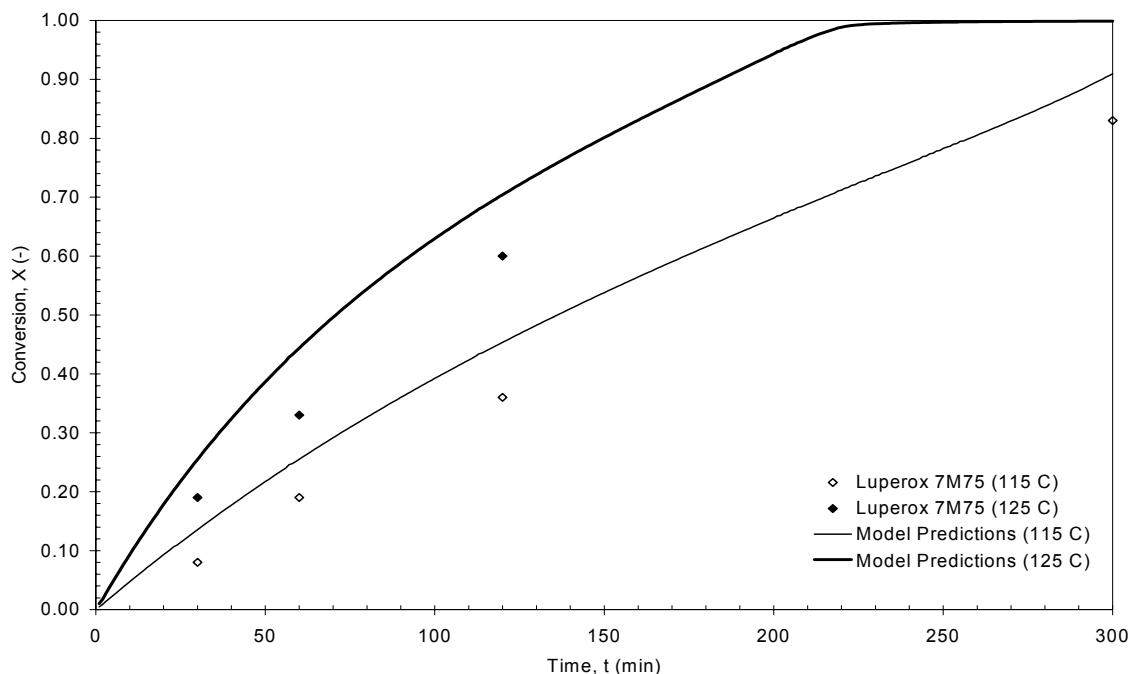


Figure A.14. Conversion as a function of time for the bulk styrene polymerization initiated by Luperox 7M75 (monofunctional, $[I]_0 = 913 \text{ ppm} = 0.00623 \text{ M}$).

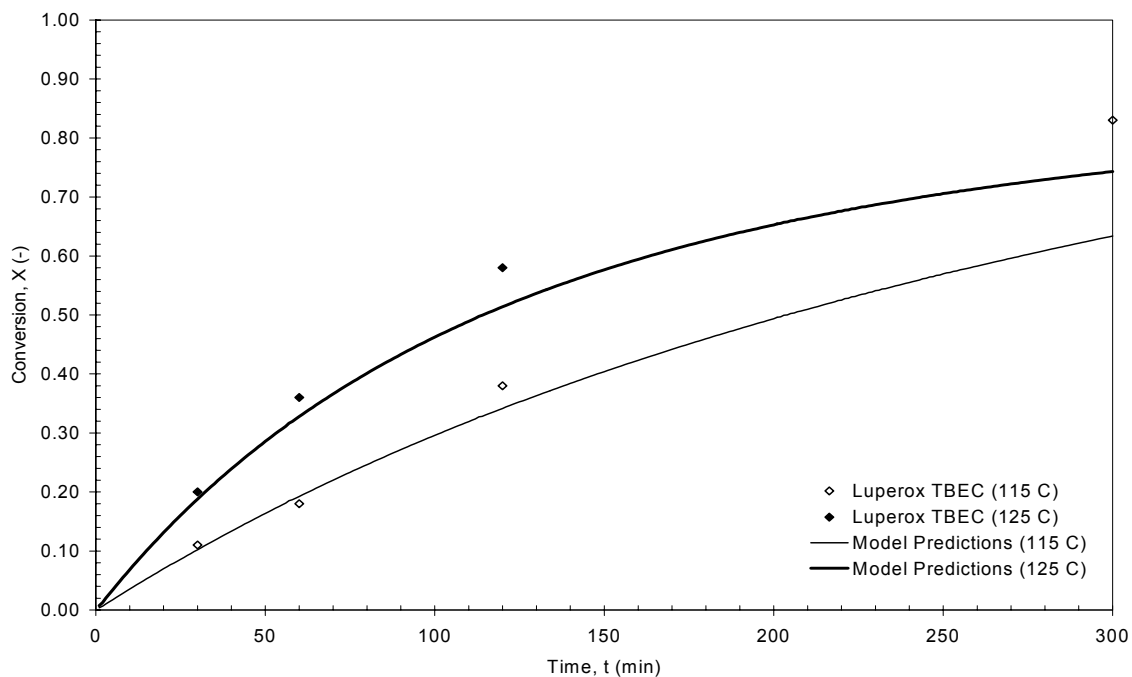


Figure A.15: Conversion as a function of time for the bulk styrene polymerization initiated by Luperox TBEC (monofunctional, $[I]_0 = 683 \text{ ppm} = 0.00250 \text{ M}$).

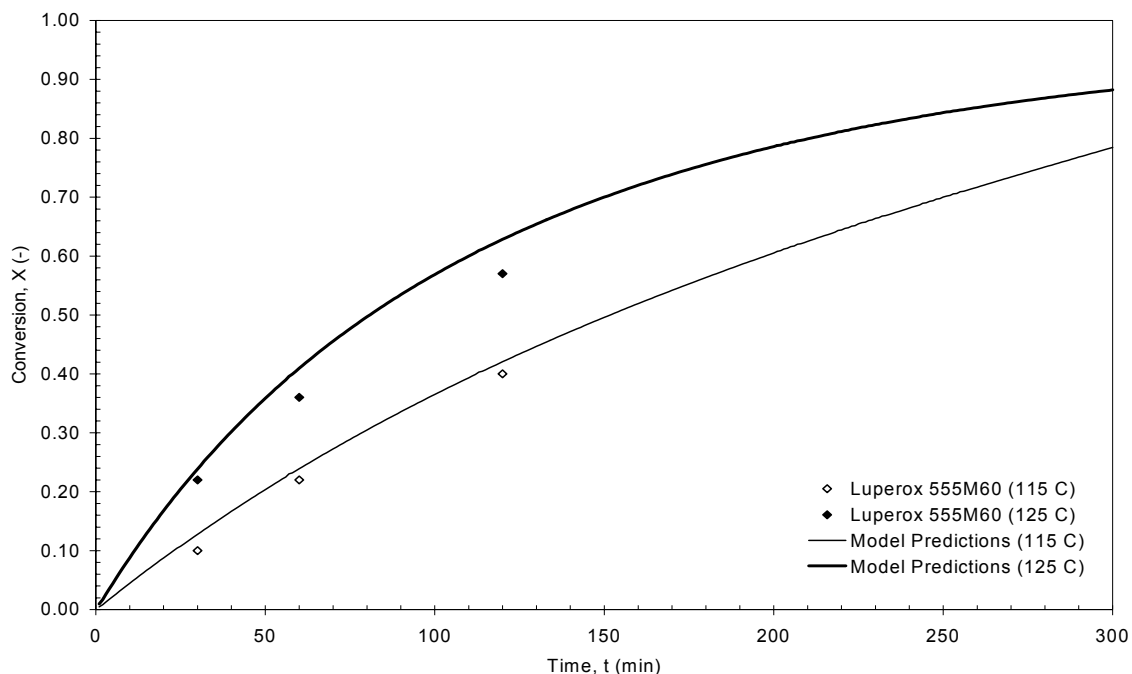


Figure A.16: Conversion as a function of time for the bulk styrene polymerization initiated by Luperox 555M60 (monofunctional, $[I]_0 = 677 \text{ ppm} = 0.00418 \text{ M}$).

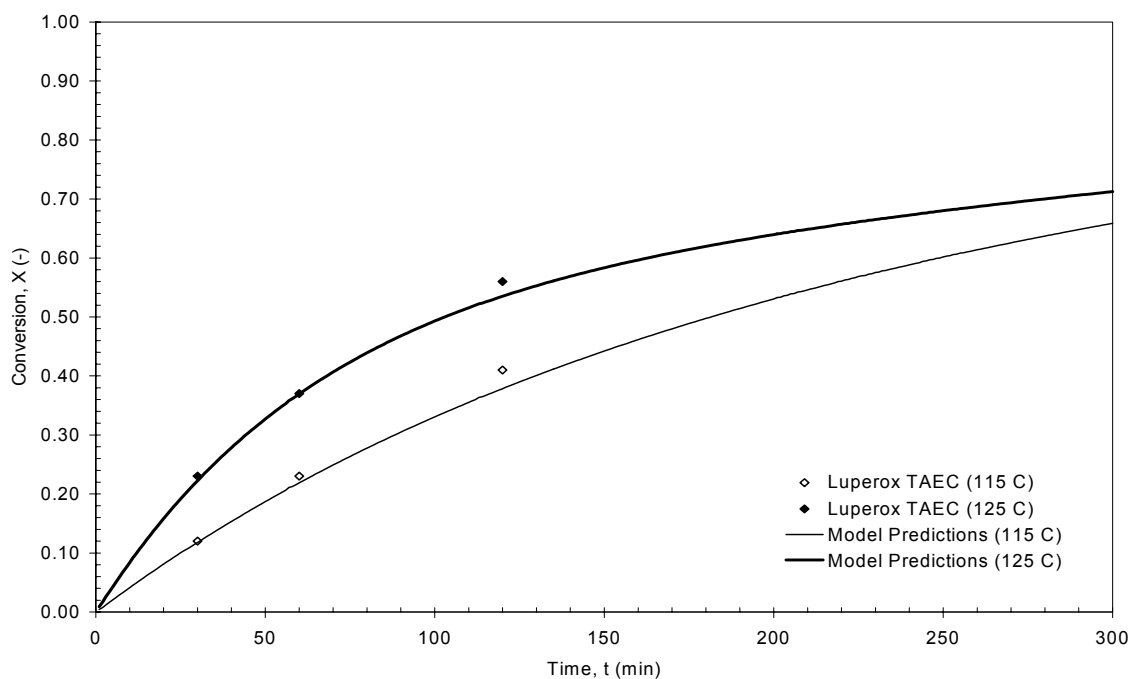


Figure A.17: Conversion as a function of time for the bulk styrene polymerization initiated by Luperox TAEC (monofunctional, $[I]_0 = 722 \text{ ppm} = 0.00250 \text{ M}$).

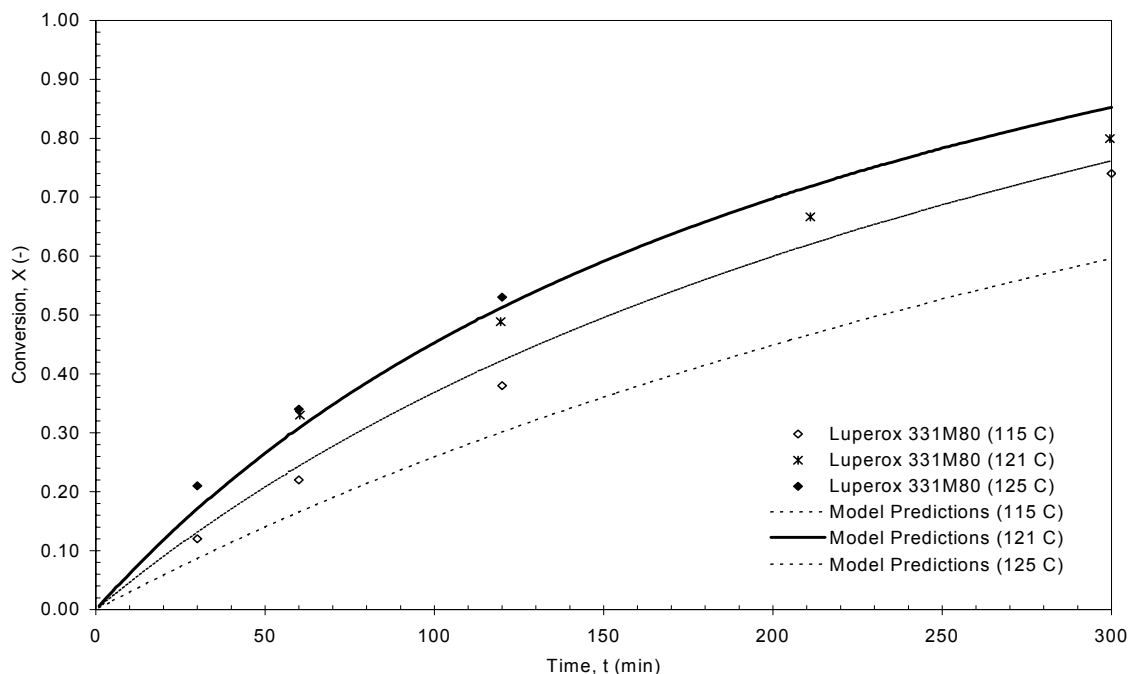


Figure A.18: Conversion as a function of time for the bulk styrene polymerization initiated by Luperox 331M80 (difunctional, $[I]_0 = 451 \text{ ppm} = 0.00156 \text{ M}$).

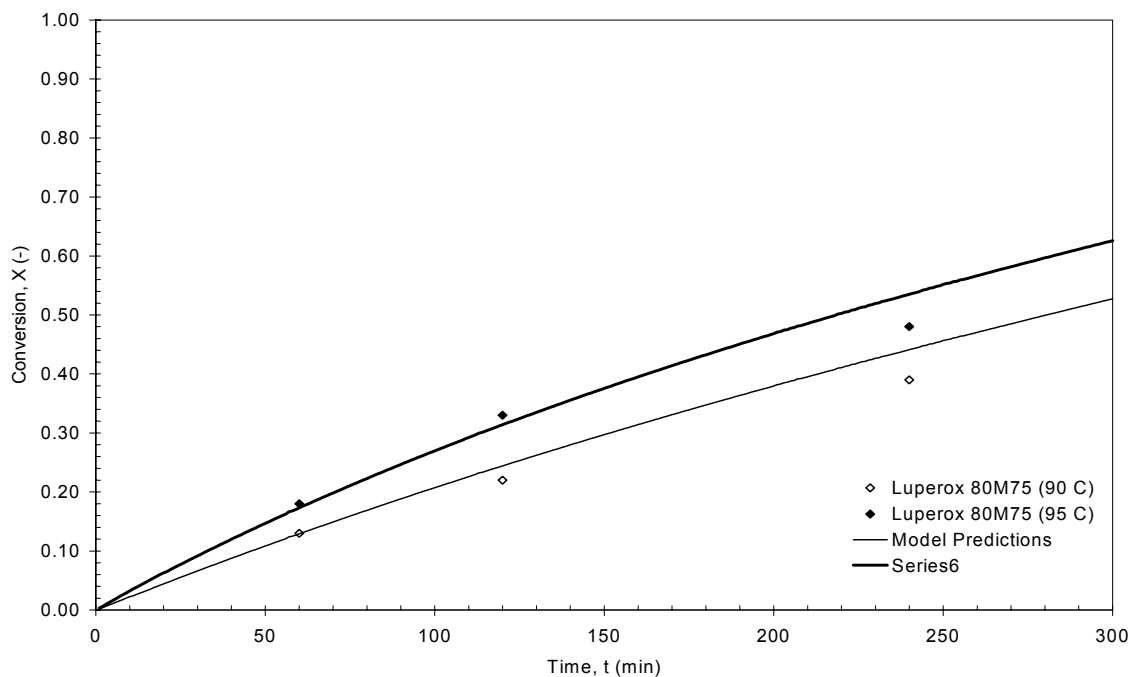


Figure A.19. Conversion as a function of time for the bulk styrene polymerization initiated by Luperox 80M75 (monofunctional, $[I]_0 = 1240 \text{ ppm} = 0.00698 \text{ M}$).

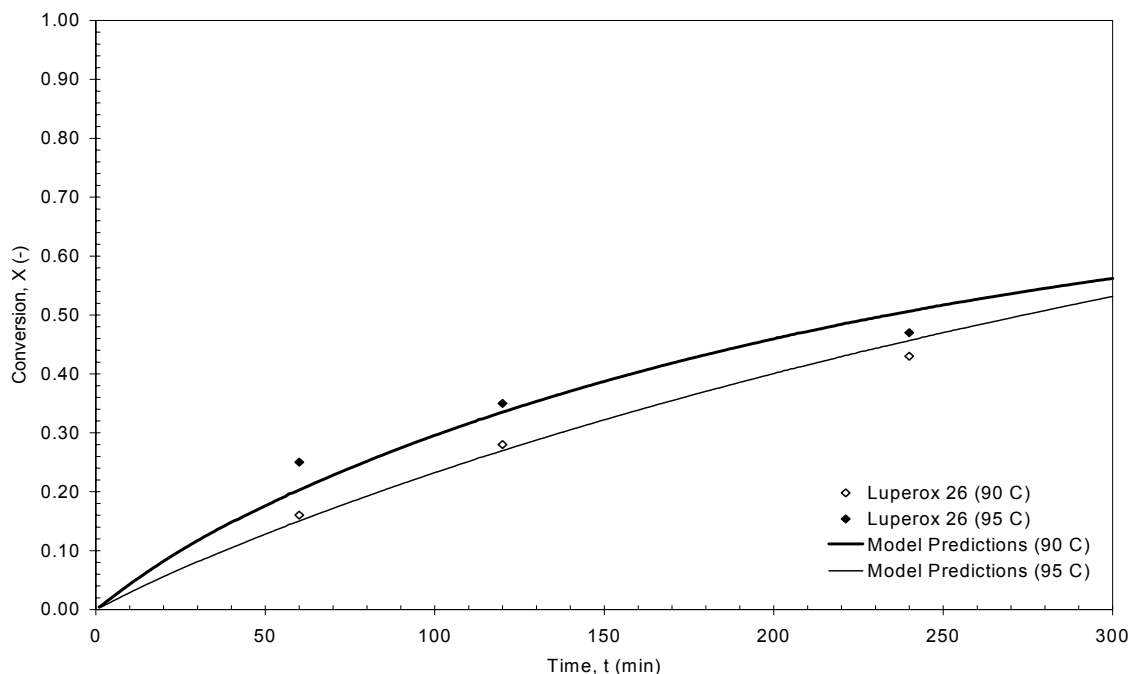


Figure A.20. Conversion as a function of time for the bulk styrene polymerization initiated by Luperox 26 (monofunctional, $[I]_0 = 1339 \text{ ppm} = 0.00559 \text{ M}$).

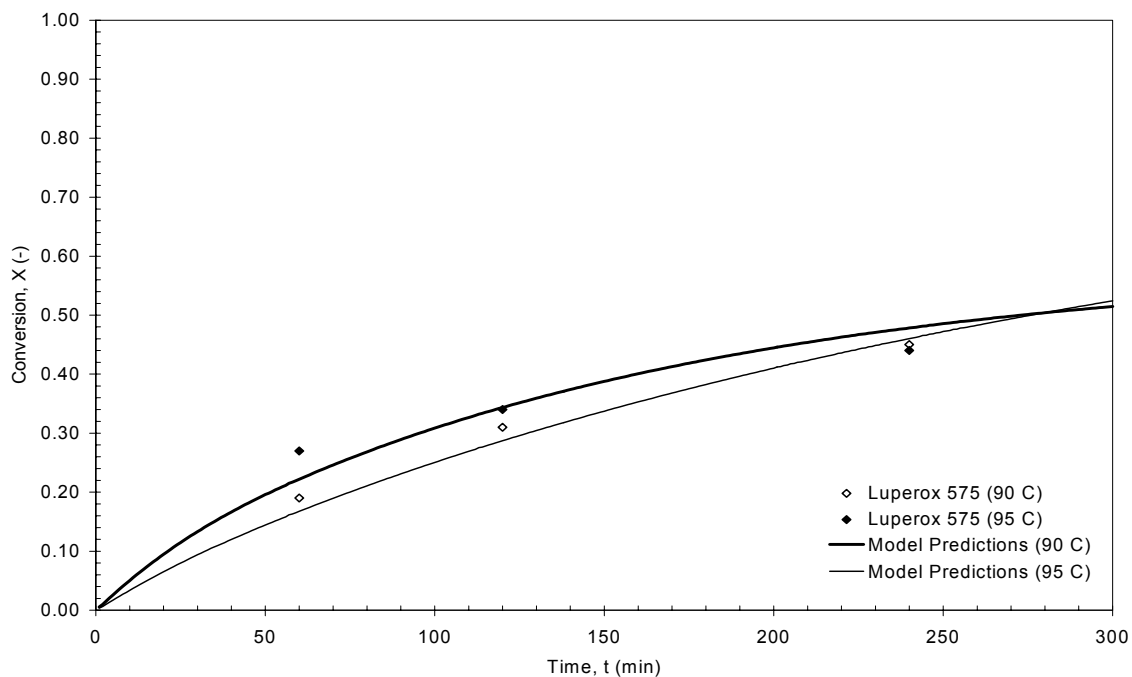


Figure A.21. Conversion as a function of time for the bulk styrene polymerization initiated by Luperox 575 (monofunctional, $[I]_0 = 1426 \text{ ppm} = 0.00559 \text{ M}$).

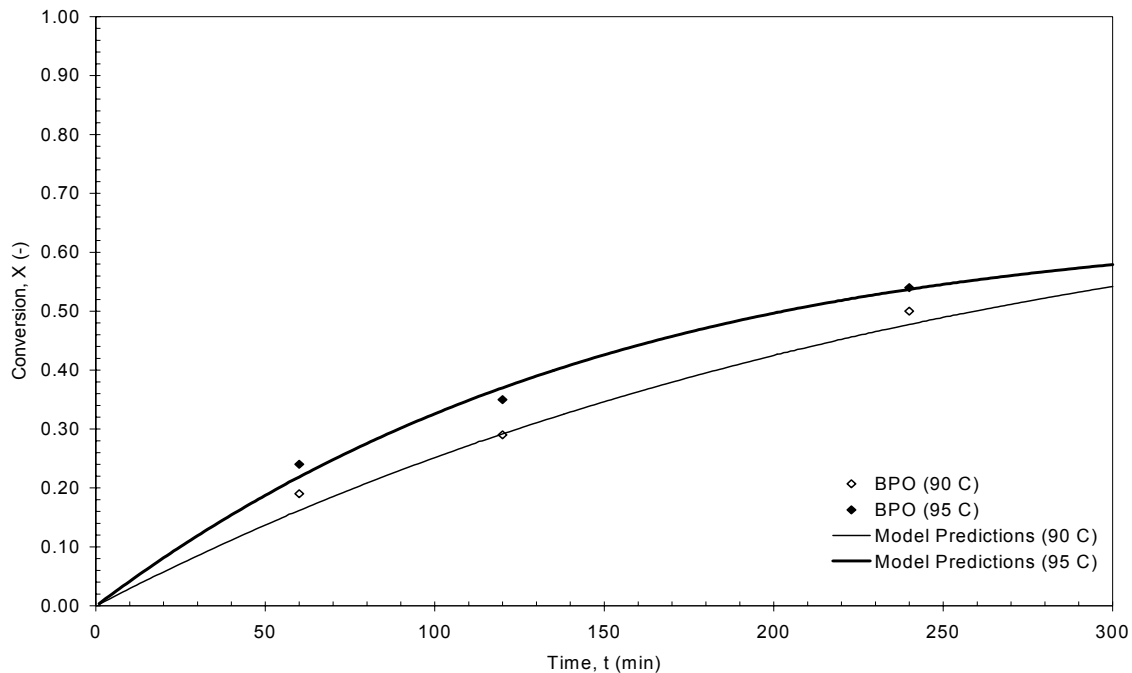


Figure A.22. Conversion as a function of time for the bulk styrene polymerization initiated by BPO (monofunctional, $[I]_0 = 1500 \text{ ppm} = 0.00558 \text{ M}$).

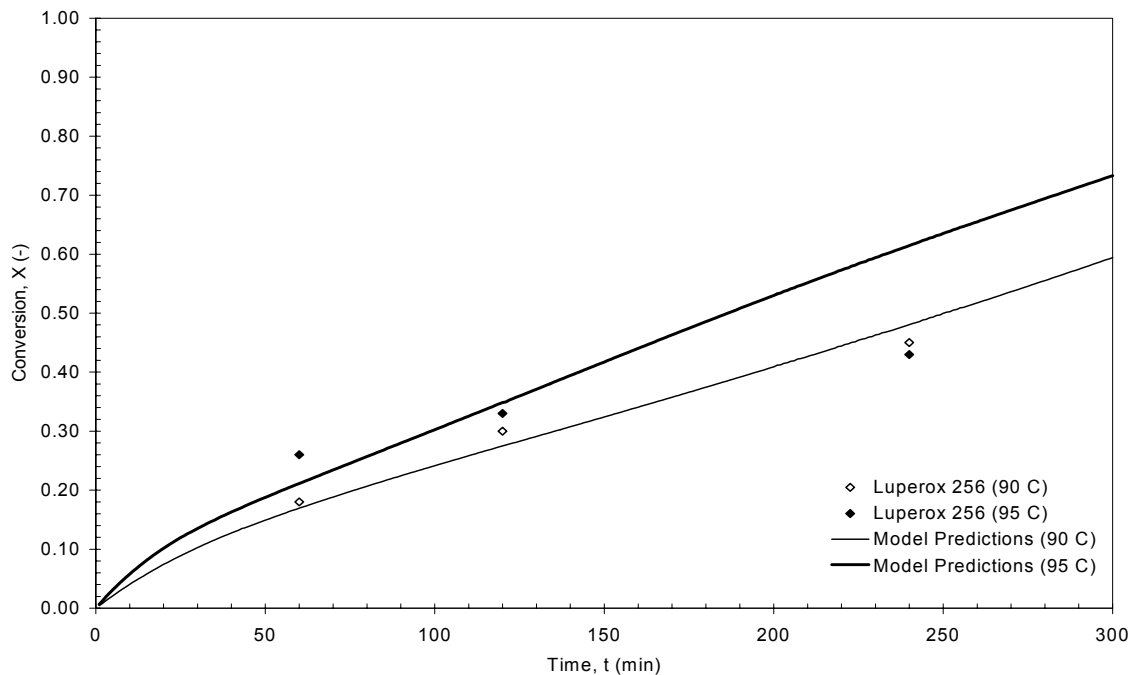


Figure A.23. Conversion as a function of time for the bulk styrene polymerization initiated by Luperox 256 (difunctional, $[I]_0 = 1336 \text{ ppm} = 0.00279 \text{ M}$).

References

1. Dhib, R., Gao, J., Penlidis, A. Simulation of free radical bulk/solution homopolymerization using mono- and bi-functional initiators. *Polymer Reaction Engineering Journal* **2000**, *8*, 299-464.
2. Cavin, L., Rouge, A., Meyer, T., Renken, A. Kinetic modeling of free radical polymerization of styrene initiated by the bifunctional initiator 2,5-dimethyl-2,5-bis(2-ethyl hexanoyl peroxy)hexane. *Polymer* **2000**, *41*, 3925-3935.
3. Villalobos, M. A., Hamielec, A. E., Wood, P. E. Kinetic model for short-cycle bulk styrene polymerization through bifunctional initiators. *Journal of Applied Polymer Science* **1991**, *42*, 629-641.
4. Gao, J., Penlidis, A. A comprehensive simulator database package for reviewing free-radical copolymerizations. *Journal of Macromolecular Science-Reviews in Macromolecular Chemistry and Physics* **1998**, *C38* (4), 651-780.
5. Ebdon, J. R., Hunt, B. J. Study of Free-Radical Polymerization of Styrene by Differential Scanning Calorimetry. *Analytical Chemistry* **1973**, *45* (4), 804-806.
6. Horie, K., Mita, I., Kambe, H. Calorimetric Investigation of Polymerization Reactions .I. Diffusion-Controlled Polymerization of Methyl Methacrylate and Styrene. *Journal of Polymer Science Part A-1-Polymer Chemistry* **1968**, *6* (9PA1), 2663-&.
7. Malavasic, T., Vizovisek, I., Lapanje, S., Moze, A. Study of the Isothermal Bulk Polymerization of Methyl Methacrylate by Differential Scanning Calorimetry. *Makromolekulare Chemie* **1974**, *175*, 873-880.

APPENDIX B - TEMPERATURE PROGRAMMING WITH DIFUNCTIONAL INITIATORS

In polymer production, it is desirable to produce a product with the best properties at the lowest cost. This can be achieved by increasing productivity while maintaining such properties as molecular weight and molecular weight distribution. Optimization policies are useful in achieving these goals and can be designed based on a good understanding of the reactions kinetics. These policies typically rely on the proper choice of an initiator (mono- versus difunctional, low versus high temperature initiator), combination of initiators, and temperature programming in order to optimize a polymerization process. An extensive amount of work has focused on the optimization of the production of polystyrene. In the past few decades, the work of Wu et al. (1) is found to be one of the most comprehensive. The group performed both theoretical and experimental studies of the bulk polymerization of styrene and determined optimal temperature policies to minimize the time to reach a final conversion and a particular number-average molecular weight. Applying a similar method to that of Wu et al. (1) this section shows the benefits of temperature programming with a difunctional initiator, Luperox 101 (2,5-dimethyl-2,5-bis (*tert*-butylperoxy)hexane) in the bulk polymerization of styrene.

The designed temperature programming profile is displayed in Figure C.1. From the conversion versus time trends (see Figure C.2) it can be seen that one can obtain shorter batch times with temperature programming operation. As well, the chosen temperature profile has ensured that stable molecular weights are produced. This is in contrast to the isothermal operation where the molecular weight averages are found to change with conversion. These results show the usefulness of temperature programming in allowing productivity enhancements and product quality improvements.

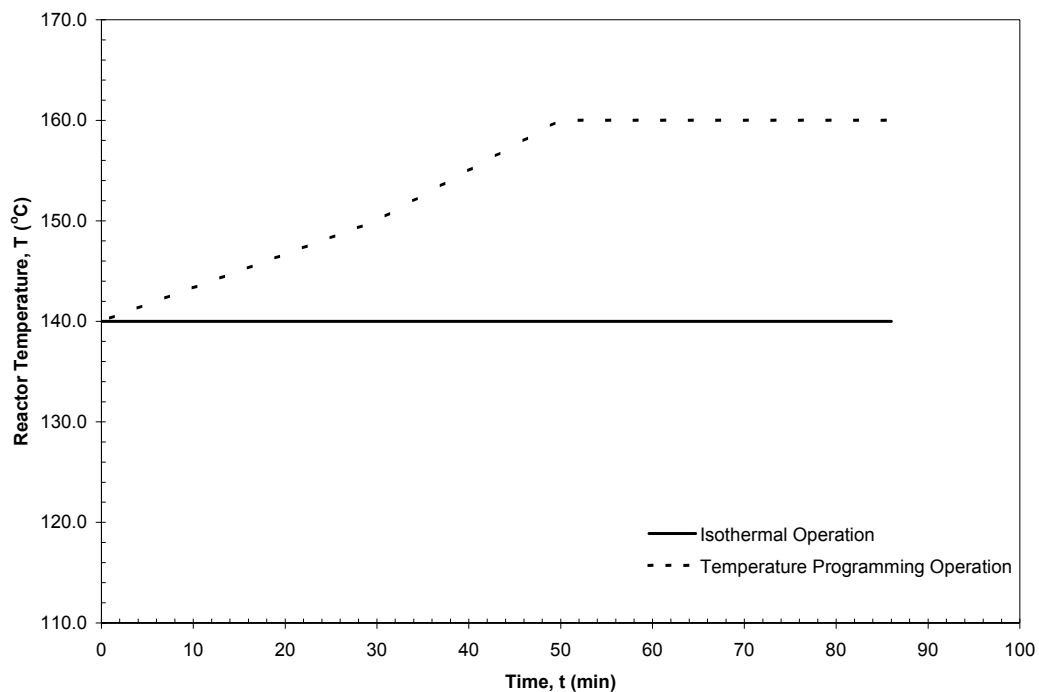


Figure B.1. Reactor temperature profiles for the bulk polymerization of styrene initiated by Luperox 101 (0.002 M) for isothermal and temperature programming operation.

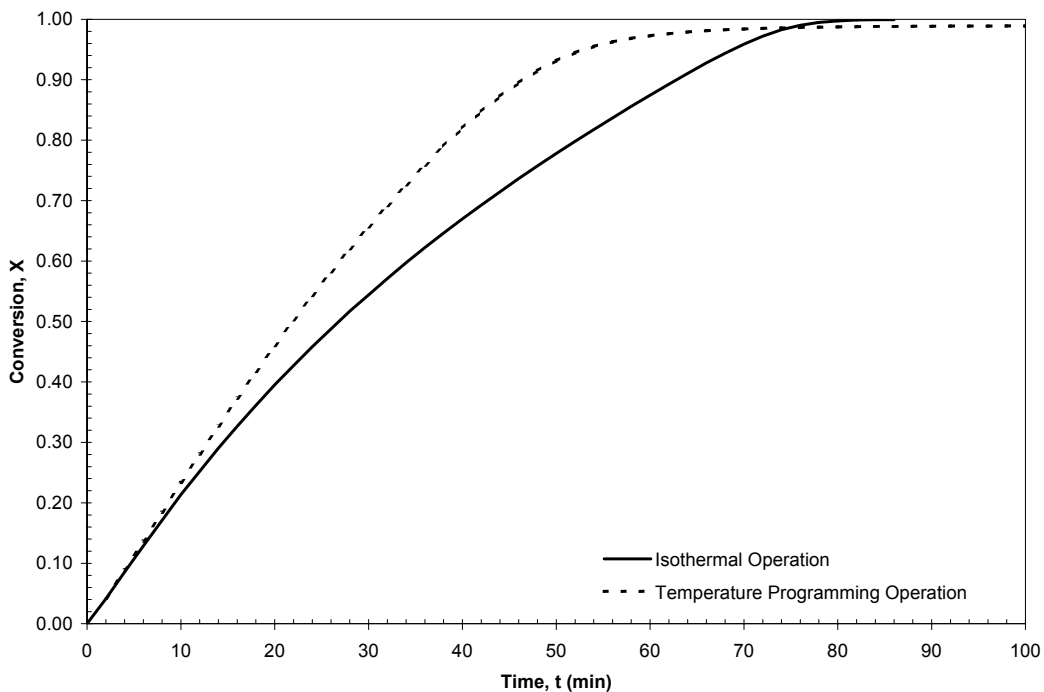


Figure B.2. Conversion as a function of time for the bulk polymerization of styrene initiated by Luperox 101 (0.002 M) for isothermal operation at 140 °C and temperature programming operation.

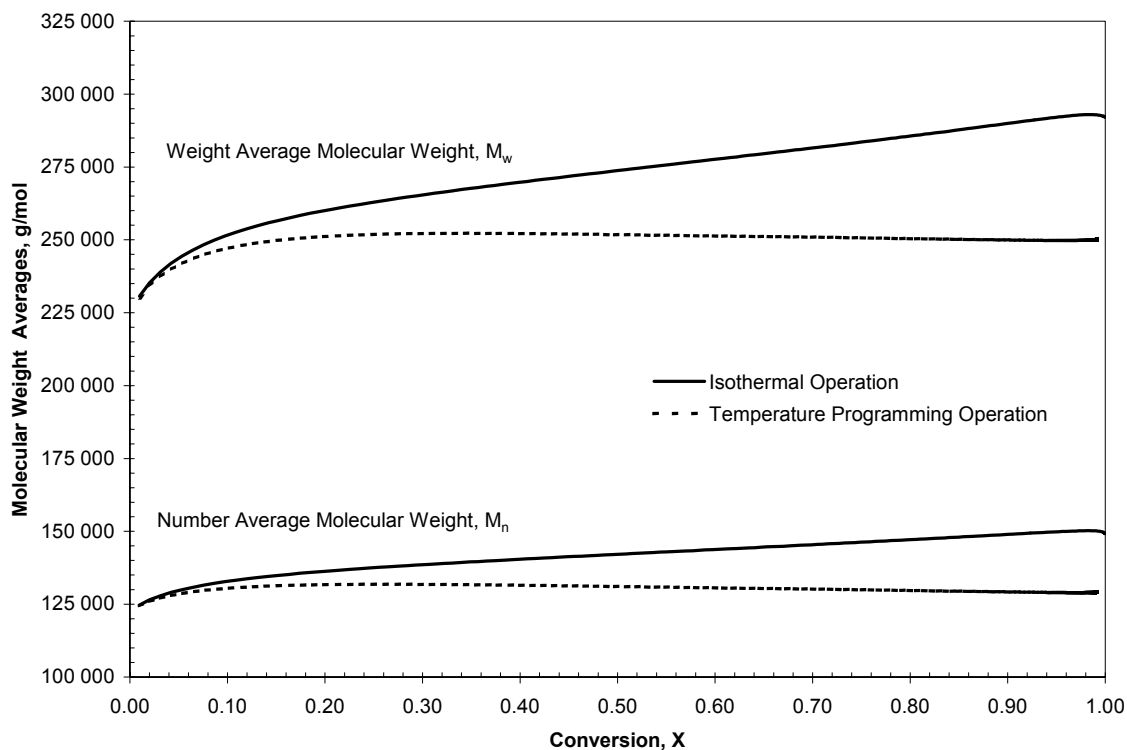


Figure B.3. Molecular weight averages for the bulk polymerization of styrene initiated by Luperox 101 (0.002 M) for isothermal operation at 140 °C and temperature programming operation.

References

1. Wu, G. Z. A., Denton, L. A., Laurence, R. L. Batch polymerization of styrene - Optimal temperature histories. *Polymer Engineering and Science* 1982, 22 (1), 1-8.

APPENDIX C - TETRAFUNCTIONAL MODEL DEVELOPMENT

This appendix contains a brief description of the model developed for a free radical polymerization initiated by a tetrafunctional initiator. The entire model including all population balances and moment equations can be obtained by contacting Professor A. Penlidis at the following address:

Department of Chemical Engineering
 University of Waterloo
 Waterloo, Ontario, Canada
 N2L 3G1

The i th moment of a radical (λ) and dead (μ) polymer species is defined as:

$$\lambda_i^{u,a,c} = \sum_{r=1}^{\infty} r^i R_r^{u,a,c} \quad \text{C.1}$$

$$\mu_i^{u,a,c} = \sum_{r=1}^{\infty} r^i P_r^{u,a,c} \quad \text{C.2}$$

where r is the chain length of a polymer species with u undecomposed functional groups, a active sites and c cores. The zeroth moment is equivalent to the total concentration of a particular species. To simplify certain equations, the following terms are defined:

$$\tilde{\lambda}_0 = \lambda_0^{5,1,2} + \lambda_0^{4,1,2} + \lambda_0^{3,1,2} + \lambda_0^{2,1,2} + \lambda_0^{1,1,2} + \lambda_0^{0,1,2} + \lambda_0^{3,1,1} + \lambda_0^{2,1,1} + \lambda_0^{1,1,1} + \lambda_0^{0,1,1} + \lambda_0^{0,1,0} \quad \text{C.3}$$

$$\tilde{\tilde{\lambda}}_0 = \lambda_0^{4,2,2} + \lambda_0^{3,2,2} + \lambda_0^{2,2,2} + \lambda_0^{1,2,2} + \lambda_0^{0,2,2} + \lambda_0^{2,2,1} + \lambda_0^{1,2,1} + \lambda_0^{0,2,1} \quad \text{C.4}$$

where $\tilde{\lambda}_0$ is the total concentration of monoradicals and $\tilde{\tilde{\lambda}}_0$ is the concentration of all di-radicals. Performing population balances on the initiator radicals allows for the initiation rate equations to be derived as:

$$R_{linear} = R_{thermal} + fk_d \left(\begin{array}{l} 4[I_4] + 3[I_3] + 2[I_2] + [I_1] \\ + 6\mu_0^{6,0,2} + 5\mu_0^{5,0,2} + 4\mu_0^{4,0,2} + 3\mu_0^{3,0,2} + 2\mu_0^{2,0,2} + \mu_0^{1,0,2} \\ + 3\mu_0^{3,0,1} + 2\mu_0^{2,0,1} + \mu_0^{1,0,1} \\ + 5\lambda_0^{5,1,2} + 4\lambda_0^{4,1,2} + 3\lambda_0^{3,1,2} + 2\lambda_0^{2,1,2} + \lambda_0^{1,1,2} \\ + 3\lambda_0^{3,1,1} + 2\lambda_0^{2,1,1} + \lambda_0^{1,1,1} \end{array} \right) \quad C.5$$

$$R_3 = 4fk_d[I_4] \quad C.6$$

$$R_2 = 3fk_d[I_3] \quad C.7$$

$$R_1 = 2fk_d[I_2] \quad C.8$$

$$R_0 = fk_d[I_1] \quad C.9$$

The following terms are grouped together to simplify the population balances:

$$\lambda_0^{\bullet,1,2} = \sum_{i=0}^5 \lambda_0^{i,1,2} = \lambda_0^{5,1,2} + \lambda_0^{4,1,2} + \lambda_0^{3,1,2} + \lambda_0^{2,1,2} + \lambda_0^{1,1,2} + \lambda_0^{0,1,2} \quad C.10$$

$$\lambda_0^{\bullet,1,1} = \sum_{i=0}^3 \lambda_0^{i,1,1} = \lambda_0^{3,1,1} + \lambda_0^{2,1,1} + \lambda_0^{1,1,1} + \lambda_0^{0,1,1} \quad C.11$$

$$\lambda_0^{\bullet,2,2} = \sum_{i=0}^4 \lambda_0^{i,2,2} = \lambda_0^{4,2,2} + \lambda_0^{3,2,2} + \lambda_0^{2,2,2} + \lambda_0^{1,2,2} + \lambda_0^{0,2,2} \quad C.12$$

$$\lambda_0^{\bullet,2,1} = \sum_{i=0}^2 \lambda_0^{i,2,1} = \lambda_0^{2,2,1} + \lambda_0^{1,2,1} + \lambda_0^{0,2,1} \quad C.13$$

$$\lambda_{total} = (\lambda_0^{\bullet,1,2} + \lambda_0^{\bullet,1,1} + \lambda_0^{0,1,0} + \lambda_0^{\bullet,2,2} + \lambda_0^{\bullet,2,1}) \quad C.14$$

where $\lambda_0^{\bullet,a,c}$ is the concentration of radical chains with a active sites and c cores and λ_{total} is the total concentration of all radicals. Monomer consumption is assumed to be predominantly due to propagation (long-chain approximation).

$$\text{Monomer} \quad \frac{1}{V} \frac{d(V[M])}{dt} = -k_p [M] \lambda_{total} \quad C.15$$

Initiator

$$\frac{1}{V} \frac{d(V[I_4])}{dt} = -4k_d[I_4] \quad \text{C.16}$$

$$\frac{1}{V} \frac{d(V[I_3])}{dt} = -3k_d[I_3] + 4(1-f)k_d[I_4] \quad \text{C.17}$$

$$\frac{1}{V} \frac{d(V[I_2])}{dt} = -2k_d[I_2] + 3(1-f)k_d[I_3] \quad \text{C.18}$$

$$\frac{1}{V} \frac{d(V[I_1])}{dt} = -k_d[I_1] + 2(1-f)k_d[I_2] \quad \text{C.19}$$

Solvent

$$\frac{1}{V} \frac{d(V[S])}{dt} = -k_{tfs}[S]\lambda_{total} \quad \text{C.20}$$

Using the radical and dead polymer balances, moment equations can be developed. As an example, the equations for linear radicals and linear dead polymer chains are shown below.

$R_r^{0,1,0}$

$$\begin{aligned} \frac{1}{V} \frac{d(V\lambda_0^{0,1,0})}{dt} = & R_{linear} - (k_{tc} + k_{td})\lambda_0^{0,1,0} (\lambda_0^{\bullet,1,2} + \lambda_0^{\bullet,1,1} + 2\lambda_0^{\bullet,2,2} + 2\lambda_0^{\bullet,2,1} + \lambda_0^{0,1,0}) \\ & + C_{tr} (\lambda_0^{\bullet,1,2} + \lambda_0^{\bullet,1,1} + 2\lambda_0^{\bullet,2,2} + 2\lambda_0^{\bullet,2,1}) \end{aligned} \quad \text{C.21}$$

$$\begin{aligned} \frac{1}{V} \frac{d(V\lambda_1^{0,1,0})}{dt} = & R_{linear} - (k_{tc} + k_{td})\lambda_1^{0,1,0} (\lambda_0^{\bullet,1,2} + \lambda_0^{\bullet,1,1} + 2\lambda_0^{\bullet,2,2} + 2\lambda_0^{\bullet,2,1} + \lambda_0^{0,1,0}) \\ & + k_p[M]\lambda_0^{0,1,0} + C_{tr} (\lambda_0^{\bullet,1,2} + \lambda_0^{\bullet,1,1} + 2\lambda_0^{\bullet,2,2} + 2\lambda_0^{\bullet,2,1} + \lambda_0^{0,1,0} - \lambda_1^{0,1,0}) \end{aligned} \quad \text{C.22}$$

$$\begin{aligned} \frac{1}{V} \frac{d(V\lambda_2^{0,1,0})}{dt} = & R_{linear} - (k_{tc} + k_{td})\lambda_2^{0,1,0} (\lambda_0^{\bullet,1,2} + \lambda_0^{\bullet,1,1} + 2\lambda_0^{\bullet,2,2} + 2\lambda_0^{\bullet,2,1} + \lambda_0^{0,1,0}) \\ & + k_p[M](2\lambda_1^{0,1,0} + \lambda_0^{0,1,0}) \\ & + C_{tr} (\lambda_0^{\bullet,1,2} + \lambda_0^{\bullet,1,1} + 2\lambda_0^{\bullet,2,2} + 2\lambda_0^{\bullet,2,1} + \lambda_0^{0,1,0} - \lambda_2^{0,1,0}) \end{aligned} \quad \text{C.23}$$

$$P_r^{0,0,0} \frac{1}{V} \frac{d(V\mu_0^{0,0,0})}{dt} = k_{td} \lambda_0^{0,1,0} (\lambda_0^{\bullet,1,2} + 2\lambda_0^{\bullet,2,2} + \lambda_0^{\bullet,1,1} + 2\lambda_0^{\bullet,2,1} + \lambda_0^{0,1,0}) + \frac{1}{2} k_{tc} (\lambda_0^{0,1,0})^2 + C_{tr} \lambda_0^{0,1,0} \quad \text{C.24}$$

$$\frac{1}{V} \frac{d(V\mu_1^{0,0,0})}{dt} = k_{td} \lambda_1^{0,1,0} (\lambda_0^{\bullet,1,2} + 2\lambda_0^{\bullet,2,2} + \lambda_0^{\bullet,1,1} + 2\lambda_0^{\bullet,2,1} + \lambda_0^{0,1,0}) + \frac{1}{2} k_{tc} (2\lambda_1^{0,1,0} \lambda_0^{0,1,0}) + C_{tr} \lambda_1^{0,1,0} \quad \text{C.25}$$

$$\frac{1}{V} \frac{d(V\mu_2^{0,0,0})}{dt} = k_{td} \lambda_2^{0,1,0} (\lambda_0^{\bullet,1,2} + 2\lambda_0^{\bullet,2,2} + \lambda_0^{\bullet,1,1} + 2\lambda_0^{\bullet,2,1} + \lambda_0^{0,1,0}) + \frac{1}{2} k_{tc} (2(\lambda_2^{0,1,0} \lambda_0^{0,1,0} + (\lambda_1^{0,1,0})^2)) + C_{tr} \lambda_2^{0,1,0} \quad \text{C.26}$$

where the transfer reaction term C_{tr} is defined as follows:

$$C_{tr} = (k_{fM} [M] + k_{fS} [S]) \quad \text{C.27}$$